Ultrafast Intersystem Crossing in Heavy-atom-Free Molecules: Effect of Polarity, Viscosity, Hydrogen Bonding and Confinement

A Thesis
Submitted in Partial Fulfillment of the Requirements
for the Degree of

DOCTOR OF PHILOSOPHY

by

ABHIJIT DUTTA

Roll No. 19107261

to the

Department of Chemistry
Indian Institute of Technology Kanpur
Kanpur, India

May 2025

This page left blank intentionally

CERTIFICATE

It is certified that the work reported in the thesis entitled "**Ultrafast Intersystem Crossing in Heavy-atom-Free Molecules: Effect of Polarity, Viscosity, Hydrogen Bonding and Confinement**" has been carried out by **Mr. Abhijit Dutta** under my supervision and has not been submitted elsewhere for a degree.

May 2025
IIT Kanpur

(Prof. Pratik Sen)
Thesis Supervisor
Department of Chemistry
Indian Institute of Technology Kanpur
Kanpur, U.P. India- 208016

This page left blank intentionally

DECLARATION

This is to certify that the thesis titled "**Ultrafast Intersystem Crossing in Heavy-atom-Free Molecules: Effect of Polarity, Viscosity, Hydrogen Bonding and Confinement**" has been authored by me. It presents the research conducted by me under the supervision of **Prof. Pratik Sen**.

To the best of my knowledge, it is an original work, both in terms of research content and narrative, and has not been submitted elsewhere, in part or in full, for a degree. Further, due credit has been attributed to the relevant state-of-the-art and collaborations (if any) with appropriate citations and acknowledgements, in line with established norms and practices.

Signature

Name: Abhijit Dutta
Programme: PhD
Department: Chemistry
Indian Institute of Technology Kanpur
Kanpur 208016

This page left blank intentionally

Department of Chemistry
Indian Institute of Technology Kanpur

Certificate of course work

This is to certify that **Mr. Abhijit Dutta** has satisfactorily completed all the courses required for the Ph.D degree. The courses include:

CHM 629A Principles of Physical Chemistry

CHM 600A Mathematics for Chemistry

CHM 684A Computer Programming for Chemistry

CHM 685A Molecule Radiation Interaction

CHM 799 Research

CHM 800A General Seminar

CHM 801A Graduate Seminar

Mr. Abhijit Dutta was admitted to the candidacy of the Ph.D degree in July 2019 after he successfully completed the written and oral qualifying examinations.

Head
Department of Chemistry
Indian Institute of Technology Kanpur
Kanpur – 208016, India

Convenor, DPGC
Department of Chemistry
Indian Institute of Technology Kanpur
Kanpur – 208016, India

This page left blank intentionally

Dedicated to

My family

This page left blank intentionally

Acknowledgements

I thank God, the ultimate superpower, for being with me throughout my PhD journey. His presence filled me with positive energy when I felt low and gave me strength during difficult times. Whenever I was confused or stuck, I felt silent guidance that helped me move forward. Every small success along the way felt like His blessing. Without His support and energy, I wouldn't have come this far.

From an academic perspective, I completed my Master's degree at IIT Bhubaneswar, where I worked on a biophysical chemistry project focused on studying the behavior of heat shock proteins associated with leprosy.

That experience gave me a basic understanding of research when I joined my Ph.D. at IIT Kanpur in July 2019. When I met my supervisor, ***Prof. Pratik Sen****, I discovered how fascinating and powerful time-resolved spectroscopy is for understanding molecular dynamics. Through his courses and lab discussions, I gained valuable knowledge about lasers and the fundamentals of light–matter interactions. His way of explaining complex concepts helped me build a strong foundation, which later became very useful in my research. After completing my coursework, I began my research under his guidance, starting with a well-known molecular system to study triplet state photophysics. However, after several months of work, I ran into experimental difficulties and was unable to interpret the results. I felt lost and could not make much progress. So, I left that project and started a new one on the blue emission of hydrophobic coumarins in SDS micelles. I worked on it for about a year and was close to finishing when, during a lab meeting, we realized that our interpretation was wrong and too speculative. That meant I had to stop that project too. It was very hard to accept two major setbacks after spending three years in the lab. I felt broken. During that time, my supervisor kept encouraging me. He said, "At least you have learned something from these failures." He understood my situation and kindly suggested that I collaborate with Prof. Tahei Tahara (RIKEN, Japan) on an interesting project involving tryptophan. I went there for a short-term project (IPA), but unfortunately, that too did not work as expected.*

When I came back to my lab after about 3.5 years, I felt like a rudderless boat lost in the ocean. But my supervisor gave me hope again. He told me that the earlier results from my first project were enough to build a meaningful story. I restarted the work, collected more data, and slowly built up the project. At the same time, he introduced me to Prof. V. Ramamurthy (University of Miami), and I began working on thionated coumarin systems. This time, I got some exciting results.

After nearly four years of hard work and struggle, I was finally able to publish my first research paper. That changed everything. I felt hopeful, energetic, and confident that I could contribute to science. With my supervisor's constant support, I was able to understand complex data and publish my second work in a reputed journal. This journey taught me that research is not only about brilliance it is about patience, hard work, and perseverance. I stopped looking back at my failures and started moving forward. The joyful moments of success I shared with my supervisor will always inspire me. A friend is someone you can talk to about your problems and ideas. A philosopher helps you stay calm and understand life better. A guide shows you the right path. My supervisor has been all three. He made me believe that every difficult problem can have a simple solution. His way of thinking, teaching, and solving problems will always stay with me and guide me in the future. Without his support, I would not have grown as a researcher, and this thesis would not have been possible. I sincerely thank him from the bottom of my heart and wish the very best to him and his family.

I am deeply grateful to ***Prof. V. Ramamurthy*** *from the* ***University of Miami, USA****, for his generous support and inspiration throughout my research journey. He introduced me to the fascinating world of thiocoumarin systems and octa acid, and kindly provided these systems for my research. Without his support, this thesis would have taken a very different shape. I still remember the excitement of our very first meeting—it's hard to put into words. Since then, every interaction with him has helped me understand my work better and learn new things. His guidance has been incredibly valuable. From the beginning of my Ph.D., his book "Principles of Molecular Photochemistry: An Introduction" has been a constant source of knowledge. I cannot think of a single research problem where I didn't refer to it. I feel truly fortunate to have had the opportunity to work with him and learn from him.*

I am sincerely grateful to ***Prof. Tahei Tahara*** *from* ***RIKEN, Japan****, for giving me the opportunity to work on a project in his laboratory. During that time, I not only gained valuable scientific knowledge but also learned important philosophical lessons that helped me appreciate the importance of making the right choices in both work and life. His guidance taught me how to present my research in a clear and meaningful way, and how to improve the quality of my work. I consider myself truly fortunate to have had the chance to work with him and learn from his wisdom.*

I would also like to thank Dr. V. Srinivasan of IISER Bhopal, for the quantum mechanical calculations in my second work.

I want to take this opportunity to express my gratitude to Prof. N. N. Nair, Dr. I. Sengupta, Dr, M. Sadhukhan for their insightful teaching during coursework. I would like to thank Prof. D. Goswami, Dr. V. G. Rao for their constant encouragement during my time as their teaching assistant.

I express my whelming acknowledgement to the Department of Chemistry, IIT Kanpur, for making a part of it and providing all the facilities. Special thanks are due to Geeta Maam for her constant cooperation and generous help.

I want to express my heartfelt gratitude to late Dr. Asish Kumar Nag and Dr. Nabakumar Bera. It was their teaching and discussions that made me love physical chemistry. I would also like to thank my Organic Chemistry teacher, Dr. Chandan Saha, for helping me realize the beauty of chemistry. I also want to acknowledge all my teachers from my childhood to my college days.

A special thanks goes to my seniors in the lab, Aritra Da, for training me on the fluorescence up-conversion and transient absorption setups. I have several fun and beautiful moments with him. I also want to thank Puspal Da (my super senior) for helping in many aspects of my research. Their guidance greatly boosted my confidence to operate these instruments independently and utilize them effectively in my research. Thanks are due to my seniors Navin Da, Ejaj Da, Nilimesh Da, Shovon Da, Shreya di and Clovis.

About my batchmates? Let me think… If I had to share everything, it would turn into another thesis on their contributions! So, keeping it short and starting with Arghya da—though he is technically a senior, we've always treated each other as batchmates. He is a truly dedicated researcher, a family man, and above all, a genuinely good human being with an incredibly positive spirit. But beyond all his admirable qualities, what inspires me most is his grounded nature despite his many achievements—something I believe he will always carry with him. I spent six wonderful years with him, and I cherish the countless memories we've made, including the nickname he gave me: "Gattu." We've shared both fun times and critical moments, and I'm truly grateful to have had Arghya da as a batchmate in the lab.

I had good fortune to other three batchmates persons, Tanmoy, Kuldeep, and Sandip, whom I cannot just mention as batchmates or labmates or friends. I remember the very first day in the lab Sandip was the guy who welcomed me in the lab. He is a very genuine and helpful guy I cannot explain it. We had a lot of fun moments in the lab. Right now, Sandip is not working with us but when I went to

Japan, he just took care me as his brother. I never felt like I was alone there. I will never forget his love, help and friendly nature.

*About **Kuldeep**—he's a brilliantly crazy guy! His hilly genes give him a unique charm and boundless energy, though he's also wonderfully impatient and chill at the same time—a truly wild combination! Beyond his vibrant personality, he's the one who made me realize that life exists outside the lab too. From morning to night, I have countless stories with him, and I honestly can't imagine anyone else filling the space he occupies in our lab. I'm truly grateful to have Kuldeep as a batchmate.*

*About **Tanmoy**? The story could go on forever! Except for a few very personal matters, we've done almost everything together. From sharing breakfast plates to midnight parties, it's hard for me to imagine a moment on campus where Tanmoy was around but not by my side—unless there was a major reason. He has a remarkable breadth of knowledge, is grounded, incredibly helpful, and a truly promising researcher. His kindness is inspiring—he's the kind of person who will pause his own work just to help someone else. Throughout my Ph.D. journey, he supported me in countless ways—from helping me write single lines to reviewing entire manuscripts. Beyond academic matters, he's been there to guide me and correct me in life too.*

*Apart from my batchmates, I shared all the above-mentioned experiences with my immediate junior, **Suman**. Although he officially joined as a junior, we were part of the same batch in most aspects, and we always treated each other like batchmates. Like others, he is a potential researcher and a genuinely helpful person. Due to the disruptions during the COVID-19 period, I wasn't able to learn the lab instruments properly in the beginning. So, we learned everything together from our seniors—making him my true partner in the lab-learning process. More than just technical learning, Suman was a constant source of support in daily life, both inside and outside the lab. We shared everything we learned with each other and helped one another in every possible way. Whenever I faced difficulties, he did his best to assist me. I honestly believe that completing my Ph.D. would have been much harder without his help. I feel truly fortunate to have had him not only as a junior but also as a lifelong friend. All of them—my batchmates and Suman—were my family here, and words will never be enough to express their importance in my life.*

I would like to acknowledge my junior, Dipankar—with whom working was always a joyful experience. I also want to thank Subhendu, Patralekha, Bhupendra, Arnab, Akash, Harshit, and Himanshu for making my time in the lab more vibrant

and memorable. I would like to mention the M.Sc. students who worked in the lab during my tenure: Bishal, Soumya, Kuntal, Subhajit, and Swagata—their enthusiasm added a refreshing energy to the lab environment.

During my Ph.D. journey, I was fortunate to cross paths with many affectionate friends, seniors, and juniors, without whom my stay at IIT Kanpur would have been dull and exhausting. It is impossible to imagine hostel life without the endless 'tea addas,' lunch/dinner table conversations, and late-night chats. I deeply cherish those moments shared with Anubhav, Aranya, Abhijit (Manna), Rajib da, Arindam da, Abir da, Bhut da, Kanyasree di, and many others. A special thanks and heartfelt mention to Subhodeep and Poulomi (my campus sister) for their constant support and presence.

And finally, to my would-be life partner, Sayanti—I don't even know where to begin. She has supported me in every possible way throughout my Ph.D. journey. Whenever I felt frustrated, depressed, or anxious, she stood by me like a true partner. I believe this journey wasn't mine alone; it was hers too. She often jokes that she deserves at least a part of my degree—and I couldn't agree more. Thank you, Sayanti, for being with me through everything.

I am grateful to the Council of Scientific and Industrial Research (CSIR), Government of India, for providing me with the research fellowship that supported my Ph.D. journey. I also acknowledge IIT Kanpur for its excellent infrastructure and research facilities. Special thanks to HPC 2010 and HPC 2013 for providing the necessary computational resources.

Most importantly, it is the unconditional love, endless patience, and immeasurable sacrifices of my brother and my parents that have shaped who I am today. I dedicate this milestone in my career to them with deepest gratitude.

Abhijit Dutta

This page left blank intentionally

Synopsis

Name of the Student	Abhijit Dutta
Roll Number:	19107261
Degree for which Thesis is Submitted:	Ph. D.
Department:	Chemistry
Supervisor:	Prof. Pratik Sen
Thesis Title:	Ultrafast Intersystem Crossing in Heavy-atom-Free Molecules: Effect of Polarity, Viscosity, Hydrogen Bonding and Confinement
Month and Year of Submission:	May, 2025

The increasing interest in light harvesting technologies highlights the need to develop molecular systems with high efficiency in triplet state formation. A high triplet efficiency is crucial for a wide range of applications, including lasers, sensing, photovoltaics, organic light-emitting diodes (OLEDs), and particularly in photodynamic therapy (PDT). While many studies have explored triplet-forming materials, detailed insights into the mechanisms of photo-induced triplet state generation are still relatively limited. Understanding these mechanisms is essential for designing effective systems.

In my thesis, I extensively examined the photophysical behavior of various heavy-atom-free molecular systems, both in solution and within confined cavities. I investigated how intrinsic and extrinsic factors influence their triplet state dynamics. This research not only expands current knowledge but also provides a solid framework for designing innovative triplet-forming systems that enhance photoluminescence applications and offer effective strategies for treating tumour cells.

Briefly, my first work was on the role of molecular motions in triplet state generation in Cu(dimethylphenanthroline)$_2$Cl complex. This molecule is known for its intriguing photophysical properties, characterized by ligand-twisting motion in the excited state transitioning from an initially perpendicular geometry to a flattened structure in unrestricted solvent media. I employed various viscous and confined environments to examine the influence of molecular vibrations on the triplet generation mechanism. It was observed that triplet state generation occurs along specific volume-changing vibrational coordinates. Subsequently, I shifted my study to thionated molecules, known for their inherently high intersystem crossing efficiency and triplet generating efficacy. The introduction of a thio-substitution for the carbonyl oxygen in coumarin 1 molecule (thiocoumarin 1, TC1) significantly altered its photophysical properties, facilitating the formation of triplets on an ultrashort timescale. I investigated the photophysical properties of TC1 in protic solvent media and discovered the detrimental impact of hydrogen bonding interactions on triplet yield. Furthermore, I found that thiocoumarins with intramolecular charge transfer (ICT) characteristics are less efficient in triplet generation compared to those without ICT. Overall, my research will contribute to the design of molecules with enhanced abilities for quantitative triplet formation.

Summary of work done

(1) Triplet State Photophysics of Bis(dimethylphenanthroline)copper(I) Might Involve Volume-Changing Molecular Motion: Ultrafast Absorption and Emission Studies (*Chem. Phys. Lett.* **2024**, *839*, 141108**)**

The steady-state spectroscopic data for bis(dimethylphenanthroline)copper(I) (Cu(dmphen)$_2$Cl) indicate that factors such as surrounding polarity, viscosity, and confinement significantly impact its phosphorescence quantum yield. Notably, high phosphorescence yields are observed in glycerol-methanol mixtures with high glycerol content, suggesting the involvement of volume-changing motions through which the triplet state decays non-radiatively to the ground state. Similar constraints

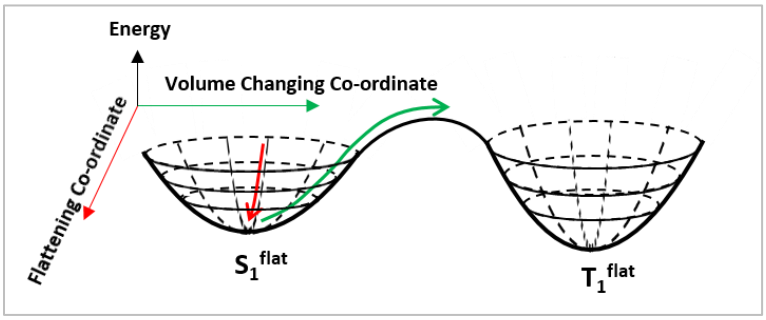

on phosphorescence yield are also seen when the complex is encapsulated within an AOT reverse micelle of varying water pool sizes, supporting this hypothesis. Temperature-dependent steady-state measurements in isoviscous glycerol/methanol mixtures suggest an energy barrier in the singlet-to-triplet conversion pathway along the same volume-changing coordinate. The pressing question concerns how environmental restrictions affect the dynamics of triplet formation in viscous or confined media. To investigate this, I first measured the fluorescence lifetime of the flattened-S_1 state, which precedes to triplet state formation, in both glycerol-methanol mixtures and confined AOT reverse micelle systems. The slower lifetime of $Cu(dmphen)_2Cl$ in high viscosity and confined media hints a delayed triplet generation. To further examine triplet generation in restricted and unrestricted environments, femtosecond transient absorption (TA) measurements were performed. These measurements revealed that triplet generation is slowed in environments with high viscosity or small water pool sizes in AOT reverse micelle. This finding underscores that triplet state decay, and its generation in this complex, involves volume-changing motion coordinates, leading to slower kinetics in restricted media. Additionally, to determine the activation energy barrier for triplet generation, I recorded TA data in isoviscous glycerol/methanol mixtures at four different temperatures ranging from 303K to 333K. From the kinetic analysis of the TA data, I calculated the rate constant for triplet generation. By employing a simple Arrhenius model, the activation energy for triplet generation in the $Cu(dmphen)_2Cl$ complex was determined to be 5.9 kJ/mol, achievable through increasing the system's temperature. This comprehensive photophysical study of $Cu(dmphen)_2Cl$ emphasizes that both the ultrafast formation and decay of the triplet state occur via volume-changing vibrational coordinates, having an activation barrier.

(2) Ultrafast Processes in Upper Excited Singlet States of Free and Caged 7-Diethylaminothiocoumarin (*J. Phys. Chem. A* **2024**, *128*, 6853-6863**)**

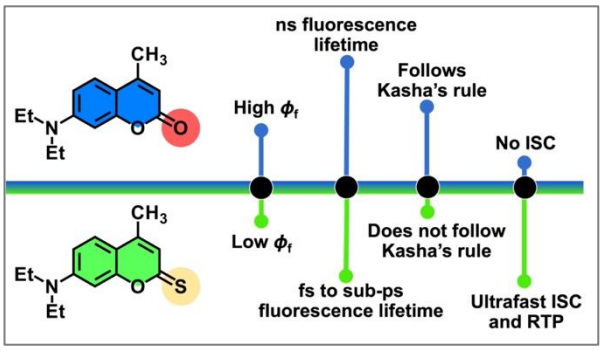

Recent literature suggests that a substitution of O-atom in carbonyl systems with a non-heavy S-atom alters the photophysical properties of the molecule, leading to quantitative triplet generation. In pursuit of an additional triplet-forming system, I selected the thio/S-atom analog of coumarin 1, namely thiocoumarin 1 (TC1), to investigate the fate of the photoexcited molecule.

The fluorescence quantum yield of TC1 is exceptionally low (~thousands of times smaller compared to the parent coumarin 1). This indicates that an efficient non-radiative process occurs from the excited singlet state. Notably, the excitation spectra are found to be red-shifted from the absorption band, suggesting that the emissive state is not coupled to the strong absorption, and a dark state exists in the molecule. Fluorescence lifetime measurements in bulk solvents (hexane, acetonitrile and dichloromethane) reveal an ultrashort singlet state lifetime ranging from 100 fs to 5 ps, in contrast to the nanosecond lifetime of the parent coumarin molecule. The fluorescence decay is mostly biexponential, likely due to the two low-lying emissive singlet states (S_1 and S_2).

To further understand the ultrafast loss of the singlet state population, transient absorption measurements were performed. These measurements confirmed that the photoexcited singlet state rapidly converts into a triplet state on a fs-ps timescale, explaining the negligible fluorescence quantum yield. Additionally, the spectral pattern also reveals that both S_1 and S_2 states are involved in generating triplet manifolds, and after several picoseconds, the higher-order triplet relaxes back to the lowest triplet state, T_1, which persists for more than 2 ns. The global analysis of the transient absorption data supports our initial hypothesis of coexisting emissive singlet states (S_1 and S_2) and population enrichment of the higher-order triplets. To

have an insight into the feasibility of singlet to triplet transitions, I conducted time-dependent density functional theory (TDDFT) calculations in acetonitrile. The results indicate that the S_1 state is dark (f=0.0054) and the S_2 state is bright (f=0.54), with both states meeting the energy and orbital criteria to transform into triplets ($S_1 \rightarrow T_1$, $S_1 \rightarrow T_3$, and $S_2 \rightarrow T_2$). This corroborates the ultrafast triplet formation behavior of the thiocoumarin molecule in bulk solvent.

As TC1 must be delivered to the target site via a water soluble carrier for its potential use in photodynamic therapy (PDT), I explored the complexation of TC1 with octa acid (OA) and studied its photophysics within the complex. TC1 and OA are found to form a 1:2 complex. Steady-state results inside the OA cavity show a strong phosphorescence emission band alongside a weak fluorescence emission band. The excitation spectra for the fluorescence emission band typically show a shift from the absorption band, while those for the phosphorescence emission band align precisely align with the main absorption. This suggests that a significant portion of the population from the S_2 state transitions to triplets. However, the S_1 state exhibits moderate fluorescence emission and triplet formation characteristics. Fluorescence lifetime and transient absorption measurements inside the cavity align with the bulk measurements, exhibiting ultrafast fluorescence decay and rapid triplet state generation involving both emissive singlet states. The comprehensive experimental and theoretical analysis elucidates the excited state behavior of this potent thio-analog of coumarin 1 molecule, characterized by efficient triplet generation.

(3) Effect of Hydrogen Bonding on the Ultrafast Intersystem Crossing in 7-Diethylaminothiocoumarin (*J. Phys. Chem. A* **2025**, In press**)**

Hydrogen bonding interaction is crucial for maintaining the structure, geometry, stability, and activity of a system, particularly in altering the excited-state dynamics of molecular systems. Such an effect on the photophysical properties of light-harvesting systems such as ketones, thioketones, and esters has been extensively reported. Following these studies, I explored on how hydrogen bonding modifies the

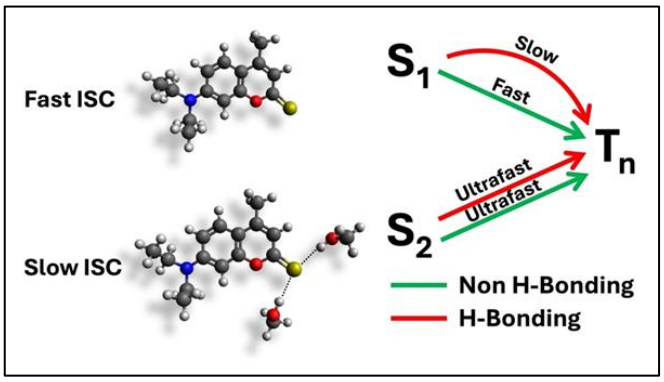

excited-state dynamics and, specifically, the intersystem crossing (ISC) process in TC1. I conducted studies using polar solvents methanol (protic) and acetonitrile (aprotic) to observe their impact on TC1's photophysical behavior. Steady-state measurements revealed that an increase in the volume fraction of methanol in acetonitrile shifts the fluorescence emission maxima toward the low-energy side, suggesting stabilization of the excited singlet state in protic methanol. This shift, along with deviations in the Lippert-Mataga plot indicates specific interactions between the solvent and the TC1 molecule. Additionally, an increase in methanol concentration correlates with higher fluorescence quantum yield and lifetime that suggests an ineffective non-radiative decay processes of the singlet excited state. Further analysis of fluorescence decay revealed an extra-long decay component of approximately 100 ps in methanol, likely attributable to a hydrogen-bonded singlet state absent in aprotic acetonitrile. Measurement of the singlet oxygen quantum yield (a measure for triplet yield) showed a decrease with increasing methanol content, indicating that hydrogen bonding restricts triplet generation. To delve deeper into triplet generation, fs-transient absorption (TA) measurements were performed in both the solvents. The global analysis of transient data showed that TC1 in methanol exhibits three emissive decay-associated spectra (~0.5 ps, 2 ps, and 66 ps), as opposed to just two in acetonitrile (~0.5 ps and 2 ps), supporting the hypothesis of a hydrogen-bonded state with emissive characteristics in methanol. Kinetic analysis of characteristics of triplet spectra demonstrated that triplet state formation from the hydrogen-bonded singlet state is slower in methanol-containing solvent and decreases further as the methanol content increases. These experimental results suggest that hydrogen bonding interactions significantly slow down the ISC process and triplet generation.

This conclusion is supported by TDDFT-based theoretical calculations, where Franck-Condon (FC) point analysis revealed that hydrogen bonding unfavorably alters energies and orbital characteristics, potentially explaining the observed slow ISC dynamics and reduced triplet yield in methanol. Building upon insights from the literature, I explored potential ISC coordinates in TC1. An examination of the twisted intramolecular charge transfer (TICT) by rotating the NEt_2 group relative to the molecular plane showed increasing singlet-triplet energy gaps, reaching a crossing point at the S_1-T_3 state, which presents an energy barrier (~0.3 eV) inaccessible at room temperature (298 K). Thus, I conclude that TC1 might not undergo triplet formation along the TICT coordinate. On the otherhand, scanning along the C=S bond stretching coordinates revealed that the S_1 and T_3 states remain energetically close, crossing in their potential well and potentially facilitating triplet formation through energy and orbital feasibilities. When explicit hydrogen bonding interactions of methanol with TC1 were considered, the transition from singlet to triplet became energetically and orbitally unfavorable, with reduced spin-orbit coupling, underscoring the significant role of hydrogen bonding along the C=S coordinate. Additionally, exploration of two other dihedral angle coordinates showed that while triplet generation is feasible in non-hydrogen-bonded solvents, hydrogen bonding interactions disfavor triplet generation along these coordinates. Overall, both experimental and theoretical findings strongly indicate that hydrogen bonding interactions play a counteractive role in triplet state generation in the thiocoumarin 1 molecule.

(4) Inhibitory Effect of Charge Transfer on Ultrafast Triplet Formation in Thiocoumarins (*Manuscript under preparation***)**

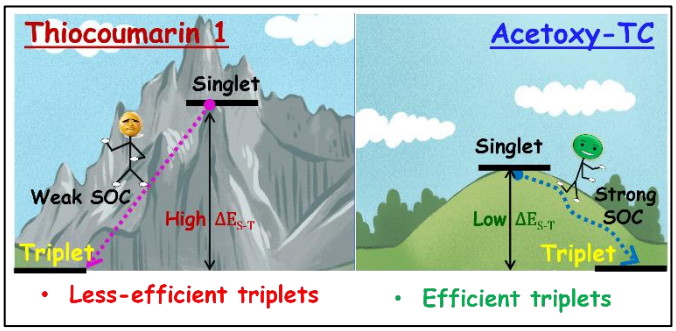

In this study, I explored the effect of charge transfer (CT) in thiocoumarin on its triplet efficiency. Behavior of CT state is notably influenced by solvent polarity, which is pivotal in determining the excited state properties of the molecule. I focus on two thio-derivatives of coumarins, differentiated by their functional groups. Of these, one has a diethyl amino group at the 7-position of the thiocoumarin structure (TC1), while the other contains an acetoxy group (Acetoxy-TC). Steady-state absorption measurements reveal that the amino-functionalized TC1 exhibits solvent polarity dependent photophysics, confirming the presence of a CT state, while in Acetoxy-TC such a dependence is not observed.

Furthermore, TC1 displays a higher fluorescence quantum yield than Acetoxy-TC across the solvents. The low fluorescence quantum yield of Acetoxy-TC, having no CT character, is corroborated by its higher singlet oxygen yield. Additionally, fluorescence lifetime measurements show that Acetoxy-TC undergoes ultrashort fluorescence decay, in contrast to the longer lifetimes found in TC1. To further probe the triplet state dynamics, femtosecond transient absorption experiments were conducted. The results revealed distinctive triplet state characteristics in Acetoxy-TC compared to TC1. The kinetic analyses indicate that while the triplet state in TC1 is generated through two singlet states including the CT state in a slower time-scale, Acetoxy-TC undergoes triplet generation via an ultrafast pathway (~200 fs). This supports the high singlet oxygen yield observed in Acetoxy-TC. These experiments in various solvent media underline the crucial yet opposing roles of intramolecular charge transfer state in the generation of triplet states in thiocoumarins.

To probe the excited state dynamics within a confined environment, I conducted photophysical studies of Acetoxy-TC encapsulated inside an octa acid (OA) cavity. Steady-state measurements revealed significantly strong phosphorescence emission

bands within the cavity, unlike those observed in bulk, suggesting minimal non-radiative decays of triplet states. Notably, the fluorescence lifetime decay of Acetoxy-TC is markedly shorter within the OA cavity compared to the TC1. Further insights were gained through transient absorption (TA) measurements performed inside the OA cavity. These experiments showed that Acetoxy-TC, which lacks a charge transfer (CT) state, forms its triplet state on an ultrafast timescale (~350 fs). In contrast, the triplet formation is relatively slow with two-time constants (~500 fs and 2-10 ps) for TC1, which features a CT state. These findings underscore that the presence of a CT state in thiocoumarins significantly influences the efficiency and kinetics of triplet state formation, acting counteractively in the process.

To elucidate the reasons behind these observations, I conducted theoretical calculations using TDDFT method. The calculations revealed that Acetoxy-TC exhibits a relatively small singlet-triplet energy gap and high spin-orbit coupling (SOC) factors, which facilitate extremely efficient intersystem crossing (ISC). Conversely, the energy gaps and SOC values in TC1, which display charge transfer (CT) characteristics, are less favorable. This difference correlates with the solvent polarity and leads to slower ISC and lower triplet yield in TC1.

This page left blank intensionally

Table of Contents

This page left blank intentionally

Chapter 1

Introduction

In this chapter, I have outlined the fundamental theories governing various photophysical processes using the Jablonski diagram, with a particular emphasis on intersystem crossing (ISC). Special focus has been given to the mechanistic aspects of ISC and the diverse factors that govern its efficiency. Throughout my thesis, I have systematically investigated the ISC dynamics of triplet-forming molecules, both in bulk solvents and within confined environments. To elucidate the triplet generation dynamics in thiocoumarin systems under spatially restricted conditions, I employed a water-soluble molecular cage, Octa Acid (OA), as the caged medium.

1.1 Light-Induced Phenomena in Molecular Systems

The interaction between light and matter is a fundamental phenomenon in light-absorbing molecules and materials. This occurs when the transition dipole moment of a molecule interacts with the electric dipole of the light wave, leading to changes in the molecule's electronic energy. These shifts can trigger a range of chemical and physical transformations within the molecule. Light-induced chemical reactions primarily proceed through bond-breaking or bond-forming pathways, resulting in the formation of new chemical species. Such light-driven reactions are classified as photochemical processes.[1–4] Alternatively, photo-excited species can dissipate energy through various electronic (radiative and non-radiative) or vibrational relaxations, collectively known as photophysical phenomena. In my thesis, I focus solely on the photophysical processes in different molecular systems under various experimental conditions.

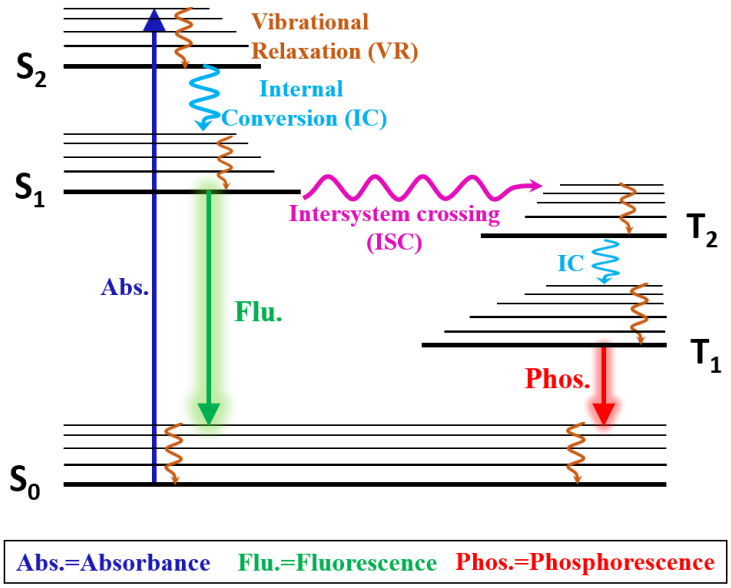

Figure 1.1.1: Jablonski diagram. Through interactions with light, ground state (S_0) molecules absorb electronic energy and become excited to higher vibrational levels of upper electronic singlet states (e.g., S_2). From these higher vibrational levels, the molecules dissipate energy and relax to the lowest vibrational level of the excited electronic state, a process known as vibrational relaxation (VR). From the lowest vibrational level of the higher electronic singlet states (S_2), the molecules undergo internal conversion (IC) to reach higher vibrational levels of the first excited singlet state (S_1). They then relax further to the lowest vibrational level of the S_1 state through the VR mechanism. Due to the large energy gap between the S_1 and S_0 states,

molecules in the lowest vibrational level of S_1 primarily release energy through a radiative process known as fluorescence. However, if molecules in the S_1 state follow an alternate pathway to triplet states (e.g., T_2), this process is called intersystem crossing (ISC). From higher electronic triplet states (e.g., T_2), they relax to the lowest vibrational level of the lowest triplet state (T_1) through both VR and IC mechanisms. From the T_1 state, the population decays to the S_0 state via either radiative or non-radiative mechanisms (IC). If the decay from T_1 to S_0 ($T_1 \rightarrow S_0$) occurs radiatively, this process is known as phosphorescence.

Light, as an electromagnetic wave, spans a broad range of frequencies responsible for inducing multiple transitions. Within the broad electromagnetic spectrum, the UV-visible region is particularly responsible for electronic transitions in molecules. The outcome of electronic excitation by light in molecular systems is often visualized through the Jablonski diagram (see Figure 1.1.1).[1–4] Upon the instantaneous absorption (10^{-14} s) of light at a specific frequency, a ground-state molecule is excited into higher vibrational levels of singlet excited states called the Franck-Condon (FC) state. These vibrationally excited molecules rapidly relax to the lowest vibrational energy level of that singlet state within an ultrafast timescale of 10^{-12} seconds, a process known as vibrational relaxation (VR). Due to small energy gaps and multiple electronic state couplings, excited molecules from higher-order singlet states (S_n) may undergo non-radiative transitions into the higher vibrational levels of the first-order singlet state (S_1). This process is referred to as internal conversion (IC). Once again, through VR, the population relaxes to the lowest vibrational levels of the S_1 state. Since the energy gap between the first singlet excited state and the ground state is relatively large, most of the excited population returns to the ground state via a radiative pathway, adhering to Kasha's law. This radiative transition between two singlet states is known as fluorescence, with typical lifetimes ranging from 10^{-12} to 10^{-9} seconds.

However, depending on the system, the singlet-state population may also take an alternative, non-radiative route into a nearby triplet state within 10^{-12} to 10^{-9} seconds. This intersystem population transfer between states with different spin characteristics is called intersystem crossing (ISC). From the lowest vibrational levels of the triplet state, the population may relax back into the ground state through

non-radiative processes, such as collisional quenching. If the population returns to the ground state via a radiative pathway, the process is termed phosphorescence. Owing to the forbidden nature of singlet-triplet transitions, phosphorescence exhibits significantly longer lifetimes, typically in the range of microseconds to milliseconds.[1–4]

1.2 Intersystem crossing (ISC): Role of Heavy-Atom Effect (HAE) and Spin-Orbit Coupling (SOC)

Intersystem crossing (ISC) is a non-radiative electronic transition between two different electronic spin states. In the diabatic representation, ISC involves transitions between pure singlet and pure triplet states (see Figure 1.2.1), where these electronic states intersect at a single point without electronic overlap. In this case, spin interconversion is strictly forbidden, and ISC can only occur through a tunnelling process. Under this condition, the electronic transitions are strongly decoupled from nuclear motion. [1,4]

However, in the adiabatic representation, singlet and triplet states are coupled via spin-orbit coupling (SOC). This coupling creates a mixed region where the Born-Oppenheimer approximation breaks down, allowing an electron to transition from the singlet to the triplet state non-adiabatically in response to small nuclear perturbations. The degree of mixing between singlet and triplet states is directly influenced by the extent of SOC between them. If the coupling is strong, significant energy splitting occurs after mixing, leading to an avoided crossing due to the repulsion between the states.[1,4]

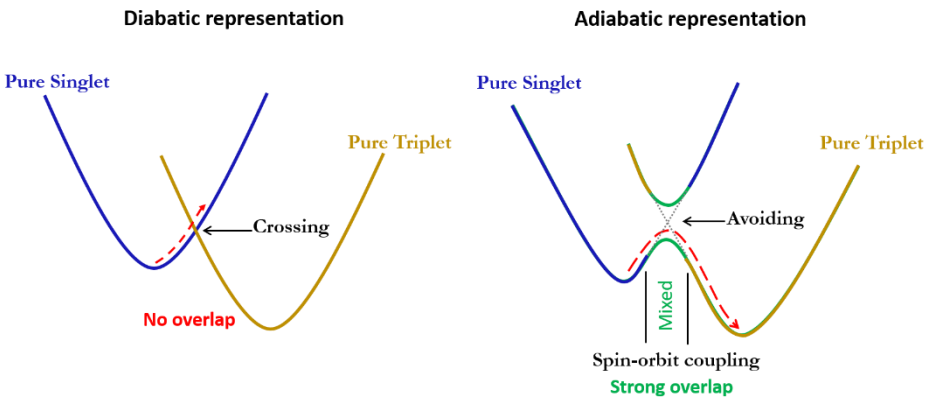

Figure 1.2.1: Diabatic and Adiabatic Representations of Singlet to Triplet Interconversion

Spin-orbit coupling (SOC) refers to the interaction between an electron's spin-angular momentum ($\vec{S}$) and its orbital angular momentum ($\vec{L}$), ensuring that the total angular momentum remains conserved.[5] It can be visualized as the interaction between the magnetic moment ($\overrightarrow{\mu_s}$) due to the spin angular momentum ($\vec{S}$) and the magnetic moment ($\overrightarrow{\mu_L}$) due to the orbital angular momentum. If the spinning electron has a gyromagnetic ratio γ, the spin magnetic moment ($\overrightarrow{\mu_s}$) can be written as

$$\overrightarrow{\mu_s} = \gamma \hbar \vec{S} \qquad (1.2.1)$$

Where,

$$\gamma = -g_e \frac{\mu_B}{\hbar} \qquad (1.2.2)$$

(μ_B is Bohr magneton, a natural unit of expressing the magnetic moment of an electron due its orbital or spin angular momentum and can be expressed as

$$\mu_B = \frac{|e|\hbar}{2m_e} \qquad (1.2.3)$$

g_e is the electronic g-factor of the electron, commonly approximated as 2. Combining equation 1.2.1 and 1.2.2,

$$\overrightarrow{\mu_s} = -g_e \mu_B \vec{S} \qquad (1.2.4)$$

When the magnetic dipole of the electron ($\overrightarrow{\mu_s}$) finds another magnetic field ($\vec{B}$), it creates a torque ($\vec{\tau}$) on the magnetic dipole which can be expressed as

$$\vec{\tau} = \overrightarrow{\mu_s} \times \vec{B} \qquad (1.2.5)$$

Using the expression of $\overrightarrow{\mu_s}$, the torque can be written as

$$\vec{\tau} = -g_e \mu_B \, \vec{S} \times \vec{B} \tag{1.2.6}$$

$$= -\frac{g_e \mu_B \, \vec{B}}{\hbar} \times \hbar \vec{S} \tag{1.2.7}$$

$$= -\overrightarrow{\omega_L} \times \hbar \vec{S} \tag{1.2.8}$$

Where, $\frac{g_e \mu_B \, \vec{B}}{\hbar}$ is the frequency vector and written as $\overrightarrow{\omega_L}$.

As the change in angular momentum is the torque,

$$\vec{\tau} = \frac{d(\hbar \vec{S})}{dt} \tag{1.2.9}$$

We can write

$$\frac{d(\vec{S})}{dt} = \overrightarrow{\omega_L} \times \vec{S} \tag{1.2.10}$$

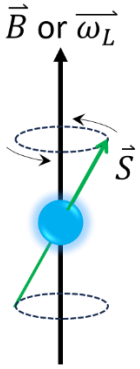

Figure 1.2.2: Larmor precession of an electron due to the torque exerted by a magnetic field $\vec{B}$ in it having spin angular momentum $\vec{S}$ and precession frequency $\overrightarrow{\omega_L}$

Due to this torque, the spin angular momentum of the electron ($\vec{S}$) start to be precise around the magnetic field vector $(\vec{B})$ with an angular frequency ($\overrightarrow{\omega_L}$). This is called the Larmor precision (see Figure 1.2.2), and the corresponding frequency is known as the Larmor frequency.

However, in the atomic/molecular system, no external magnetic field is present rather magnetic field is provided by the nucleus. For such a system during the calculation of interaction energy of the electron-magnetic field, we must consider the magnetic field at the site of the electron due to the nucleus. According to Bio-Savart law when a charged (say electron around the nucleus) particle moves around a point it creates a magnetic field at the nucleus.[6] In different frames, the atomic

system can also be visualized as an electron is stationary and the nucleus is rotating around the stationary electron. In such case, an electron with charge e and a nucleus with charge Ze, are present at the distance r, and the magnetic field generated by the nucleus at the electron site is

$$B' = \frac{\mu_0}{4\pi}\frac{|Ze|\,\vec{v}\times\hat{r}}{r^2} \quad (1.2.11)$$

Where,

μ_0 is the permeability of free space,

Ze is the charge of the nucleus, (Z=atomic number)

v is the velocity of the electron,

r is the distance between the electron and the nucleus,

$\hat{r}$ is the unit vector along the electron-nucleus line ($\hat{r} = \frac{\vec{r}}{r}$).

Therefore, the spin-orbit interaction energy Hamiltonian $\left(\widehat{\mathcal{H}}_{SO}\right)$ is associated with the interaction of the electron's magnetic moment with the magnetic field created by its orbital motion (B') can be expressed as

$$\widehat{\mathcal{H}}_{SO} = -\overrightarrow{\mu_e}.\overrightarrow{B'} = \vec{\omega}_L.\hbar\vec{S} \quad (1.2.12)$$

However, this expression does not consider the relativistic precision effect of the electron acceleration and its rotation of the nucleus, called Thomas precession. Therefore, the corrected interacting Hamiltonian can be written as

$$\widehat{\mathcal{H}}_{SO} = (\vec{\omega}_L + \vec{\omega}_T).\hbar\vec{S} \quad (1.2.13)$$

Where, $\vec{\omega}_T$ is the Thomas precession vector and equal to $-\frac{1}{2}\vec{\omega}_L$ and therefore equation 1.2.13 can be modified as

$$\widehat{\mathcal{H}}_{SO} = \frac{1}{2}\vec{\omega}_L.\hbar\vec{S} \quad (1.2.14)$$

This Thomas factor $\left(\frac{1}{2}\right)$ adjusts the strength of the spin-orbit coupling due to the precession of the electron's spin in its rest frame. Therefore, by using the expression of $\overrightarrow{\mu_e}$ the corrected spin-orbit Hamiltonian can be written as

$$\widehat{\mathcal{H}}_{SO} = \frac{-(-g_e\mu_B\,\vec{S}).\overrightarrow{B'}}{2} \quad (1.2.15)$$

$$= \frac{g_e \mu_B \vec{S}.\overrightarrow{B'}}{2} \quad (1.2.16)$$

Incorporating the expression of μ_B from equation 1.2.3 and

$$= \frac{g_e \vec{S}}{2}\left(\frac{|e|\hbar}{2m_e}\right)\left(\frac{\mu_0}{4\pi}\right)\frac{|Ze|\,\vec{v}\times\vec{r}}{r^3} \quad (1.2.17)$$

By replacing, $\mu_0\varepsilon_0 = \frac{1}{c^2}$ (Where, ε_0 is the permittivity of the vacuum)

$$= \frac{g_e\vec{S}}{2}\left(\frac{|e|\hbar}{2m_e\varepsilon_0 c^2}\right)\left(\frac{1}{4\pi}\right)\frac{|Ze^2|\,\vec{v}\times\vec{r}}{r^3} \quad (1.2.18)$$

Multiplying m_e in both numerator and denominator

$$= \frac{g_e \vec{S}}{2}\left(\frac{|e|\hbar}{2{m_e}^2\varepsilon_0 c^2}\right)\left(\frac{1}{4\pi}\right)\frac{|Ze|\,m_e\vec{v}\times\vec{r}}{r^3} \quad (1.2.19)$$

By replacing the orbital angular momentum vector $m_e\vec{v}\times\vec{r}$ as $\hbar\vec{L}$ the equation 1.2.19 can be further written as

$$\widehat{\mathcal{H}}_{SO} = \frac{g_e\vec{S}}{2}\left(\frac{|e|\hbar}{2{m_e}^2\varepsilon_0 c^2}\right)\left(\frac{1}{4\pi}\right)\frac{|Ze^2|\,\hbar\vec{L}}{r^3} \quad (1.2.20)$$

$$= \frac{g_e \vec{S}}{2}\left(\frac{Z|e^2|\hbar^2}{2{m_e}^2\varepsilon_0 c^2}\right)\left(\frac{1}{4\pi}\right)\frac{\vec{L}}{r^3} \quad (1.2.21)$$

$$= \frac{g_e}{2}\left(\frac{Z|e^2|\hbar^2}{8\pi{m_e}^2\varepsilon_0 c^2}\right)\frac{\vec{L}.\vec{S}}{r^3} \quad (1.2.22)$$

$$= AZ\,\frac{\vec{L}.\vec{S}}{r^3}; \quad (1.2.23)$$

Where $A = \frac{g_e}{2}\left(\frac{Z|e^2|\hbar^2}{8\pi{m_e}^2\varepsilon_0 c^2}\right)$

This is the final expression spin -orbit coupling Hamiltonian and the expectation value of this Hamiltonian can be written as

$$\langle\widehat{\mathcal{H}}_{SO}\rangle = \langle\frac{AZ}{r^3}\rangle\,\langle\vec{L}.\vec{S}\rangle \quad (1.2.24)$$

In the equation 1.2.24, the first term is the spin-orbit coupling factor, ζ_{SO}. Therefore,

$$\langle\widehat{\mathcal{H}}_{SO}\rangle = \zeta_{SO}\langle\vec{L}.\vec{S}\rangle \quad (1.2.25)$$

Determination of $\langle\vec{L}.\vec{S}\rangle$ is quite straight forward.

$$\vec{J}^2 = \left(\vec{L}+\vec{S}\right).\left(\vec{L}+\vec{S}\right) = \vec{L}^2 + \vec{S}^2 + 2\vec{L}.\vec{S} \quad (1.2.26)$$

Rearrangement gives

$$\vec{L}.\vec{S} = \frac{1}{2}\left[\vec{J}^2 - \vec{L}^2 - \vec{S}^2\right] \quad (1.2.27)$$

Hence,

$$\langle\vec{L}.\vec{S}\rangle = \frac{1}{2}\left[\langle\vec{J}^2\rangle - \langle\vec{L}^2\rangle - \langle\vec{S}^2\rangle\right] = \frac{1}{2}[j(j+1) - l(l+1) - s(s+1)] \quad (1.2.28)$$

To determine its value, we need to integrate the expression of ζ_{SO}

$$\zeta_{SO} = \langle\frac{AZ}{r^3}\rangle = \left\langle R(r)_{n,l}\middle|\frac{AZ}{r^3}\middle|R(r)_{n,l}\right\rangle \quad (1.2.29)$$

$$\Rightarrow \zeta_{SO} = \int_0^\infty {R(r)_{n,l}}^2 \frac{AZ}{r^3} r^2 dr = AZ\int_0^\infty {R(r)_{n,l}}^2 r^{-3+2} dr \quad (1.2.30)$$

The solution to the above integration can be done by using the Gamma function below.

$$\int_0^\infty r^{k+2}{R(r)_{n,l}}^2 dr = {a_0}^k Z^{-k} P_k(n,l) \quad (1.2.31)$$

In the case of, $k = -3$. Therefore,

$$\zeta_{SO} = AZ{a_0}^{-3} Z^3 P_{-3}(n,l) = \frac{A}{{a_0}^3}\frac{Z^4}{n^3(l+1)(l+{}^1/_2)l} \quad (1.2.32)$$

And

$$\langle\widehat{H}_{SO}\rangle = \frac{A}{2{a_0}^3}\frac{Z^4}{n^3(l+1)(l+{}^1/_2)l}[j(j+1) - l(l+1) - s(s+1)] \quad (1.2.33)$$

Therefore, if we estimate $\langle\widehat{H}_{SO}\rangle$ for H-atom for $n = 2$ and $l = 1$, we will get value in the order of $10^{-5}eV$ which is insignificant due to the very weak spin-orbit coupling interaction. However, as $\zeta_{SO} \propto Z^4$, dictates that for heavy-atom containing molecule, the strength of spin-orbit coupling is extremely high. Therefore, the introduction of heavy atoms externally or internally to a system has been a well-known technique to increase spin-orbit coupling and facilitate ISC. This phenomenon is referred to as the heavy atom effect (HAE). [7–23]

If we estimate $\langle\widehat{H}_{SO}\rangle$ for the hydrogen atom with $n = 2$ and $l = 1$, the resulting value is on the order of $10^{-5}eV$, which is negligible due to the very weak spin-orbit coupling interaction. However, since $\zeta_{SO} \propto Z^4$, the spin-orbit coupling strength

increases dramatically for molecules containing heavy atoms. Thus, introducing heavy atoms, either externally or internally into a system, is a well-known method to enhance spin-orbit coupling and facilitate intersystem crossing (ISC).

1.2.1 Spin-Interconversion Mechanism in Singlet-Triplet non-Radiative ISC Transition

Introducing heavy atoms enhances spin-orbit coupling (SOC), thereby increasing the likelihood of spin interconversion. This interconversion can occur via two pathways: (1) Spin-flipping and (2) Spin-rephrasing (see Figure 1.2.3). In the spin-flip mechanism, the electron undergoes a direct flip of its spin while transitioning between electronic states of different spin multiplicities (e.g., from a singlet to a triplet state or vice versa), with minimal change in orbital angular momentum. This mechanism requires strong SOC to facilitate the spin change. In contrast, the spin-rephrasing mechanism involves changes in both orbital and spin angular momenta. The electron not only flips its spin but also shifts its orbital configuration (e.g., moving from a π-orbital to an n-orbital), making this pathway consistent with El-Sayed's rule for intersystem crossing (ISC).

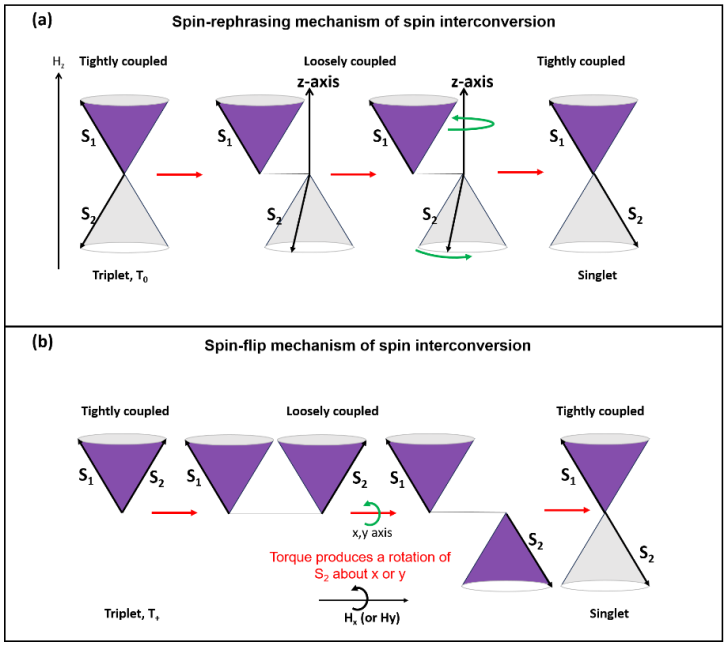

Figure 1.2.3: Spin Interconversion Mechanism of Singlet and Triplet States

1.2.2 Selection Rule of Intersystem Crossing (ISC)

As discussed in Section 1.2.1, intersystem crossing (ISC) can occur via either a "spin-flip" or "spin-rephrasing" mechanism. In any horizontal transition between electronic states, both energy and momentum are conserved, which also applies to non-radiative ISC from a singlet to triplet state. However, ISC involves a change in spin-angular momentum. To conserve total angular momentum, this change must be compensated by another form of angular momentum. In a two-electron spin system, ISC possibilities for a molecule involving p-orbitals can be visualized as follows: During a spin-flip, if the electron remains in the same orbital ($P_y \rightarrow P_y$), there is no change in orbital angular momentum, preventing a spin transition (see Figure 1.2.4). Conversely, if the electron jumps from a $P_y \rightarrow P_x$ orbital, the system's orbital angular momentum changes by one unit, corresponding to a 90° rotation about the z-axis. This change in orbital angular momentum leads to a corresponding change in spin-angular momentum, thus conserving the total angular momentum of the system. For effective changes in orbital angular momentum, the interconverting orbitals (P_y and P_x) must be degenerate. Spin-orbit coupling (SOC) facilitates mixing between spin states and generates orbital angular momentum due to the $P_y \rightarrow P_x$ transition, leading to a spin-flip.

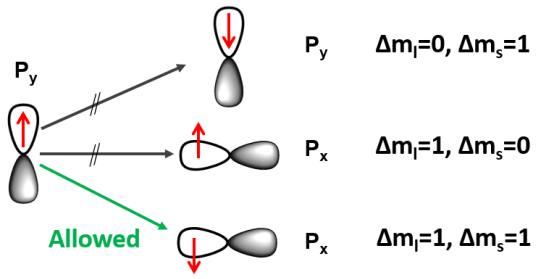

Figure 1.2.4: Conservation of Angular Momentum of an ISC Transition Involving p-orbitals

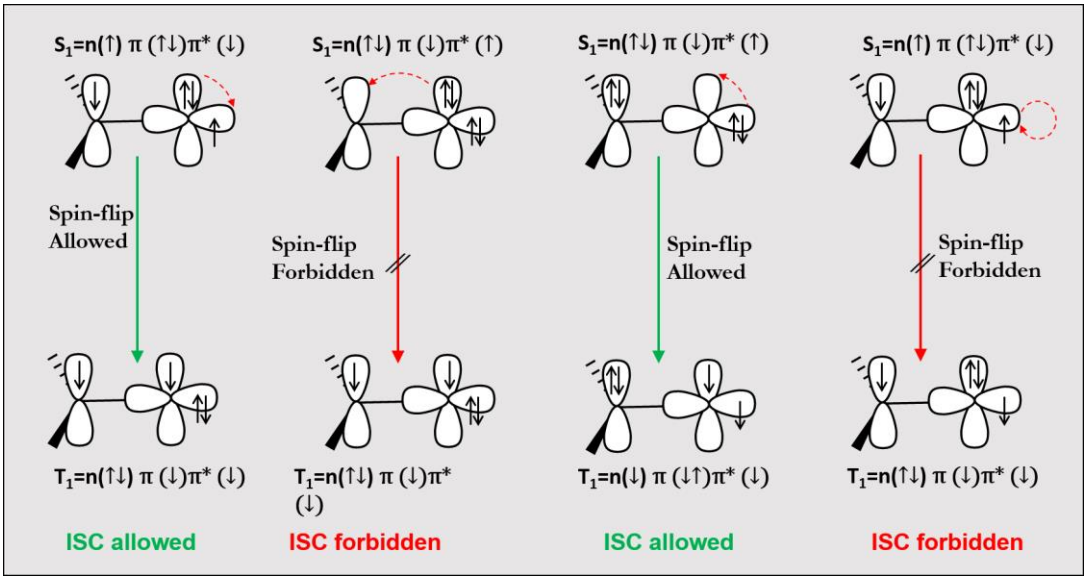

Figure 1.2.5: Possible Singlet to Triplet ISC Transition in Carbonyl Compounds

Carbonyl systems serve as an excellent example for understanding SOC. In these systems, the singlet state can arise from an nπ* or ππ* configuration, and four possible electronic transitions are illustrated in Figure 1.2.5. For S_1 (nπ*) to T_1 (nπ*) or S_1 (ππ*) to T_1 (ππ*) transitions, the orbitals remain unchanged during spin transition, resulting in no change in orbital angular momentum. Consequently, spin-flip cannot be compensated by orbital angular momentum, rendering these transitions forbidden. However, in the case of ISC from S_1 (ππ*) to T_1 (nπ*) or S_1 (nπ*) to T_1 (ππ*), orbital configurations change, leading to a shift in orbital angular momentum, which compensates for the spin-angular momentum and allows the spin-flip to occur. Therefore, these transitions (nπ* → ππ* or ππ* → nπ*) are allowed, leading to the deduction of the selection rule (El-Sayed's rule) for the $S_1 \rightarrow T_1$ transition (see Figure 1.2.6).

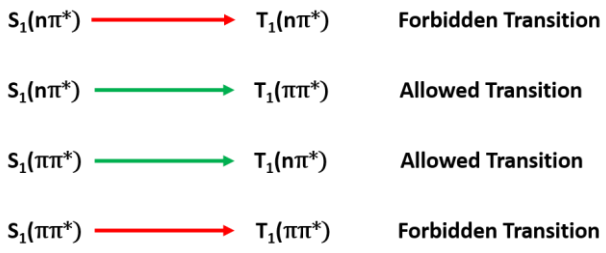

Figure 1.2.6: El-Sayed Selection Rule ISC Process in Carbonyl Compounds

1.2.3 Vibronically Assisted ISC

As discussed in the previous section, the potential of heavy atoms to significantly alter the SOC is well established. In an ultrafast time scale, the non-radiative transition breaks the universal Born-Oppenheimer (BO) approximation and is thus governed by the matrix elements acting between the same multiplicity i.e. Internal conversion (IC). The same can also be applied to electronic states of different spin-multiplicities. In this regime, states are not coupled only through the SOC but are mixed non-adiabatic and spin-orbit coupling. Therefore, according to the Pauli's approximation, the electronic Hamiltonian can be written as

$$\hat{\mathcal{H}}_{el} = \hat{\mathcal{H}}_{es} + \hat{\mathcal{H}}_{so} \tag{1.2.34}$$

Where, $\hat{\mathcal{H}}_{es}$ is the electrostatic Hamiltonian and diagonal elements represent the energies of the spin-free states and $\hat{\mathcal{H}}_{so}$ is the spin-orbit coupling Hamiltonian.

Thus, the addition of $\hat{\mathcal{H}}_{so}$ make the electronic Hamiltonian ($\hat{\mathcal{H}}_{so}$) is a non-pure Hamiltonian i.e. mixture of singlet and triplet states. This electronic Hamiltonian (a combination of both $\hat{\mathcal{H}}_{el}$ and $\hat{\mathcal{H}}_{so}$) only considers a certain reference geometry of the nuclear coordinate. However, in reality, these individual Hamiltonians can also depend on the nuclear geometry i.e. Q. Thus, the electronic Hamiltonian ($\hat{\mathcal{H}}_{el}$) can be further written as

$$\hat{\mathcal{H}}_{el} = \hat{\mathcal{H}}_{es}(Q_o) + \hat{\mathcal{H}}_{so}(Q_o) + \sum_{\alpha} \left[\frac{\partial \hat{\mathcal{H}}_{es}}{\partial Q_\alpha} + \frac{\partial \hat{\mathcal{H}}_{so}}{\partial Q_\alpha}\right]\Big|_{Q_o} \tag{1.2.35}$$

Q_o is the reference geometry (FC geometry)

It is evident from equation 1.2.35 that coupling elements depend on the vibrational degrees of freedom α of specific molecular vibrations and allow the mixing among equilibrium configurations of close-lying states with different spin-multiplicities.

Therefore, the total contribution from the spin-orbit coupling can be written as,

$$\hat{\mathcal{H}}_{so} = \hat{\mathcal{H}}_{so}(Q_o) + \sum_\alpha \frac{\partial \hat{\mathcal{H}}_{so}}{\partial Q_\alpha} Q_\alpha \quad (1.2.36)$$

The first part of the Hamiltonian is only contributed by the direct spin-orbit coupling of the electronic states and the second part of the equation is contributed by the vibrational spin-orbit coupling along a particular coordinate Q. Considering the higher-order (mainly second order) dependence, the above equation 1.2.36 can further be modified as

$$\hat{\mathcal{H}}_{so} = \hat{\mathcal{H}}_{so}(Q_o) + \sum_\alpha \frac{\partial \hat{\mathcal{H}}_{so}}{\partial Q_\alpha} Q_\alpha + \frac{1}{2}\sum_\alpha \sum_\beta \frac{\partial^2 \hat{\mathcal{H}}_{so}}{\partial Q_\alpha \partial Q_\beta} Q_\alpha Q_\beta \quad (1.2.37)$$

Considering the transition from the S_1 state to the T_1 state

$$\hat{\mathcal{H}}_{so} = \langle \psi_{S_1} | \hat{\mathcal{H}}_{so} | \psi_{T_1} \rangle + \sum_\alpha \frac{\partial \langle \psi_{S_1} | \hat{\mathcal{H}}_{so} | \psi_{T_1} \rangle}{\partial Q_\alpha} Q_\alpha + \frac{1}{2}\sum_\alpha \sum_\beta \frac{\partial^2 \langle \psi_{S_1} | \hat{\mathcal{H}}_{so} | \psi_{T_1} \rangle}{\partial Q_\alpha \partial Q_\beta} Q_\alpha Q_\beta \quad (1.2.38)$$

However, according to Albrecht,[24] there are two other spin-vibronic processes of ISC and incorporating those possibilities, the final expression of $\hat{\mathcal{H}}_{so}$ can be modified as

$$\hat{\mathcal{H}}_{so} = \langle \psi_{S_1} | \hat{\mathcal{H}}_{so} | \psi_{T_1} \rangle + \sum_\alpha \frac{\partial \langle \psi_{S_1} | \hat{\mathcal{H}}_{so} | \psi_{T_1} \rangle}{\partial Q_\alpha} Q_\alpha + \frac{1}{2}\sum_\alpha \sum_\beta \frac{\partial^2 \langle \psi_{S_1} | \hat{\mathcal{H}}_{so} | \psi_{T_1} \rangle}{\partial Q_\alpha \partial Q_\beta} Q_\alpha Q_\beta + \sum_n \frac{\langle \psi_{S_1} | \hat{\mathcal{H}}_{so} | \psi_{T_n} \rangle \langle \psi_{T_n} | \hat{\mathcal{T}}_N | \psi_{T_1} \rangle}{E_{T_2} - E_{S_1}} + \sum_m \frac{\langle \psi_{S_m} | \hat{\mathcal{H}}_{so} | \psi_{T_1} \rangle \langle \psi_{S_1} | \hat{\mathcal{T}}_N | \psi_{S_m} \rangle}{E_{S_2} - E_{T_1}} \quad (1.2.39)$$

where ψ represents the molecular wave function for a particular state, $\hat{\mathcal{T}}_N$ represents the vibronic mixing and $\hat{\mathcal{T}}_N = \sum_\alpha \frac{\partial \hat{\mathcal{H}}_{es}}{\partial Q_\alpha}\Big|_0 Q_\alpha$. The third part of the above expression is the coupling between the spin-vibronic operator with the vibronic coupling factor in the triplet manifolds and the last part is the coupling between the spin-vibronic operator with the vibronic coupling factor in the singlet manifolds.

The efficiency of intersystem crossing (ISC) is highly influenced by the energy gap between states, spin-orbit coupling (SOC), and non-adiabatic coupling between states of different spin multiplicities. Direct SOC, often associated with heavy atom

substitution, and El-Sayed's rule are commonly used to assess ISC rates in rigid molecules with strongly localized electronic states. However, in molecules with greater structural flexibility, deviations from these standard rules are observed. These deviations stem from the potential mixing of energy states, driven by vibrational modes within the molecules. Several studies on benzene, naphthalene, pyrene-based compounds have already investigated the role of vibrational motions in enhancing ISC efficiency.[25–31] Beyond conjugated aromatic molecules, research has also focused on how metal-metal vibrations facilitate ISC. In xanthone derivative, spin mixing of ISC occurs along the C═O elongation coordinate. Additionally, our work on the carbonyl-based compound benzanthrone revealed that both in-plane C=O vibrations and out-of-plane molecular vibrations impact the ISC process.[32] Therefore, accounting for vibrational contributions in ISC is essential. Our recent studies demonstrated that C-X bond vibrations significantly influence ISC in halo-coumarins.[33]

1.2.4 Effects of Surrounding Rigidity and Micellar Confinement in ISC Dynamics

The relaxation dynamics of the photoexcited state in a molecule are significantly influenced by the polarity and viscosity of the surrounding environment.[32,34–46] For positively solvatochromic dyes, the extent of solvation is strongly dependent on the solvent's polarity. Beyond polarity, factors such as viscosity and the confinement of the medium can also profoundly impact the photophysical behavior of the excited state. In molecular rotor systems, non-radiative transitions are particularly sensitive to the confinement and viscosity of the medium.[34,42,44,45] Notably, the polarity and environments, leading to altered excited state dynamics within the structurally rigid space. Numerous studies have shown that photophysical properties like solute translation, rotation, solvation, and other behaviors can vary significantly in confined systems.[41,47–51] Micelle and reverse micelle systems are especially popular

due to their ease of synthesis and high-water solubility. Reverse micelles, such as those formed with sodium bis(2-ethylhexyl) sulfosuccinate (AOT), serve as excellent models for studying nanoconfined aqueous environments.[52–56] AOT reverse micelles, with their narrow size distribution dictated by the water loading ratio, offer a tuneable core size and microenvironmental rigidity, both of which impact the photophysical properties of molecules within the micelle.[57–59] Specifically, the confinement can have a significant impact on intersystem crossing (ISC) and phosphorescence behavior due to increased structural rigidity, which may slow down the motion of the vibrational modes of singlet excited states responsible for the ISC process.[60–62]

1.2.5 Transition Metal Complexes and ISC

In light-harvesting complexes (LHC), intersystem crossing (ISC) plays a crucial role in transitioning energy from the singlet to the triplet state, which is key for energy conversion and transfer processes. Numerous reports from the past depicts how metal complexes contributed into the field of generating triplet over the years (see Table 1).

Table 1. Important Metal complexes having ultrafast triplet characteristics

Complex Type	Type of ISC transition	ISC Time	Year[references]
$[Fe(bpy)_3]^{2+}$	^{1}MLLCT→^{3}MLLCT	≤30 fs	2007[63]
$Cr(acac)^3$	$^4T_2$→^2E	<100 fs	2006[64]
$[Fe(bpy)_3]^{2+}$	^{3}MLCT→^{5}T	~130 fs	2009[65]
$[Fe(tren(py)_3]^{2+}$	^{1}MLCT→^{5}T	~190 fs	2008[66]
$[Fe(phen)_3]^{2+}$	^{3}MLCT→^{5}T	~220 fs	2011[67]

$[Fe(PMH)_3]^{2+}$ $[Fe_2(PMH)_3]^{4+}$ $[FeZn(PMK)_3]^{4+}$	$^1MLCT \rightarrow {}^5T$	<80 fs	2008[68]
Fe-porphyrins	Ligated to unligated myoglobin	~150 fs	2004[69]
$[Ru(bpy)_3]^{2+}$	$^1MLLCT \rightarrow {}^3MLLCT$	≤30 fs	2006[70]
$Fe^{II}(bpy)_3]^{2+}$	$^1MLLCT \rightarrow {}^3MLLCT$	≤ 150fs	2018[71]
ZnTPP	$S_1 \rightarrow T_1$	4-160 ps	2011[72]
$[Cu(dmphen)_2]^{+}$		7.4 ps	2011[73]
$[Re(L)(CO)_3(bpy)]^{1+}$ L=Cl L=Br L=I L=etpy	$^1MLLCT \rightarrow {}^3MLLCT$	85 fs 130 fs 150 fs 130 fs	2008[74]
Pt acetylide complexes	S_1-T_1	70 fs to 2.1 ps	2009[75]
$[Fe(bmip)_2]^{2+}$	$^1MLCT \rightarrow {}^3MC$ $^1MLCT \rightarrow$ $^3MLCT \rightarrow {}^3MC$	100 fs 9.0 ps	2021[76]
$Pt^{IV}Br_6^{2-}$	$^1T_{1g} \rightarrow {}^3T_{1g}$	140 fs	2020[77]
$ReCl(CO)_3(bpy)$	$S_1 \rightarrow T_1$ $S_2 \rightarrow T_2$	800-1000 fs	2022[78]
$[Re(CO)_3(im)(phen)]^{+}$	$^1MLCT \rightarrow {}^3MLCT$	8 fs and 420 fs	2019[79]
$Mo_2(O_2C$-9-anthracene$)_4$	$^1MLCT \rightarrow {}^3MLCT$	~10 ps	2006[80]
Pt_2POP	$^1A_{2u} \rightarrow {}^3A_{2u}$	10-30 ps	2011[81]
carbene metal-amide studied herein. M = Cu (Cu-Cz), Ag (Ag-Cz), Au (Au-Cz).	$^1CT \rightarrow {}^3CT$	30-1700 ps	2020[82]

$[Cu(dmp)_2](PF_6)$	S_1-T_1	9-20 ps	2015[83]
Nitronaphthalene derivatives	$S_1 \rightarrow T_n$	~1 ps	2019[84]
$[M(imidazole)(CO)_3(phenanthroline)]^+$ (M = Mn, Re)	$S_2 \rightarrow T_n$	10-50 fs	2018[85]
$Pt(Br)_6$	$^1T_{1g} \rightarrow {}^3T_{1g}$	<150 fs	2011[86]
dinuclear Pt(II) complexes	^{1}MMLCT$\rightarrow{}^3$MMLCT	<1 ps	2023[87]
platinum(II) dimer complexes	^{1}MMLCT$\rightarrow{}^3$MMLCT	<1 ps	2021[88]

Among various metal complexes, copper-based complexes—particularly those with phenanthroline ligands such as Cu(x-phen)$_2$ are especially useful and easy to synthesize.[89–92] This enables rapid ISC from the singlet to triplet states, producing long-lived triplet states essential for energy transfer. The combination of the heavy-atom effect from the copper and the planar structure of the phen ligands contributes to efficient ISC, making the complex ideal for applications like solar energy harvesting and photocatalysis.[93,94] complexes, the transition from the singlet to triplet state occurs through structural flattening of the initially excited singlet state, followed by activation along the metal-ligand vibrational coordinates.[95] To investigate how surrounding rigidity or confinement affects the intersystem crossing (ISC) behavior in such complexes, I specifically selected the $[Cu(dmphen)_2]Cl$ molecule, where "dmphen" denotes 2,9-dimethyl-1,10-phenanthroline. In addition to micelles, γ-cyclodextrin is often considered for studying excited-state dynamics; however, due to its open cavity structure, it cannot fully isolate the guest molecule from the bulk medium. Therefore, I explored the excited-state ISC dynamics of this complex both in a bulk viscous glycerol–methanol mixture and within AOT reverse micelles of varying water pool sizes. These findings are discussed in detail in

Chapter 3 of my thesis. This experimental setup enables a comparative study of ISC behavior in different environments, offering insights into how molecular confinement and medium viscosity influence the excited-state dynamics of copper-based complexes.

1.2.6 ISC Affinity of thio-Carbonyl Compounds

Thiocarbonyl compounds, where sulfur replaces oxygen atoms (as in thioamides or thioketones), exhibit efficient intersystem crossing (ISC) due to sulfur's heavy-atom effect, which enhances spin-orbit coupling.[96,97] Upon photoexcitation, thiocarbonyl compounds typically transition to the singlet excited state (S_1). However, due to efficient ISC, the population rapidly shifts to the triplet excited state (T_1), which plays a crucial role in their photophysical and photochemical behavior.[98–102] Triplet states in thiocarbonyl compounds tend to be more reactive than singlet states, leading to different chemical pathways, such as phosphorescence or reactions with other molecules, as seen in photocatalysis.[101,103–105]

Examples:

a) **Thioamides**: These sulfur analogs of amides, where sulfur replaces carbonyl oxygen, are often used in photoinduced biological studies due to the reactivity of sulfur's triplet states.[106]

b) **Thioketones**: Thioketones, such as thioacetone, undergo efficient ISC, leading to phosphorescence as they transition from singlet to triplet states. Their ability to form triplet states makes them valuable in applications like molecular materials.[99,107–110]

c) **Thiourea**: Thiourea and its derivatives (e.g., N, N'-Dimethylthiourea) play a critical role in ISC due to sulfur’s strong spin-orbit coupling. In photocatalysis and photodynamic therapy (PDT), these compounds are useful for generating

reactive triplet states and singlet oxygen ($^1O_2$), vital for selective chemical reactions and as therapeutic agents in cancer treatment.[99,111–115]

d) **Thionated Dyes**: Dyes like thioxanthone show improved ISC efficiency when oxygen is substituted with sulfur, making them crucial in photochemical applications, such as UV-curable coatings and polymerization photoinitiators.[99,115]

e) **Thionated Metal Complexes**: Thionated ligands enhance ISC in metal complexes, such as Ruthenium(II)–thioether, improving their utility in light-harvesting and photocatalytic applications. These complexes are instrumental in dye-sensitized solar cells, where ISC enhances energy transfer from singlet to triplet states, used for therapeutic application.[116]

f) **Organic Electronics**: Thionated compounds, such as thionated BODIPY (boron-dipyrromethene) dyes, are key in organic electronics. Their high ISC rates improve device performance in OLEDs and organic photovoltaic cells (OPVs) by enabling efficient charge separation and energy transfer.[117]

Studying intersystem crossing (ISC) in thionated compounds is crucial for optimizing their photophysical and photochemical properties, with implications spanning applications from energy conversion to medical therapies. Owing to the growing interest in thionated compounds—attributed to their unique photophysical behavior compared to their canonical oxygen-containing analogues—I investigated the excited-state dynamics of the thionated derivative of the fluorescent dye Coumarin 1, namely thiocoumarin 1, in bulk solvents. These findings are presented in **Chapter 4** of my thesis.

1.2.7 Photoexcited ISC Dynamics Inside Caged Octa acid Capsule

Octa acid (OA) is an organic cavitand, first synthesized by Gibb in 2004,[118,119] characterized by a bucket-like shape with two distinct openings. The larger opening

measures 11.4 Å in diameter, while the smaller one is 5.5 Å. The cavitand's outer height is 13.7 Å, with an inner cavity that has a depth of about 6 Å and a diameter of 9.1 Å at its widest point. Importantly, these inner walls of the cavity are non-polar, while eight carboxylic acid groups extend from the outer surface, giving the molecule its name "Octa acid." OA is soluble in aqueous buffers at pH 7.4 due to its carboxylic acid groups. It forms host-guest complexes with organic molecules, typically in a 1:1, 1:2, or 2:2 ratio, depending on the guest's size, shape, and concentration. For instance, naphthalene and anthracene can form both 1:2 and 2:2 complexes, while larger molecules like tetracene or pyrene can only form 1:2 complexes due to their size.

One of OA's key features is that it absorbs UV light below 300 nm, making it ideal for studying encapsulated molecules that absorb in the visible spectrum without interference. OA's host-guest complexes also have dynamic properties; studies by Jayraj *et al*. show that the capsular structure formed by two OA molecules can partially open and close on a microsecond timescale.[119,120] However, during the nanosecond-scale excited state lifetime of a guest molecule, the capsule typically remains closed, enabling the investigation of photophysical processes within the OA cavity. Additionally, the encapsulation process can clarify turbid solutions of hydrophobic molecules in water, and the stoichiometry of the resulting complexes is usually confirmed through 1H-NMR titration.

Earlier literature on the coumarin kinds of molecule has depicted that the photophysical properties inside the OA cavity quite different from the bulk solvent media due to its non-polar hydrophobic core and complete bulk separation. Along with the photophysical properties, Das *et al*. depicted the possibility of anthracene excimer formation and its dynamics inside this OA cavity.[121] Studies on the ISC dynamics of halo-coumarins confined within cavities have revealed the active involvement of C–X vibrational modes in facilitating the intersystem crossing process.[33] It is well established that triplet-state systems are highly beneficial for photodynamic therapy (PDT) applications. However, to effectively utilize these

molecular systems, it is essential to deliver them to the reactive site using an appropriate carrier. Octa acid (OA), due to its high solubility and ability to provide a non-polar capsular environment, serves as an excellent carrier by protecting the triplet state from direct interaction with water. Therefore, I investigated the excited-state dynamics of thiocoumarin 1 within the confined OA cavity. The findings of this study, which reveal significant alterations in ISC efficiency and other excited-state behaviors under confinement, are discussed in detail alongside the corresponding bulk solvent measurements in **Chapter 4** of my thesis.

1.2.8 Role of Hydrogen Bonding in ISC: A Brief Overview

Hydrogen bonding can modulate electronic states and energy levels, affecting both radiative and non-radiative photophysical processes.[32,108,122–127] This modification of electronic structure changes the relative energies of singlet and triplet states, which can either enhance or reduce the ISC rate depending on the energy gaps and Franck-Condon factors. Since ISC is facilitated by spin-orbit coupling, hydrogen bonding may sometimes increase spin-orbit coupling by altering the local electronic environment, potentially promoting ISC.[128] It some system, hydrogen bonding alters the electron density distribution, affecting singlet-triplet mixing and ISC efficiency, particularly in systems where ISC is driven by charge-transfer character.[129] Recent reports also demonstrated that hydrogen bonding can influence vibrational modes coupled to electronic transitions, thereby impacting non-radiative processes such as intersystem crossing (ISC).[124,130] These changes in vibrational modes may either increase or decrease ISC efficiency. Overall, current understanding suggests that hydrogen bonding can either promote or inhibit intersystem crossing (ISC), depending on how it modulates the electronic structure, vibrational coupling, and spin–orbit interactions within the system.[131–135] To unravel the effects of hydrogen bonding interactions on the excited-state behavior of my chosen molecule, thiocoumarin 1, I studied its photophysics in the hydrogen bond-donating solvent

methanol and compared the results with those obtained in the aprotic solvent acetonitrile. These findings are presented in **Chapter 5** of my thesis.

1.2.9 Photoinduced Charge Transfer and ISC Modulation in Amino Thiocoumarins

Aminocoumarins are a group of compounds that consist of a coumarin backbone modified by amino groups. These compounds are renowned for their unique photophysical properties, which make them useful in a range of applications such as fluorescence imaging and phototherapy.[136–138] Upon absorbing light, an electron is excited from the highest occupied molecular orbital (HOMO) of the donor, typically the amino group, to the lowest unoccupied molecular orbital (LUMO) of the acceptor, which is the coumarin core. This light-induced excitation results in the formation of a charge transfer (CT) state, where charges are separated between the donor and acceptor regions of the molecule.[139–143] The CT state can either remain localized or become delocalized, depending on the surrounding molecular environment and the specific structural attributes of the aminocoumarin. The efficiency of charge transfer in aminocoumarins is heavily influenced by the nature and position of substituents on the coumarin backbone.[144,145] Electron-donating groups, such as amino groups, can enhance the donor properties, whereas electron-withdrawing groups help stabilize the acceptor.[144,146,147] Apart from the traditional acceptors species, the thionation of the lactone carbonyl oxygen at position 2 lead to a significant redshift in the absorption and the emission maxima of a 7-(*N*,*N*-dialkylamino) coumarin.[148–150] Therefore, solvent polarity plays a critical role in stabilizing the charge-transfer (CT) state and can consequently alter the rate of ISC dynamics by enhancing the stability of the charge-separated state.[151,152] In particular when the CT state lies lower in energy than the locally excited singlet states the ISC efficiency is very high.[153–157]. The CT state can also enhance spin-orbit coupling, particularly in aminocoumarins that contain heavy atoms such as iodine or bromine, which further increases the probability of ISC.[33] After forming the CT state, the

system may relax to the triplet state through non-radiative pathways, bypassing fluorescence. This process leads to an increase in ISC efficiency and generates longer-lived triplet states, often involved in energy transfer or photochemical reactions. Therefore, it is understood that if the molecule possesses this energy alignment, then the presence of the CT state can reduce fluorescence due to the rapid conversion to triplet states. This variation in singlet lifetimes has important implications for designing systems used in light harvesting or therapeutic applications.[104,158] However, if the singlet state character is such that it gets destabilizes upon increasing solvent polarity, then it enhances the singlet to triplet energy gaps and causes slow ISC. Sujit *et al.* reported that aminothiocoumarins include a variant with an amino substitution at the 7-position and others featuring an array of parent, alkoxy, and acetoxy substitutions.[105] All seven thiocoumarins exhibit phosphorescence at 77 K, though those with amino substitution display both fluorescence and phosphorescence. It is also found that these amino derivatives show charge transfer behaviour and have strong polarity dependence in the steady state absorption and emission spectrum. Therefore, it is expected that the ISC dynamics will differ significantly between amino-derivatives possessing charge-transfer (CT) states and other thio-derivatives. We believe that the presence of such CT character opens new avenues for investigating how this behavior influences ISC dynamics in thiocoumarins. To explore this, I studied the excited-state dynamics of the acetoxy-substituted thio-derivative of thiocoumarin, referred to as Acetoxy-TC, and compared its dynamics with those of the CT-state-forming TC1 molecule. A detailed account of this comparative study is presented in **Chapter 6** of my thesis.

References

(1) Turro, N. J. *Modern Molecular Spectroscopy*; The Benjamin/Cummings Pub. Company: US., 1978.

(2) Valeur, B.; Berberan-Santos, M. N. *Molecular Fluorescence*; Wiley-VCH Verlag GmbH & Co. KGaA: Weinheim, Germany., 2012.

(3) Lakowicz, J. R. *Principles of Fluorescence Spectroscopy*; Springer US: Boston, MA., 2006.

(4) Turro, N. J.; Ramamurthy, V.; Scaiano, J. C. *Modern Molecular Photochemistry of Organic Molecules*; University Science Books, Sausalito, California., 2010.

(5) McGlynn S. P.; Azumi, T.; Kinoshita, M. *Molecular Spectroscopy of the Triplet State*; Prentice Hall, Englewood Cliffs, NJ, 1969.

(6) Griffiths, D. J. *Introduction to Electrodynamics*; Prentice-Hall, Englewood Cliffs, NJ., 1999.

(7) Thomas J. Penfold; Gindensperger, E.; Daniel, C.; Marian, C. M. Spin-Vibronic Mechanism for Intersystem Crossing. *Chem. Rev.* **2018**, *118*, 6975–7025.

(8) Solovyov, K. N.; Borisevich, E. A. Intramolecular Heavy-Atom Effect in the Photophysics of Organic Molecules. *Phys.-Usp.* **2005**, *48*, 231–253.

(9) Kasha, M. J. The Triplet State. *J. Chem. Edu.* **1984**, *61*, 204–215.

(10) Lewis, G. N.; Kasha, M. Phosphorescence and the Triplet State. **1938**, *71*, 191.

(11) Lewis, G. N.; Kasha, M. Phosphorescence in Fluid Media and the Reverse Process of Singlet-Triplet Absorption. *J. Am. Chem. Soc.* **1945**, *67*, 994–1003.

(12) Kasha, M. Phosphorescence and the Role of the Triplet State in the Electronic Excitation of Complex Molecules. *Chem. Rev.* **1947**, *41*, 401–419.

(13) Mcclure, D. S. Triplet-Singlet Transitions in Organic Molecules. Lifetime Measurements of the Triplet State. *J. Chem. Phys.* **1949**, *17*, 905–913.

(14) El-Sayed, M. A. Theoretical Considerations Concerning the Intramolecular Heavy-Atom Effect on the Phosphorescence Process: C_{2v} Symmetric Dihalonaphthalene. *J Chem Phys* **1965**, *43*, 2864–2872.

(15) Murata, S.; Iwanaga, C.; Toda, T.; Kokubun, H. Fluorescence and Radiationless Transitions from the Second Excited States of Azulene Derivatives. *Berichte der Bunsengesellschaft für physikalische Chemie* **1972**, *76*, 1176–1183.

(16) Eber, G.; Schneider, S.; Dörr, F. On the Importance of Intersystem Crossing for the Deactivation of the S2 State of Halogeno Derivatives of Azulene. *Chem. Phys. Lett.* **1977**, *52*, 59–62.

(17) Abou-Zied, O. K.; Sinha, H. K.; Steer, R. P. Van Der Waals Complexes of 2-Chloro-, 2-Methyl-, and 1,3-Dimethylazulene with Rare Gases: Microscopic Solvent Shifts, Structures, and Binding Energies. *J. Phys. Chem. A* **1997**, *101*, 7989–7997.

(18) Roy, J. K.; Goodman, L. Halogen Enhancement of Singlet-Triplet Transitions: Part I. Low-Resolution Polarization of Halophenanthrene Spectra. *J. Mol. Spectr.* **1966**, *19*, 389–406.

(19) Ginsburg, J. L.; Goodman, L. Halogen Enhancement of Singlet–Triplet Transitions. II. Vibronic Paths in Phenanthrene. *J. Chem. Phys.* **1970**, *52*, 2369–2374.

(20) Najbar, J.; Jarzeba, W.; Urbanek, Z. H. Internal Heavy-Atom Effect on the T1 States of Monochloroquinolines and Monochloronaphthalenes. *Chem. Phys.* **1983**, *79*, 245–253.

(21) Najbar, J.; Jarzba, W.; Hochstrasser, R. M. Non-Radiative Decay of the T1 States of Chloronaphthalenes and Protonated Chloroquinolines at 77 K. *Chem. Phys.* **1985**, *95*, 1–8.

(22) Jarzęba, W.; Najbar, J.; Ciosłowski, J. Internal Heavy Atom Effects for Chloro- and Bromoquinolines. *J. Mol. Spectr.* **1986**, *141*, 469–474.

(23) Lewanowicz, A.; Lipiński, J.; Ruziewicz, Z.; Szymczak, A.; Szynkarczuk, J. Position-Dependent Effects of Internal Heavy Atoms on Highly Resolved Electronic Spectra and Luminescence Properties of Some Quinoxalines Substituted at the Homocyclic Ring. *J. Lumin.* **1989**, *43*, 85–102.

(24) Albrecht, A. C. Vibronic—Spin-Orbit Perturbations and the Assignment of the Lowest Triplet State of Benzene. *J. Chem. Phys.* **1963**, *38*, 354–365.

(25) Hosokai, T.; Matsuzaki, H.; Nakanotani, H.; Tokumaru, K.; Tsutsui, T.; Furube, A.; Nasu, K.; Nomura, H.; Yahiro, M.; Adachi, C. Evidence and Mechanism of Efficient Thermally Activated Delayed Fluorescence Promoted by Delocalized Excited States. *Sci. Adv.* **2017**, *3*, e1603282.

(26) Di, D.; Romanov, A. S.; Yang, L.; Richter, J. M.; Rivett, J. P. H.; Jones, S.; Thomas, T. H.; Jalebi, M. A.; Friend, R. H.; Linnolahti, M.; Bochmann, M.; Credgington, D. High-Performance Light-Emitting Diodes Based on Carbene-Metal-Amides. *Science (1979)* **2017**, *356*, 159–163.

(27) Zobel, J. P.; Nogueira, J. J.; González, L. Mechanism of Ultrafast Intersystem Crossing in 2-Nitronaphthalene. *Chem. Eur. J.* **2018**, *24*, 5379–5387.

(28) Baba M.; Saitoh M.; Kowaka Y.; Taguma K.; Yoshida K.; Semba Y.; Kasahara S.; Yamanaka T.; Ohshima Y.; Hsu Y-Chu.; Hsien L. Sheng. Vibrational and Rotational Structure and Excited-State Dynamics of Pyrene. *J. Chem. Phys.* **2009**, *131*, 224314.

(29) Penfold, T. J.; Spesyvtsev, R.; Kirkby, O. M.; Minns, R. S.; Parker, D. S. N.; Fielding, H. H.; Worth, G. A. Quantum Dynamics Study of the Competing Ultrafast Intersystem Crossing and Internal Conversion in the Channel 3 Region of Benzene. *J. Chem. Phys.* **2012**, *137*, 204310.

(30) Minns, R. S.; Parker, D. S. N.; Penfold, T. J.; Worth, G. A.; Fielding, H. H. Competing Ultrafast Intersystem Crossing and Internal Conversion in the "'channel 3'" Region of Benzene. *Phys. Chem. Chem. Phys.* **2010**, *12*, 15607–15615.

(31) Parker, D. S. N.; Minns, R. S.; Penfold, T. J.; Worth, G. A.; Fielding, H. H. Ultrafast Dynamics of the S1 Excited State of Benzene. *Chem. Phys. Lett.* **2009**, *469*, 43–47.

(32) Bhowmik, S.; Dutta, A.; Sen, P. Ultrafast Intersystem Crossing in Benzanthrone: Effect of Hydrogen Bonding and Viscosity. *J. Phys. Chem. A* **2024**, *128*, 6864–6878.

(33) Das, A.; Ghosh, S. K.; Ramamurthy, V.; Sen, P. Vibration-Assisted Intersystem Crossing in the Ultrafast Excited-State Relaxation Dynamics of Halocoumarins. *J. Phys. Chem. A* **2022**, *126*, 1475–1485.

(34) Haidekker, M. A.; Brady, T. P.; Lichlyter, D.; Theodorakis, E. A. Effects of Solvent Polarity and Solvent Viscosity on the Fluorescent Properties of Molecular Rotors and Related Probes. *Bioorg Chem* **2005**, *33*, 415–425.

(35) Tao, W.; Zhao, Z.; Kang, J.; Li, Z.; Zhu, J.; Zuo, Y.; Huang, M.; Cui, J.; Yu, J.; Liu, Y.; Fang, W.; Li, Y. Solvent Polarity-Driven Modulation of Excited

States: A DFT and Spectroscopic Analysis. *J. Photochem. Photobiol. A: Chem.* **2025**, *459*, 115992.

(36) Wang, P. Y.; Hsu, Y. C.; Chen, P. H.; Chen, G. Y.; Liao, Y. K.; Cheng, P. Y. Solvent-Polarity Dependence of Ultrafast Excited-State Dynamics of Trans-4-Nitrostilbene. *Phys. Chem. Chem. Phys.* **2023**, *26*, 788–807.

(37) Zhang, W.; Ma, Y.; Song, H.; Miao, R.; Kong, J.; Zhou, M. Deciphering the Photophysical Properties of Naphthalimide Derivatives Using Ultrafast Spectroscopy. *Phys. Chem. Chem. Phys.* **2024**, *26*, 4607–4613.

(38) Shi, H. X.; Bao, H. W.; Wu, G. Y. Solvation Controlled Excited-State Dynamics in a Donor-Acceptor Phenazine-Imidazole Derivative. *RSC. Adv.* **2024**, *14*, 17071–17076.

(39) Greißel, P. M.; Beneventi, G. M.; Weiß, R.; Wollny, A. S.; Dubey, R. K.; Melle-Franco, M.; Clark, T.; Mateo-Alonso, A.; Guldi, D. M. Intramolecular Singlet Fission in Individual Graphene Nanoribbons─Competition with a Charge Transfer. *J. Am. Chem. Soc.* **2025**, *147*, 11277–11290.

(40) Kainda, R.; Kumar Behera, S.; Dehury, A. K.; Chaudhary, Y. S. Deciphering the Photophysical Properties of Nonplanar Heterocyclic Compounds in Different Polarity Environments. *J. Phys. Chem. B* **2025**, *129*, 1323–1330.

(41) Conyard, J.; Stacko, P.; Chen, J.; McDonagh, S.; Hall, C. R.; Laptenok, S. P.; Browne, W. R.; Feringa, B. L.; Meech, S. R. Ultrafast Excited State Dynamics in Molecular Motors: Coupling of Motor Length to Medium Viscosity. *J. Phys. Chem. A* **2017**, *121*, 2138–2150.

(42) Ghosh, R.; Kushwaha, A.; Das, D. Conformational Control of Ultrafast Molecular Rotor Property: Tuning Viscosity Sensing Efficiency by Twist Angle Variation. *J. Phys. Chem. B* **2017**, *121*, 8786–8794.

(43) Liao, K.; Pan, Y.; Wu, Z.; Yao, W.; Miao, X.; Lu, X.; Fan, Q.; Hu, W. Viscosity Effects on Excited-State Dynamics of Indocyanine Green for Phototheranostic. *Chem. Asian J.* **2022**, *17*, e202200112.

(44) Ehrlich, R. S.; Dasgupta, S.; Jessup, R. E.; Teppang, K. L.; Shiao, A. L.; Jeoung, K. Y.; Su, X.; Shivkumar, A.; Theodorakis, E. A.; Paesani, F.; Yang, J. Excited State Rotational Freedom Impacts Viscosity Sensitivity in Arylcyanoamide Fluorescent Molecular Rotor Dyes. *J. Phys. Chem. B* **2024**, *128*, 3946–3952.

(45) Liu, X.; Chi, W.; Qiao, Q.; Kokate, S. V.; Cabrera, E. P.; Xu, Z.; Liu, X.; Chang, Y. T. Molecular Mechanism of Viscosity Sensitivity in BODIPY Rotors and Application to Motion-Based Fluorescent Sensors. *ACS Sens.* **2020**, *5*, 731–739.

(46) Santra, S.; Mora, A. K.; Nath, S. Ultrafast Isomerization vs Bond Twisting Process – Role of a Proton. *J. Photochem. and Photobiol. A: Chem.* **2023**, *437*, 114474.

(47) Das, A.; Sharma, G.; Kamatham, N.; Prabhakar, R.; Sen, P.; Ramamurthy, V. Ultrafast Solvation Dynamics Reveal That Octa Acid Capsule's Interior Dryness Depends on the Guest. *J. Phys. Chem. A* **2019**, *123*, 5928–5936.

(48) Gu, B.; Gu, Y.; Chernyak, V. Y.; Mukamel, S. Cavity Control of Molecular Spectroscopy and Photophysics. *Acc. Chem. Res.* **2023**, *56*, 2753–2762.

(49) Singh, M. K.; Pal, H.; Koti, A. S. R.; Sapre, A. V. Photophysical Properties and Rotational Relaxation Dynamics of Neutral Red Bound to β-Cyclodextrin. *J. Phys. Chem. A* **2004**, *108*, 1465–1474.

(50) Retna Raj, C.; Ramaraj, R. Influence of Cyclodextrin Complexation on the Emission of Thioflavin T and Its Off-on Control. *J. Photochem. and Photobiol. A: Chem.* **1999**, *122*, 39–46.

(51) Wang, R.; Yuan, L.; Macartney, D. H. A Green to Blue Fluorescence Switch of Protonated 2-Aminoanthracene upon Inclusion in Cucurbit[7]Uril. *Chem. Commun.* **2005**, 47, 5867–5869.

(52) Belletête, M.; Lachapelle, M.; Durocher, G. Polarity of AOT Micellar Interfaces: Use of the Preferential Solvation Concepts in the Evaluation of the Effective Dielectric Constants. *J. Phys. Chem.* **1990**, *94*, 5337–5341.

(53) Abel, S.; Waks, M.; Urbach, W.; Marchi, M. Structure, Stability, and Hydration of a Polypeptide in AOT Reverse Micelles. *J. Am. Chem. Soc.* **2006**, *128*, 382–383.

(54) Vasquez, V. R.; Williams, B. C.; Graeve, O. A. Stability and Comparative Analysis of AOT/Water/Isooctane Reverse Micelle System Using Dynamic Light Scattering and Molecular Dynamics. *J. Phys. Chem. B* **2011**, *115*, 2979–2987.

(55) Mat'usová, A.; Moody, G.; Dowding, P. J.; Eastoe, J.; Camp, P. J. Experimental and Simulation Study of Reverse Micelles Formed by Aerosol-OT and Water in Non-Polar Solvents. *Phys. Chem. Chem. Phys.* **2024**, *26*, 27772–27782.

(56) Jana, R.; Seth, D. Photophysical Study of Styryl Derivatives with Macrocyclic Host and the Effect of Addition of Cholesterol and Neurotransmitter. *J. Photochem. and Photobiol. A: Chem.* **2022**, *427*, 113842.

(57) Guchhait, B.; Biswas, R.; Ghorai, P. K. Solute and Solvent Dynamics in Confined Equal-Sized Aqueous Environments of Charged and Neutral Reverse Micelles: A Combined Dynamic Fluorescence and All-Atom Molecular Dynamics Simulation Study. *J. Phys. Chem. B* **2013**, *117*, 3345–3361.

(58) Dutta, P.; Sen, P.; Mukherjee, S.; Halder, A.; Bhattacharyya, K. Solvation Dynamics in the Water Pool of an Aerosol-OT Microemulsion. Effect of Sodium Salicylate and Sodium Cholate. *J. Phys. Chem. B* **2003**, *107*, 10815–10822.

(59) Maitra, A. Determination of Size Parameters of Water-Aerosol OT-Oil Reverse Micelles from Their Nuclear Magnetic Resonance Data. *J. Phys. Chem.* **1984**, *88*, 5122–5125.

(60) Hirata, S.; Totani, K.; Kaji, H.; Vacha, M.; Watanabe, T.; Adachi, C.; Hirata, S.; Vacha, M.; Totani, K.; Watanabe, T.; Kaji, H.; Adachi, C. Reversible Thermal Recording Media Using Time-Dependent Persistent Room Temperature Phosphorescence. *Adv. Opt. Mat.* **2013**, *1*, 438–442.

(61) Hirata, S.; Totani, K.; Zhang, J.; Yamashita, T.; Kaji, H.; Marder, S. R.; Watanabe, T.; Adachi, C. Efficient Persistent Room Temperature Phosphorescence in Organic Amorphous Materials under Ambient Conditions. *Adv. Funct. Mater.* **2013**, *23*, 3386–3397.

(62) Kabe, R.; Notsuka, N.; Yoshida, K.; Adachi, C. Afterglow Organic Light-Emitting Diode. *Adv. Mater.* **2016**, *28*, 655–660.

(63) Gawelda, W.; Cannizzo, A.; Pham, V.-T.; Van Mourik, F.; Bressler, C.; Chergui, M. Ultrafast Nonadiabatic Dynamics of $[Fe^{II}(Bpy)_3]^{2+}$ in Solution. *J. Am. Chem. Soc.* **2007**, *129*, 8199–8226.

(64) Juban Eric A.; Smeigh Amanda L.; Monat Jeremy E.; McCusker James K. Ultrafast Dynamics of Ligand-Field Excited States. *Coord. Chem. Rev.* **2006**, *250*, 1783–1791.

(65) Consani, C.; Prémont-Schwarz, M.; Elnahhas, A.; Bressler, C.; Van Mourik, F.; Cannizzo, A.; Chergui, M. Vibrational Coherences and Relaxation in the High-Spin State of Aqueous [FeII(Bpy)3]2+. *Angew. Chem. Int. Ed.* **2009**, *48*, 7184–7187.

(66) Smeigh, A. L.; Creelman, M.; Mathies, R. A.; McCusker, J. K. Femtosecond Time-Resolved Optical and Raman Spectroscopy of Photoinduced Spin Crossover: Temporal Resolution of Low-to-High Spin Optical Switching. *J. Am. Chem. Soc.* **2008**, *130*, 14105–14107.

(67) Tribollet J.; Galle G.; Jonusauskas G.; Deldicque D.; Tondusson M.; Letard J.F.; Freysz E. Transient Absorption Spectroscopy of the Iron(II) $[Fe(Phen)_3]^{2+}$ Complex: Study of the Non-Radiative Relaxation of an Isolated Iron(II) Complex. *Chem. Phys. Lett.* **2011**, *513*, 42–47.

(68) Lapini A.; Foggi P.; Bussotti L.; Righini R.; Dei A. Relaxation Dynamics in Three Polypyridyl Iron(II)-Based Complexes Probed by Nanosecond and Sub-Picosecond Transient Absorption Spectroscopy. *Inorganica Chim. Acta.* **2008**, *361*, 3937–3943.

(69) Champion, P. M.; Rosca, F.; Ionascu, D.; Cao, W.; Ye, X. Rapid Timescale Processes and the Role of Electronic Surface Coupling in the Photolysis of Diatomic Ligands from Heme Proteins. *Faraday Discuss.* **2004**, *127*, 123–135.

(70) Cannizzo, A.; Van Mourik, F.; Gawelda, W.; Zgrablic, G.; Bressler, C.; Chergui, M.; Cannizzo, [A; Van Mourik, F.; Gawelda, W.; Zgrablic, G.; Bressler, C.; Chergui, M. Broadband Femtosecond Fluorescence Spectroscopy of $[Ru(Bpy)_3]^{2+}$. *Angew. Chem. Int. Ed.* **2006**, *45*, 3174–3176.

(71) Zhang, Y.; Bennett, K.; Mukamel, S. Monitoring Ultrafast Spin Crossover Intermediates in an Iron(II) Complex by Broad Band Stimulated X-Ray Raman Spectroscopy. *J. Phys. Chem. A* **2018**, *122*, 6524–6531.

(72) Colvin, M. T.; Smeigh, A. L.; Giacobbe, E. M.; Conron, S. M. M.; Ricks, A. B.; Wasielewski, M. R. Ultrafast Intersystem Crossing and Spin Dynamics of Zinc Meso-Tetraphenylporphyrin Covalently Bound to Stable Radicals. *J. Phys. Chem. A* **2011**, *115*, 7538–7549.

(73) Iwamura, M.; Watanabe, H.; Ishii, K.; Takeuchi, S.; Tahara, T. Coherent Nuclear Dynamics in Ultrafast Photoinduced Structural Change of Bis(Diimine)Copper(I) Complex. *J. Am. Chem. Soc.* **2011**, *133*, 7728–7736.

(74) Cannizzo, A.; Blanco-Rodríguez, Ana. M.; Nahhas, A. El; Šebera, J.; Záliš, S.; Vlček, A.; Chergui, M. Femtosecond Fluorescence and Intersystem Crossing in Rhenium(I) Carbonyl-Bipyridine Complexes. *J. Am. Chem. Soc.* **2008**, *130*, 8967–8974.

(75) Ramakrishna, G.; Goodson, T.; Joy, E. R. H.; Cooper, T. M.; McLean, D. G.; Urbas, A. Ultrafast Intersystem Crossing: Excited State Dynamics of Platinum Acetylide Complexes. *J. Phys. Chem. C* **2009**, *113*, 1060–1066.

(76) Gaffney, K. J. Capturing Photochemical and Photophysical Transformations in Iron Complexes with Ultrafast X-Ray Spectroscopy and Scattering. *Chem. Sci.* **2021**, *12*, 8010–8025.

(77) Melnikov, A. A.; Pozdnyakov, I. P.; Chekalin, S. V.; Glebov, E. M. Direct Measurement of Ultrafast Intersystem Crossing Time for the PtIVBr62− Complex. *Mendeleev Commun.* **2020**, *30*, 509–511.

(78) Šrut, A.; Mai, S.; Sazanovich, I. V.; Heyda, J.; Vlček, A.; González, L.; Záliš, S. Nonadiabatic Excited-State Dynamics of $ReCl(CO)_3(Bpy)$ in Two Different Solvents. *Phys. Chem. Chem. Phys.* **2022**, *24*, 25864–25877.

(79) Mai, S.; González, L. Unconventional Two-Step Spin Relaxation Dynamics of $[Re(CO)_3(Im)(Phen)]^+$ in Aqueous Solution. *Chem. Sci.* **2019**, *10*, 10405–10411.

(80) Burdzinski, G. T.; Ramnauth, R.; Chisholm, M. H.; Gustafson, T. L. Direct Observation of a ^{1}MLCT State by Ultrafast Transient Absorption Spectroscopy in $Mo_2(O_2C\text{-}9\text{-}Anthracene)_4$. *J. Am. Chem. Soc.* **2006**, *128*, 6776–6777.

(81) Van Der Veen, R. M.; Cannizzo, A.; Van Mourik, F.; Vlček, A.; Chergui, M. Vibrational Relaxation and Intersystem Crossing of Binuclear Metal Complexes in Solution. *J. Am. Chem. Soc.* **2011**, *133*, 305–315.

(82) Eng, J.; Thompson, S.; Goodwin, H.; Credgington, D.; Penfold, T. J. Competition between the Heavy Atom Effect and Vibronic Coupling in Donor–Bridge–Acceptor Organometallics. *Phys. Chem. Chem. Phys* **2020**, *22*, 4659–4667.

(83) Garakyaraghi, S.; Danilov, E. O.; McCusker, C. E.; Castellano, F. N. Transient Absorption Dynamics of Sterically Congested Cu(I) MLCT Excited States. *J. Phys. Chem. A* **2015**, *119*, 3181–3193.

(84) Zobel, J. P.; González, L. Nonadiabatic Dynamics Simulation Predict Intersystem Crossing in Nitroaromatic Molecules on a Picosecond Time Scale. *ChemPhotoChem* **2019**, *3*, 833–845.

(85) Fumanal, M.; Gindensperger, E.; Daniel, C. Ultrafast Intersystem Crossing vs Internal Conversion in α-Diimine Transition Metal Complexes: Quantum Evidence. *J. Phys. Chem. Lett.* **2018**, *9*, 5189–5195.

(86) Zheldakov, I. L.; N. Ryazantsev, M.; Tarnovsky, A. N. Wavepacket Motion via a Conical Intersection in the Photochemistry of Aqueous Transition-Metal Dianions. *J. Phys. Chem. Lett.* **2011**, *2*, 1540–1545.

(87) Rafiq, S.; Weingartz, N. P.; Kromer, S.; Castellano, F. N.; Chen, L. X. Spin–Vibronic Coherence Drives Singlet–Triplet Conversion. *Nature* **2023**, *620*, 776–781.

(88) Kim, P.; Valentine, A. J. S.; Roy, S.; Mills, A. W.; Chakraborty, A.; Castellano, F. N.; Li, X.; Chen, L. X. Ultrafast Excited-State Dynamics of Photoluminescent Pt(II) Dimers Probed by a Coherent Vibrational Wavepacket. *J. Phys. Chem. Lett.* **2021**, *12*, 6794–6803.

(89) Pallenberg, A. J.; Koenig, K. S.; Barnhartlb, D. M. Synthesis and Characterization of Some Copper(I) Phenanthroline Complexes. *Inorg. Chem* **1995**, *34*, 2833–2840.

(90) Gómez-Coca, R. B.; Kapinos, L. E.; Holý, A.; Vilaplana, R. A.; González-Vílchez, F.; Sigel, H. Intramolecular Stacking Interactions in Ternary Copper(II) Complexes1 Formed with 2,2′-Bipyridine or 1,10-Phenanthroline and 9-(4-Phosphonobutyl)Adenine (DPMEA), the Carba Relative of the Antiviral Nucleotide Analogue 9-[2-(Phosphonomethoxy)Ethyl]Adenine (PMEA). *J. Inorg. Biochem.* **2001**, *84* (1), 39–46.

(91) Sogukomerogullari, H. G.; Başaran, E.; Sarıoğlu, A. O.; Köse, A.; Akkoç, S. Synthesis, Characterization, Photoluminescence Properties and Antiproliferative Activity of New Pd(II), Ni(II) and Cu(II) Mixed Complexes Bearing Schiff Base Ligand and 1,10-Phenanthroline. *ChemistrySelect* **2023**, *8*, e202301014.

(92) Sogukomerogullari, H. G.; Sarıoğlu, A. O.; Kepekçi, R. A.; Türkmenoğlu, B.; Morcali, M. H. Copper(II), Cobalt(II), Nickel(II), and Iron(II) Mixed Complexes Formed by Schiff Base and 1,10-Phenanthroline as Secondary Chelates: Preparation, Characterization, Antimicrobial, Antioxidant, and Molecular Docking Studies. *Inorganica Chim Acta* **2025**, *583*, 122692.

(93) See, C. E.; Housecroft, E.; Housecroft, C. E.; Constable, E. C. Solar Energy Conversion Using First Row D-Block Metal Coordination Compound Sensitizers and Redox Mediators. *Chem. Sci.* **2022**, *13*, 1225–1262.

(94) Cetin, M. M.; Hodson, R. T.; Hart, C. R.; Cordes, D. B.; Findlater, M.; Casadonte, D. J.; Cozzolino, A. F.; Mayer, M. F. Characterization and Photocatalytic Behavior of 2,9-Di(Aryl)-1,10-Phenanthroline Copper(I) Complexes. *Dalton Trans.* **2017**, *46*, 6553–6569.

(95) Gourlaouen, C.; Daniel, C. Towards Optimized Photoluminescent Copper(I) Phenanthroline-Functionalized Complexes: Control of the Photophysics by Symmetry-Breaking and Spin–Orbit Coupling. *Materials* **2022**, *15*, 5222.

(96) Cui, G.; Fang, W. H. State-Specific Heavy-Atom Effect on Intersystem Crossing Processes in 2-Thiothymine: A Potential Photodynamic Therapy Photosensitizer. *J. Chem. Phys.* **2013**, *138*, 44315.

(97) Acquah, C.; Hoehn, S.; Krul, S.; Jockusch, S.; Yang, S.; Seth, S. K.; Lee, E.; Xiao, H.; Crespo-Hernández, C. E. Electronic Relaxation Pathways in Thio-Acridone and Thio-Coumarin: Two Heavy-Atom-Free Photosensitizers Absorbing Visible Light. *Phys. Chem. Chem. Phys.* **2024**, *26*, 28980–28991.

(98) Coyle, J. D. The Photochemistry of Thiocarbonyl Compounds. *Tetrahedron* **1985**, *41* (23), 5393–5425.

(99) Bingham, N. M.; Abousalman-Rezvani, Z.; Collins, K.; Roth, P. J. Thiocarbonyl Chemistry in Polymer Science. *Polym. Chem.* **2022**, *13*, 2880–2901.

(100) Rao, V. P. The Photoreactivity of Thiocarbonyl Compounds. *Sulfur Reports* **1992**, *12*, 359–399.

(101) Iyer, A.; Clay, A.; Jockusch, S.; Sivaguru, J. Evaluating Brominated Thioxanthones as Organo-Photocatalysts. *J. Phys. Org. Chem.* **2017**, *30*, e3738.

(102) Pollum, M.; Crespo-Hernández, C. E. Communication: The Dark Singlet State as a Doorway State in the Ultrafast and Efficient Intersystem Crossing Dynamics in 2-Thiothymine and 2-Thiouracil. *J. Chem. Phys.* **2014**, *140*, 071101.

(103) Ashwood, B.; Pollum, M.; Crespo-Hernández, C. E. Photochemical and Photodynamical Properties of Sulfur-Substituted Nucleic Acid Bases. *Photochem. Photobiol.* **2019**, *95*, 33–58.

(104) Tong, S.; Cheng, Y.; Liu, H.; Pang, Y.; Lin, X.; Hu, Z.; Wu, F. Thionation of Conjugated Porphyrin with Enhanced Photodynamic and Photothermal Effects for Cancer Therapy. *J. Photochem. Photobiol. A: Chem.* **2025**, *459*, 116085.

(105) Ghosh, S. K.; Valloli, L. K.; Unny, D.; Sivaguru, J.; Jockusch, S.; Ramamurthy, V. Room Temperature Phosphorescence of 2-Thioxo-Coumarins in Aqueous Solution Promoted by Octa Acid Inclusion. *J. Photochem. Photobiol. A: Chem.* **2024**, *451*, 115510.

(106) Culik, R. M.; Jo, H.; DeGrado, W. F.; Gai, F. Using Thioamides To Site-Specifically Interrogate the Dynamics of Hydrogen Bond Formation in β-Sheet Folding. *J. Am. Chem. Soc.* **2012**, *134*, 8026–8029.

(107) Bailey, W. F.; Bartelson, A. L.; Wiberg, K. B. Contrasting Reactions of Ketones and Thioketones with Alkyllithiums: A Coordinated Experimental and Computational Investigation. *J. Am. Chem. Soc.* **2012**, *134*, 3199–3207.

(108) Khadka, D.; Kulasekharan, R.; Ramamurthy, V. Role of Supramolecular Steric Compression during Photoinduced Intramolecular Hydrogen Abstraction Reactions of Ketones and Thioketones. *J. Photochem. and Photobiol. A: Chem.* **2023**, *437*, 114442.

(109) Murai, T. The Construction and Application of C=S Bonds. *Top. Curr. Chem.* **2018**, *376*, 1–21.

(110) Szymański, M.; Balicki, M.; Binkowski, M.; Kubicki, J.; Maciejewskia, A.; Pawłowska, E.; Wróżowa, T. EFFECTS OF SOLUTE-SOLVENT INTERACTIONS ON RADIATIONLESS DECAY OF THIOKETONES

EXCITED TO THEIR S_2-AND T_1-STATES. *Acta Phys Pol A* **1996**, *89*, 527–546.

(111) Sharma, S. K.; Wu, Y.; Steinbergs, N.; Crowley, M. L.; Hanson, A. S.; Casero, R. A.; Woster, P. M. (Bis)Urea and (Bis)Thiourea Inhibitors of Lysine-Specific Demethylase 1 as Epigenetic Modulators. *J Med Chem.* **2010**, *53*, 5197-5212.

(112) Han, J.; Dong, H.; Xu, Z.; Wang, J.; Wang, M. Synthesis and Activity of Novel Acylthiourea with Hydantoin. *Int. J. Mol. Sci.* **2013**, *14*, 19526–19539.

(113) Madabhushi, S.; Mallu, K. K. R.; Vangipuram, V. S.; Kurva, S.; Poornachandra, Y.; Ganesh Kumar, C. Synthesis of Novel Benzimidazole Functionalized Chiral Thioureas and Evaluation of Their Antibacterial and Anticancer Activities. *Bioorg Med Chem Lett.* **2014**, *24*, 4822–4825.

(114) Crank, G.; Neville, M.; Ryden, R. Thiourea Derivatives of 2-Aminooxazoles Showing Antibacterial and Antifungal Activity. *J. Med. Chem.* **1973**, *16*, 1402–1405.

(115) Seto, R.; Matsumoto, K.; Endo, T. Selective Nucleophilic Additions to Poly(Methacrylate)s Containing Isothiocyanate Moieties in the Side Chains and Their Application in Cross-Linking. *J. Polym. Sci. Part A: Polym. Chem.* **2014**, *52*, 1832–1842.

(116) Hudej, R.; Kljun, J.; Kandioller, W.; Repnik, U.; Turk, B.; Hartinger, C. G.; Keppler, B. K.; Miklavčič, D.; Turel, I. Synthesis and Biological Evaluation of the Thionated Antibacterial Agent Nalidixic Acid and Its Organoruthenium(II) Complex. *Organometallics* **2012**, *31*, 5867–5874.

(117) Xiao Y.; Huang X.; Feng J.; Ni Z.; Gai L.; Xiao X.; Sui X.; Lu H. A Simple Route toward Triplet-Forming Thionated BODIPY-Based Photosensitizers. *Dyes and Pigments* **2022**, *200*, 110167.

(118) Gibb, C. L. D.; Gibb, B. C. Well-Defined, Organic Nanoenvironments in Water: The Hydrophobic Effect Drives a Capsular Assembly. *J. Am. Chem. Soc.* **2004**, *126*, 11408–11409.

(119) Ramamurthy, V. Photochemistry within a Water-Soluble Organic Capsule. *Acc. Chem. Res.* **2015**, *48*, 2904–2917.

(120) Jayaraj, N.; Jockusch, S.; Kaanumalle, L. S.; Turro, N. J.; Ramamurthy, V. Dynamics of Capsuleplex Formed between Octaacid and Organic Guest Molecules - Photophysical Techniques Reveal the Opening and Closing of Capsuleplex. *Can. J. Chem.* **2011**, *89*, 203–213.

(121) Das, A.; Danao, A.; Banerjee, S.; Raj, A. M.; Sharma, G.; Prabhakar, R.; Srinivasan, V.; Ramamurthy, V.; Sen, P. Dynamics of Anthracene Excimer Formation within a Water-Soluble Nanocavity at Room Temperature. *J. Am. Chem. Soc.* **2021**, *143*, 2025–2036.

(122) Burdzinski, G.; Maciejewski, A.; Buntinx, G.; Poizat, O.; Toele, P.; Zhang, H.; Glasbeek, M. Femtosecond Fluorescence Up-Conversion and Transient Absorption Studies of the S_2 State in the Hydrogen-Bonded Benzopyranthione–Water Complex. *Chem. Phys. Lett.* **2004**, *393*, 102–106.

(123) Krystkowiak, E.; Bachorz, R. A.; Maciejewski, A. Hydrogen-Bonded 4H-1-Benzopyrane-4-Thione–Water Complexes Properties in the S_2 Excited State: The Mechanism and Dynamics of Deactivation. *Phys. Chem. Chem. Phys.* **2016**, *18*, 492–502.

(124) Rabe, E. J.; Goldwyn, H. J.; Hwang, D.; Masiello, D. J.; Schlenker, C. W. Intermolecular Hydrogen Bonding Tunes Vibronic Coupling in Heptazine Complexes. *J. Phys. Chem. B* **2020**, *124*, 11680–11689.

(125) Su, Y.; Li, K.; Yu, X. Theoretical Studies on the Fluorescence Enhancement of Benzaldehydes by Intermolecular Hydrogen Bonding. *J. Phys. Chem. B* **2019**, *123* (4), 884–890.

(126) Krystkowiak, E.; Koput, J.; Maciejewski, A. Hydrogen Bond Effects in the Ground and Excited Singlet States of 4H-1-Benzopyrane-4-Thione in Water—Theory and Experiment. *Phys. Chem. Chem. Phys.* **2012**, *14*, 8842–8851.

(127) Lawrence, A. H.; Liao, C. C.; de Mayo, P.; Mayo, de; Ramamurthy, V. Thione Photochemistry. Cycloaddition in a Saturated System. *J. Am. Chem. Soc.* **1976**, *98*, 2219–2226.

(128) Guo, Y.; Zhong, Y.; Wu, Z.; Wang, C.; Wang, Y.; Zhang, Ji.; Wang, H.; Zhao, G. The Hydrogen Bond Effect on Excited State Mechanism for 2-Isopropyl Thioxanone in Protic Solvents: Experimental and Theoretical Investigation. *J. Mol. Liq.* **2022**, *345*, 117012.

(129) Zhao, G. J.; Han, K. L. Role of Intramolecular and Intermolecular Hydrogen Bonding in Both Singlet and Triplet Excited States of Aminofluorenones on Internal Conversion, Intersystem Crossing, and Twisted Intramolecular Charge Transfer. *J. Phys. Chem. A* **2009**, *113*, 14329–14335.

(130) Wang, L.; Qin, Y.; Cheng, Y.; Fan, W.; Yang, S.; Zheng, L.; Cao, Q. Intermolecular Hydrogen Bonds Induce Restriction of Access to the Dark State for Triggering Aggregation-Induced Emission. *J. Mater. Chem. C* **2022**, *10*, 5356–5363.

(131) Kumar Venkatraman, R.; Kayal, S.; Barak, Ar.; Orr-Ewing, A. J.; Umapathy, S. Intermolecular Hydrogen Bonding Controlled Intersystem Crossing Rates of Benzophenone. *J. Phys. Chem. Lett.* **2018**, *9*, 1642–1648.

(132) Shimada, H.; Nakamura, A.; Yoshihara, T.; Tobita, S. Intramolecular and Intermolecular Hydrogen-Bonding Effects on Photophysical Properties of 2′-Aminoacetophenone and Its Derivatives in Solution. *Photochem. Photobiol. Sci.* **2005**, *4*, 367–375.

(133) Nogueira, J. J.; Oppel, M.; González, L. Enhancing Intersystem Crossing in Phenotiazinium Dyes by Intercalation into DNA. *Angew. Chem. Int. Ed.* **2015**, *54*, 4375–4378.

(134) Kitamura, M.; Baba, H. Substitution and Hydrogen Bonding Effects on Fluorescence and Intersystem Crossing in Naphthaldehydes and Their Derivatives. *Bull. Chem. Soc. Jpn.* **1975**, *48*, 1191–1195.

(135) Jiang Meng-Huan; Li Mai-Ning; Zhao Yu; Liu Yu-Hui; Gao Jun; Zhu Chaoyuan. ESIPT-Induced Intersystem Crossing Leads to Tautomer Fluorescence Quenching for 3-Mercapto-2-(4-(Trifluoromethyl) Phenyl)-4H-Chromen-4-One Molecule. *J. Photochem. & Photobiol., A: Chem.* **2025**, *459*, 116111.

(136) Feng J.; Gao T.; Morlet-Savary F.; Schmitt M.; Dietlin C.; Zhang J.; Xiao P.; Dumur F.; Lalevée J. Sunlight-Driven Photoinitiating Systems for Photopolymerization and Application in Direct Laser Writing. *Polym. Chem.* **2024**, *15*, 2899–2912.

(137) Zhang, Z.-Y.; Li, Z.-J.; Tang, Y.-H.; Xu, L.; Zhang, D.-T.; Qin, T.-Y.; Zhang, Z.-Y.; Li, Z.-J.; Tang, Y.-H.; Xu, L.; Zhang, D.-T.; Qin, T.-Y.; Wang, Y.-L. Recent Research Progress in Fluorescent Probes for Detection of Amyloid-β In Vivo. *Biosensors (Basel)* **2023**, *13*, 990.

(138) Hasegawa, R.; Iwakiri, S.; Kubo, Y. Synthesis and Triplet Sensitization of Bis(Arylselanyl)BOPHYs; Potential Application in Triplet-Triplet Annihilation Upconversion. *New J. Chem.* **2021**, *45*, 6091–6099.

(139) Retig, W.; Klock, A. Intramolecular Fluorescence Quenching in Aminocoumarines. Identification of an Excited State with Full Charge Separation. *Can. J. Chem.* **1985**, *63*, 1649–1653.

(140) Liu, X.; Cole, J. M.; Xu, Z. Substantial Intramolecular Charge Transfer Induces Long Emission Wavelengths and Mega Stokes Shifts in 6-Aminocoumarins. *J. Phys. Chem. C* **2017**, *121*, 13274–13279.

(141) Debnath, T.; Ghosh, H. N. An Insight of Molecular Twisting of Coumarin Dyes. *ChemistrySelect* **2020**, *5*, 9461–9476.

(142) Dahiya, P.; Kumbhakar, M.; Mukherjee, T.; Pal, H. Effect of Protic Solvents on Twisted Intramolecular Charge Transfer State Formation in Coumarin-152 and Coumarin-481 Dyes. *Chem. Phys. Lett.* **2005**, *414*, 148–154.

(143) Nath, S.; Kumbhakar, M.; Pal, H. Effect of H-Bonding on the Photophysical Behaviour of Coumarin Dyes. *Hydrogen Bonding and Transfer in the Excited State* **2010**, *1*, 419–431.

(144) Izquierdo-García, E.; Rovira, A.; Forcadell, J.; Bosch, M.; Marchán, V. Exploring Structural–Photophysical Property Relationships in Mitochondria-Targeted Deep-Red/NIR-Emitting Coumarins. *Int. J. Mol. Sci.* **2023**, *24*, 17427.

(145) Sharma, S. J.; Sekar, N. Deep-Red/NIR Emitting Coumarin Derivatives - Synthesis, Photophysical Properties, and Biological Applications. *Dyes and Pigments* **2022**, *202*, 110306.

(146) Fournier, L.; Aujard, I.; Le Saux, T.; Maurin, S.; Beaupierre, S.; Baudin, J. B.; Jullien, L. Coumarinylmethyl Caging Groups with Redshifted Absorption. *Chem. Eur. J.* **2013**, *19*, 17494–17507.

(147) Matikonda, S. S.; Ivanic, J.; Gomez, M.; Hammersley, G.; Schnermann, M. J. Core Remodeling Leads to Long Wavelength Fluoro-Coumarins. *Chem. Sci.* **2020**, *11*, 7302–7307.

(148) Fournier, L.; Gauron, C.; Xu, L.; Aujard, I.; Le Saux, T.; Gagey-Eilstein, N.; Maurin, S.; Dubruille, S.; Baudin, J. B.; Bensimon, D.; Volovitch, M.; Vriz,

S.; Jullien, L. A Blue-Absorbing Photolabile Protecting Group for in Vivo Chromatically Orthogonal Photoactivation. *ACS Chem. Biol.* **2013**, *8* (7), 1528–1536.

(149) Dutta, A.; Ghosh, S. K.; Mandal, S.; Srinivasan, V.; Ramamurthy, V.; Sen, P. Ultrafast Processes in Upper Excited Singlet States of Free and Caged 7-Diethylaminothiocoumarin. *J. Phys. Chem. A* **2024**, *128*, 6853–6863.

(150) Ghosh, S. K.; Chatterjee, S.; Boruah, P. P.; Mandal, S.; Da Silva, J. P.; Srinivasan, V.; Ramamurthy, V. A Supramolecular Approach towards the Photorelease of Encapsulated Caged Acids in Water: 7-Diethylaminothio-4-Coumarinyl Molecules as Triggers. *Photochem. Photobiol. Sci.* **2024**, *23*, 2057–2073.

(151) Nad, S.; Kumbhakar, M.; Pal, H. Photophysical Properties of Coumarin-152 and Coumarin-481 Dyes: Unusual Behavior in Nonpolar and in Higher Polarity Solvents. *J. Phys. Chem. A* **2003**, *107*, 4808–4816.

(152) Maity, B.; Chatterjee, A.; Seth, D. Photophysics of a Coumarin in Different Solvents: Use of Different Solvatochromic Models. *Photochem. and Photobiol.* **2014**, *90*, 734–746.

(153) Liu, D.; El-Zohry, A. M.; Taddei, M.; Matt, C.; Bussotti, L.; Wang, Z.; Zhao, J.; Mohammed, O. F.; Di Donato, M.; Weber, S. Long-lived Charge-transfer State Induced by Spin-Orbit Charge Transfer Intersystem Crossing (SOCT-ISC) in a Compact Spiro Electron Donor/Acceptor Dyad. *Angew. Chem. Int. Ed.* **2020**, *59*, 11591–11599.

(154) Gould, I. R.; Boiani, J. A.; Gaillard, E. B.; Goodman, J. L.; Farid, S. Intersystem Crossing in Charge-Transfer Excited States. *J. Phys. Chem. A* **2003**, *107*, 3515–3524.

(155) Xu, J.; Zeng, H.; Wang, K.; Peng, S.; Chen, X.; Zhang, Y.; Wu, D.; Xia, J. High-Yield Triplet States from Charge-Transfer-Mediated Intersystem

Crossing in a Thionated Perylene Dimer. *J. Phys. Chem. C* **2024**, *128*, 20967–20973.

(156) Hou, Y.; Zhang, X.; Chen, K.; Liu, D.; Wang, Z.; Liu, Q.; Zhao, J.; Barbon, A. Charge Separation, Charge Recombination, Long-Lived Charge Transfer State Formation and Intersystem Crossing in Organic Electron Donor/Acceptor Dyads. *J. Phys. Chem. C* **2019**, *7*, 12048–12074.

(157) Dance, Z. E. X.; Mickley, S. M.; Wilson, T. M.; Ricks, A. B.; Scott, A. M.; Ratner, M. A.; Wasielewski, M. R. Intersystem Crossing Mediated by Photoinduced Intramolecular Charge Transfer: Julolidine - Anthracene Molecules with Perpendicular π Systems. *J. Phys. Chem. A* **2008**, *112*, 4194–4201.

(158) Gemenetzidis, E.; Shavorskaya, O.; Xu, Y. Z.; Trigiante, G. Topical 4-Thiothymidine Is a Viable Photosensitiser for the Photodynamic Therapy of Skin Malignancies. *J Dermatolog Treat.* **2011**, *24*, 209–214.

Chapter 2

Experimental

This chapter covers the details of the experimental methods used in this thesis. I have explicitly written the detailed instrumentation and data analysis procedure for time-correlated single photon counting, femtosecond transient absorption spectroscopy, and fluorescence up-conversion spectroscopy used in my research works. Besides, a brief description of density functional theory has also been provided. I have also described the procedure of complexation between Octa acid as host and hydrophobic probe molecules as guests.

2.1. Steady State Measurements

Steady-state absorption spectra were recorded using a Shimadzu UV-2450 spectrophotometer (Japan), which is equipped with a deuterium and halogen lamp as the light source and a photomultiplier tube (PMT) as the detector. Steady-state emission spectra were obtained with a Fluoromax-4 spectrofluorometer (Horiba Jobin-Yvon, USA), featuring a 150W xenon arc lamp as the excitation source and a photomultiplier tube detector (190–850 nm range). Time-gated emissions were performed on a FS920CDT Edinburgh fluorimeter or FLS1000 Photoluminescence Spectrometer (Edinburgh Instruments, UK) employing a quartz dewar filled with liquid nitrogen. Fluorescence quantum yield of different samples was calculated through the following equation.

$$\left(\varphi_f\right)_{Sample} = \frac{I_{Sample}}{I_{Ref}} \times \frac{A_{Ref}}{A_{Sample}} \times \frac{n^2_{Sample}}{n^2_{Ref}} \times \left(\varphi_f\right)_{Ref} \quad (2.1.1)$$

Where, I_{Sample} and I_{Ref} are the area integrated emission intensity for the sample and reference respectively, A_{Sample} and A_{Ref} are the absorption at the corresponding excitation wavelength for the sample and reference, n_{Sample} and n_{Ref} are the refractive index at room temperature for the sample and reference, and $\left(\varphi_f\right)$ is the known fluorescence quantum yield of the reference.

To quantify the triplet population of my studied systems, singlet oxygen phosphorescence measurements were carried out. The characteristic phosphorescence emission of singlet oxygen, centered at 1270 nm, was recorded using a Horiba Fluoromax-Plus-C-P spectrofluorimeter (Horiba, USA) equipped with a liquid nitrogen-cooled InGaAs detector, which offers high sensitivity up to 1650 nm. To eliminate interference from the visible region of the emission spectrum, an 800 nm long-pass filter was used to block shorter wavelengths. Optical density (OD) all samples were around 0.3–0.4 at the excitation wavelength. To ensure complete oxygen saturation, pure oxygen was purged into the solutions at constant pressure for 30 minutes. The oxygenated samples were then transferred to a quartz cuvette with a 1 cm pathlength for measurement. Upon photoexcitation to the singlet

excited state, if the sample undergoes intersystem crossing (ISC), it populates the triplet state, which can subsequently transfer its energy to ground-state molecular oxygen ($^3O_2$), producing singlet oxygen ($^1O_2$). The generated $^1O_2$ emits phosphorescence in the 1200–1350 nm region, with a characteristic maximum at 1270 nm, which was detected using a near-infrared (NIR) detector. Temperature has a significant influence on the intensity of singlet oxygen phosphorescence: at elevated temperatures, enhanced non-radiative losses from the triplet state reduce the phosphorescence signal, whereas at lower temperatures, the efficiency of triplet energy transfer decreases due to the diffusion-controlled nature of the process. Our measurements indicated that 10 °C is the optimal temperature for maximizing the phosphorescence intensity in our system. Hence, all experiments were performed at this temperature. The singlet oxygen phosphorescence spectra were recorded for each sample, and the singlet oxygen quantum yield (φ_{SO}) was determined by using a relative comparison method using chrysazin in acetonitrile.[1] Singlet oxygen quantum yield was calculated through the expression as

$$(\varphi_{SO})_{Sample} = \frac{I_{Sample}}{I_{Ref}} \times \frac{A_{Ref}}{A_{Sample}} \times (\varphi_{SO})_{Ref} \quad (2.1.2)$$

Where, I_{Sample} and I_{Ref} are the area integrated emission intensity for the sample and reference respectively, A_{Sample} and A_{Ref} are the absorption at the corresponding excitation wavelength for the sample and reference, and (φ_f) is the known singlet oxygen quantum yield of the reference i.e. $(\varphi_{SO})_{Ref}$.

2.2. Time-Correlated Single Photon Counting (TCSPC) Method

2.2.1. Basic Principle

The fundamental concept behind fluorescence lifetime measurement is to excite the sample with a short delta function pulse and track the gradual decay in fluorescence intensity with time. However, there are several challenges associated with this measurement. Firstly, the fluorescence decay times of most organic samples are extremely short, typically in the nanosecond range. To capture fluorescence lifetimes

accurately, a detector with an ultrafast response is required, which is challenging to achieve. Moreover, to fully characterize a sample, it’s not sufficient to measure just the fluorescence lifetime; we also need the complete fluorescence decay profile, often an exponential decay pattern. However, capturing such short lifetimes necessitates a detector having a picosecond-level time response to resolve nanosecond-range decay components accurately. Even with high-speed photodiodes and GHz oscilloscopes, it is difficult to achieve this level of resolution, and the weak emission signal from the sample may be insufficient to generate a detectable electric signal after passing through the optics. Consequently, an analog measurement cannot reliably capture the full decay waveform of fluorescence.

The time-correlated single photon counting (TCSPC) method, pioneered by Bollinger and Thomas in 1961, offers an effective solution to these challenges. In TCSPC, each photon's arrival time at the detector is measured relative to the excitation pulse, allowing for a highly precise and efficient measurement of fluorescence decay profiles.[2,3] This process is repeated over many cycles until a histogram of the decay waveform is generated. TCSPC is particularly sensitive to low-level signals due to its statistical approach. In TCSPC measurements, a high repetition rate laser source is used. The principle is that detecting a single photon within each pulse period is unlikely, and detecting two photons is even more so. Therefore, only the first photon detected between two consecutive excitations of the sample is considered. The excitation pulse acts as the "start" signal, while the first detected photon serves as the "stop" signal. The time difference between these signals is measured and stored. Following the single-photon detection criterion, there may be cycles with no detected photon, which is acceptable, as photon detection per cycle is random, and the distribution will emerge statistically over many repetitions. Whenever a photon is detected in a cycle, a count of 1 is recorded in memory, and its arrival time is noted. The critical component in this data recording process is the time-to-amplitude converter (TAC). The excitation pulse sends a synchronization signal (the "start" signal) to the TAC, initiating the charging of an internal capacitor.

When the emission photon, or "stop" signal, is detected, the capacitor stops charging. During this interval, the capacitor voltage increases linearly, creating a voltage ramp. An analog-to-digital converter, called a multichannel analyzer (MCA), stores the magnitude of this voltage in a designated channel based on the time. Over repeated cycles, the complete histogram is stored in the MCA. To adhere to the one-photon-per-cycle principle, the experimental stop rate should be kept below 2% of the start rate. This ratio is essential when accounting for the "dead time" of the electronics, which is the minimum time required to detect two successive photons. If the stop rate is too high, multiple photons may arrive within one cycle, and the first emitted photon might not be detected first if it falls within the electronics' dead time. This can lead to "pulse pile-up," resulting in an overrepresentation of certain points in the histogram.[2,3]

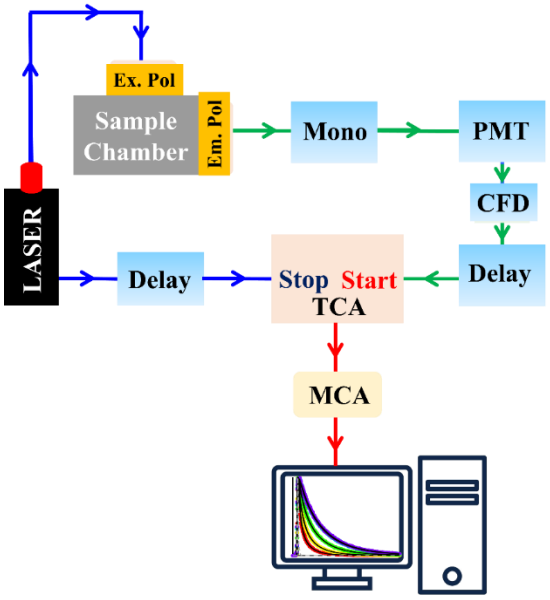

Figure 2.2.2.1: Schematic diagram of a standard TCSPC setup along with typical lifetime decay data

The detector in a modern TCSPC setup is a multichannel plate photomultiplier tube (MCP PMT). The advantage of using an MCP PMT over single-electron response detectors or standard PMTs lies in its reduced transit time spread (TTS), which significantly impacts the instrument's time resolution. When a photoelectron is generated at the cathode of a PMT, it undergoes amplification in the dynodes. This

multiplication process results in a group of electrons with varying velocities that may follow different paths to the anode, leading to a distribution of transit times, defined as the TTS. MCP PMTs exhibit lower TTS compared to regular PMTs, which makes them preferable as TTS directly affects the instrument response.

The electronics' rise and fall times in the TCSPC setup introduces time jitter in the measurement. Additionally, the random amplification of optical signals by the detector may cause amplitude jitter in the electric signal. If a simple discriminator is used to transmit signals to the TAC, it may trigger when the leading edge of an electric pulse exceeds a certain threshold, introducing inconsistencies. To address this, a constant fraction discriminator (CFD) is employed in TCSPC. A CFD triggers a signal to the TAC at a constant fraction of the pulse height, effectively reducing height-induced time jitters. The instrument response function (IRF) of a TCSPC system, recorded by measuring the signal from a scattering process, is influenced by factors such as laser pulse width, TTS, and additional time jitters in the setup. A schematic diagram illustrating the components of a TCSPC setup is shown in Figure 2.2.1.1.

In my experiments, I have used the TCSPC instrument LifeSpec II from Edinburgh Instruments, U.K. This instrument is equipped with thermoelectrically cooled Hamamatsu R3809-50 MCP PMT with intrinsic detector response <25 ps. The excitation sources are picosecond pulse diode lasers (EPL-series) from the same company. For my experiments, I have used 375 and 405 nm diode lasers with 80 ps pulse width. The IRF of this instrument measured by scattering from Ludox suspension was 120 ps. All the data were acquired at Magic Angle polarization to avoid any contribution from the rotational diffusion of the molecules. The data obtained from the instrument was analyzed in FAST and DAS software respectively. A brief overview of the fitting procedure is presented here.

2.2.2. Data Analysis Procedure

The data analysis procedure is complex because the excitation pulse is not a delta function; it has a finite width in the time domain, and the instrument's IRF also has a finite width. These factors influence the data, resulting in the measured fluorescence decay becoming a convolution of the IRF and the actual fluorescence intensity decay.

$$I(t) = \int_0^t P(t)F(t - t')dt' \quad (2.2.2.1)$$

Using this convolution to fit the data is challenging, as the problem is inherently ill-posed. Accurate fitting requires the exact form of the IRF or prompt, a theoretical model of the fluorescence, and minimized experimental noise. Consequently, most commercial software, like FAST or DAS, applies iterative methods or specifically the non-linear least squares method to extract fluorescence lifetimes. Initially, the pure fluorescence intensity decay is estimated as a sum of lifetime components, each weighted by their respective amplitudes, as follows.[4–8]

$$F(t) = \sum_{i=1}^{n} a_i e^{-\frac{t}{\tau_i}} \quad (2.2.2.2)$$

$$\sum_{i=1}^{n} a_i = 1 \quad (2.2.2.3)$$

Here, τ_i represents the lifetime components, and a_i represents their respective amplitudes. The IRF profile is recorded using a scatter, as mentioned previously, but is measured at the excitation wavelength rather than the emission wavelength, which is fundamentally inaccurate. Nonetheless, recording the IRF with the same number of channels is necessary for reconvolution. Since this reconvolution is performed in a quantized manner, i.e., on a per-channel basis, a sum is used in place of integration in equation 2.2.2.1. The IRF is considered as a series of δ-functions, each with distinct amplitudes across channels. The measured data can thus be expressed as[4–8]

$$I(t) = \sum_{t_i=0}^{t} P(t)F(t - t_i)\Delta t \quad (2.2.2.4)$$

In the equation above, Δt represents the time per channel. Two additional parameters are required in the final fitting equation. A slight mismatch in the time-zero positions between the IRF and intensity decay data is accounted for by a shift parameter (Δ). Additionally, a noise factor (A) is included for accurate fitting. Altogether, the final form of the equation is

$$D(t) = A + I(t + \Delta) \quad (2.2.2.5)$$

The consistency of the assumed model is tested by the "goodness of the fit".[4–8]

$$\chi^2 = \sum_{j=1}^{n} \frac{[Y(j)-D(j)]^2}{\sigma_j^2} \quad (2.2.2.6)$$

In the above equation, $Y(j)$ is the fitted data, $D(j)$ is the experimental data and σ_j^2 is the standard deviation. However, χ^2 is not the best choice for many data points. Instead, a quantity ${\chi^2}_R$ is defined as

$$\chi_R^2 = \frac{\chi^2}{n-p} \quad (2.2.2.7)$$

In this context, *n* denotes the number of data points, while *p* represents the number of fitting parameters. For TCSPC (Time-Correlated Single Photon Counting) measurements, *n* is typically much larger than *p*. The goodness of fit is evaluated using the chi-squared χ^2 statistic, which is minimized by adjusting the fitting parameters within a multiexponential decay model. The fit is considered acceptable based on the comparative χ^2 values obtained for different parameter sets. However, a key challenge of this iterative approach is the reliance on intuition when selecting the appropriate model, as multiple models may yield statistically similar fits. Therefore, incorporating prior knowledge about the system is essential to ensure reliable and physically meaningful TCSPC fitting.

2.3. Femtosecond Fluorescence up-conversion spectroscopy

2.3.1. Basic Principle

Fluorescence up-conversion spectroscopy operates on the principle of cross-correlation between the emission from an electronically excited molecule and a gate beam. This optical gating of fluorescence was first described by Hallidy and Topp in 1977.[9] The use of femtosecond lasers has allowed this technique to measure fluorescence intensity decays across the sub-picosecond to nanosecond time domains.[10–13] In this method, the second harmonic of a femtosecond oscillator (here, a mode-locked Ti:laser operating at frequency (ω_1)) is employed to electronically excite the sample.

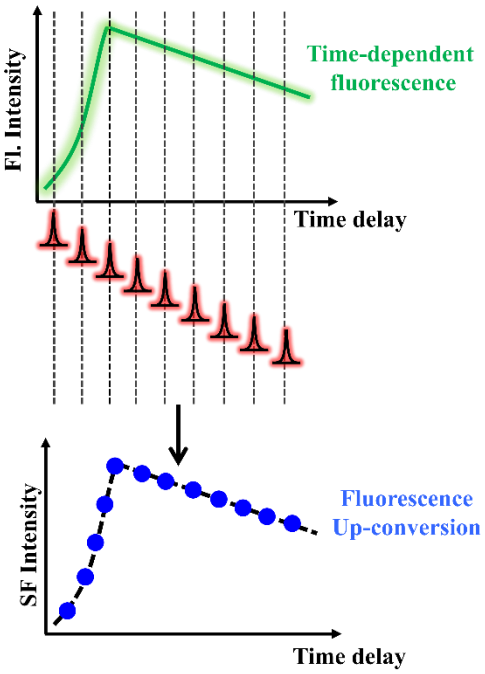

Figure 2.3.1.1. Schematic principle of fluorescence up-conversion spectroscopy

As shown in Figure 2.3.1.1, the arrival of the excitation pulse at the sample establishes time zero (t=0), leading to the emission of incoherent fluorescent light (ω_2) from the excited molecules. This fluorescent light is mixed with the gate pulse essentially the residual fundamental gate light arriving at t=τ in a nonlinear crystal

(such as β-barium borate or potassium di-deuterium phosphate), generating the sum frequency (ω_3) of the two signals.

$$\omega_3 = \omega_1 + \omega_2 \quad (2.3.1.1)$$

The arrival time of the gate pulse is controlled by a mechanical delay stage. It can be demonstrated that, at any given moment, the intensity of the sum frequency light (I_{sum}) is proportional to the cross-correlation function of the fluorescence (I_{fl}) and gate beam (I_G).[10]

$$I_{sum} \propto \int_{-\infty}^{+\infty} I_{fl}(t) I_G(t-\tau) dt \quad (2.3.1.2)$$

The sum frequency light is only generated when the gate pulse is present in the crystal, and thus, we can achieve time resolution comparable to laser pulse width.

2.3.2. Instrumental setup

The schematic optical layout of the instrument (FOG 100, CDP Systems, Moscow, Russia), along with the external laser source, is illustrated in Figure 2.3.2.1. The setup employs a mode-locked Ti:laser (Mai-Tai HP, Spectra Physics, USA) operating at an 80 MHz repetition rate with an average power of ~2.5 W and a pulse width of ~100 fs as the fundamental frequency radiation ω_1. The light is focused onto a β-barium borate crystal (BBO, 0.2 mm thickness) to generate the second harmonic ($2\omega_1$) of the fundamental light, which serves as the excitation source for the sample.

The generated second harmonic, along with the fundamental light, is collimated by lens L_2 onto a dichroic mirror/beamsplitter (DM_1), which separates the input beam into excitation and gate beams. The reflected excitation beam then passes through a Berek polarizer (B) to adjust its polarization. Neutral density filters (ND filters, F) are placed before the polarizer to control the intensity of the excitation light, and cut-off filters are used to eliminate any residual fundamental light. The excitation beam is then directed by another beamsplitter (BS_1) and focused onto the rotating sample

cell (S) using lens L_3. The fluorescence emission from the sample (ω_2)is collected by lens L_4 and passed through a second cut-off filter (F_2) to block the excitation light ($2\omega_1$). The gate beam is directed by mirrors M_3 and M_4 to a gold-coated retroreflector (RR) mounted on a mechanical delay line, which is controlled by software. Both the emission and the gate pulse are collected by lens L_5 and focused onto a second nonlinear BBO crystal (0.2 mm or 0.5 mm thick) to generate the sum frequency i.e. $\omega_3 = \omega_1 + \omega_2$ of the two incident beams.

In the experiments described in this thesis, the fluorescence is in the visible region, the gate pulse is in the near-IR region, and the resulting sum frequency is in the UV region. The emission and gate beams are blocked from reaching the detector using an iris and appropriate cut-off filters (F_3). Lens L_7 then focuses the sum frequency light onto the input slit of the monochromator. The monochromator selects the sum frequency signal, which is detected by a photomultiplier tube (PMT) coupled with a photon counting device. Data acquisition, monochromator, and optical delay line control are managed by LUMEX software (CDP Corp).

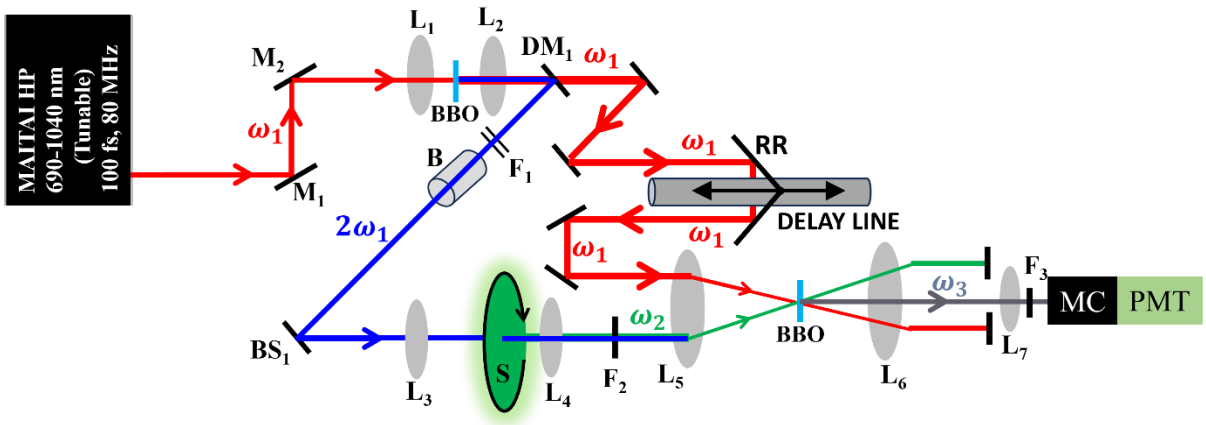

Figure 2.3.2.1 Schematic optical diagram of femtosecond fluorescence up-conversion

2.3.3. Principle of Second Harmonic and Sum Frequency Generation

Fluorescence up-conversion spectroscopy involves generating the sum frequency from the fluorescence emitted by the sample and the gate beam, as well as producing the second harmonic of the fundamental beam for excitation. Both of these processes are examples of nonlinear optical phenomena, which are discussed in this section. Under normal conditions, i.e., in the presence of low-intensity light, the medium's response to light is linear. In this case, optical behavior can be described using a linear refractive index for the medium. However, when exposed to intense, high-power laser light, the medium's response deviates from linearity. The electric field associated with such high-intensity radiation can alter the refractive index of the medium, giving rise to nonlinear effects.[14–16] The medium's response to the electric field of propagating electromagnetic radiation can be represented by a Taylor expansion of the dielectric polarization density (the dipole moment per unit volume) or, more simply, the induced polarization (P_k) as a function of the electric field (E_i) at time t.

$$P_k(t) = \epsilon_0\left(\chi_{ik}^{(1)}E_i(t) + \chi_{ijk}^{(2)}E_i(t)E_j(t) + \chi_{ijlk}^{(3)}E_i(t)E_j(t)E_l(t) + \cdots\right) \quad (2.3.3.1)$$

In the equation above, ϵ_0 represents the permittivity of vacuum, and $\chi^{(n)}$ denotes the n-th order optical susceptibility of the medium, which is an $(n+1)$ order tensor. On the right side of Equation 2.3.3.1, the first term corresponds to the linear response, while the higher-order terms represent the medium's nonlinear responses. For simplicity, P_k and E_i are treated as scalar quantities, considering the nonlinear optical process in a specific direction. Both second harmonic and sum frequency generation are second-order nonlinear phenomena, so I will refer only to the second-order polarization as[14–16]

$$P^{(2)}(t) = \epsilon_0\chi^{(2)}E^2(t) \quad (2.3.3.2)$$

Now let us consider the second-order response to a monochromatic input field of frequency ω is given by

$$E(t) = \mathcal{E}exp(-i\omega t) + \mathcal{E}^*exp(i\omega t) \quad (2.3.3.3)$$

In the above equation, $\mathcal{E}$ is the field amplitude. Plugging equation 2.3.3.3 to equation 2.3.3.2 we get the second-order response of the medium as

$$P^{(2)}(t) = 2\epsilon_0 \mathcal{E}\mathcal{E}^* + \left(\epsilon_0 \chi^{(2)} \mathcal{E}^2 exp(-i2\omega t) + \epsilon_0 \chi^{(2)} \mathcal{E}^{*2} exp(i2\omega t)\right) \quad (2.3.3.4)$$

The first term in equation 2.3.3.4 represents a constant static field, known as optical rectification, while the second term describes an output with a frequency twice that of the input field, known as second harmonic generation.[14–16] It's essential to note that the even-order terms in equation 2.3.3.1 will vanish if the crystal possesses inversion symmetry; thus, second harmonic generation occurs only in specific nonlinear optical (NLO) crystals. Another crucial aspect of nonlinear processes, such as frequency doubling, is the phase matching among interacting waves. This phase matching ensures that the amplitude contributions of the output wave from different parts of the NLO crystal are in phase at the crystal's end. In second harmonic generation, we produce light with twice the frequency, and its wave vector $k_{2\omega}$ is given by

$$k_{2\omega} = \frac{2\omega}{c} n_{2\omega} \quad (2.3.3.5)$$

In the above equation, c represents the speed of light and $n_{2\omega}$ is the refractive index for the second harmonic light. Similarly, the wave vector for the input light is given by

$$k_{\omega} = \frac{\omega}{c} n_{\omega} \quad (2.3.3.6)$$

In frequency doubling within a crystal, phase matching is achieved when $k_{2\omega} = k_{\omega}$, or equivalently, $n_{2\omega} = n_{\omega}$. However, dispersion prevents this condition from naturally occurring. To overcome this, birefringent crystals are used, where the refractive index differs for light of different polarizations. Phase matching is then achieved by using extraordinary polarization for ω and ordinary polarization for 2ω, such that $n_o(2\omega) = n_e(\omega)$. Additionally, the intensity of the sum frequency signal generated in an NLO crystal of a given thickness is given by

$$I_{sig}(\lambda) \propto \left(\frac{L}{\lambda}\right)^2 sinc^2\left(\frac{\Delta k L}{2}\right) \quad (2.3.3.7)$$

$$\Delta k(\lambda) = \frac{4\pi}{\lambda}\left(n_\lambda - n_{\frac{\lambda}{2}}\right) \quad (2.3.3.8)$$

Therefore, phase matching is effective only for light of a specific wavelength. However, femtosecond laser pulses possess a broad spectral bandwidth, and the efficiency of frequency doubling across this bandwidth is governed by the full width at half maximum (FWHM) of the $sinc^2\left(\frac{\Delta kL}{2}\right)$ function, where Δk is the phase mismatch and L is the crystal length. In our case, as described in the previous section, a BBO crystal with a thickness of approximately 0.2 mm was used. Since BBO is a negatively birefringent crystal, the phase-matching condition is satisfied only when the input (fundamental) radiation is ordinarily polarized and the generated second harmonic light is extraordinarily polarized. In the setup I used, a BBO crystal was also employed to generate the sum frequency signal by mixing the sample's emitted fluorescence with the gate pulse. In sum frequency generation (SFG), two incident beams of different wavelengths—or equivalently, different frequencies—interact within a nonlinear medium to produce a new beam whose frequency is the sum of the two inputs.[14–16]

$$E(t) = \mathcal{E}_1 exp(-i\omega_1 t) + \mathcal{E}_2 exp(-i\omega_2 t) + c.c. \quad (2.3.3.9)$$

Here, $c.c.$ denotes complex conjugate. Replacing equation 2.3.3.9 into equation 2.3.3.2 gives us

$$P^{(2)}(t) = 2\epsilon_0(\mathcal{E}_1\mathcal{E}_1^* + \mathcal{E}_2\mathcal{E}_2^*) + \epsilon_0\chi^{(2)}[\mathcal{E}_1^2 exp(-2i\omega_1 t) + \mathcal{E}_2^2 exp(-2i\omega_2 t) + 2\mathcal{E}_1\mathcal{E}_2 exp(-2i(\omega_1 + \omega_2)t) + 2\mathcal{E}_1\mathcal{E}_2^* exp(-2i(\omega_1 - \omega_2)t) + c.c.] \quad (2.3.3.10)$$

In this case, the nonlinear interaction can give rise to sum frequency $(\omega_1 + \omega_2)$, difference frequency $(\omega_1 - \omega_2)$, and optical rectification signals. Phase matching plays a critical role in determining the efficiency of these processes. Depending on the phase-matching condition, either the sum frequency or the difference frequency signal will be generated with significantly higher intensity. For sum frequency generation (SFG), the phase matching condition requires that the wave vectors of the interacting beams satisfy[11–16]

$$k_3 = k_1 + k_2 \quad (2.3.3.11)$$

In the equation above, k_3 represents the wave vector of the sum frequency light, while k_1 and k_2 represent those of the input beams. In a crystal, the refractive index experienced by one polarization of light can be adjusted by changing the angle. For simplicity, if we consider a uniaxial crystal, where $n_x = n_y = n_o$ and $n_z = n_e$ with the z-axis as the optical axis, we can express the phase-matching condition as follows:[11–16]

$$\frac{1}{n_e^2(\theta)} = \frac{cos^2\theta}{n_o^2(\theta)} + \frac{sin^2\theta}{n_o^2(\theta)} \qquad (2.3.3.12)$$

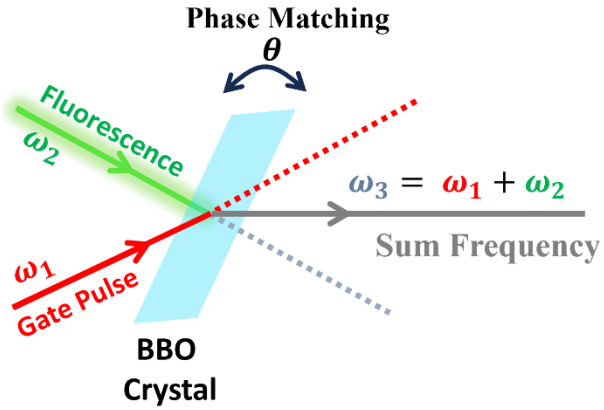

Figure 2.3.3.1 Schematic diagram depicting sum frequency generation in a BBO crystal

It should be noted that there are two primary types of phase matching: Type 1, where the output wave has a different polarization from the input waves, and Type 2, where one of the input waves has a different polarization than the other two. In my setup, the sample fluorescence was collected with a lens, and any leaking excitation light was removed using a cut-off filter. The gate beam and fluorescence beam were then focused onto the BBO crystal through another lens. As I have measured fluorescence intensity decay at various wavelengths for different samples, data acquisition at a particular wavelength required rotating the BBO crystal to the appropriate phase-matching angle. This ensured that the intensity of the sum frequency signal, generated from the gate light and the specific wavelength of fluorescence, was maximized. It's worth mentioning that most fluorescence up-conversion systems utilize only Type 1 phase matching.

To collect fluorescence intensity decays at magic-angle polarization, the pump beam was rotated relative to the gate beam to a specific angle using a Berek compensator. The Berek compensator consists of a uniaxial crystal, which, when tilted at a specific angle, makes the axis in the plane of incidence extraordinary, allowing light of a certain wavelength to be rotated to any desired angle depending on the tilt.

2.3.4. Data Analysis Procedure

When measuring the fluorescence intensity decay of a fluorophore with a long lifetime, we can approximate the excitation pulse as a δ-function, implying it has no width in the time domain. However, in femtosecond fluorescence up-conversion spectroscopy, we deal with lifetime components in the sub-picosecond time domain, rendering this assumption invalid, as no optical pulse has zero width. Additionally, as the laser pulse passes through various dispersive optics, it naturally broadens. Nonlinear optical (NLO) crystals also introduce dispersion, resulting in an overall instrument response function (IRF) with a finite, non-negligible width.

In my setup, I measured the IRF before each experiment using the Raman signal of water, which is shifted by about 3300 cm^{-1} relative to the excitation light.[11–13,17] The Raman scattering process has zero-time delay, so when the sum frequency of the water Raman and gate beams was generated, the temporal profile of the pulses was preserved. The intensity of the water Raman signal at different time delays reflects the cross-correlation function, as described in equation 2.3.1.2. By replacing the sample cell with a water cell and measuring the decay at a specific wavelength, I obtained an IRF that could be accurately modelled by a Gaussian function with a full width at half maximum (FWHM) of approximately 250 fs.

$$G(x) = \frac{1}{\sigma\sqrt{2\pi}} e^{-(x-\mu)^2/2\sigma^2} \qquad (2.3.4.1)$$

In the above equation, σ is the width parameter of the Gaussian and μ is the x-axis position of the function. The FWHM (H) of the above function is given by

$$H = 2\sigma\sqrt{2\ln 2} \approx 2.3548\sigma \qquad (2.3.4.2)$$

For simplicity, we assume excitation occurs instantaneously at zero time, so I used a Gaussian function with μ=0 for data analysis. In time-resolved fluorescence lifetime measurements using pulsed light, the decay curve is influenced by the finite width of the pulse, which can distort very short-lifetime components. Extracting the true intensity decay from such data is essential, particularly for short-lived species. This process of isolating the actual signal from any extraneous contributions is called deconvolution. Fluorescence intensity decays obtained from femtosecond fluorescence up-conversion measurements are convolutions of the instrument response function (IRF) and the sample's actual decay profile. To derive the lifetime components, I fitted each decay curve to a convolution of the IRF with a sum of exponential functions. Here, I briefly present the convolution of a Gaussian IRF with a single exponential function, which can also be extended to multiple exponential components. Setting, $\mu = 0$ in equation 2.3.4.1

$$G(x) = \frac{1}{\sigma\sqrt{2\pi}} e^{-x^2/2\sigma^2} \tag{2.3.4.3}$$

$$S(x) = exp(-\frac{x}{\tau}) \tag{2.3.4.4}$$

In equation 2.3.4.4, τ is the lifetime. Now the convolution is defined as

$$I(t) = G(x) * S(x) = \frac{1}{\sigma\sqrt{2\pi}} \int_0^\infty exp\left(-\frac{x}{\tau}\right) exp\left(-(t-x)^2/2\sigma^2\right) dx =$$

$$\frac{1}{\sigma\sqrt{2\pi}} \int_0^\infty exp\left(-\frac{\left(x^2+t^2+\frac{2\sigma^2 x}{\tau}-2tx\right)}{2\sigma^2}\right) dx \tag{2.3.4.5}$$

Now using the transformation,

$$z = \frac{\left(x-\left(t-\frac{\sigma^2}{\tau}\right)\right)}{\sigma\sqrt{2}} \tag{2.3.4.6}$$

$$\frac{\left(x^2+t^2+\frac{2\sigma^2 x}{\tau}-2tx\right)}{2\sigma^2} = z^2 + \frac{1}{\tau}\left[t - \frac{\sigma^2}{2\tau}\right] \tag{2.3.4.7}$$

Using equations 2.3.4.6 and 2.3.4.7 in equation 2.3.4.5 we get,

$$I(t) = \frac{1}{\sqrt{\pi}} exp\left(-\frac{1}{\tau}\left(t - \frac{\sigma^2}{2\tau}\right)\right) \int_{-\left(\frac{t-\frac{\sigma^2}{\tau}}{\sigma\sqrt{2}}\right)}^{\infty} exp(-z^2)dz \quad (2.3.4.8)$$

Now the error function is introduced as

$$erf(x) = \frac{2}{\sqrt{\pi}} \int_0^x exp(-z^2)\, dz \quad (2.3.4.9)$$

Here, it should be noted that error function is an odd function which means $erf(x) = erf(-x)$. Now introducing the error function in equation 2.3.4.9 gives

$$I(t) = \frac{1}{\sqrt{\pi}} exp\left(\frac{\sigma^2}{2\tau^2} - \frac{t}{\tau}\right)\left(1 - erf\left(\frac{\sigma^2 - t\tau}{\sqrt{2}\sigma t}\right)\right) \quad (2.3.4.10)$$

The above equation was applied to fit the fluorescence intensity decay data, where equation 2.3.4.10 represents the convolution of a single exponential function with a Gaussian. However, fitting the data often requires more than one exponential term. Since convolution is a linear operation that adheres to both the distributive and additive properties, equation 2.3.4.10 was expanded for multiexponential fitting as a summation of multiple exponential functions, each convolved with the same Gaussian and weighted accordingly. Therefore, in this thesis, any mention of multiexponential fitting refers to this expanded convoluted model. All up-conversion data fitting was performed using IGOR Pro (WaveMetrics, Inc.) software.

2.4. Time-Resolved Emission Spectra

Fluorescence intensity decay over time at a specific wavelength, recorded using techniques like TCSPC or fluorescence up-conversion spectroscopy, reveals details about excited-state processes. Another key approach to studying photoexcited molecules is time-resolved emission spectra (TRES). Unlike steady-state emission spectra—which reflect a time-averaged view of TRES—analyzing TRES provides critical insights into dynamic excited-state phenomena such as charge transfer and excited-state reactions.[7,18–22] Additionally, TRES can shed light on how excited

molecules interact with surrounding solvents.[7] Although earlier methods for recording TRES at different times were often affected by instrument response distortions,[18–22] it is now possible to derive TRES by combining fluorescence decays measured across various wavelengths throughout the emission range.[7,18–22] This method provides a robust, high-resolution picture of excited-state dynamics (for details, see Chapter 1).

$$I(\lambda, t) = \frac{I_{ss}(\lambda)}{\sum_i a_i \tau_i} \sum_{i=0}^{n} a_i e^{-t/\tau_i} \qquad (2.4.1)$$

As outlined in equation 2.4.1, recording the fluorescence intensity decay at a specific wavelength, along with knowledge of the steady-state intensity, allows us to reconstruct the time-dependent intensity profile. This approach was applied across several wavelengths to gather multiple data points, enabling the construction of each TRES. Each of these spectra was then fitted to a lognormal function, as described by Maroncelli and Fleming, to accurately represent the time-resolved emission behavior.[20,21]

$$L(\nu) = g_0 exp\left\{-\ln 2\left(\frac{\ln\left(1+\frac{2b(\nu-\nu_p)}{\Delta}\right)}{b}\right)^2\right\} \qquad (2.4.2)$$

In the above equation, g_0, b, ν_p, Δ represent the peak height, asymmetry parameter, peak frequency, and width parameter, respectively. The width parameter Δ, is related to the full width at half maximum (FWHM), denoted as Γ, by the following relationship[20,21]

$$\Gamma = \Delta\left(\frac{\sinh(b)}{b}\right) \qquad (2.4.3)$$

The fitting was performed using IGOR Pro software, and the resulting parameters were analyzed to gain insights into various excited-state processes. These findings and their implications will be discussed in detail in the relevant sections.

2.5. Femtosecond Broadband Transient Absorption Spectroscopy

2.5.1. Basic Principle

Femtosecond molecular dynamics can be studied by various methods, with pump-probe techniques being among the most widely used. One prominent example is broadband transient absorption spectroscopy. In typical pump-probe experiments, an ultrashort laser pulse, known as the pump, initiates a non-stationary molecular state, and the evolution of this excited state is then monitored by a second, time-delayed pulse called the probe.[23–26] In transient absorption spectroscopy, resonant excitation is applied, meaning that the pump pulse populates the excited electronic state, and this population decays over time, unlike the instantaneous response seen in Raman spectroscopy.[23–26] The dynamics observed in the excited state depend on the choice of the probe pulse, which may be monochromatic or broadband and span the UV-Visible or IR regions, each revealing different photophysical properties of the molecule.[23–26] Additionally, the effect of the pump pulse can be detected either through changes in characteristics (such as intensity) of the probe or through subsequent events triggered by the probe itself post-pump interaction. Transient absorption spectroscopy demonstrates the first case, observing the change in probe intensity due to the pump's action.[23–26] We observe the first case in transient absorption spectroscopy.

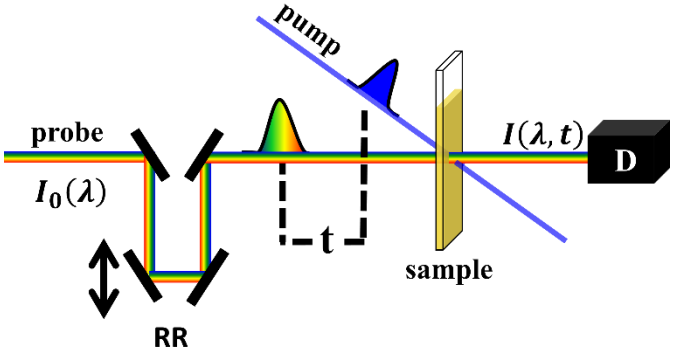

Figure 2.5.1.1. Schematic representation of transient absorption spectroscopy experiment

In our lab setup, either 400 nm or 266 nm light was used as the pump to excite a fraction of molecules to their electronic excited states. A visible white light continuum (WLC) probe, spanning 450–750 nm, is then passed through the sample at various delay times, controlled by a mechanical delay stage, while the pump light is diverted. The detector monitors the change in probe light intensity across these delays, as shown schematically in Figure 2.5.1.1. The probe intensity is kept significantly lower than that of the pump to prevent any unintended multistep or multiphoton interactions from the probe itself. Detection is conducted simultaneously over the probe spectrum range at specific time points, repeating across multiple delay times in a time-gated manner.[23–26] Since this is an absorption spectroscopy setup, the probe light intensity change follows the Lambert-Beer law.

$$I(\lambda, t) = I_0(\lambda) \times 10^{-\varepsilon(\lambda)N(t)l} \quad (2.5.1.1)$$

In equation 2.5.1.1, $I_0(\lambda)$ and $I(\lambda, t)$ represent the intensities of the probe light before and after it passes through the sample, respectively, at a delay time t, as depicted in Figure 2.5.1.1. The time zero is defined as the specific delay position where the pump and probe pulses reach the sample simultaneously. Here, $\varepsilon(\lambda)$ denotes the molar extinction coefficient at wavelength λ, $N(t)$ is the population of the excited state at time t after pump excitation, and l is the path length of the sample. Based on Figure 2.5.1.1 and equation 2.5.1.1, the absorbance $A(\lambda, t)$ is therefore given by

$$A(\lambda, t) = log \frac{I_0(\lambda)}{I(\lambda,t)} = \varepsilon(\lambda)N(t)l \quad (2.5.1.2)$$

In transient absorption techniques, the key observed quantity is the change in absorbance due to the presence or absence of the pump pulse. This change, $\Delta A(\lambda, t)$, can be mathematically expressed as:

$$\Delta A(\lambda, t) = A(\lambda, t) - A(\lambda) \quad (2.5.1.3)$$

$$\Delta A(\lambda, t) = log \frac{I_0(\lambda)}{I(\lambda,t)} - log \frac{I_0(\lambda)}{I(\lambda)} = log \frac{I(\lambda)}{I(\lambda,t)} \quad (2.5.1.4)$$

Equation 2.5.1.4 describes how the observable quantity, $\Delta A(\lambda, t)$, can be obtained by measuring the probe intensity with and without the sample being illuminated by the pump. Thus, we can express this as

$$\Delta A(\lambda, t) = log \frac{I^{probe}}{I^{probe}_{pump}} \quad (2.5.1.5)$$

In equation 2.5.1.5, it is important to note that I^{probe} is measured with the pump light completely blocked by a chopper. The population created or depleted by the pump light evolves over time, meaning that as $N(t)$ changes, so does $\Delta A(\lambda, t)$, allowing us to track the photophysical dynamics of the system. Additionally, because the observable $N(t)$ does not include an $I_0(\lambda)$ term, there is no need to measure the probe intensity before the sample, meaning a single-beam spectrophotometer is sufficient. However, to further reduce noise in the probe signal, dual-beam spectrophotometers are commonly used. This pump-probe technique, being an absorption spectroscopy method, can detect both radiative and non-radiative processes depending on the spectral range of the probe.[23–26] Four primary processes can be observed in transient absorption spectroscopy, as illustrated in Figure 2.5.1.2 and detailed below.

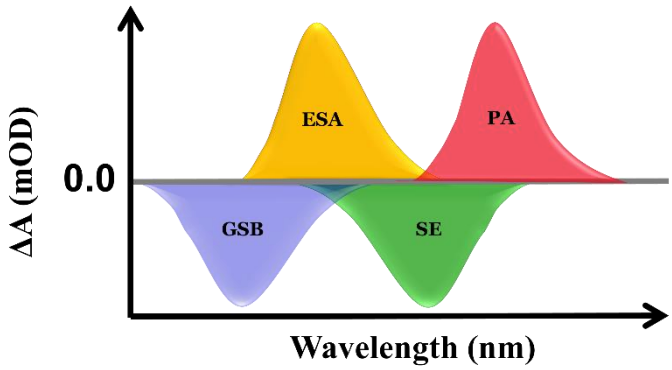

Figure 2.5.1.2. Contribution of different photophysical processes in transient absorption spectra

Ground State Bleaching (GSB): When the pump pulse excites a portion of molecules from the ground state to the excited state, the population in the ground state decreases. As a result, fewer ground-state molecules are available to absorb the probe light following pump excitation, leading to a lower absorption compared to the case without pump excitation i.e., $I^{probe} < I^{probe}_{pump}$. This causes a negative ΔA spectrum, which diminishes as the time delay between the pump and probe increases

due to the gradual return of excited molecules to the ground state. This signal, indicating reduced ground-state absorption, is referred to as ground state bleaching (GSB).

Stimulated Emission (SE): In addition to spontaneous emission (fluorescence) that returns molecules from the excited to the ground state, a resonating photon from external radiation can trigger emission from the excited state in a process known as stimulated emission. Here, if the probe pulse includes frequencies that resonate with the transitions between the excited and ground states (including vibrational levels), it can induce stimulated emission from molecules excited by the pump. The stimulated emission photons travel in the same direction as the probe photons, thereby increasing the detected probe intensity at specific wavelengths after pump excitation. This means $I^{probe} < I^{probe}_{pump}$, resulting in a negative ΔA signal in the transient absorption spectrum. This SE signal resembles the molecule's spontaneous emission spectrum and remains Stokes-shifted relative to the GSB signal, though there may be considerable overlap at very short delay times. The SE signal diminishes over time as the excited-state population decays through various radiative and non-radiative processes, assuming the probe intensity is low enough not to significantly alter the excited-state population.

Excited State Absorption (ESA): Transient absorption spectroscopy enables the detection of transitions that are inaccessible to fluorescence techniques, such as excited state absorption (ESA). When the pump pulse excites molecules to a specific electronic excited state, certain wavelengths in the probe light may resonate with the energy gap between this excited state and a higher-energy state, allowing the excited-state molecules to absorb the probe light. This transition, which does not occur in the absence of the pump, results in $I^{probe} > I^{probe}_{pump}$, producing a positive ΔA signal in the transient absorption spectrum.

Product Absorption (PA): Product absorption (PA) is another distinct feature in transient absorption spectroscopy that is challenging to capture with fluorescence techniques. After excitation, molecules may undergo transformations or excited-

state reactions, such as photoinduced electron or proton transfer, resulting in new transient species. These newly formed species can absorb the probe light, leading to an increase in detected probe intensity. This creates a positive ΔA signal in the transient absorption spectrum, as $I^{probe} > I^{probe}_{pump}$.

The ability to observe these four phenomena—ground state bleaching, stimulated emission, excited state absorption, and product absorption makes transient absorption spectroscopy an exceptionally powerful technique. However, its effectiveness can be limited by several factors, notably the spectral spread of the probe and the instrument response, which may restrict the detection of one or more of these processes.

2.5.2. Instrumental Setup

The femtosecond broadband transient absorption spectrometer used in our studies is a commercially available model (Femto-Frame-II, IB Photonics, Bulgaria), with its optical layout illustrated in Figure 2.5.2.1. This system is powered by an 800 nm output from a Ti:regenerative amplifier (SpitfirePro XP, Spectra-Physics, USA), which is pumped by a 20-W Q-switched Nd:laser (Empower, Spectra-Physics, USA) and seeded by a Ti-Sapphire femtosecond oscillator (MaiTai SP, Spectra-Physics, USA). The setup provides a pulse width of approximately 80 fs at a 1 kHz repetition rate, measured using a commercial autocorrelator. The fundamental 800 nm beam is divided by beamsplitter BS_1, creating two paths: one for generating the pump light and the other for the probe. The pump light is produced inside a JANOS tripler, also from IB Photonics. Here, the 800 nm beam is focused onto a BBO crystal, generating a 400 nm second harmonic. This 400 nm light, along with residual 800 nm light, passes through a waveplate and onto a second BBO crystal to generate the 266 nm third harmonic, following the principles in Section 2.3.3. Dichroic mirrors then separate these beams, directing either the 400 nm or 266 nm light as the excitation source via mirrors M_6 or M_7.

The probe path is routed through mirror M_5 to a retroreflector (RR) on a mechanical delay stage via mirrors MB_1, MB_2, and MB_3, allowing for a maximum 2 ns delay between pump and probe pulses. A small portion of the 800 nm beam is further split by BS_2 to illuminate a photodiode (PD) for controlling the chopper, while the main portion passes through a linear neutral density filter (ND_1) and an iris, focusing onto a 0.3 mm sapphire crystal via lens L_4.

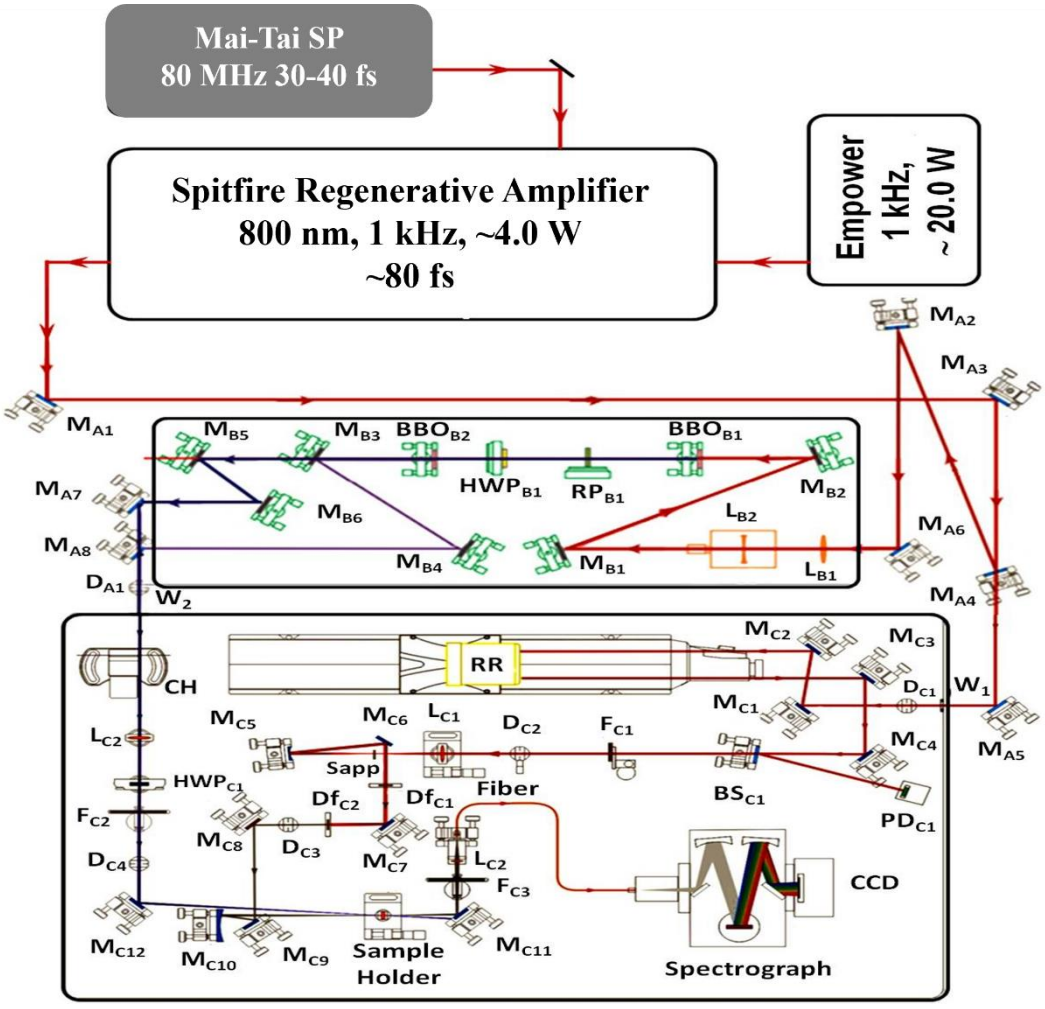

Figure 2.5.2.1. Optical layout of the femtosecond broadband transient absorption spectrometer

Thus, a white light continuum (WLC) probe spanning 450–750 nm is generated in the sapphire crystal (Sapp). The characteristics and shape of the WLC probe are controlled by the power and beam shape, which are adjusted with a neutral density (ND) filter and iris. After generation, the WLC probe is collected by parabolic mirror

MB_5 and directed through two notch filters (N_1 and N_2) that block residual 800 nm fundamental radiation, using mirrors MB_6 and MB_7. The probe light is then focused on the sample with parabolic mirror MB_{10}.

Meanwhile, the pump light passes through a chopper, and its polarization is adjusted relative to the probe using a half-wave plate. The power of the pump is controlled with a rotating ND filter (ND_2), and lens L_3 along with mirror MB_{12} focuses the pump beam to overlap with the probe beam in the sample cuvette, achieving a focal spot size of 100–200 µm. The chopper periodically blocks the pump beam to allow measurements without pump excitation, as previously described. Polarization control ensures that measurements are unaffected by any system anisotropy.

After passing through the sample, the probe beam is focused onto a 200 µm optical fiber cable using mirror MB_{11}, with ND filter (ND_3) adjusting the intensity of the probe light reaching the detector. The detector, a CCD spectrograph, captures the probe light scattered by a pair of diffraction gratings. Because the pump beam is angled slightly relative to the probe, it does not reach the detector. The zero-time point is calibrated by observing the signal of a reference sample (C152 in ethanol, in this case) and adjusting the delay accordingly. The entire setup is managed by software on the LABVIEW platform, with pump power maintained at ~5–10 µW during measurements. Steady-state absorption spectra are recorded before and after each experiment to verify that no photodegradation occurs in the sample.

For temperature dependent measurement, the temperature was maintained using a peltier temperature controller with a 2 °C accuracy. All the experiments were performed at 25 °C if not mentioned otherwise.

2.5.3. Instrument Response Function (IRF) and Chirp

In broadband transient absorption spectroscopy, the instrument response function (IRF) is determined by the cross-correlation of the pump and probe pulses.[27–29] While pulses are typically broadened when passing through optical elements, in pump-probe setups, additional factors such as instantaneous artifacts, group velocity

dispersion (GVD), and high-power pulse effects can influence data quality and IRF acquisition.

One such artifact is two-photon absorption (TPA), where a sample simultaneously absorbs photons from both the pump and spectrally broad probe pulse, causing unwanted changes in probe absorbance.[27–29] Another possible effect is stimulated Raman amplification (SRA), which may occur if the pump and probe frequencies are closely matched;[28,29] however, the spectral separation in this setup mitigates this issue, and SRA remains short-lived and within the IRF timescale. Cross-phase modulation (XPM) is yet another effect, arising when the intense pump light alters the refractive index of the medium, shifting the probe light spectrum primarily at time zero.[28,29] Each of these artifacts has a linear dependence on pump intensity and can be minimized by using a lower pump intensity, a higher optical density in the sample, and a less-chirped WLC probe. Still, these effects can notably influence IRF measurements.

In this setup, the IRF was measured by filling the sample cuvette with pure solvents, allowing the femtosecond pump pulse to generate an instantaneous, non-resonant signal, such as stimulated Raman scattering, impulsive Raman scattering, or off-resonant transient birefringence, which provide the pump-probe cross-correlation.[23,28–31] Two critical factors group velocity dispersion (GVD) and resulting chirp must be considered for accurate IRF and data analysis.

GVD is an optical effect where different wavelengths travel at different speeds through a medium, causing the red end of the probe spectrum to arrive faster than the blue. As the probe travels through the optics and sample, this wavelength-dependent spread over time introduces chirp, shifting the time zero position across wavelengths. Although GVD does not alter the sample's intrinsic dynamics, knowing the chirp allows for accurate cross-wavelength comparisons and global fitting. The chirp can be estimated by tracking the time-zero position of the pure solvent response across the probe spectrum.[23,28–31]

In addition to GVD, XPM from the pump on a chirped probe distorts the IRF shape, so the solvent response is modeled using a Gaussian function along with its first and

second derivatives to capture this modulation.[28–31] After measuring the solvent response, it is fitted across different wavelengths using a Gaussian function along with its first and second derivatives to accurately capture the IRF shape. The time positions obtained from these fits at various wavelengths are then used to estimate the chirp present in the data. To correct for this chirp, a polynomial fit is applied, and a specific position in the spectrum is designated as the time zero reference.

In Figure 2.5.3.1, I present the IRF measured across multiple wavelengths in solvents like acetonitrile, methanol, and chloroform, along with corresponding Gaussian fits. The Gaussian width varies between 50–60 fs, depending on the wavelength. Applying the width-to-FWHM relation from equation 2.3.4.2, the IRF is estimated to be around 120–140 fs. The figure clearly illustrates a trend where the IRF center shifts toward longer times at the probe's longer wavelengths, indicating a wavelength-dependent delay due to dispersion effects.

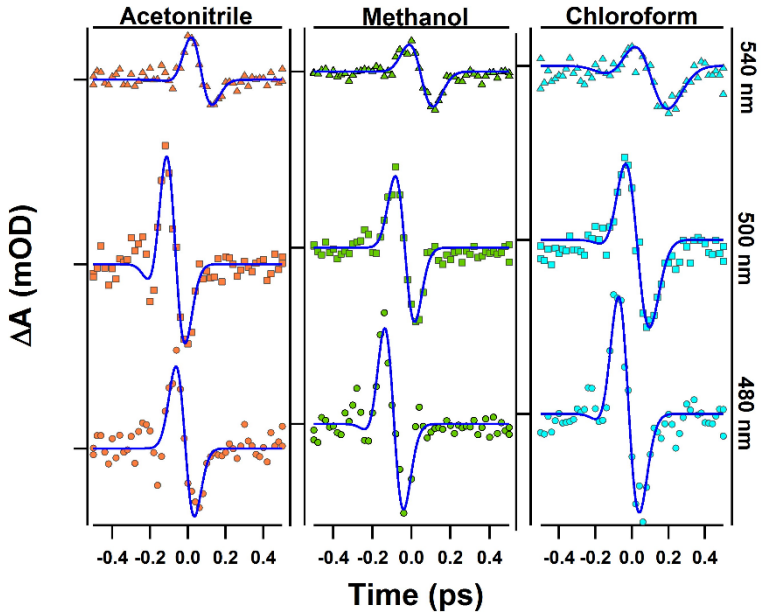

Figure 2.5.3.1. The IRF of the transient absorption setup was recorded in acetonitrile, methanol, and chloroform using a 400 nm pump. The solid blue lines indicate fitting.

2.5.4. Data Analysis

Broadband transient absorption spectroscopy generates large datasets that are analyzed simultaneously or "globally." This two-way dataset involves two independent experimental variables—time and wavelength—necessitating a model-based global analysis approach. For data analysis, I used the open-source Java-based software GLOTARAN, with operational details outlined in references 31[32] and 32[33]. Here, I briefly summarize the procedure.

In transient absorption data analysis, it is assumed that the data exhibits homogeneity, meaning that a single set of parameters can effectively describe the dataset, and that the overall dynamics can be attributed to distinct species or reaction pairs within the system. The data includes contributions from all the photophysical processes discussed in the previous section, across various times and wavelengths. Since the experiment is absorption-based, Beer-Lambert's law applies. Additionally, the dataset is considered as a superposition of spectral properties, each weighted by the concentration of the contributing species, allowing for a comprehensive analysis of the system's dynamic behavior.

$$\psi(t,\lambda) = \sum_{l=1}^{n_{comp}} c_l(t)\varepsilon_l(\lambda) \qquad (2.5.4.1)$$

In this formalism, $c_l(t)$ represents the concentration of the l-th component at time t, and $\varepsilon_l(\lambda)$ is the extinction coefficient of that component at wavelength λ. A typical global analysis can resolve up to 10 such components, with the minimum number of components needed to be determined based on prior knowledge of the system.

The data can be fitted using two approaches: by applying known concentration profiles $c_l(t)$, termed the kinetic model, or by using known extinction coefficients $\varepsilon_l(\lambda)$, known as the spectral model. In this study, we assume concentration profiles that vary exponentially with time, so the objective is to fit $\psi(t,\lambda)$ with a sufficient number of exponential components, each convoluted with the instrument response function (IRF). The IRF is modelled as a Gaussian, and the convolution of an exponential with a Gaussian, as described in Section 2.3.4, is used here.

The experimental dataset is structured as an m×n matrix, with measurements taken across mmm wavelengths at n time points. One approach to identify the number of independent components in this matrix is singular value decomposition (SVD), which is defined as[32,33]

$$\psi(t,\lambda) = \sum_{n=1}^{n_{max}} u_n(t) w_n(\lambda) SV_n \quad (2.5.4.2)$$

So, the minimum number of parameters required for fitting was initially estimated using singular value decomposition (SVD). Once this baseline was established, the entire dataset was fitted simultaneously by applying a sum of exponential functions convoluted with the Gaussian-modeled IRF. To account for dispersion effects across the wavelengths, a polynomial function was incorporated into the fitting process to model the wavelength-dependent temporal shifts accurately. This approach allowed for a comprehensive global fit, capturing both the kinetic and spectral dynamics in the dataset.

2.6. Density Functional Theory (DFT) Calculations

Predicting the photophysical behavior of a molecule requires a thorough understanding of its electronic structure in both ground and excited states, the energy gaps between these levels, electron density distributions in molecular orbitals, and more. Additionally, examining how electronic state energies shift with changes in molecular geometry provides valuable insights for photochemists into a molecule's properties.[34–38] Computational chemistry plays a crucial role in this analysis, and for this thesis, I used density functional theory (DFT) calculations extensively. All calculations were conducted using Gaussian 16, and results were visualized with GaussView 05 software.[39]

Density functional theory (DFT) is among the most powerful tools for modeling molecular electronic structure.[34–38] The theory's foundational papers were published in 1964 and 1965, leading to Walter Kohn's Nobel Prize in Chemistry in 1998.[40,41] While DFT was used for ground-state geometry and electronic structure

calculations, excited-state calculations require time-dependent potentials, which are incorporated in time-dependent density functional theory (TDDFT). In this section, I will outline the fundamental concepts underlying these methods, which formed the basis for the computations, without delving into detailed theoretical explanations. Here, I will discuss the basic concepts underlying the computations performed, focusing on the foundational approach without detailed theoretical explanations.

For any quantum chemical calculation of the ground state, the objective is to solve the time-independent Schrödinger equation. Under the Born-Oppenheimer approximation, this equation is simplified by separating the nuclear and electronic motions, allowing it to be expressed as

$$\widehat{H}_{el}\psi_{el} = E_{el}\psi_{el} \quad (2.6.1)$$

In an N-electron M-nuclei system the electronic Hamiltonian is given by

$$\widehat{H}_{el} = -\frac{1}{2}\sum_{i=1}^{N}\nabla_i^2 - \sum_{i=1}^{N}\sum_{A=1}^{M}\frac{Z_A}{r_{iA}} + \sum_{i=1}^{N}\sum_{j>i}^{N}\frac{1}{r_{ij}} \quad (2.6.2)$$

The challenge with equation 2.6.2 is that it cannot be solved exactly without significant approximations, and even then, constructing an accurate wavefunction is complex due to the numerous degrees of freedom involved. Additionally, the wavefunction itself is a non-observable quantity, making it impossible to measure directly.[34–38] In density functional theory (DFT), the state of the system is defined by the electron density of interacting electrons, rather than by their individual interactions—a concept that applies to any system of fermions.[34–38] Unlike, the wavefunction, electron density is observable, meaning it can be measured, and calculations do not require knowledge of every coordinate to determine expectation values.[34–38] The first Hohenberg-Kohn theorem establishes that the electron density uniquely determines all ground-state properties of the system.[34–38] Consequently, the total energy ($E[\rho]$) of the system is a functional of the electron density (ρ) in the presence of an external potential ($v_{ext}(r)$) , such as the electric field generated by the nuclei.[34–38]

$$E[\rho] = F[\rho] + \int v_{ext}(r)\rho(r)dr \quad (2.6.3)$$

The second Hohenberg-Kohn theorem states that the variational principle applies to $E[\rho]$; thus, the energy $E[\rho]$ reaches a minimum when ρ corresponds to the equilibrium electron density. Here, $F[\rho]$ is a universal functional, meaning it is independent of any external potential.[34–38]

The approach for calculating this functional was provided by the Kohn-Sham theorem, which expresses the ground-state electronic energy $E[\rho]$ as:

$$E[\rho] = -\frac{1}{2}\sum_{i=1}^{N}\langle\psi_i|\nabla_i^2|\psi_i\rangle - \int\sum_{A=1}^{M}\frac{Z_A}{r_{Ai}}\rho(r)dr + \frac{1}{2}\int\int\frac{\rho(r_1)\rho(r_2)}{r_{12}}dr_1dr_2 + E_{xc} \quad (2.6.4)$$

In the Kohn-Sham formulation of density functional theory, the total energy $E[\rho]$, of a system is broken down into four key terms: the kinetic energy of a system of non-interacting electrons, the electron-nucleus attraction, the electron-electron Coulomb repulsion, and the exchange-correlation energy E_{xc}, which accounts for the intricate quantum effects of electron exchange and correlation. The exchange-correlation term E_{xc} is unknown and thus approximated by various functional forms. In this approach, the ground-state electron density ρ is determined by single-electron Kohn-Sham orbitals.[34–38]

$$\rho(r) = \sum_{i=1}^{N}|\psi_i(r)|^2 \quad (2.6.5)$$

One commonly used approximation for the exchange-correlation energy is the Local Density Approximation (LDA), which assumes that the inhomogeneous electron density of a solid or liquid can be approximated by the properties of a homogeneous electron gas. However, more sophisticated methods have been developed, such as hybrid functionals, which offer improved accuracy. Among these, the Becke, 3-parameter, Lee-Yang-Parr (B3LYP) functional is particularly popular in chemistry. Hybrid functionals like B3LYP blend the orbital-dependent Hartree-Fock approach with explicit density functionals, such as LDA and the Generalized Gradient Approximation (GGA), to better account for both local and non-local electron interactions.[34–38]

Another essential aspect of computational chemistry is the choice of basis set, which provides a mathematical representation of atomic orbitals. In Gaussian-based

calculations, I used split-valence basis sets, such as 6-31+G(d,p). This approach, initially proposed by Boys and further developed by Pople, replaces Slater-type orbitals (STOs) with Gaussian-type orbitals (GTOs), which are computationally more efficient.[34–38,42,43] However, Gaussian orbitals do not precisely replicate the behavior of Slater-type orbitals, especially at shorter interatomic distances. To address this limitation, a linear combination of multiple Gaussian functions each called a primitive Gaussian is used to approximate the desired orbital shape.[34–38,42,43]
The split-valence basis sets, such as 6-31+G(d,p), use a contracted Gaussian function (a sum of several Gaussian primitives)[34–38,42,43] to model inner-shell orbitals and a larger number of Gaussians to represent valence orbitals. For example, in 6-31+G(d,p), the core (inner-shell) orbital is represented by a combination of six Gaussian primitives, while the valence shell has a split structure with one compact component represented by a combination of three Gaussians and an extended component represented by a single Gaussian. The "6" represents the core Gaussian primitives, "3-1" denotes the split in the valence shell, and "G" signifies the use of Gaussian-type orbitals.[42,43]
In Orca-based calculations, I have used the def2-TZVP basis set. Solvation effects were modelled in the conductor like polarizable continuum model (CPCM). This family of basis sets was developed by F. Weigend and R. Ahlrichs, and it is designed to provide a balanced level of accuracy and computational efficiency across a wide range of elements. The def2 basis sets are particularly popular in computational chemistry, especially for density functional theory (DFT) and correlated methods (like MP2 and CCSD), due to their consistency, coverage of the periodic table, and integration with effective core potentials (ECPs) for heavier elements.[44–46]
In def2-TZVP, the valence shell is represented by three Gaussian basis functions (known as "triple-zeta"), which is crucial for accurately modeling electron distribution in the valence orbitals, especially in systems with complex bonding. The basis set includes polarization functions, which are higher angular momentum functions (like d-functions for main-group elements and f-functions for transition metals). These polarization functions allow orbitals to distort and better represent

molecular environments, especially where electron distribution shifts due to bonding or nearby charges. The "def2" prefix indicates that this basis set is the second generation of the original "def" (default) basis sets developed by Ahlrichs.[47] This version improves upon the accuracy and consistency of the original def-TZVP basis set. The def2 family is comprehensive, covering nearly all elements up to radon (Rn), with parameters optimized for each one.[47,48] Compared to older basis sets (like 6-31G(d,p)), def2-TZVP is better optimized to reduce the Basis Set Superposition Error (BSSE), which is important for accurately modeling intermolecular interactions, such as in non-covalent complexes.[48,49]

In photochemistry, calculating vertical excitation energy is essential for aligning theoretical predictions with experimental absorption spectra and for exploring molecular dynamics in the excited state through geometry scans. While standard DFT methods focus on ground-state properties, they lack the framework for calculating excited-state properties, leading to the development of time-dependent density functional theory (TDDFT). TDDFT extends DFT by analyzing the system's response to an external perturbation, such as polarizability in response to an external electric field. The core concept involves solving the time-dependent many-particle Schrödinger equation, allowing TDDFT to capture electronic excitations and dynamic properties essential for studying excited states in molecular systems.

$$i\frac{\partial}{\partial t}\psi(r_1, r_2 \cdots\cdots r_N, t) = \hat{H}(t)\psi(r_1, r_2 \cdots\cdots r_N, t) \qquad (2.6.6)$$

In the time-independent Schrödinger equation, we solve for stationary eigenstates of the system, yielding discrete energy levels and fixed states. However, in the time-dependent Schrödinger equation, we instead track the time evolution of a quantum state under a time-dependent Hamiltonian $\hat{H}(t)$. This Hamiltonian $\hat{H}(t)$ consists of terms for kinetic energy and electron-electron interactions, along with an external potential ($\hat{V}_{ext}(\{r\}, t)$), which represents interactions with an external perturbation (like an oscillating electric field) and is expressed as a sum of one-body potentials. This approach enables TDDFT to model how an electronic system responds to time-

dependent external fields, capturing dynamic properties essential for simulating excited states and electronic transitions.[50–54]

$$\hat{V}_{ext}(\{r\},t) = \sum_{i=1}^{N} v_{ext}(r_i,t) \quad (2.6.7)$$

In TDDFT, the system's time evolution is influenced by an external potential, such as light or radiation. Runge and Gross demonstrated that there exists a one-to-one correspondence between time-dependent potentials and resulting electron densities. This means that if two different time-dependent potentials act on the same initial state of a system, they will produce distinct time-dependent densities.[50–54]

However, unlike in standard DFT, the variational principle cannot be directly applied in TDDFT since energy is not conserved in a time-dependent context.[50–54] Instead, a quantity called the quantum mechanical action (A_{xc}) is defined to replace energy as a guiding functional. Runge and Gross further adapted the Kohn-Sham equations, showing that the exchange-correlation potential (v_{xc}) in TDDFT can be derived as the functional derivative of this action.[50–54] This modification allows TDDFT to effectively capture time-dependent electronic behavior by leveraging the properties of (A_{xc}) in place of a variational energy approach.

$$v_{xc}(\rho) = \frac{\partial A_{xc}}{\partial \rho} \quad (2.6.8)$$

Since the exact form of the exchange-correlation functional is unknown even for the ground state, the adiabatic local density approximation (ALDA) is typically applied in TDDFT. This involves using the same functional form for both ground and excited states. However, TDDFT also encounters the causality problem, which requires that response functions remain zero until the external perturbation (such as light) is applied. Van Leeuwen addressed the causality issue in 1998 by establishing proper boundary conditions for TDDFT.[50–54]

In TDDFT, adiabatic approximations are commonly applied to the exchange-correlation potential, which generally works well when the excited state closely resembles the ground state. For instance, the photoabsorption cross-section, a key quantity in photochemistry, is determined by the imaginary part of the system's dynamic polarizability, estimated through the linear density response to a small

external perturbation. Additionally, TDDFT has been adapted to calculate specific photoabsorption phenomena such as double excitations, transitions to higher excited states, and charge-transfer states through various modifications introduced by researchers in recent years.[50–54]

In DFT and TDDFT computations using Gaussian software or Orca-based program, solvent effects can be incorporated via the self-consistent reaction field (SCRF) method, which places the solute molecule within a cavity surrounded by a reaction field to simulate solvent influence.[34–38,55] The most widely used approach, and the one applied in all solvent-dependent calculations in this study, is the Polarizable Continuum Model (PCM) or Conductor like Polarizable Continuum Model (CPCM). PCM or CPCM calculates the free energy of a molecule as a sum of its electrostatic energy, dispersion-repulsion free energy, and cavitation energy, where the solute is placed within an Onsager cavity defined by the van der Waals radii of its constituent atoms.[55,56] In this model, solvent effects are treated as a dielectric continuum, mirroring the solvent's polarity, but it does not account for specific solvation interactions, such as hydrogen bonding. PCM therefore provides a generalized solvent effect, suitable for capturing polarity influences but without the granularity of explicit solute-solvent interactions.

2.7. Materials

The synthesis and characterization of $[Cu(dmphen)_2]Cl$ was done according to the earlier report.[57] Dioctyl sulfosuccinate sodium salt (AOT) was purchased from Sigma and vacuum-dried before being used. Malachite green (MG) (Aldrich) was recrystallized from the water before use. High-performance liquid chromatography (HPLC) grade glycerol and acetone (Aldrich), methanol (Spectrochem), DCM and Acetonitrile (ThermoFischer Scientific), and n-heptane (TCI) were used without further purification. AOT reverse micelles having different water pool sizes were prepared by using double distilled water. Thio-dervatives of the coumarin molecules (abbreviated as thiocoumarin) were synthesized by following the reported

procedures.[58] Coumarin-1 and Coumarin-481 (Exciton Inc., USA) were used as received. Octa acid (OA) was synthesized, purified, and characterized following the published procedure.[59] The singlet oxygen-forming standard molecule, Chrysazin was purchased from TCI Chemicals and used as received.

2.8. Synthetic procedures

I would like to express my gratitude to Prof. V. Ramamurthy and his group in University of Miami, USA for the synthesis of octa acid (OA), thiocoumarins.

2.8.1 Synthesis of Thiocoumarin 1 (TC1)

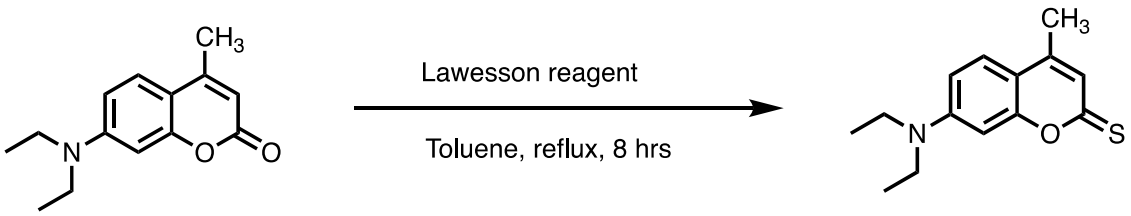

Thiocoumarin 1 was synthesized by following the literature procedure.[58,60,61] A mixture of 1 g (4.32 mmol, 1equiv.) of coumarin-1 and 1.399 g (3.45 mmol, 0.8 equiv.) Lawesson reagent was dissolved in 20 ml dry toluene and refluxed for 8 hrs in the dark under a nitrogen atmosphere. The progress of the reaction was monitored by TLC. Upon completion, the reaction mixture was filtered through Whatman filter paper, and the solvent was evaporated completely using a rotary evaporator. The crude was purified by column chromatography (30% ethyl acetate/hexane). The column-purified product precipitated with cold ethanol solvent, yielding a yellow-colored solid. The isolated product weighed 769 mg (72% yield). ^{1}H NMR (400 MHz, $CDCl_3$) d (ppm): 7.46 (d, J = 8.4 Hz, 1H), 6.95 (s, 1H), 6.71- 6.74 (m, 2H), 3.44 (q, J = 7.2 Hz, 4H), 2.31 (s, 3H), 1.23 (t, J = 7.2 Hz, 6H). NMR spectrum matches with reported spectra.[62]

2.8.2 Synthesis of 7-Acetoxy Thiocoumarin (Acetoxy-TC)

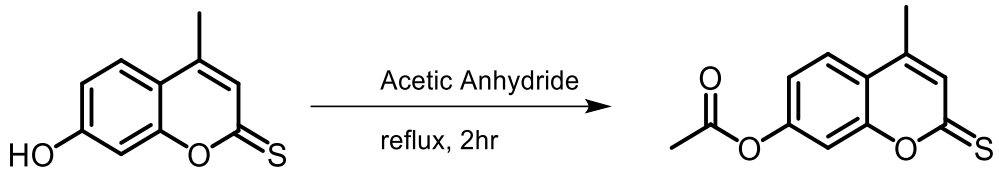

This acetoxy-derivative of coumarin was synthesized by following the literature procedure.[63] Coumarin (2.18 g, 10 mmol) was dissolved in 5 mL acetic anhydride and refluxed for 2 h. After completion of the reaction, the reaction mixture was poured into ice-cold water. A solid precipitate was formed, filtered, and dried for 1 day in airflow. The crude was recrystallized with 95% ethanol to obtain the acetoxy derivative as a white solid (2.6 g, 96% yield). To get the thio-derivative of the acetoxy coumarin same protocol as thiocoumarin 1 was used. The isolated acetoxy-TC product features: ^{1}H NMR (500 MHz, DMSO-d6) d (ppm): 7.91 (d, J = 8.5 Hz, 1H), 7.48 (s, 1H), 7.28- 7.30 (d, J = 8.5 Hz, 1H), 7.26 (s, 1H), 2.41 (s, 3H), 2.33 (s, 3H); ^{13}C NMR (125 MHz, $CDCl_3$) d (ppm): 197.22, 168.58, 156.59, 153.31, 143.58, 128.69, 125.29, 119.34, 119.27, 110.30, 21.17, 18.06; ESI-HRMS: Calculated for $C_{12}H_{11}O_3S$ $[M+H]^+$ = 235.0429, observed:235.0425.

References

(1) Gollnick, K.; Held, S.; Martire, D. 0; Braslavsky, S. E. Hydroxyanthraquinones as Sensitizers of Singlet Oxygen Reactions: Quantum Yields of Triplet Formation and Singlet Oxygen Generation in Acetonitrile. *J. Photochem. Photobiol. A: Chem.* **1992**, *69*, 155–165.

(2) Bollinger, L. M.; Thomas, G. E. Measurement of the Time Dependence of Scintillation Intensity by a Delayed-Coincidence Method. *Rev. Sci. Instrum.* **1961**, *32*, 1044–1050.

(3) O'Connor, D. V. and P. D. *Time-Correlated Single Photon Counting*; Academic Press, London, 1984.

(4) Lakowicz, J. R. *Techniques: 1 Topics in Fluorescence Spectroscopy*; Springer US: Boston, 2002; Vol. 1.

(5) Castleman, A. W.; Toennies, J. P.; Zinth, W. *Advanced Time-Correlated Single Photon Counting Techniques*; Eds.; Springer Series in Chemical Physics; Springer Berlin Heidelberg: Berlin, Heidelberg, 2005; Vol. 81.

(6) Becker, W. Introduction to Multi-Dimensional TCSPC. *Chem. Phys.* **2015**, *111*, 1–63.

(7) Lakowicz, J. R. *Principles of Fluorescence Spectroscopy*; Springer US: Boston, MA, 2006.

(8) Smith, D. A.; McKenzie, G.; Jones, A. C.; Smith, T. A. Analysis of Time-Correlated Single Photon Counting Data: A Comparative Evaluation of Deterministic and Probabilistic Approaches. *Methods Appl Fluoresc* **2017**, *5*, 042001.

(9) Hallidy, L. A.; Topp, M. R. Picosecond Luminescence Detection Using Type-II Phase-Matched Frequency Conversion. *Chem. Phys. Lett.* **1977**, *46*, 8–14.

(10) Kahlow, M. A.; Jarzęba, W.; DuBruil, T. P.; Barbara, P. F. Ultrafast Emission Spectroscopy in the Ultraviolet by Time-gated Upconversion. *Rev. Sci. Instrum.* **1988**, *59*, 1098–1109.

(11) Shah, J. Ultrafast Luminescence Spectroscopy Using Sum Frequency Generation. *IEEE J Quantum Electron* **1988**, *24*, 276–288.

(12) Wirth, M. J. INSTRUMENTATION. *Anal. Chem.* **1990**, *62*, 270A-277A.

(13) Xu, J.; Knutson, J. R. Chapter 8 Ultrafast Fluorescence Spectroscopy via Upconversion: Applications to Biophysics. *Methods Enzymol* **2008**, *450*, 159–183.

(14) Boyd, R. *Nonlinear Optics*, 3rd ed.; Academic Press, San Diego, CA., 2008.

(15) Shen, Y. R. *Principles of Nonlinear Optics*; Wiley-Interscience,New York, NY, USA, 1984.

(16) Zernike, F.; Midwinter, J. E. *Applied Nonlinear Optics*; John Wiley & Sons, Ltd., New York, 1973.

(17) Moore, J. H.; Spencer, N. D. *Encyclopedia of Chemical Physics and Physical Chemistry. Volume 3, Applications*; Spencer, N. D., Moore, J. H., Eds.; CRC Press, 2023; Vol. 3.

(18) Brearley, A. M.; Strandjord, A. J. G.; Flom, S. R.; Barbara, P. F. Picosecond Time-Resolved Emission Spectra: Techniques and Examples. *Chem. Phys. Lett.* **1985**, *113*, 43–48.

(19) Fleming, G. R.; Gijzeman, O. L. J.; Freed, K. F.; Lin, S. H. Theory for Time Resolved Emission Spectra. *J. Chem. Soc., Faraday Trans.* **1975**, *71*, 773–780.

(20) Homg, M. L.; Gardecki, J. A.; Papazyan, A.; Maroncelli, M. Subpicosecond Measurements of Polar Solvation Dynamics: Coumarin 153 Revisited. *J. Phys. Chem* **1995**, *99*, 17311–17337.

(21) Maroncelli, M.; Fleming, G. R. Picosecond Solvation Dynamics of Coumarin 153: The Importance of Molecular Aspects of Solvation. *J. Chem. Phys.* **1987**, *86*, 6221–6239.

(22) Easter, J. H.; DeToma, R. P.; Brand, L. Nanosecond Time-Resolved Emission Spectroscopy of a Fluorescence Probe Adsorbed to L-Alpha-Egg Lecithin Vesicles. *Biophys J* **1976**, *16*, 571–583.

(23) Berera, R.; van Grondelle, R.; Kennis, J. T. M. Ultrafast Transient Absorption Spectroscopy: Principles and Application to Photosynthetic Systems. *Photosynth Res* **2009**, *101*, 105–118.

(24) Ruckebusch, C.; Sliwa, M.; Pernot, P.; de Juan, A.; Tauler, R. Comprehensive Data Analysis of Femtosecond Transient Absorption Spectra: A Review. *Journal of Photochemi. and Photobiol. C: Photochem. Rev.* **2012**, *13*, 1–27.

(25) Ceroni, P. *The Exploration of Supramolecular Systems and Nanostructures by Photochemical Techniques*; Lecture Notes in Chemistry; Springer Netherlands: Dordrecht, 2018; Vol. 78.

(26) Rullière, C. *Femtosecond Laser Pulses: Advanced Texts in Physics*, 2nd ed.; Springer New York: New York, NY, 2005.

(27) Mouton, N.; Sliwa, M.; Buntinx, G.; Ruckebusch, C. Deconvolution of Femtosecond Time-Resolved Spectroscopy Data in Multivariate Curve Resolution. Application to the Characterization of Ultrafast Photo-Induced Intramolecular Proton Transfer. *J. Chemom.* **2010**, *24*, 424–433.

(28) Ziólek, M.; Lorenc, M.; Naskrecki, R. Determination of the Temporal Response Function in Femtosecond Pump-Probe Systems. *Appl Phys B* **2001**, *72*, 843–847.

(29) Lorenc, M.; Ziolek, M.; Naskrecki, R.; Karolczak, J.; Kubicki, J.; Maciejewski, A. Artifacts in Femtosecond Transient Absorption Spectroscopy. *Appl Phys B* **2002**, *74*, 19–27.

(30) Cho, M.; Du, M.; Scherer, N. F.; Fleming, G. R.; Mukamel, S. Off-resonant Transient Birefringence in Liquids. *J. Chem. Phys.* **1993**, *99*, 2410–2428.

(31) Kovalenko, S. A.; Ernsting, N. P.; Ruthmann, J. Femtosecond Hole-Burning Spectroscopy of the Dye DCM in Solution: The Transition from the Locally Excited to a Charge-Transfer State. *Chem. Phys. Lett.* **1996**, *258*, 445–454.

(32) Van Stokkum, I. H. M.; Larsen, D. S.; Van Grondelle, R. Global and Target Analysis of Time-Resolved Spectra. *Biochimica et Biophysica Acta (BBA) - Bioenergetics* **2004**, *1657*, 82–104.

(33) Snellenburg, J. J.; Laptenok, S.; Seger, R.; Mullen, K. M.; van Stokkum, I. H. M. Glotaran: A Java-Based Graphical User Interface for the R Package TIMP. *J. Stat. Softw.* **2012**, *49*, 1–22.

(34) Koch, W.; Holthausen, M. C. *A Chemist's Guide to Density Functional Theory*, 2nd ed.; Wiley-VCH Verlag GmbH Weinheim, FRG, 2001.

(35) Parr, R. G. Density Functional Theory of Atoms and Molecules. *Horizons of Quantum Chemistry* **1980**, 5–15.

(36) Jones, R. O.; Gunnarsson, O. The Density Functional Formalism, Its Applications and Prospects. *Rev. Mod. Phys.* **1989**, *61*, 689.

(37) Kohn, W. Nobel Lecture: Electronic Structure of Matter-Wave Functions and Density Functionals. *Rev. Mod. Phys.* **1998**, *71*, 1253.

(38) Burke, K. Perspective on Density Functional Theory. *J. Chem. Phys.* **2012**, *136*, 150901.

(39) Frisch, M. J.; et al. Gaussian 09, Revision E.01. *Gaussian, Inc., Wallingford CT* **2009**.

(40) Kohn, W.; Sham, L. J. Self-Consistent Equations Including Exchange and Correlation Effects. *Phys. Rev.* **1965**, *140*, A1133–A1138.

(41) Hohenberg, P.; Kohn, W. Inhomogeneous Electron Gas. *Phys. Rev.* **1964**, *136*, B864–B871.

(42) Davidson, E. R.; Feller, D. Basis Set Selection for Molecular Calculations. *Chem. Rev.* **1986**, *86*, 681–696.

(43) McQuarrie, D. A.; Simon, J. D. *Physical Chemistry: A Molecular Approach*; University Science Books, Sausalito, California, 2011.

(44) Rappoport, D. Property-Optimized Gaussian Basis Sets for Lanthanides. *J. Chem. Phys.* **2021**, *155*, 124102.

(45) Xu, X.; Truhlar, D. G. Accuracy of Effective Core Potentials and Basis Sets for Density Functional Calculations, Including Relativistic Effects, as Illustrated by Calculations on Arsenic Compounds. *J. Chem. Theory Comput.* **2011**, *7*, 2766–2779.

(46) Xu, X.; Truhlar, D. G. Performance of Effective Core Potentials for Density Functional Calculations on 3d Transition Metals. *J. Chem. Theory Comput.* **2012**, *8*, 80–90.

(47) Ahlrichs, R.; Bär, M.; Häser, M.; Horn, H.; Kölmel, C. Electronic Structure Calculations on Workstation Computers: The Program System Turbomole. *Chem. Phys. Lett.* **1989**, *162*, 165–169.

(48) Weigend, F.; Ahlrichs, R. Balanced Basis Sets of Split Valence, Triple Zeta Valence and Quadruple Zeta Valence Quality for H to Rn: Design and Assessment of Accuracy. *Phys. Chem. Chem. Phys.* **2005**, *7*, 3297–3305.

(49) Pitman, S. J.; Evans, A. K.; Ireland, R. T.; Lempriere, F.; McKemmish, L. K. Benchmarking Basis Sets for Density Functional Theory Thermochemistry Calculations: Why Unpolarized Basis Sets and the

Polarized 6-311G Family Should Be Avoided. *J. Phys. Chem. A* **2023**, *127*, 10295–10306.

(50) Chong, D. P. *Recent Advances in Density Functional Methods*, Ed.; Recent Advances in Computational Chemistry; World Scientific Publishing Co. Pte. Ltd., Singapore, 1995.

(51) Capaz, R. B. *Time-Dependent Density-Functional Theory: Concepts and Applications*; Oxford University Press, Oxford, New York, 2012; Vol. 44.

(52) Atkins, P. W.; Friedman, R. S. *Molecular Quantum Mechanics*, 3rd ed.; Oxford University Press, 1997.

(53) Casida, M. E. Time-Dependent Density-Functional Theory for Molecules and Molecular Solids. *J. Mol. Struct. Theochem.* **2009**, *914*, 3–18.

(54) Runge, E.; Gross, E. K. U. Density-Functional Theory for Time-Dependent Systems. *Phys. Rev. Lett.* **1984**, *52*, 997.

(55) Tomasi, J.; Mennucci, B.; Cammi, R. Quantum Mechanical Continuum Solvation Models. *Chem. Rev.* **2005**, *105* (8), 2999–3093.

(56) Onsagbr, L. Electric Moments of Molecules in Liquids. *J. Am. Chem. Soc.* **1936**, *58*, 1486–1493.

(57) Pallenberg, A. J.; Koenig, K. S.; Barnhartlb, D. M. Synthesis and Characterization of Some Copper(I) Phenanthroline Complexes. *Inorg. Chem.* **1995**, *34*, 2833–2840.

(58) Jesberger, M.; Davis, T. P.; Barner, L. Applications of Lawesson's Reagent in Organic and Organometallic Syntheses. *Synthesis-Stuttgart* **2003**, 13, 1929–1958.

(59) Gibb, C. L. D.; Gibb, B. C. Well-Defined, Organic Nanoenvironments in Water: The Hydrophobic Effect Drives a Capsular Assembly. *J. Am. Chem. Soc.* **2004**, *126*, 11408–11409.

(60) Gandioso, A.; Contreras, S.; Melnyk, I.; Oliva, J.; Nonell, S.; Velasco, D.; García-Amorós, J.; Marchán, V. Development of Green/Red-Absorbing Chromophores Based on a Coumarin Scaffold That Are Useful as Caging Groups. *J. Org. Chem.* **2017**, *82*, 5398–5408.

(61) Ghosh, S. K.; Valloli, L. K.; Unny, D.; Sivaguru, J.; Jockusch, S.; Ramamurthy, V. Room Temperature Phosphorescence of 2-Thioxo-Coumarins in Aqueous Solution Promoted by Octa Acid Inclusion. *J. Photochem. Photobiol. A: Chem.* **2024**, *451*, 115510.

(62) Gandioso, A.; Contreras, S.; Melnyk, I.; Oliva, J.; Nonell, S.; Velasco, D.; García-Amorós, J.; Marchán, V. Development of Green/Red-Absorbing Chromophores Based on a Coumarin Scaffold That Are Useful as Caging Groups. *J. Org. Chem.* **2017**, *82*, 5398–5408.

(63) Xi, G. L.; Liu, Z. Q. Coumarin Moiety Can Enhance Abilities of Chalcones to Inhibit DNA Oxidation and to Scavenge Radicals. *Tetrahedron* **2014**, *70*, 8397–8404.

Chapter 3

Triplet State Photophysics of Bis(dimethylphenanthroline)copper(I) Might Involve Volume-Changing Molecular Motion: Ultrafast Absorption and Emission Studies

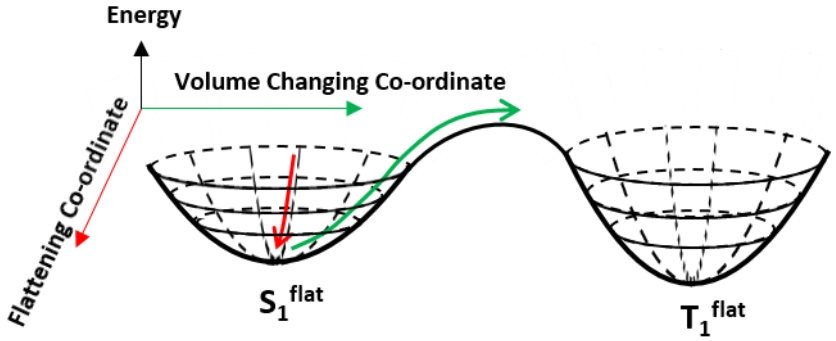

Abhijit Dutta, Suman Bhowmik, and Pratik Sen, *Chem. Phys. Lett.* **2024**, *839*, 141108

Study of triplet photophysics has remained a contemporary field for the last eight decades due to its wide-ranging applications. Many recent studies deciphered the influence of molecular vibrations on the electronic coupling for facile intersystem crossing (ISC) in numerous metal complexes. Through a combined analysis of steady-state and time-resolved spectroscopies, we identified the role of environmental rigidity on the triplet photophysics of bis(dimethylphenanthroline)copper(I) chloride ([Cu(dmphen)$_2$]Cl). Our experiments suggest an involvement of volume-changing coordinate in ISC of [Cu(dmphen)$_2$]Cl having an activation energy barrier of 5.9 kJ mol^{-1}. This insight can be useful in the research and development of efficient triplets.

3.1 Introduction

Molecules with high triplet yield and lifetime are of major interest in recent times due to their immense importance in the realms of chemistry, physics, and materials science for application in photocatalysis, photon up-conversion, and ability to sensitize other triplets [1–5]. They are also promising candidates to harvest light in organic photovoltaic cells, thus having potential to revolutionize the renewable energy technologies [6–8]. In general, these triplet states cannot be accessed directly through photoexcitation of the ground singlet state because that would violate the spin selection rule. In most cases, triplet states are produced through intersystem crossing (ISC), which is a dynamic process that results from spin-orbit coupling (SOC) between electronic states that have different spin multiplicities [9–11]. Vibrational levels of excited singlet states are typically spin-orbit coupled to the dense manifold of vibrational levels of a low-lying triplet state. As a consequence, inorganic metal-ligand complexes, especially those involving transition metals, display a significant inclination toward achieving an efficient triplet state [12–15].

A knowledge of the ISC mechanism in a system is essential to design a molecule with higher triplet quantum yield or higher triplet lifetime. The heavy atom effect (HAE) is one of the most contributing factors in the SOC matrix in ISC due to its quadratic dependence on atomic number [16–18]. There are several other reports of strong ISC without HAE include (a) singlet fission, (b) twisted induced, (c) charge recombination, etc. [19–22]. The vibrational contribution along with the electronic coupling in ISC was neglected in the earlier research. In the last few years, the idea of vibration assisted ISC has been explored drastically [23–26]. Recently, we unveiled the significant impact of carbon-halogen bond vibrations on the ISC in halo-coumarins [27]. The strong involvement of spin-vibronic motion on the ISC has also been studied by the Daniel group [28]. Recent studies by Chen's and Chergui's group explored the effect of vibrational wave packet motions and structural dynamics on the ISC dynamics of several bimetallic complexes [23,24,29].

Among various phosphorescent metal complexes, Bis(dimethylphenanthroline)copper(I) chloride [Cu(dmphen)$_2$]Cl ; Scheme 3.1) has been studied extensively [30–35]. Recent studies also revealed that this molecule shows thermally activated delayed fluorescence (TADF) behaviour which can be used as a constituents in organic light emitting diode (OLED) material and a replacement material for traditional phosphorescent materials [36]. Various research groups have delved into the detailed excited-state photophysics of [Cu(dmphen)$_2$]$^+$ in the last two decades [30–32,34,35,37–39]. In dichloromethane, this complex exhibits a strong absorption band around 460 nm, due to $S_2 \leftarrow S_0$ transition, accompanied by a minor absorption shoulder around 550 nm from $S_1 \leftarrow S_0$ transition [34,35]. Furthermore, it demonstrates phosphorescence in the range of 700-800 nm. The electronic ground state of this molecule (S_0) has the D_{2d} symmetry, where two ligands are perpendicularly attached to the central copper metal ion. Following initial excitation to the S_2 state (possessing D_{2d} symmetry), the complex rapidly returns to the S_1 state within ~45 fs while maintaining its geometry. Subsequently, from the S_1 perpendicular state, it transform to a new singlet state with structural distortions, known as the S_1 flattened state, on a timescale of 700-900 fs [34,35]. This photoinduced structural change was explained by metal-to-ligand charge transfer (MLCT) followed by dihedral ligand rotation through the Jahn-Teller effect of the d^9 electronic configuration central copper ion. The flattened S_1 state subsequently progresses to a nearby triplet state (called T_1 flattened state) in a 7-10 ps time scale [34,35]. The resulting triplet state exhibits a phosphorescence emission band with ~41 ns lifetime. Investigations involving various substituted phenanthroline ligands and solvent dependent studies infer that the structural distortion follows an inner-sphere mechanism [40]. However, until now, there is no detailed investigation on the ISC of the flattened S_1 state to the triplet state.

In the present study, the specific focus lies in gaining a mechanistic view on the triplet crossover of the flattened S_1 state of [Cu(dmphen)$_2$]$^+$. With the help of femtosecond fluorescence up-conversion and transient absorption spectroscopy, we observed a moderate viscosity dependence on the ISC dynamics and confirmed it to

be an activated process. In combination with the theoretical result, we propose ligand-metal vibration could be an important channel for triplet formation in $[Cu(dmphen)_2]^+$.

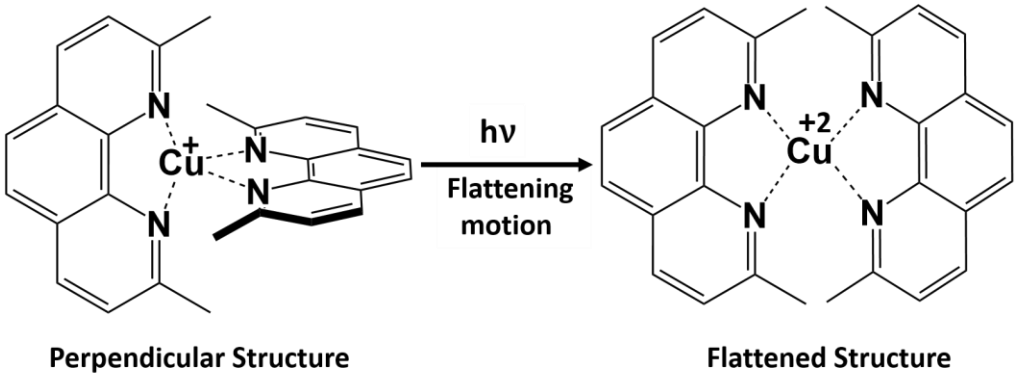

Scheme 3.1. Molecular structure and photoinduced flattening of Bis(dimethylphenanthroline)copper(I) complex.

3.2 Results and Discussions

Steady State Experiments. Figure 3.1.1a depicts the steady state absorption spectra of $[Cu(dmphen)_2]Cl$ in four solvents ranging from non-polar DCM to highly polar water, where no appreciable shift in the absorption maxima is observed. Though the absorption characteristics of $[Cu(dmphen)_2]Cl$ is insensitive to the polarity and viscosity of the solvent medium, the photoluminescence feature changes significantly as shown in figure 3.2.1b. When examining the photoluminescence property of $[Cu(dmphen)_2]Cl$ in the same four solvent solvents, a notable change in the emission intensity is evident. The intense band around 730 nm region is identified as phosphorescence [35]. By taking malachite green (MG) as standard, the calculated values of phosphorescence quantum yield of $[Cu(dmphen)_2]Cl$ in four different solvents are $9.0 \pm 1.3 \times 10^{-5}$ (DCM), $1.1 \pm 0.2 \times 10^{-5}$ (Glycerol), $3.8 \pm 0.9 \times 10^{-6}$ (Water), and $2.9 \pm 1.1 \times 10^{-6}$ (MeOH). (Figure 3.2.1c) This variation strongly implies that along with the solvent polarity, solvent viscosity also plays a crucial role in the excited state property of $[Cu(dmphen)_2]Cl$. To check the effect of viscosity on the photophysics, we have used glycerol/methanol binary solvent mixtures as the solvent media. By adjusting the composition of methanol and

glycerol, medium's viscosity can be altered significantly (0.54 to 187 cP) [41,42] without much change in the polarity (at 20℃ $\in_{Glycerol}$ ~42.5 and $\in_{Methanol}$ ~33.6) [43]. From figures 3.2.1d and 3.2.1g it becomes apparent that the phosphorescence intensity increases with an increase in the proportion of glycerol in the glycerol/methanol mixture, thus the medium viscosity. This suggests an involvement of large amplitude motion in the non-radiative decay channel of the triplet state.

To investigate if this viscosity effect is specific to the glycerol/methanol mixture at constant temperature and to glycerol at varying temperature, or extends to other constrained media, we opted for an aerosol OT (AOT) reverse micelle (RM) system. Here, we can manipulate the viscosity of the water pool of the RM formed by AOT in n-heptane medium by adjusting the water content within it [44]. In figure 3.2.1e, the steady-state emission spectra of $[Cu(dmphen)_2]Cl$ in AOT RM of varying water contents (defined by W_0=[Water]/[Surfactant]) are depicted. We observed that with a decrease in the water pool size of the AOT RM (W_0=50 to 2.5) the phosphorescence intensity increases gradually (see Figure 3.2.1h). A decrease in the W_0 increases the viscosity as well as the structural rigidity of the surrounding of $[Cu(dmphen)_2]Cl$, which may lead to an increase in the phosphorescence intensity. This increase in environmental rigidity seems to impose a greater likelihood of radiative decay. The observations suggest that as we elevate the viscosity of the surrounding medium, it restricts non-radiative decay pathways, consequently resulting in a higher phosphorescence quantum yield.

Furthermore, to check the effects of temperature on the steady-state phosphorescence emission, a temperature-dependent study has been undertaken by taking different compositions of glycerol/methanol mixture (60-90%) with varying the temperature in such a way that the viscosity of the medium remains similar (~58-68 cP) [42]. The result is depicted in figure 3.2.1f. We observed a monotonous increase in the phosphorescence quantum yield with an increase in the temperature (Figure 3.2.1i). An increased phosphorescence yield with an increase in the temperature could be due to the activation energy barrier between the S_1-flattened state and the T_1-flattened state, which is overcome easily at higher temperatures, leading to an efficient ISC

and consequently an increase in the triplet state population. Along with this or alternatively, the initial T_1-flattened state may converted through an activation energy barrier to another stable triplet state, which is emissive. According to a recent theoretical report by Gourlaouen *et al*. on several Cu(I)-phenanthroline complexes suggests that the formation of the emissive triplet state (T_1) occurs via T_2 state along the ligand dihedral flattening coordinate. The calculated value of the spin-orbit coupling (SOC) for the $S_1 \rightarrow T_2$ transition is very high over the $S_1 \rightarrow T_1$ transition, which also justifies the $S_1 \rightarrow T_2$ transition. In addition, they have also shown that S_1 and T_1 states have two minima separated by a potential energy barrier along the Cu-ligand distance coordinate [45]. This theoretical result is in accordance to our proposition for observing high phosphorescence quantum yield of $[Cu(dmphen)_2]Cl$ at high temperatures in a glycerol. We propose that the influence of viscosity on the fate of the flattened-T_1 state of $[Cu(dmphen)_2]Cl$ primarily stems from the restriction imposed on certain types of structural change in the excited manifold of $[Cu(dmphen)_2]Cl$. To understand the role of viscosity in the formation of the triplet state, we performed femtosecond time-resolved absorption and emission studies.

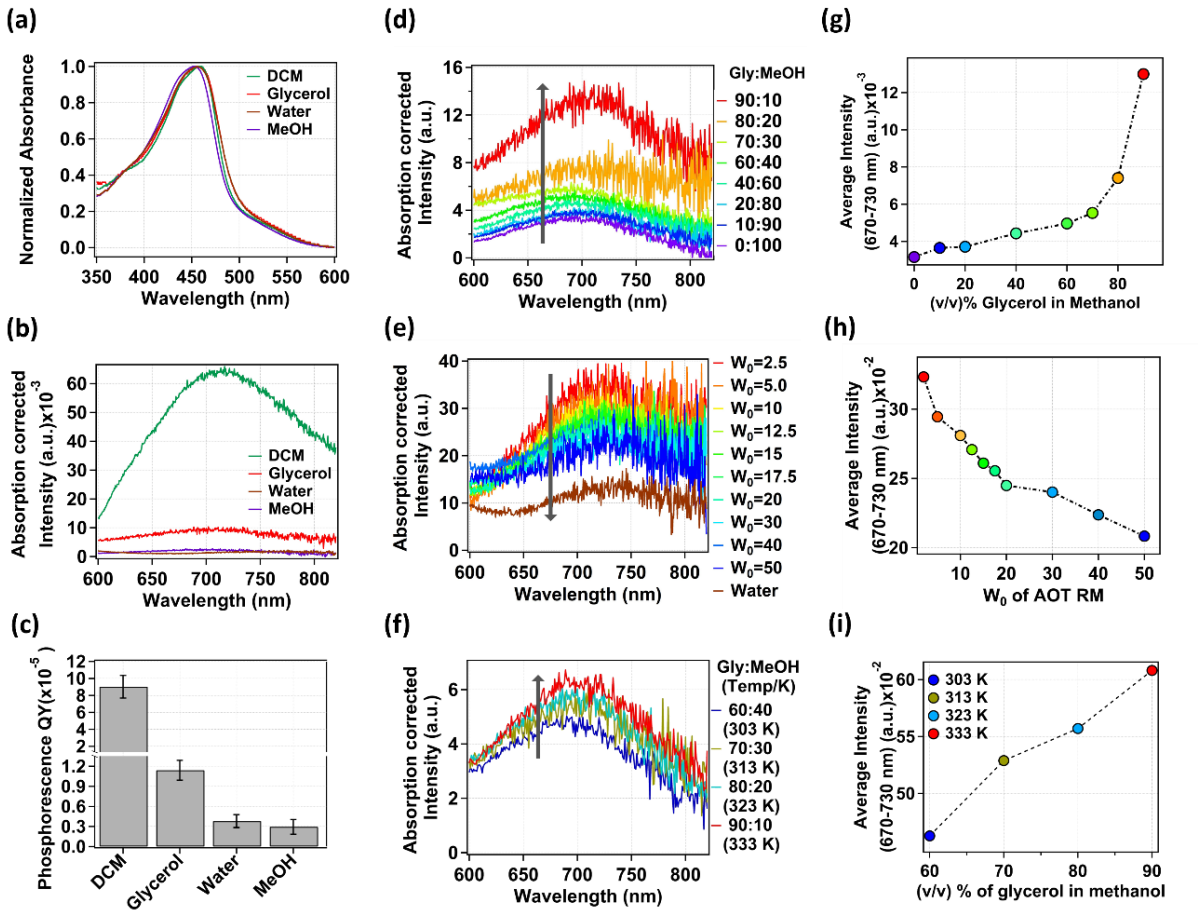

Figure 3.2.1. Steady-state (a) absorption spectra, (b) emission spectra and (c) phosphorescence quantum yields of $[Cu(dmphen)_2]Cl$ in dichloromethane (DCM), glycerol, water and methanol (MeOH). Steady-state emission spectra of $[Cu(dmphen)_2]Cl$ in (d) various mixtures of glycerol in methanol (v/v), (e) water-pool of AOT reverse micelle (RM) of different sizes (W_0=2.5 to 50) along with the bulk water and (f) four different glycerol/methanol mixtures (Blue 60:40, Brown 70:30, Cyan 80:20 and red 90:10 v/v) at four different temperatures where viscosity remains similar. The trend in the average phosphorescence intensity in (g) various glycerol/methanol mixtures (h) various AOT RM systems and (i) four different glycerol/methanol mixtures of similar viscosity. All emission spectra were recorded at an excitation wavelength of 450 nm.

Femtosecond Fluorescence Up-conversion Study. An earlier report on $[Cu(dmphen)_2]^+$ in DCM suggests that the long component of the biexponential fluorescence decay at 630 nm corresponds to population transfer from the flattened-S_1 state to the flattened-T_1 state through the ISC process.[40] Following this information, we recorded the fluorescence decay of $[Cu(dmphen)_2]Cl$ in two different glycerol/methanol mixtures (10% (v/v) and 90% (v/v) glycerol in methanol) at 630 nm and fitted the same to a bi-exponential function with deconvolution (See

Figure 3.2.2). From the normalized transients, we can see that in case of 90% (v/v) glycerol in methanol, the fluorescence decay is slower (with a long component of 11.5 ps) compared to that in the 10% (v/v) glycerol in methanol (with a long component of 5.3 ps).

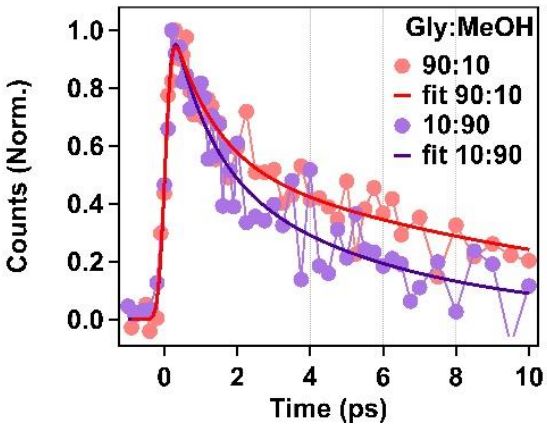

Figure 3.2.2. Normalized fluorescence decay of $[Cu(dmphen)_2]Cl$ at 630 nm in the glycerol/methanol mixtures: 10% v/v glycerol (purple) and 90% v/v glycerol (red) in methanol, upon excitation at 400 nm at 25°C.

From this observation we conclude that the formation of the triplet state gets slower as the viscosity of the medium increases. Hence, it is reasonable to assert that the viscosity of the surrounding medium retarded the volume changing motion of the flattened singlet state in $[Cu(dmphen)_2]Cl$ to go towards flattened triplets. Such a retardation in ISC is likewise observed in the AOT-RM system with various W_0s. Figure 3.2.3 illustrates that as the water pool size of the AOT-RM decreases, the fluorescence decay becomes progressively slower, with the fastest decay observed in bulk water. For W_0=10, the long component of the bi-exponential decay is found to be 6.9 ps, which gradually decreases upon increasing the water pool size of the RM and becomes 4.0 ps in W_0=50 (Table 3.2.1). In bulk water, the long component of the fluorescence decay becomes much faster (2.7 ps). Based on this observation we propose that ISC coordinate in $[Cu(dmphen)_2]Cl$ involves volume changing motion. However, as the 630 nm signal is not solely controlled by the flattened-S_1 → flattened-T_1 process [35], we cannot extract the time scale of triplet state formation

from this study. Therefore, we performed a femtosecond transient absorption spectroscopic measurement.

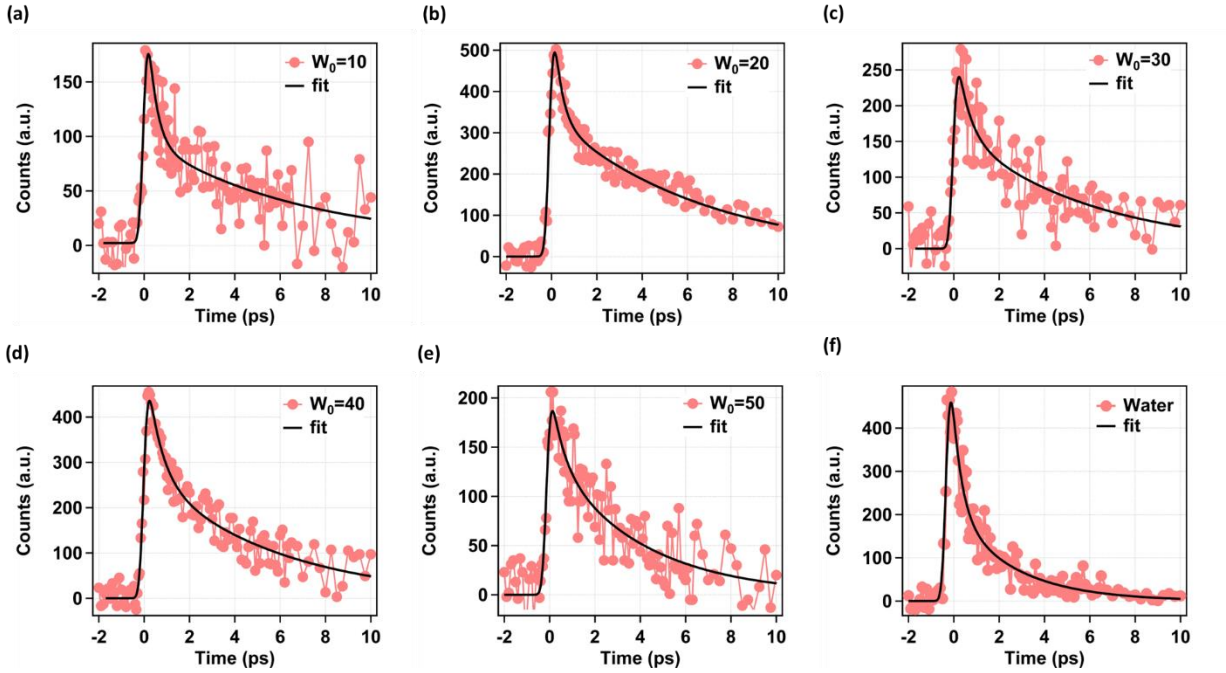

Figure 3.2.3. Fluorescence decay of $[Cu(dmphen)_2]Cl$ at 630 nm in AOT RM of five different water pool sizes (a) W_0=10, (b) W_0=20, (c) W_0=30, (d) W_0=40, (e) W_0=50 and in (f) bulk water at 25°C. The excitation wavelength was 400 nm.

Table 3.2.1. Fitting parameters of the fluorescence decays of $[Cu(dmphen)_2]Cl$ in two glycerol/methanol mixtures (90% and 10% v/v glycerol), in various AOT RM (W_0=10 to 50) and in bulk water at 630 nm at 25°C.

System	a_1	τ_1 (fs)	a_2	τ_2 (ps)
Glycerol:MeOH (90:10 v/v)	0.47	1141	0.53	11.5
Glycerol:MeOH (10:90 v/v)	0.48	992	0.52	5.3
AOT RM W_0=10	0.64	368	0.36	6.9
AOT RM W_0=20	0.52	350	0.48	6.7
AOT RM W_0=30	0.47	543	0.53	5.9
AOT RM W_0=40	0.49	624	0.51	5.7
AOT RM W_0=50	0.38	563	0.62	4.0
Water	0.64	414	0.36	2.7

Transient Absorption (TA) Study. The results of the femtosecond transient absorption (fs-TA) study of $[Cu(dmphen)_2]Cl$ in glycerol/methanol mixture and

AOT RM system of different pool sizes are presented in figure 3.2.4, 3.2.5 respectively. In both systems, the transient signal features a broad positive band with a peak around 560 nm (Figure 3.2.4a and 3.2.4b), which has been assigned to the flattened-S_1 state, following earlier studies [33,34,40]. Additionally, two low intensity satellite bands centred at 650 nm and 730 nm are also observed, which intensified at longer delay times (see figures 3.2.4a/3.2.4c for 10% (v/v) glycerol in methanol and figures 4b/4d for 90% (v/v) glycerol in methanol). Following the previous studies, these two bands are assigned to the triplet states [34,40]. To track the formation of the triplet state (ISC rate) of $[Cu(dmphen)_2]Cl$, we monitored the kinetics at 730 nm. Figures 3.2.4c and 3.2.4f depicts the kinetics at 730 nm in 10% and 90% glycerol in methanol, respectively. With an increase in the glycerol proportion, the triplet state formation becomes slower (5.5 ps in 10% glycerol in methanol to 10.4 ps in 90% glycerol in methanol, see Table 3.2.2). This result clearly suggests a role of volume changing motion in the triplet state formation of $[Cu(dmphen)_2]Cl$.

The fs-TA spectra of $[Cu(dmphen)_2]Cl$ inside AOT RM (Figure 3.2.5) is very similar to that in glycerol/methanol mixture suggesting of same excited state features. Fitted transients at 730 nm are depicted in figure 3.2.6 and fitting parameters are tabulated in Table 3.2.2. The ISC time is found to be 5.0 ps for W_0=10 AOT-RM, and becomes faster on increasing the water pool size. In bulk water the ISC time is found to be 1.8 ps. A reduction in the structural rigidity and micro-viscosity of the medium is probably the reason for this observation. From the comprehensive data on the kinetics of triplet formation it is evident that the reaction coordinate involves a volume changing motion.

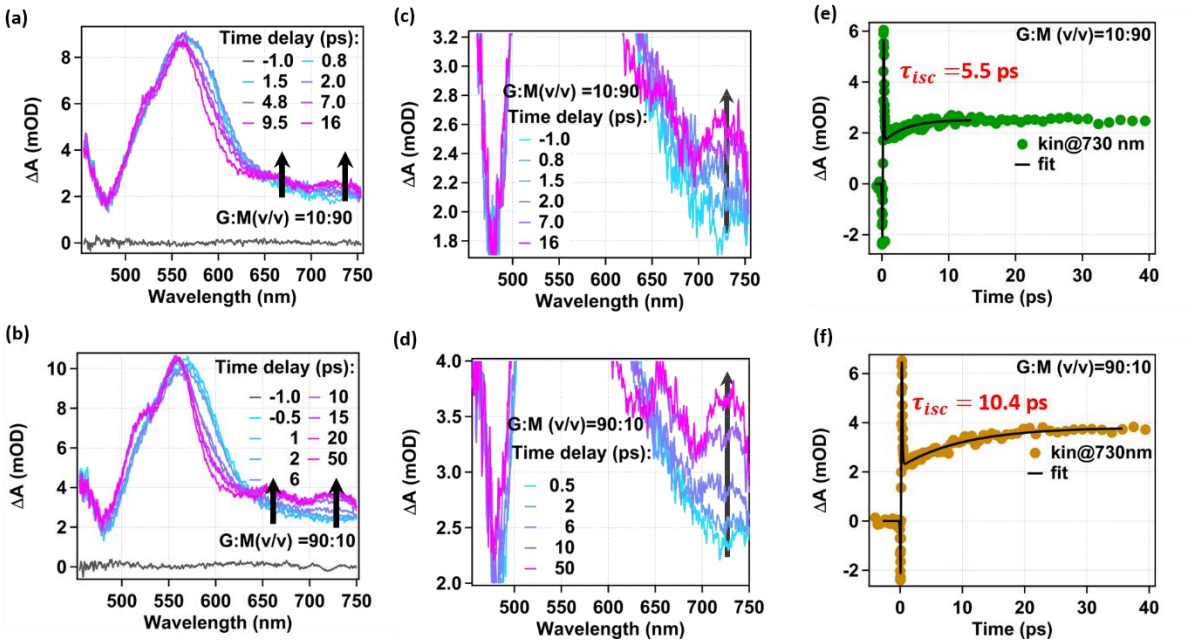

Figure 3.2.4. Femtosecond transient absorption (TA) studies of $[Cu(dmphen)_2]Cl$ in glycerol/methanol mixtures. TA spectra at some selective delays in (a) 10 % (v/v) glycerol in methanol and (b) 90 % (v/v) glycerol in methanol at 25°C. The transient data in the 650-750 nm of 4a and 4b are magnified and shown in 4c and 4d, respectively. Fitted transient kinetics at 730 nm in (e) 10 % (v/v) glycerol in methanol and (f) 90% (v/v) glycerol in methanol. Samples were excited at 400 nm.

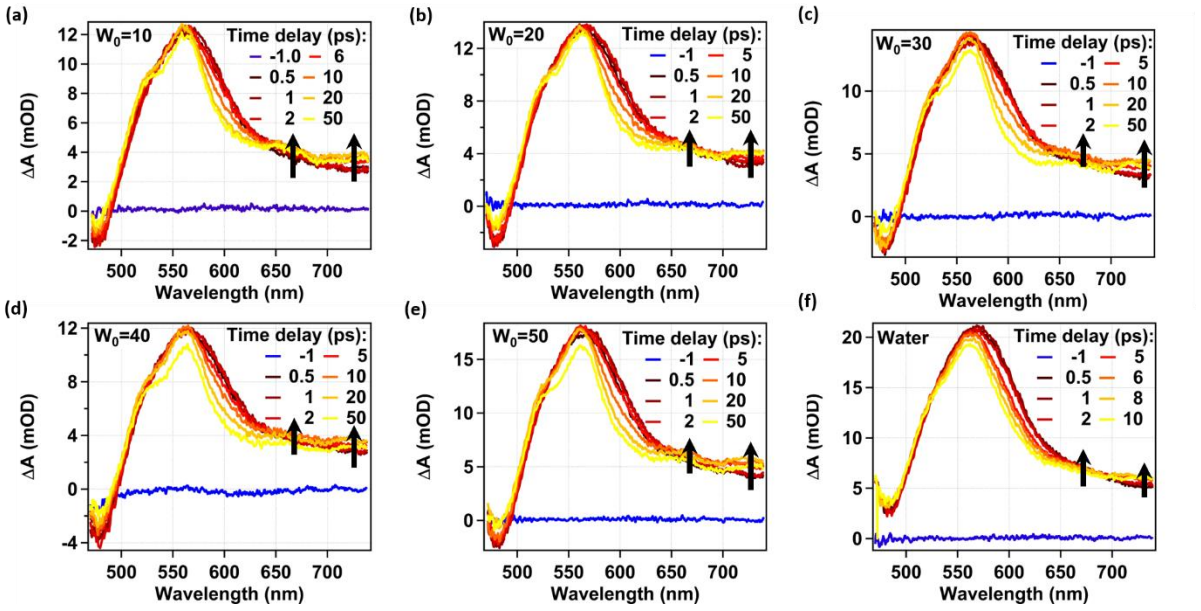

Figure 3.2.5. Transient absorption spectra of $[Cu(dmphen)_2]Cl$ at 25°C in AOT RM of five different water pool sizes (a) W_0=10, (b) W_0=20, (c) W_0=30, (d) W_0=40, (e) W_0=50 and (f) bulk water upon exciting at 400 nm at 25°C.

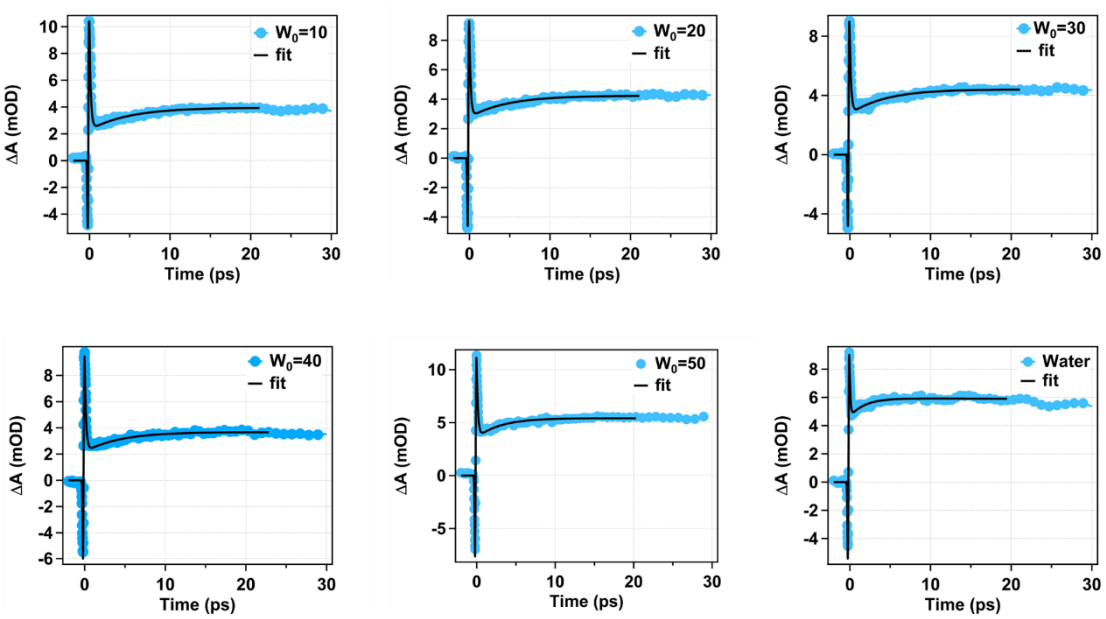

Figure 3.2.6. Kinetics of transient absorption signal of $[Cu(dmphen)_2]Cl$ at 730 nm in AOT RM of five different water pool sizes (a) W_0=10, (b) W_0=20, (c) W_0=30, (d) W_0=40, (e) W_0=50 and (f) Bulk water at 25°C. Samples were excited at 400 nm.

Table 3.2.2. ISC time-scale extracted from TA signal of $[Cu(dmphen)_2]Cl$ at 730 nm in glycerol/methanol mixtures, in various AOT RMs and in bulk water at 25°C.

System	ISC time (ps)
Glycerol:MeOH (90:10 v/v)	10.4
Glycerol:MeOH (10:90 v/v)	5.5
AOT RM W0=10	5.0
AOT RM W0=20	4.8
AOT RM W0=30	4.5
AOT RM W0=40	4.4
AOT RM W0=50	4.2
Water	1.8

Recently, Gourlaouen *et al*. theoretically established the involvement of ligand-Cu-ligand breathing motion in the ISC coordinate of Cu-phenanthrene complex, which is in line to our proposition.[45] According to their study, Cu-ligand distance coordinate S_1 state has two minima, which finally reaches the lowest energy triplet state. Indeed, upon excitation, the system can access both energy minima, and these minima are interconnected through an energy barrier. This feature contributes to the complex dynamics and pathways involved in the intersystem crossing (ISC) process. To

determine the barrier height between S_1 and T_1, temperature-dependent fs-TA measurement of $[Cu(dmphen)_2]Cl$ was performed in different glycerol-methanol compositions where the viscosity of the medium remains similar (~58-68 cP). The result is presented in figure 3.2.7 and the fitting parameters are tabulated in table 3.2.3. On increase in the temperature, the rate of the triplet state formation becomes faster. The rate constant of triplet formation i.e. k_{ISC} is estimated by taking the reciprocal of the growth time component of 730 nm kinetics considering that the rate constant for the depopulation of the flattened-S_1 state to the ground state is insignificant (see Supplementary Material for details). The Arrhenius plot of the variation of the rate constant of triplet formation with temperature (Table 3.2.3 and Figure 3.2.7b) yields an activation energy of 5.9 kJ mol^{-1}. The barrier height for the triplet formation is low, implying that it can be readily overcome by fluctuations in the surrounding medium of $[Cu(dmphen)_2]Cl$ due to the temperature.

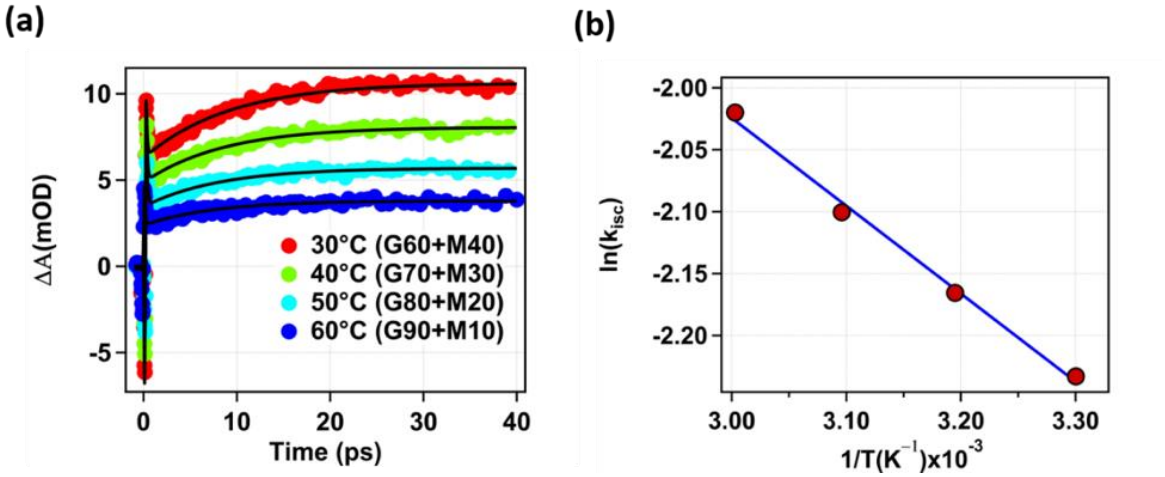

Figure 3.2.7. (a) Kinetics of transient signal of $[Cu(dmphen)_2]Cl$ at 730 nm in various glycerol/methanol mixtures at given temperatures. The mixture composition and the temperature were chosen carefully so that viscosity of the medium remains similar at those temperatures (Samples were excited at 400 nm) (b) Arrhenius plot for the determination of activation energy barrier of ISC.

Table 3.2.3. ISC time-scale extracted from TA signal of [Cu(dmphen)$_2$]Cl at 730 nm in glycerol/methanol mixtures at given temperature as presented in figure 3.2.7a. The rate constant of triplet formation is calculated by taking the inverse of the growth time of triplet formation.

Temp (K)	Growth time (ps)	Rate constant, k (ps^{-1})	$\ln(k)$	Inverse Temp (1/K)
303	9.3	0.108	–2.226	0.003300
313	8.7	0.115	-2.163	0.003195
323	8.2	0.122	-2.104	0.003096
333	7.5	0.133	-2.017	0.003003

Rate constant for ISC:

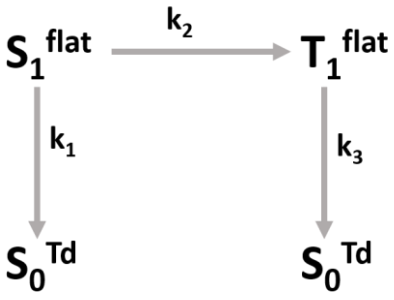

In the above scheme, as proposed in our study, k_1 is the decay rate constant of S_1^{flat} state to S_0^{Td} state, k_2 is the rate constant of ISC (i.e. k_{ISC}) from S_1^{flat} state to T_1^{flat} state, and k_3 is the decay rate constant of T_1^{flat} state to S_0^{Td} state. Thus, we can write,

$$-\frac{d\left[S_1^{flat}\right]}{dt} = (k_1 + k_2)\left[S_1^{flat}\right] \text{ and } -\frac{d\left[T_1^{flat}\right]}{dt} = -k_2\left[S_1^{flat}\right] + k_3\left[T_1^{flat}\right] \quad (3.2.1)$$

The solution of the above two equations allows one to comprehend how the triplet state population changes as a function of time, which is shown below.

$$\left[T_1^{flat}\right] = \frac{k_2\left(S_1^{flat}\right)^0}{k_3 - k_1 - k_2}\left\{e^{-(k_1+k_2)t} - e^{-k_3 t}\right\} \quad (3.2.2)$$

where, $\left(S_1^{flat}\right)^0$ is the maximum population of the S_1^{flat} state

Iwamura *et al.* already reported the radiative rate constants (k_r) for different excited state manifolds of ([Cu(dmphen)$_2$] in dichloromethane. In particular, k_r for S_1^{flat}

state is in the order of 10^6 s^{-1}.[33] Considering that there is no non-radiative channel operating between S_1^{flat} and S_0^{Td} sates, k_r is assumed to be k_1. From the fluorescence up-conversion and transient absorption measurements we found that the time constants of triplet formation are in the order of 10^{10} s^{-1}. This allows us to neglect the contribution of k_1 compared to k_2 in the formation of the T_1^{flat} state, i.e. $k_1 \ll k_2$. Thus, we can write time-dependent T_1^{flat} population as

$$\left[T_1^{flat}\right] = \frac{k_2\left(S_1^{flat}\right)^0}{k_3 - k_2}\{e^{-k_2 t} - e^{-k_3 t}\} \quad (3.2.3)$$

$$= \frac{k_2\left(S_1^{flat}\right)^0}{k_3 - k_2}\{e^{-k_2 t} - e^{-k_3 t}\} \quad (3.2.4)$$

$$= \frac{k_2\left(S_1^{flat}\right)^0}{k_3 - k_2}\{e^{-k_2 t}\} - \frac{k_2\left(S_1^{flat}\right)^0}{k_3 - k_2}\{e^{-k_3 t}\} \quad (3.2.4)$$

$$= -A(e^{-k_2 t}) + A(e^{-k_3 t}), \text{ as } k_2 > k_3 \text{ and } A = \frac{k_2\left(S_1^{flat}\right)^0}{k_2 - k_3} \quad (3.2.5)$$

Here, the first and second terms indicate the population growth and decay of the T_1^{flat} state, respectively. Under this condition, we consider that the growth time component may be used to describe the rate constant (k_{ISC}) of the ISC process.

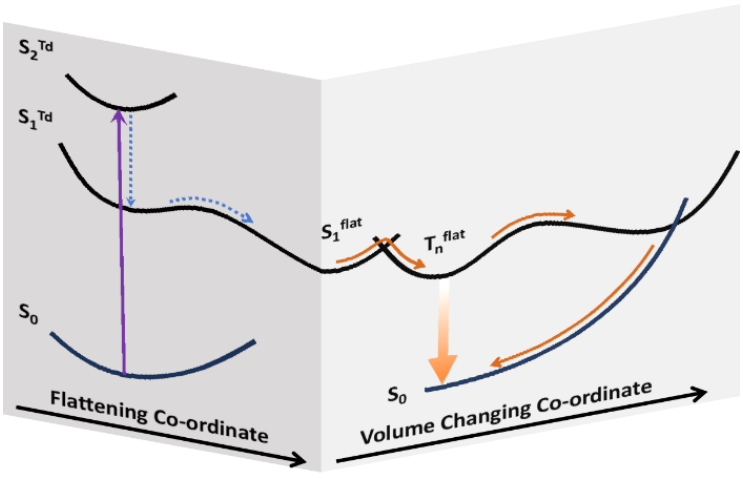

Scheme 3.2.2. A schematic of general relaxation mechanism for photoexcited $[Cu(dmphen)_2]Cl$.

From the analysis of our experimental observations, we present an overall relaxation process of the photoexcited $[Cu(dmphen)_2]Cl$ in scheme 2, where we have successfully captured the effect of surrounding viscosity on the excited state ISC dynamics involving volume changing reaction coordinate. We believe that this result will add a new insight into the recent understanding of vibration-assisted intersystem crossing process.

3.3. Conclusions

The present study proposed the involvement of volume changing motion in the singlet-triplet dynamics and also in the fate of the triplet state of $[Cu(dmphen)_2]Cl$ using steady-state and time-resolved absorption and emission spectroscopies. By controlling the viscosity and confinement in glycerol/methanol binary solvent mixture and water pool size of AOT-RM, we conclude that molecular vibration might play a crucial role in deciding the phosphorescence quantum yield of $[Cu(dmphen)_2]Cl$. The femtosecond transient absorption study in combination with the fluorescence up-conversion investigation reveal that the triplet formation dynamics is in the order of few ps. The strong viscosity/confinement dependence of this time constant leads us to propose that the ISC coordinate involves a volume changing motion in $[Cu(dmphen)_2]Cl$. From the temperature dependent femtosecond transient absorption experiments in glycerol/methanol mixtures, where the viscosity remains similar at different temperatures, the activation barrier is estimated to be 5.9 kJ mol^{-1}. A recent theoretical study also revealed the existence of an activation energy barrier in the ISC channel along the copper-ligand distance coordinate.[45] This comprehensive understanding revealed the significance of molecular vibrations in governing ISC in $[Cu(dmphen)_2]Cl$, which is an activated process. We believe that our study will add a significant contribution to the contemporary research on vibration assisted ISC.

References

1. Gemenetzidis, E.; Shavorskaya, O.; Xu, Y. Z.; Trigiante, G. Topical 4-Thiothymidine Is a Viable Photosensitiser for the Photodynamic Therapy of Skin Malignancies. *J Dermatolog Treat.* **2011**, *24*, 209–214.
2. Steiner, F.; Lupton, J. M.; Vogelsang, J. Role of Triplet-State Shelving in Organic Photovoltaics: Single-Chain Aggregates of Poly(3-Hexylthiophene) versus Mesoscopic Multichain Aggregates. *J. Am. Chem. Soc.* **2017**, *139*, 9787–9790.
3. Sakamoto, Y.; Izawa, S.; Ohkita, H.; Hiramoto, M.; Tamai, Y. Triplet Sensitization via Charge Recombination at Organic Heterojunction for Efficient Near-Infrared to Visible Solid-State Photon Upconversion. *Commun Mater* **2022**, *3*, 76.
4. Grancini, G.; De Bastiani, M.; Martino, N.; Fazzi, D.; Egelhaaf, H. J.; Sauermann, T.; Antognazza, M. R.; Lanzani, G.; Caironi, M.; Franco, L.; Petrozza, A. The Critical Role of Interfacial Dynamics in the Stability of Organic Photovoltaic Devices. *Phys. Chem. Chem. Phys.* **2014**, *16*, 8294–8300.
5. Elliott, L. D.; Kayal, S.; George, M. W.; Booker-Milburn, K. Rational Design of Triplet Sensitizers for the Transfer of Excited State Photochemistry from UV to Visible. *J. Am. Chem. Soc.* **2020**, *142*, 14947–14956.
6. Wang, R.; Xu, J.; Fu, L.; Zhang, C.; Li, Q.; Yao, J.; Li, X.; Sun, C.; Zhang, Z. G.; Wang, X.; Li, Y.; Ma, J.; Xiao, M. Nonradiative Triplet Loss Suppressed in Organic Photovoltaic Blends with Fluoridated Nonfullerene Acceptors. *J. Am. Chem. Soc.* **2021**, *143*, 4359–4366.
7. Hedley, G. J.; Ruseckas, A.; Samuel, I. D. W. Light Harvesting for Organic Photovoltaics. *Chem. Rev.* **2017**, *117*, 796–837.
8. Yanai, N.; Kimizuka, N. New Triplet Sensitization Routes for Photon Upconversion: Thermally Activated Delayed Fluorescence Molecules, Inorganic Nanocrystals, and Singlet-to-Triplet Absorption. *Acc. Chem. Res.* **2017**, *50*, 2487–2495.

9. Lewis, G. N.; Kasha, M. Phosphorescence and the Triplet State. *J. Am. Chem. Soc.* **1944**, *66*, 2100–2116.
10. Marian, C. M. Spin-Orbit Coupling and Intersystem Crossing in Molecules. Wiley Interdiscip Rev *Comput Mol Sci* **2012**, *2*, 187–203.
11. Furlani, T. R.; King, H. F. Theory of Spin-Orbit Coupling. Application to Singlet-Triplet Interaction in the Trimethylene Biradical. *J. Chem. Phys.* **1984**, *82*, 5577–5583.
12. Kim, J. W.; Kang, D. G.; Kim, S. K.; Joo, T. Role of Coherent Nuclear Motion in the Ultrafast Intersystem Crossing of Ruthenium Complexes. *Phys. Chem. Chem. Phys*. **2020**, *22*, 25811–25818.
13. Van Veenendaal, M.; Chang, J.; Fedro, A. J. Model of Ultrafast Intersystem Crossing in Photoexcited Transition-Metal Organic Compounds. *Phys. Rev. Lett.* **2010**, *104*, 067401.
14. Van Der Veen, R. M.; Cannizzo, A.; Van Mourik, F.; Vlček, A.; Chergui, M. Vibrational Relaxation and Intersystem Crossing of Binuclear Metal Complexes in Solution. *J. Am. Chem. Soc.* **2011**, *133*, 305–315.
15. Jones, R. W.; Auty, A. J.; Wu, G.; Persson, P.; Appleby, M. V.; Chekulaev, D.; Rice, C. R.; Weinstein, J. A.; Elliott, P. I. P.; Scattergood, P. A. Direct Determination of the Rate of Intersystem Crossing in a Near-IR Luminescent Cr(III) Triazolyl Complex. *J. Am. Chem. Soc.* **2023**, *145*, 12081–12092.
16. Uppili, S.; Marti, V.; Nikolaus, A.; Jockusch, S.; Adam, W.; Engel, P. S.; Turro, N. J.; Ramamurthy, V. Heavy-Cation-Induced Phosphorescence of Alkanones and Azoalkanes in Zeolites as Hosts: Induced S_1 ($n\pi^*$) to T_1 ($n\pi^*$) Intersystem Crossing and S0 to T1 ($n\pi^*$) Absorption. *J. Am. Chem. Soc.* **2000**, *122*, 11025–11026.
17. Romanova, Z. S.; Deshayes, K.; Piotrowiak, P. Remote Intermolecular "Heavy-Atom Effect": Spin-Orbit Coupling across the Wall of a Hemicarcerand. *J. Am. Chem. Soc.* **2001**, *123*, 2444–2445.
18. Mońka, M.; Serdiuk, I. E.; Kozakiewicz, K.; Hoffman, E.; Szumilas, J.; Kubicki, A.; Park, S. Y.; Bojarski, P. Understanding the Internal Heavy-

Atom Effect on Thermally Activated Delayed Fluorescence: Application of Arrhenius and Marcus Theories for Spin-Orbit Coupling Analysis. *J. Mater. Chem. C* ***2022***, *10*, 7925–7934.

19. Nagarajan, K.; Mallia, A. R.; Reddy, V. S.; Hariharan, M. Access to Triplet Excited State in Core-Twisted Perylenediimide. *J. Phys. Chem. C* **2016**, *120*, 8443–8450.
20. Tsuneda, T.; Taketsugu, T. Singlet Fission Initiating Triplet Generations of BODIPY Derivatives through π -Stacking: A Theoretical Study. *Sci Rep* **2022**, *12*, 19714.
21. Dong, Y.; Sukhanov, A. A.; Zhao, J.; Elmali, A.; Li, X.; Dick, B.; Karatay, A.; Voronkova, V. K. Spin-Orbit Charge-Transfer Intersystem Crossing (SOCT-ISC) in Bodipy-Phenoxazine Dyads: Effect of Chromophore Orientation and Conformation Restriction on the Photophysical Properties. *J. Phys. Chem. C* **2019**, *123*, 22793–22811.
22. Mikulchyk, T.; Karuthedath, S.; De Castro, C. S. P.; Buglak, A. A.; Sheehan, A.; Wieder, A.; Laquai, F.; Naydenova, I.; Filatov, M. A. Charge Transfer Mediated Triplet Excited State Formation in Donor-Acceptor-Donor BODIPY: Application for Recording of Holographic Structures in Photopolymerizable Glass. *J. Mater. Chem. C* **2022**, *10*, 11588–11597.
23. Mewes, L.; Ingle, R. A.; Megow, S.; Böhnke, H.; Baranoff, E.; Temps, F.; Chergui, M. Ultrafast Intersystem Crossing and Structural Dynamics of $[Pt(Ppy)(\mu\text{-}TBu_2pz)]_2$. *Inorg. Chem.* **2020**, *59*, 14643–14653.
24. Kim, P.; Valentine, A. J. S.; Roy, S.; Mills, A. W.; Castellano, F. N.; Li, X.; Chen, L. X. Ultrafast Branching in Intersystem Crossing Dynamics Revealed by Coherent Vibrational Wavepacket Motions in a Bimetallic Pt(II) Complex. *Faraday Discuss.* **2022**, *237*, 259–273.
25. Marian, C. M. Spin-Orbit Coupling and Intersystem Crossing in Molecules. *WIREs Comput Mol Sci* **2012**, *2*, 187–203.

26. Rafiq, S.; Weingartz, N. P.; Kromer, S.; Castellano, F. N.; Chen, L. X. Spin–Vibronic Coherence Drives Singlet–Triplet Conversion. *Nature* **2023**, *620*, 776–781.

27. Das, A.; Ghosh, S. K.; Ramamurthy, V.; Sen, P. Vibration-Assisted Intersystem Crossing in the Ultrafast Excited-State Relaxation Dynamics of Halocoumarins. *J. Phys. Chem. A* **2022**, *126*, 1475–1485.

28. Mandal, S.; Daniel, C. Spin-Vibronic Mechanism at Work in a Luminescent Square-Planar Cyclometalated Tridentate Pt(II) Complex: Absorption and Ultrafast Photophysics. *Phys. Chem. Chem. Phys.* **2023**, *25*, 18720–18727.

29. Farrow, G. A.; Quick, M.; Kovalenko, S. A.; Wu, G.; Sadler, A.; Chekulaev, D.; Chauvet, A. A. P.; Weinstein, J. A.; Ernsting, N. P. On the Intersystem Crossing Rate in a Platinum(II) Donor-Bridge-Acceptor Triad. *Phys. Chem. Chem. Phys.* **2021**, *23*, 21652–21663.

30. Garakyaraghi, S.; McCusker, C. E.; Khan, S.; Koutnik, P.; Bui, A. T.; Castellano, F. N. Enhancing the Visible-Light Absorption and Excited-State Properties of Cu(I) MLCT Excited States. *Inorg. Chem.* **2018**, *57*, 2296–2307.

31. Zhang, Y.; Schulz, M.; Wächtler, M.; Karnahl, M.; Dietzek, B. Heteroleptic Diimine–Diphosphine Cu(I) Complexes as an Alternative towards Noble-Metal Based Photosensitizers: Design Strategies, Photophysical Properties and Perspective Applications. *Coord. Chem. Rev.* **2018**, *356*, 127–146.

32. Brown-Xu, S.; Fumanal, M.; Gourlaouen, C.; Gimeno, L.; Quatela, A.; Thobie-Gautier, C.; Blart, E.; Planchat, A.; Riobé, F.; Monnereau, C.; Chen, L. X.; Daniel, C.; Pellegrin, Y. Intriguing Effects of Halogen Substitution on the Photophysical Properties of 2,9-(Bis)Halo-Substituted Phenanthrolinecopper(I) Complexes. *Inorg. Chem.* **2019**, *58*, 7730–7745.

33. Iwamura, M.; Takeuchi, S.; Tahara, T. Real-Time Observation of the Photoinduced Structural Change of Bis(2,9-Dimethyl-1,10-Phenanthroline)Copper(I) by Femtosecond Fluorescence Spectroscopy: A

Realistic Potential Curve of the Jahn-Teller Distortion. *J. Am. Chem. Soc.* **2007**, *129*, 5248–5256.

34. Iwamura, M.; Watanabe, H.; Ishii, K.; Takeuchi, S.; Tahara, T. Coherent Nuclear Dynamics in Ultrafast Photoinduced Structural Change of Bis(Diimine)Copper(I) Complex. *J. Am. Chem. Soc.* **2011**, *133*, 7728–7736.
35. Iwamura, M.; Takeuchi, S.; Tahara, T. Substituent Effect on the Photoinduced Structural Change of Cu(i) Complexes Observed by Femtosecond Emission Spectroscopy. *Phys. Chem. Chem. Phys.* **2014**, *16*, 4143–4154.
36. Sandoval-Pauker, C.; Santander-Nelli, M.; Dreyse, P. Thermally Activated Delayed Fluorescence in Luminescent Cationic Copper(i) Complexes. *RSC Adv.* **2022**, *12*, 10653–10674.
37. Chen, L. X.; Shaw, G. B.; Novozhilova, I.; Liu, T.; Jennings, G.; Attenkofer, K.; Meyer, G. J.; Coppens, P. MLCT State Structure and Dynamics of a Copper(I) Diimine Complex Characterized by Pump-Probe x-Ray and Laser Spectroscopies and DFT Calculations. *J. Am. Chem. Soc.* **2003**, *125*, 7022–7034.
38. Du, L.; Lan, Z. Ultrafast Structural Flattening Motion in Photoinduced Excited State Dynamics of a Bis(Diimine) Copper(i) Complex. *Phys. Chem. Chem. Phys.* **2016**, *18*, 7641–7650.
39. Gimeno, L.; Phelan, B. T.; Sprague-Klein, E. A.; Roisnel, T.; Blart, E.; Gourlaouen, C.; Chen, L. X.; Pellegrin, Y. Bulky and Stable Copper(I)-Phenanthroline Complex: Impact of Steric Strain and Symmetry on the Excited-State Properties. *Inorg. Chem.* **2022**, *61*, 7296–7307.
40. Shaw, G. B.; Grant, C. D.; Shirota, H.; Castner, E. W.; Meyer, G. J.; Chen, L. X. Ultrafast Structural Rearrangements in the MLCT Excited State for Copper(I) Bis-Phenanthrolines in Solution. *J. Am. Chem. Soc.* **2007**, *129*, 2147–2160.
41. Rajbongshi, B. K.; Rafiq, S.; Bhowmik, S.; Sen, P. Ultrafast Excited State Relaxation of a Model Green Fluorescent Protein Chromophore:

Femtosecond Fluorescence and Transient Absorption Study. *J. Mol. Struct.* **2023**, *1275*, 134538.

42. Afshar Ghotli, R.; Abdul Aziz, A. R.; Atadashi, I. M.; Hasan, D. B.; Kong, P. S.; Aroua, M. K. Selected Physical Properties of Binary Mixtures of Crude Glycerol and Methanol at Various Temperatures. *Journal of Industrial and Engineering Chemistry* **2015**, *21*, 1039–1043.
43. Haidekker, M. A.; Brady, T. P.; Lichlyter, D.; Theodorakis, E. A. Effects of Solvent Polarity and Solvent Viscosity on the Fluorescent Properties of Molecular Rotors and Related Probes. *Bioorg. Chem.* **2005**, *33*, 415–425.
44. Rafiq, S.; Yadav, R.; Sen, P. Microviscosity inside a Nanocavity: A Femtosecond Fluorescence up-Conversion Study of Malachite Green. *J. Phys. Chem. B* **2010**, *114*, 13988–13994.
45. Gourlaouen, C.; Daniel, C. Towards Optimized Photoluminescent Copper(I) Phenanthroline-Functionalized Complexes: Control of the Photophysics by Symmetry-Breaking and Spin–Orbit Coupling. *Materials* **2022**, *15*, 5222.

This page left blank intentionally

Chapter 4

Ultrafast Processes in Upper Excited Singlet States of Free and Caged 7-Diethylaminothiocoumarin

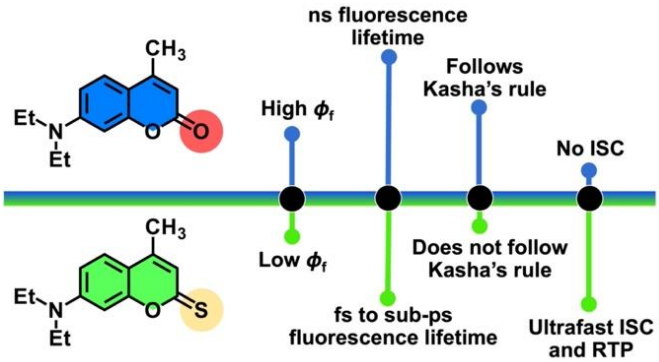

Abhijit Dutta, Sujit Kumar Ghosh, Satyajit Mandal, Varadharajan Srinivasan, Vaidhyanathan Ramamurthy and Pratik Sen, *J. Phys. Chem. A* **2024**, 128, 33, 6853–6863.

The photochemistry and photophysics of thiocarbonyl compounds, analogues of carbonyl compounds with sulfur, have long been overshadowed by their counterparts. However, recent interest in visible light reactions has reignited attention towards these compounds due to their unique excited state properties. This study delves into the ultrafast dynamics of 7-diethylaminothiocoumarin (TC1), a close analogue of a well-known probe molecule coumarin 1 (C1), to estimate intersystem crossing rates, understand the mechanism of fluorescence and phosphorescence, and evaluate TC1's potential as a solvation dynamics probe. Enclosing TC1 within an organic capsule indicates its potential applications even in aqueous environments. Ultrafast studies reveal a dominant sub-picosecond intersystem crossing process, indicating the importance of upper excited singlet and triplet states in the molecule's photochemistry. The distinct fluorescence and phosphorescence origins, along with the presence of closely spaced singlet excited states, support the observed efficient intersystem crossing. The sulfur atom alters the excited state behavior, shedding light on reactive triplet states and paving the way for further investigations.

4.1 Introduction

The photochemistry and photophysics of thiocarbonyl compounds, i.e. the sulfur analogues of carbonyl compounds, have been overlooked for decades in favor of carbonyl compounds.[1-4] Despite the undesirable characteristics such as foul smell and poor stability, these molecules have been established to possess interesting excited state properties such as emission[5] and reactivity from upper excited states[3] and quantitative rapid conversion to lower triplet from excited singlet manifold.[6] Fortunately, smell is compensated by attractive color of these molecules. Recent interest in conducting reactions with visible light, has refocussed the attention on molecules containing thiocarbonyl chromophore.[7-10]

One of the current authors' interest in thiocarbonyl compounds dates back to early 1970s.[11-13] Towards the waning years of his activities in this area, his group noted that thiocoumarins possess close to unity quantum yield of intersystem crossing (ISC) as well as several properties similar to diaryl, dialkyl and arylalkyl thioketones.[14-16] Unfortunately, unlike in thioketones, since S_2 and S_1 states are closer in energy in thiocoumarin it was not possible to identify reactions from upper excited states and unequivocally identify the electronic nature of the state from which the weak fluorescence and strong phosphorescence originate.[17] At that time, due to lack of ultrafast facilities, the rate and the origin of ISC could not be determined. In this article we have fulfilled the gap by probing the ultrafast dynamics of 7-diethylaminothiocoumarin (TC1, Scheme 1 for structure), a close analogue 7-diethylaminocoumarin (C1, Scheme 1). Our interest in TC1, as opposed to the parent thiocoumarin, derives from the central role of the analogous C1 in molecular photochemistry and photophysics. C1 is a well-known probe to monitor solvation dynamics in various media[18-24] and derivatives of it have served as photoprotecting groups in organic photochemistry.[25-28] We hoped that TC1 will display similar properties and thought therefore it is important to gain knowledge of its photophysics. Our goals in the current undertaking were to estimate the rates of ISC from the singlet manifold to the triplet, to understand the mechanism of ISC, to

identify the origin of fluorescence and phosphorescence and to establish the viability of using TC1 as a probe to monitor solvation dynamics.

It is well known that the excited molecules possessing thiocarbonyl chromophore are deactivated through physical[29] and chemical quenching by self, solvent and oxygen.[1, 3, 12, 30-40] To isolate the molecule from the above solvent surroundings, another molecule of its own kind and oxygen, the excited state dynamics of a single TC1 molecule enclosed within an organic capsule formed by two molecules of octa acid (Scheme 1) was investigated.[41-45] As expected, the dynamics were cleaner than in organic solvents and intense phosphorescene was recorded even at room temperature indicating that the TC1 molecule even in millisecond time scale was not exposed to exterior water molecules and oxygen.[46] As discussed below, the excited singlets live only for subpicsecond and in that time scale, certainly, the encaged TC1 is not expected to interact with any other molecules except the walls of the capsule. Thus, we were able to monitor the dynamics of an encaged TC1 molecule in aqueous solution at room temperature.

There have been a few ultrafast studies on thiocarbonyl molecules including parent thiocoumarin (TC).[47-51] A short S_2 lifetime of 100 fs[47] was reported in TC, being attributed to the presence of a conical intersection between S_2 to S_1. ISC is suggested to occur from S_1 to T_1. A series of indepth ultrafast studies on thiocarbonyl substituted nucleic acid bases reveal that the S_2 state of these molecules live only for a few hundred of fs.[49-51] Once again, the short lifetime of S_2 is attributed to the presence of a conical intersection leading S_2 to S_1. The ISC to T_2 and T_1 is proposed to occur from S_1. Direct crossing from S_2 to the triplet manifold is suggested to be only a minor pathway. However, an early study suggested direct T_2 formation from S_2 of dialkyl thioketones.[52] The rapid ISC in these systems is suggested to involve crossing from S_2 to T_2 followed by internal conversion to T_1. Interestingly, even photoreactions are speculated to originate from T_2.[13, 53] Thus, in addition to S_1 and T_1, upper excited singlet and triplet states could play a role in the photochemistry and photophysics of TC1. The extraordinarily short lifetimes and high triplet yields

reported for thiocarbonyl substituted nucleic acid bases and various thioketones, prompted us to undertake a detailed ultrafast studies on TC1.

It is well-known that thiocarbonyls react with solvents from upper excited states and deactivate by interacting with solvent C-H bonds.[29, 37-38, 54-55] These make the study in organic solvents as well as OA encaged TC1 challenging, We believe the insights we gain from the current study with TC1 would help us exploit systems like TP1 (Scheme 4.1.1) as a photoprotecting group.[26] Surprisingly, we found that the absorption and excitation spectra for fluorescence in TC1 do not overlap suggesting that there is a hidden state with almost negligible absorption co-efficient.[56] Furthermore, we have made progress in identifying the states involved in the singlet-triplet crossing and measured the corresponding rates. However, the mechanistic origin of the fast ISC remains to be determined.

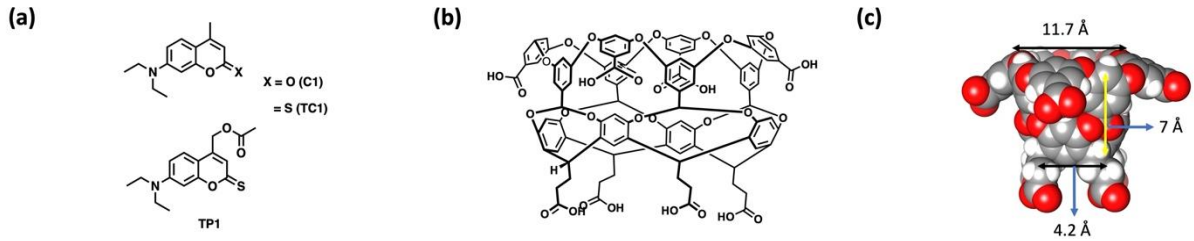

Scheme 4.1.1: (a) Molecular structure of 7-diethylaminocoumarin (coumarin-1 or C1), 7-diethylaminothiocoumarin (thiocoumarin-1 or TC1) and 7-diethylaminothiocoumarin phototrigger (TP1) (b) Chemical structure of water-soluble octa acid (OA) cavitand (c) Three-dimensional structure of OA cavitand.

4.2 Results and Discussion

Our initial studies revealed the fluorescence quantum yield (ϕ_f) of TC1 to be exceptionally low (~10^{-4}) compared to its oxygen analog C1 (0.73).[57] Further, the ϕ_f of TC1 was found to depend strongly on the solvent (see Table 4.2.1). In addition, the excitation spectrum of the fluorescence did not fully match with the

absorption. These unusual observations prompted us to undertake ultrafast experiments whose results are discussed below.

4.2.1 Steady-state and time-resolved absorption/emission studies in solution. The steady-state absorption and emission spectra of TC1 in various polar and nonpolar solvents are shown in Figures 4.2.1a and 4.2.1b. In acetonitrile the absorption maximum is at 456 nm with the molar absorption coefficient (ε) of 43,500±750 M^{-1} cm^{-1} (see Figure 4.2.2). This is about two times higher than for C1.[58] Upon decreasing the polarity of the solvent a hypsochromic shifts of the absorption (left panel) and the emission (right panel) maxima are observed (see Table 4.2.1) suggesting the excited state dipole moment of TC1 to be higher than that of the ground state.

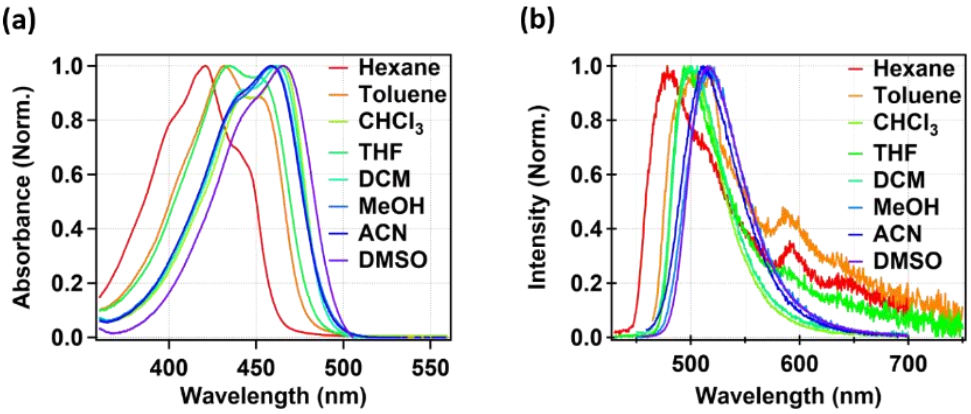

Figure 4.2.1. Steady-state (a) absorption and (b) emission spectra of TC1 in different solvents; hexane (λ_{ex} = 400 nm), toluene (λ_{ex} = 450 nm), chloroform (λ_{ex} = 440 nm), THF (λ_{ex} = 400 nm), DCM (λ_{ex} = 440 nm), MeOH (λ_{ex} = 440 nm), ACN (λ_{ex} = 440 nm), and DMSO (λ_{ex} = 440 nm) at 25°C All the absorption/emission measurements were done in aerated condition without any special treatment.

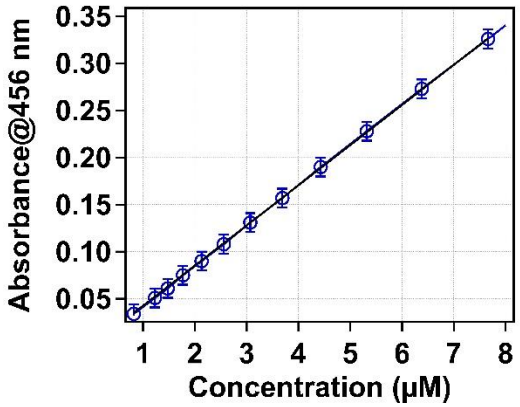

Figure 4.2.2. Calculation of the molar extinction coefficient (ε) of TC1 through the steady-state absorption measurement in aerated condition at 25°C. Steady-state absorbance of TC1 in ACN solvent at 456 nm vs concentration of the probe TC1 dye. From the linear equation fit of Lambert-Beer's law we have found the molar extinction coefficient (ε) of TC1 is ~43500±750 M^{-1} cm^{-1} at 456 nm.

Table 4.2.1. Experimental absorption maxima, emission maxima, and fluorescence quantum yield ($\emptyset_f$) of TC1 in different solvents.

Medium	$\boldsymbol{\lambda_{abs}^{max}}$ **(nm)**	$\boldsymbol{\lambda_{em}^{max}}$ **(nm)**	$\boldsymbol{\phi_f}$
Gas phase	Nil	Nil	Nil
Hexane	401,421,445	480,512,590,645 (λ_{ex}=400 nm)	0.000583
Toluene	432,452	502,590,640 (λ_{ex}=450 nm)	0.00183
Diethyl ether	426,446	483,586 (λ_{ex}=400 nm)	Nil
Chloroform	442,464	497 (λ_{ex}=440 nm)	Nil
THF	434,453	497 (λ_{ex}=400 nm)	0.00145
DCM	442,462	500 (λ_{ex}=440 nm)	0.000469
Methanol	439,460	518 (λ_{ex}=440 nm)	0.0036
Acetonitrile	440,458	515 (λ_{ex}=440 nm)	0.00027
DMSO	445,466	516 (λ_{ex}=440 nm)	0.00133

In nonpolar solvents (e.g. hexane, tetrahydrofuran and toluene), the major emission band near 500 nm is accompanied by two low intensity bands at 595 nm and 640 nm. In line with the previous works on thio-analogs of cyclic thioketones and thiocoumarins, we attribute these bands to phosphorescence.[1,4,5,46] Emission recorded under oxygen and nitrogen saturated conditions (Figure 4.2.3a) confirmed the long wavelength emission to be phosphorescence. The emission with maxima at 595 and 640 nm that was weak under aerated conditions was completely quenched upon bubbling the solution with oxygen. However, saturation of the solution with nitrogen brought back the emission. This observation leads us to conclude the origin of the 595 nm and 640 nm bands to be the triplet state. This observation is quite interesting as it established that thio-coumarin compounds are potential room temperature phosphorescence (RTP) molecules and might have wide applicability. A similar observation is also observed for TC1 in acetonitrile (see Figure 4.2.3b). To further confirm the origin, the emission spectra at 77 K in ethanol (polar) and methylcyclohexane (non-polar) glasses were recorded. From the spectra shown in Figures 4.2.4a-b we note an increase in intensities of the 595 nm and 640 nm bands upon lowering the temperature. This is due to suppression of oxygen and self-quenching in a rigid glassy medium, phenomena well-established for thiocarbonyl systems in solution.[1, 3] The gated emission spectrum after 0.1 ms of the excitation, shown in Figure 4.2.3c, contains only bands above 580 nm. The emission decay monitored at 595 nm could be fitted to a single exponential function with a lifetime of 4.2 ms (Figure 4.2.3d). The long lifetime, intense emission at 77 K and oxygen quenching in solution support our conclusion that the long wavelength emission in non-polar solvents at room temperature is phosphorescence.

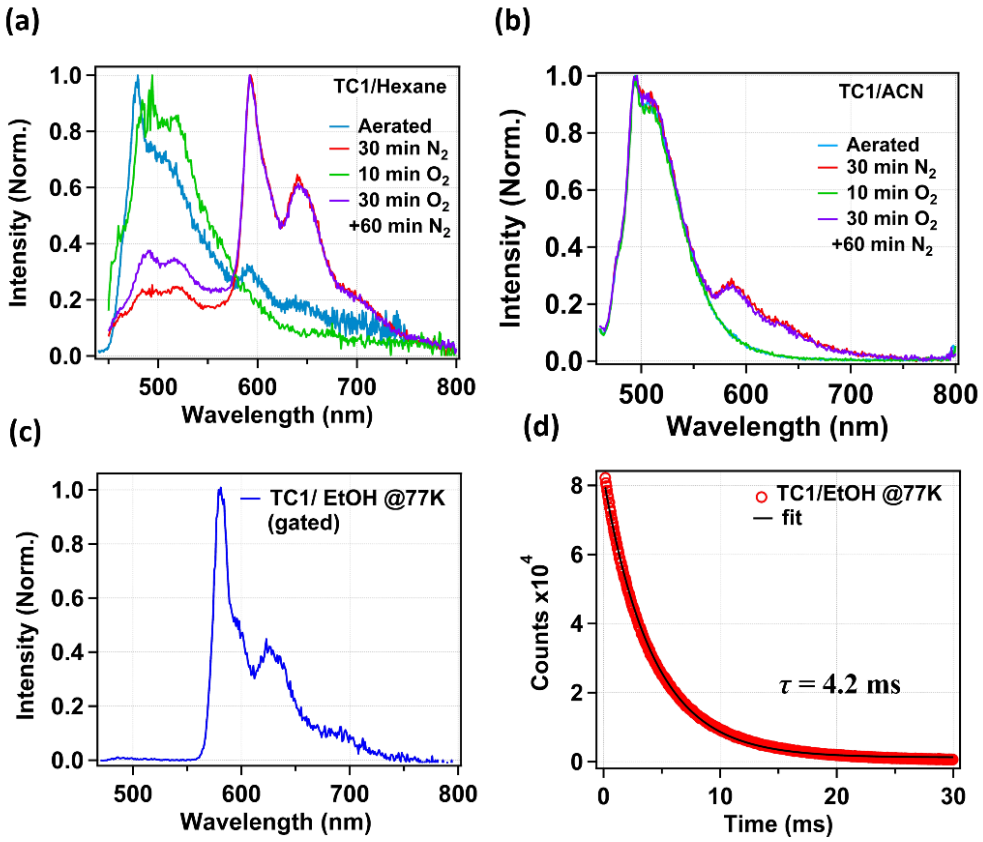

Figure 4.2.3. Steady-state emission in O_2/N_2 purged condition, time-gated emission spectroscopy, and lifetime measurement: (a,b) Steady-state emission of TC1 in hexane and ACN in aerated and different purged conditions (λ_{ex}= 400 nm and 430 nm for Hexane and ACN respectively) (c) Time-gated emission spectra (λ_{ex} = 445 nm, delay 0.1 ms, gate width 3 ms) in EtOH glass a 77 K (d) Emission lifetime decay at 595 nm of TC1 in EtOH glass at 77 K.

To understand the origin of the fluorescence, the excitation spectra of TC1 in both polar and non-polar solvents were recorded and these with the absorption spectra are presented in Figures 4.2.5a-d. Surprisingly, the excitation spectrum of TC1 is red-shifted to absorption spectra in all the solvents. For C1 the excitation spectrum matches exactly with the absorption spectrum, which signifies that the emissive state is coupled with the Franck-Condon state (see Figure 4.2.6). Earlier photophysical studies on parent thiocoumarin molecules reported the exact matching of excitation spectrum with the absorption spectrum.[48] However, as seen in Figure 4.2.5a-d, in TC1 the excitation spectrum does not match with the absorption spectrum, and this

led us to conclude that the emissive state is not coupled to the FC state of the molecule.

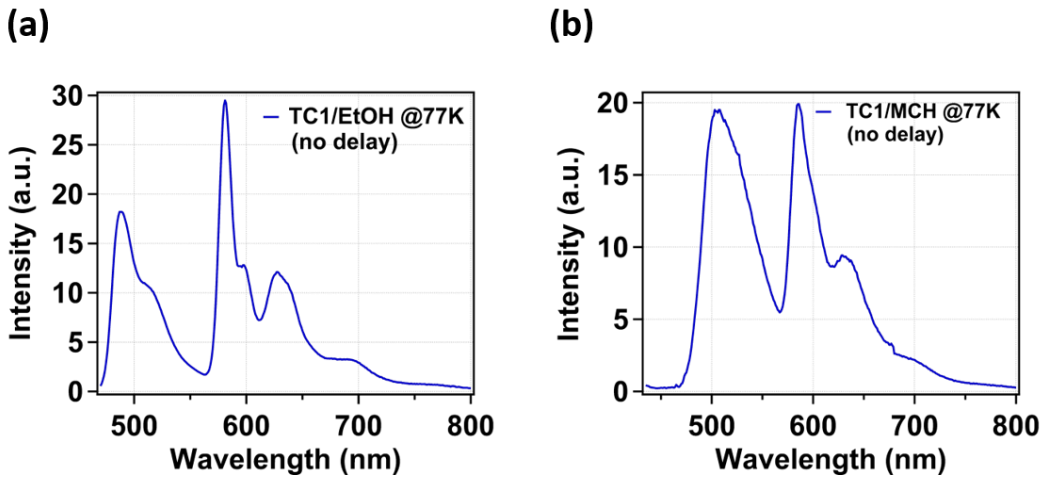

Figure 4.2.4. Steady-state non-gated low temperature (77 K) emission spectral measurement: (a) TC1 in ethanol (EtOH, λ_{ex}=457 nm) and (b) in methylcyclohexane (MCH, λ_{ex}=422 nm).

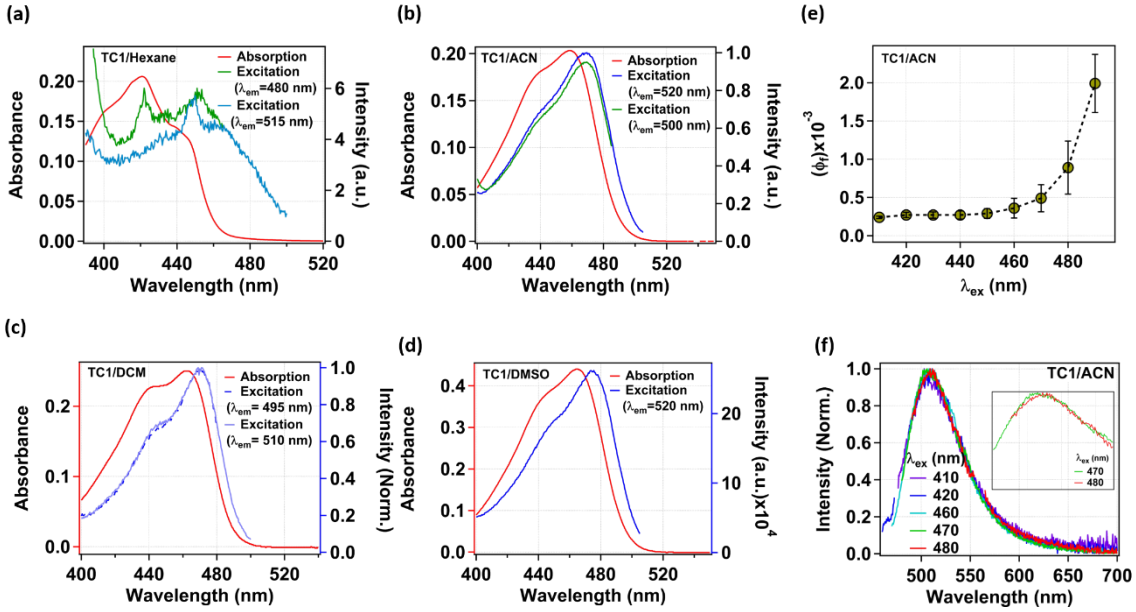

Figure 4.2.5. Steady-state excitation, emission spectral measurement and fluorescence quantum yield measurement: Excitation spectra (right axis) and absorption spectra (left axis) of TC1 in (a) hexane (Hex) and (b) acetonitrile (ACN), (c) dichloromethane (DCM) and (d) dimethylsulphoxide (DMSO) in aerated condition at 25°C (λ_{em} for excitation spectral measurements are indicated in the figures). (e) Excitation wavelength-dependent fluorescence quantum yield of TC1 in ACN solvent (Using the reference quantum yield 0.032 of coumarin

481 in 50 % ethanol). (f) Steady-state emission spectra of TC1 in ACN at various excitation wavelengths in aerated condition at 25°C (The insignificant shift of the fluorescence maximum position is highlighted in the inset figure)

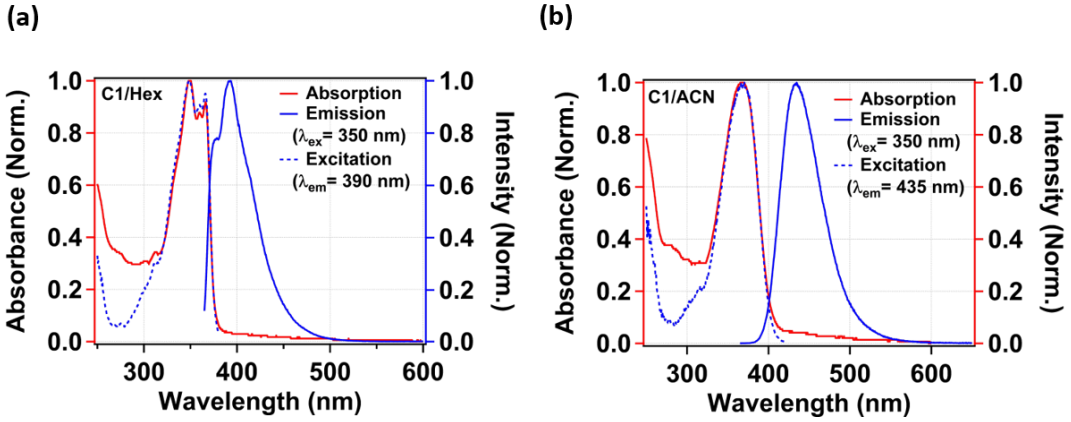

Figure 4.2.6. Steady-state absorption, emission, excitation spectral measurement: Absorption spectra (left axis, red solid line), emission spectra (right axis, blue solid line), and excitation spectra (right axis, blue dotted line) of TC1 in (a) hexane (Hex) and (b) acetonitrile (ACN) in aerated condition at 25°C (λ_{em} and λ_{ex} for excitation and emission spectral measurements are indicated in the figures).

To probe the origin of the unusual shift in the fluorescence excitation spectrum, we measured the excitation wavelength dependent fluorescence quantum yield (ϕ_f) (Figure 4.2.5e). According to Vavilov's rule, ϕ_f should be independent of the excitation wavelength for molecules emitting from the lowest excited singlet state, which is valid for most fluorophores. However, for TC1 in acetonitrile, we observed a 7-fold increase in ϕ_f upon changing the excitation wavelength from 440 nm ($\phi_f = 2.7 \times 10^{-4}$) to 490 nm ($\phi_f = 19.9 \times 10^{-4}$) (see Table 4.2.2 for measured data).

Table 4.2.2: Excitation wavelength-dependent fluorescence quantum yield (ϕ_f) of TC1 in ACN solvent

Excitation wavelength **(nm)**	$\boldsymbol{\phi_f}$
410	0.00024 $\pm$1.6e^{-05}
420	0.00027 $\pm$3.6e^{-05}
430	0.00027 $\pm$4.1e^{-05}

440	0.00027 $\pm$5.4e^{-05}
450	0.00029 $\pm$6.3e^{-05}
460	0.00036 $\pm$0.000129
470	0.00049 $\pm$0.000177
480	0.00089 $\pm$0.000346
490	0.00199 $\pm$0.00038

This observation indicates the presence of a highly fluorescent low energy state that is feebly accessible by direct light absorption. We believe, the red-shifted state is strongly emissive, but has very low absorption cross-section. We propose that the measured absorption spectrum is a linear combination of the two lowest singlet excited states. Two orders lower ϕ_f in TC1 with respect to C1 is likely to be the result of the presence of faster non-radiative channels in the singlet manifold.

The fluorescence lifetime of TC1 in hexane, acetonitrile and dichloromethane at their corresponding emission maxima is measured using femtosecond fluorescence up-conversion technique; decay traces are displayed in Figure 4.2.7. In hexane, the lifetime of TC1 is found to be single exponential with a time constant of 150 fs. In the case of acetonitrile, the decay was best fitted to a biexponential function with two time constants of 1.2 ps (43%) and 4.7 ps (57%). The fluorescence decay time constants of TC1 in hexane, acetonitrile, dichloromethane are tabulated in Table 4.2.3. The fluorescence decay of TC1 in dichloromethane shows a bi-exponential behavior, like in acetonitrile.

The origin of two lifetime components in acetonitrile and dichloromethane is proposed to be two closely spaced excited singlet states. If it is true, then we must expect a change in the excitation spectrum if the emission is monitored at different wavelengths. However, we have not seen any spectral shift of the excitation spectrum by changing the observed emission wavelength in acetonitrile and dichloromethane (see Figure 4.2.5b, 4.2.5c).

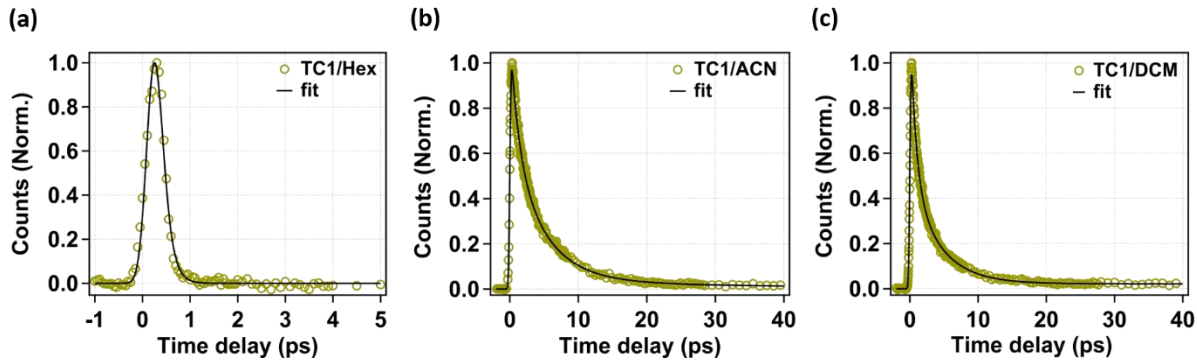

Figure 4.2.7. Fluorescence lifetime decays of TC1 in (a) hexane (Hex) (λ_{em} = 490 nm); (b) acetonitrile (ACN) (λ_{em} = 520 nm), and (c) dichloromethane (DCM) (λ_{em} = 510 nm) at 25 °C. All the fluorescence decays were measured in aerated conditions.

Table 4.2.3: Fitted kinetic parameters of TC1 in specified solvents in their fluorescence emission maximum.

Solvent	**a_1**	**τ_1 (ps)**	**a_2**	**τ_2 (ps)**
Hexane	1	0.15	-	-
ACN	0.43	1.2	0.57	4.7
DCM	0.83	0.6	0.17	4.2

Error in fitted time constants: ±30 fs for ultrafast growth component, ±0.2 ps for picosecond component

This is probably due to the large difference in the fluorescence quantum yield of the two emissive states in TC1. Quite likely the one with the larger quantum yield contributes to the overall emission. Earlier reports on parent thiocoumarin (TC) attributed the biexponential fluorescence decay to the equilibrated and unequilibrated vibrational energy levels of the singlet excited state.[48] If this is true, then we would expect a gradual shift in the emission spectra upon changing the excitation wavelength as was reported for TC. However, in this study, we have not seen any gradual shift of the emission maxima of TC1 in acetonitrile on changing the excitation wavelength (see Figure 4.2.5f). Rather, we observed a negligible shift in the emission maximum beyond a certain excitation wavelength (see Figure 4.2.5f inset figure). This indicates that the two emissive states of TC1 are not due to

different vibrational levels within a single excited singlet manifold. In the case of TC1, in all likelihood, atleast two distinct electronic states play a role in this unusual phenomenon. Consistent with this, as discussed above, two lifetimes were measured in acetonitrile and dichloromethane. Most likely in the case of hexane, the limited time resolution of our instrument (IRF~250 fs) missed the second component.

The combined fluorescence quantum yield and lifetime data suggest that most of the excited state population in TC1 is dispersed through non-radiative pathways. The occurrence of intense phosphorescence in low-temperature glass,[46] suggests that ISC is the most probable non-radiative channel operating in the excited singlet manifold of TC1. To authenticate this proposal, a femtosecond transient absorption study was conducted. Transient absorption spectra of TC1 in hexane and acetonitrile at different probe delay times are presented in Figure 4.2.8. At very early times, a negative band appears that matches the steady-state emission spectrum (see Figure 4.2.9), which is assigned to the stimulated emission (SE) band. This negative band converted to a broad positive band within a few picoseconds, that partially decays (until ~80-90 ps in both hexane and acetonitrile) and then remains unaltered till 1 ns (time window of our measurement). The positive band (460 nm to 730 nm) is assigned to the excited state absorption (ESA) band of the triplet state. The spectral feature of the ESA band in the early time (2 ps and 10 ps in the case of hexane and acetonitrile, respectively) was found to be different compared to the same in the later time regime. The former has been assigned to the ESA of higher order triplet (T_n), whereas, the ESA band at the later time is assigned to the (T_1) state. Radiationless decay of T_n to T_1 is a spin-allowed process, observation of a fast decay of the T_n state is not surprising.

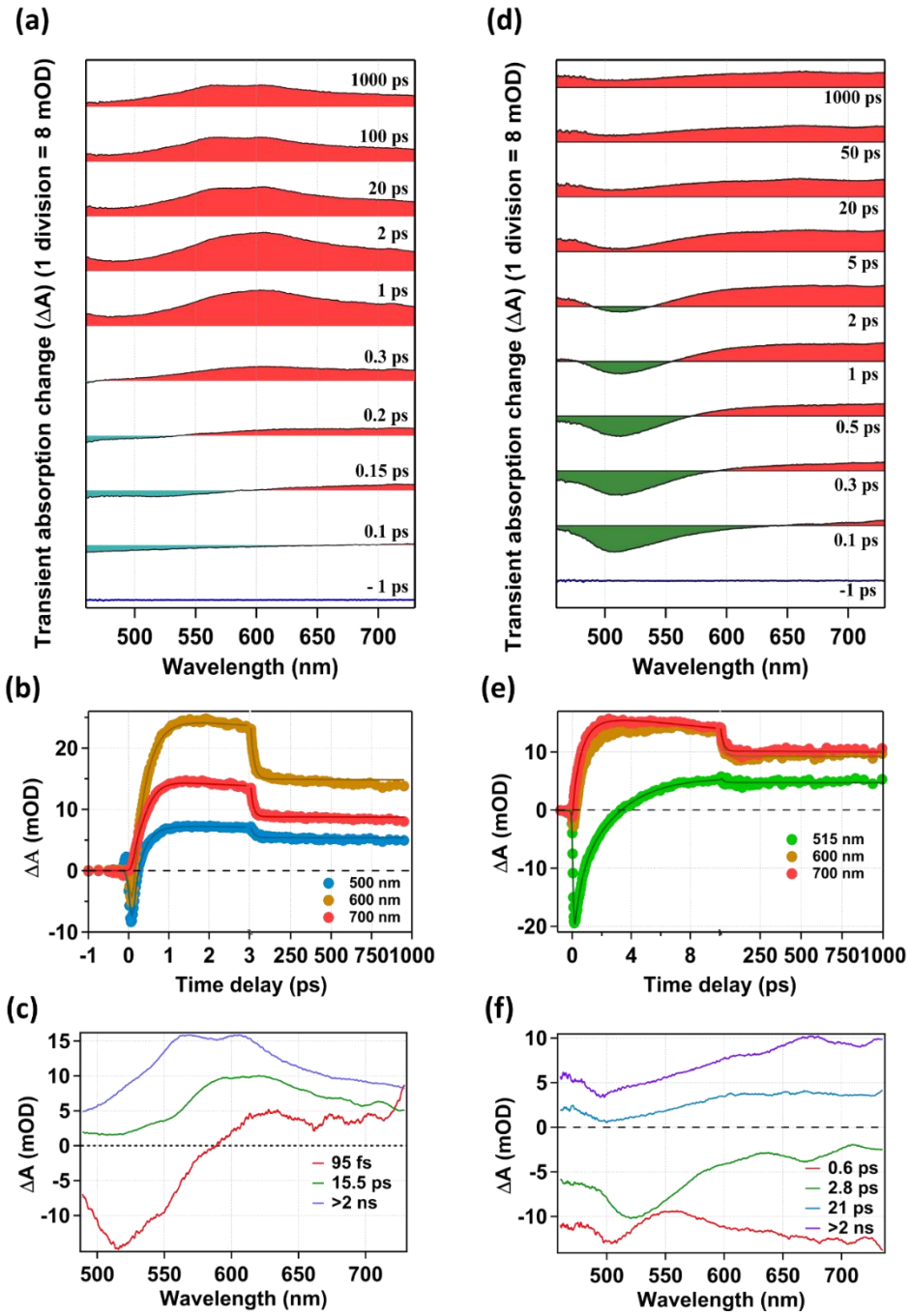

Figure 4.2.8. Transient absorption response (pump, 400 nm, probe, 460-730 nm) of TC1 in hexane (left panel) and acetonitrile (right panel). (a, d) TA spectra at some representative delay times for hexane (Hex) and acetonitrile (ACN) respectively. In Hex, the TA spectra consist of extremely feeble SE around 500 nm (cyan) and strong ESA over the whole probe spectral window (red). In ACN, spectra consist of SE around 520 nm (Green) and ESA above 600 nm (red) . (b, e) Fitted kinetics of TC1 in Hex and ACN solvent at three selective wavelengths of the whole probe window spectra. (c, f) Decay-associated spectra from the global analysis of TA data in Hex and ACN solvent. For TC1 in Hex solvent, three global time constants are 95 fs, 15.5 ps, and > 2 ns, and in ACN solvent, four global time constants are 0.6 ps, 2.8 ps, 21 ps, and > 2 ns. Both the transient measurements were done in aerated condition.

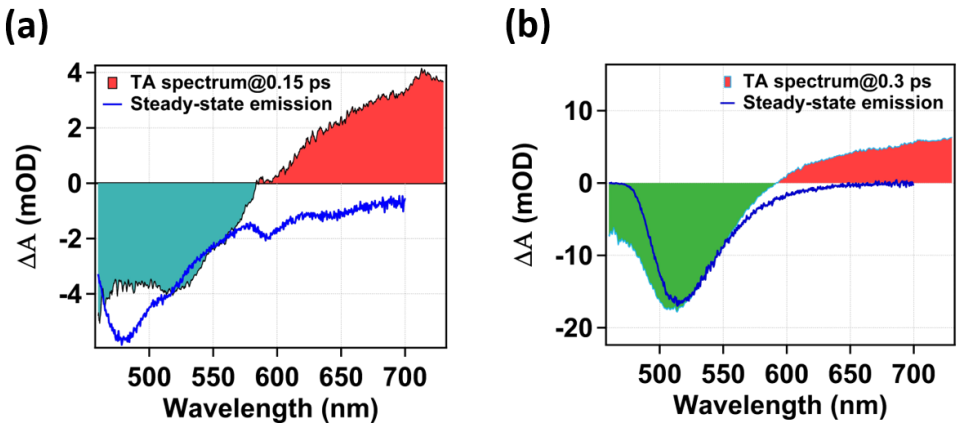

Figure 4.2.9. Match of the inverted steady-state emission spectra of TC1 with the time-resolved SE bands from TA measurement: TC1 in (a) Hexane (left) (b) Acetonitrile (right) at specified delay time. All the measurements were performed in aerated condition.

Similar transient spectral characteristics of TC1 have been found in dichloromethane (see Figure 4.2.10a). Thus, we believe the excited singlet decays to the upper triplet that relaxes to T_1. To get an idea about the time scale of triplet formation, we performed the kinetic analysis of the transient spectra (see Figures 4.2.8b,e, and Table 4.2.4). In hexane, we observed a rise time of 220 fs, which closely matches the fluorescence lifetime of TC1. This observation indicates an ultrafast ISC for TC1 in hexane. The existence of the second emissive state of TC1 could not be resolved in hexane due to the limited time resolution of the instrument. On the other hand, in case of TC1 in acetonitrile, we observed two distinct rise time components (~500 fs and ~2 ps). Interestingly, during the lifetime measurement of TC1 in acetonitrile, we observed two decay time constants. A similar kinetic feature was observed in dichloromethane (see Figure 4.2.10b). This is what we expected from our proposition of the existence of two emissive states in TC1.

Table 4.2.4: Fitted data of single point kinetic analysis of TC1 in specified solvents at three mentioned wavelengths.

Solvent	Spectral range (nm)	a_1	τ_1 (ps)	a_2	τ_2 (ps)	a_3	τ_3 (ps)	a_4	τ_4 (ns)
Hexane	498-502			-0.016	0.25	0.002	20.0	0.0054	> 10
	598-602			-0.014	0.32	0.01	19.8	0.014	> 10
	698-702			-0.017	0.22	0.005	16.1	0.008	> 10
ACN	513-517	-0.011	0.45	-0.035	2.45	-0.018	15.7	0.005	> 10
	598-602	-0.013	0.47	-0.008	2.08	0.007	18.2	0.009	> 10
	698-702	-0.012	0.55	-0.004	1.54	0.007	16.4	0.01	> 10
DCM	513-517	-0.024	0.34	-0.034	1.90	0.007	40.0	0.007	> 10
	598-602	-0.013	0.40	-0.005	2.15	0.005	39.6	0.011	> 10
	698-702	-0.034	0.31	-0.003	1.99	0.004	33.0	0.011	> 10

Error in fitted time constants: $\pm$30 fs for ultrafast growth component, $\pm$0.2 ps for picosecond growth component and $\pm$2 ps for intermediate decay components

To get a better idea of the involvement of a number of excited states in the photophysical process of TC1, we performed global analysis of TA data to identify the decay-associated spectra (DAS). Figure 4.2.8c presents three DAS obtained for TC1 in hexane. The DAS for the 95 fs component has a strong SE feature, while the 15.5 ps and >2 ns components have a prominent ESA features, where the amplitude and sharpness of the former are smaller compared to the latter. On the other hand, we observed four DAS components for TC1 in acetonitrile (see Figure 4.2.8f), where the fast components (0.6 ps and 2.8 ps) are of SE type, and the other two components (21 ps and >2 ns) are of ESA type. The 2.8 ps DAS matches well with the steady-state emission spectrum, while the 600 fs DAS probably represents the other short-lived emissive state, we proposed above. The spectral features of the long-lived DAS (21 ps and >2 ns) are broad in nature. The >2 ns DAS has been assigned to the lowest triplet state (T_1) for both in hexane and acetonitrile. The 15.5 ps and 21 ps components of TC1 in hexane and acetonitrile, respectively, are of ESA type. We presume these are the higher triplet states (T_n), which converts to the T_1 state via internal conversion (IC). Similar DAS components (two SE type and two ESA type) have also been obtained for TC1 in dichloromethane (see Figure 4.2.10c), and we

assign them in the same line as in acetonitrile. It has also been observed that by changing the polarity of the solvents from Hexane to DCM to ACN, the hump position becomes red-shifted, suggesting that the T_1 state has $\pi - \pi^*$ character.

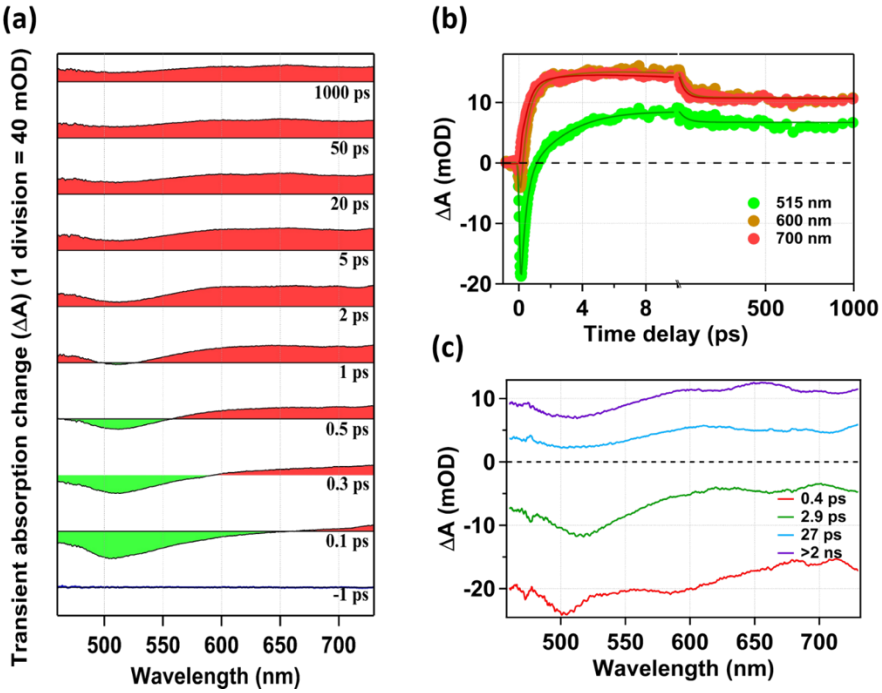

Figure 4.2.10. Transient absorption (TA) response (pump, 400 nm, probe, 460-730 nm) of TC1 in dichloromethane (DCM): (a) TA spectra at some representative delay times for DCM. In DCM solvent also, the TA spectra consist of SE around 515 nm (green) and strong ESA over the whole probe spectral window (red) (b) Fitted kinetics of TC1 in DCM at three selective wavelengths of the whole probe window spectra (c) Decay-associated spectra from the global analysis of TA data in DCM. For TC1 in DCM solvent, four global time constants are 0.4 ps, 2.9 ps, 27 ps and > 2 ns. All the measurements were performed in aerated condition.

If the proposition of two emissive states having different lifetimes in TC1 is true, one should observe a shift in the fluorescence spectrum as a function of time. At early time, the emission will be observed from both the states, whereas, at the later time, emission will be observed only from the long-lived state. To check the same we re-constructed the time resolved emission spectra (TRES) from the measured fluorescence decays at different wavelengths throughout the emission band (see Figure 4.2.11a,b). Consistent with the above expectation, a small change in the spectral maximum was observed. However, as acetonitrile is a polar solvent, it may

also solvate the excited state of TC1 leading to a shift in the emission spectrum, that contributes to the observed shift. Nevertheless, the observed dynamics of spectral shift found to be quite slow (10-12 ps) compared to the computed peak frequency shift due to the solvation dynamics in acetonitrile using the bi-exponential solvation time constants of 0.089 ps (69%) and 0.63 ps (31%)[23] as shown in Figure 4.2.11c. In addition, it has also been observed that after photoexcitation the peak frequency marginally shifts until 1 ps (see Figure 4.2.11d), which indicate that the LE state of TC1 achieved through 400 nm excitation is not solvatochromic in nature. Overall, the results authenticate the proposition of the existence of two singlet emissive states in TC1.

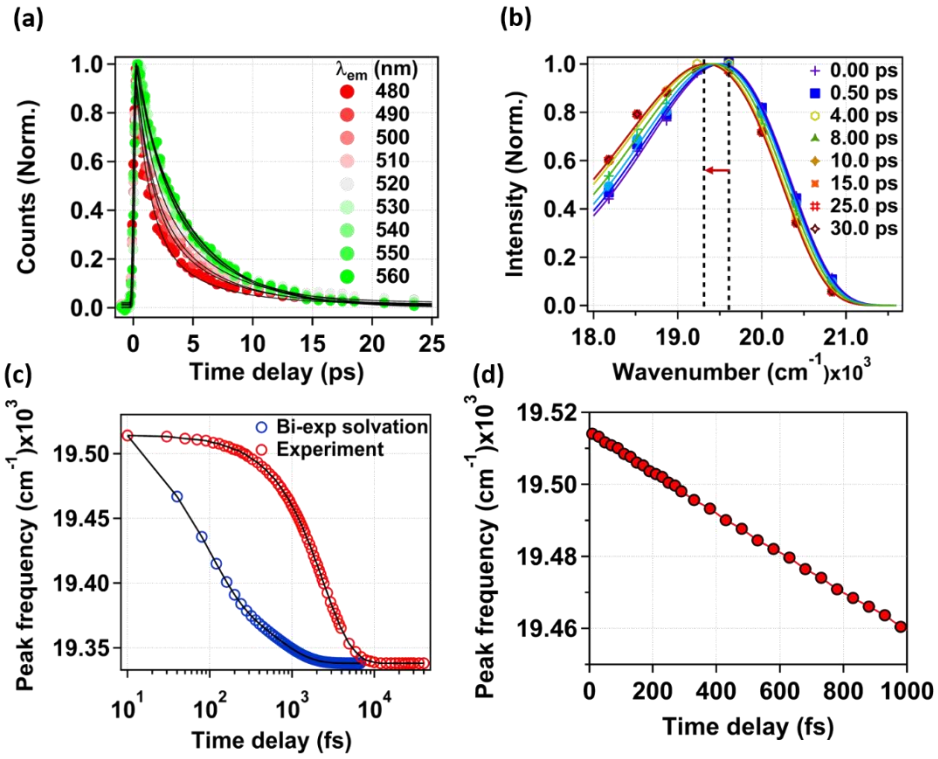

Figure 4.2.11. (a) Fluorescence lifetime decay of TC1 in acetonitrile at various emission wavelengths (480-560 nm) in Fluorescence Up-conversion. (λ_{ex}=400 nm) (b) Time-resolved emission spectra (TRES) of TC1 in ACN are constructed from the fitted coefficients of the fluorescence transients (c) Comparison of time-dependent fluorescence peak frequency shift and excited state solvation dynamics related peak frequency shift simulated from the bi-exponential solvation time constants of 0.089 ps (69%) and 0.63 ps (31%)[23]. The TRES shows that the fluorescence peak frequency shift is occurring up to 10-12 ps. (d) Time-dependent

fluorescence peak frequency shift related to the solvation of the excited state dipole of TC1 in acetonitrile (ACN). All the fluorescence decays were measured in aerated conditions.

4.2.2 Steady-state and time-resolved absorption/emission studies within a confined capsule. Octa acid is known to form closed capsular host-guest capsular complexes with varieties of guest molecules.[42-43, 45] The use of OA as host allows us to examine the excited state dynamics of TC1 within a highly confined non-polar OA capsule. Given that excited thioketones are known to be highly reactive in organic solvent media and relax through interaction with C—H bonds of solvents,[3, 12, 13, 54] a well-defined and restricted environment medium is appropriate to gain a better insight into the excited state dynamics of TC1. Recently we established by ^{1}H NMR that OA forms a 2:1 host-guest complex with TC1 in borate buffer solution (pH 7.4).[46] In this study, steady-state absorption and fluorescence measurements were utilized to monitor the binding of TC1 to OA cavity (Figures 4.2.12a,b). A drastic change in the absorption and fluorescence characteristics of TC1 was observed when OA was added to TC1 in water (borate buffer). Consistent with our previous work,[59] the above experiments suggested that the formation of OA–TC1 capsular complex is a two step process (see Figures 4.2.12c,d). The binding constant for the formation of 1:1 complex (TC1@OA) is estimated to be 2.5×10^{5} M^{-1}, whereas, the binding constant of the 1:2 (guest to host; TC1@OA_2)) complex is quite high (3.1×10^{11} M^{-2}). For a solution of 3 μM TC1 and 17 μM OA, the amount of free TC1, 1:1 complex (TC1@OA) and 1:2 complex (TC1@OA_2) are estimated to be <1%, 3% and 96%, respectively.

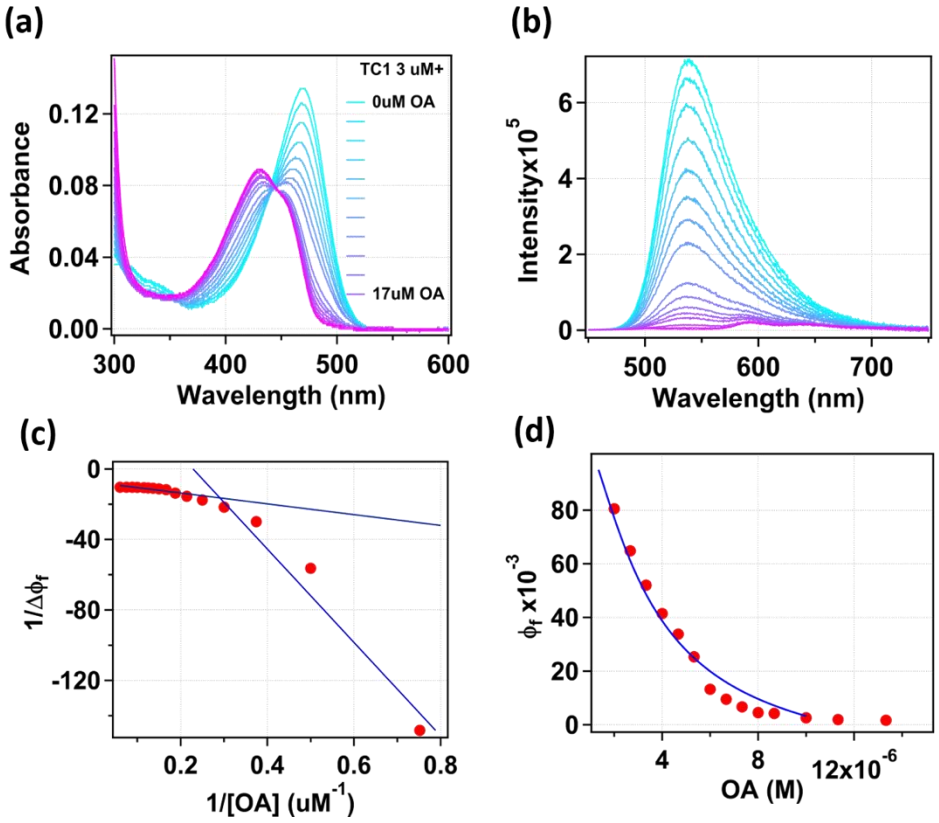

Figure 4.2.12. Absorbance and fluorescence titration of TC1 (3 μM) with octa acid (OA). Change in (a) Absorption (b) Emission upon gradual addition of octa acid (0-17 μM) (c) Plot of $1/\Delta\phi_f$ vs 1/[OA] for TC1 in borate buffer (d) Plot of emission quantum yield (ϕ_f) of TC1 vs [OA] in borate buffer with varying concentrations of OA. All the spectral measurements were performed in N_2-purged conditions.

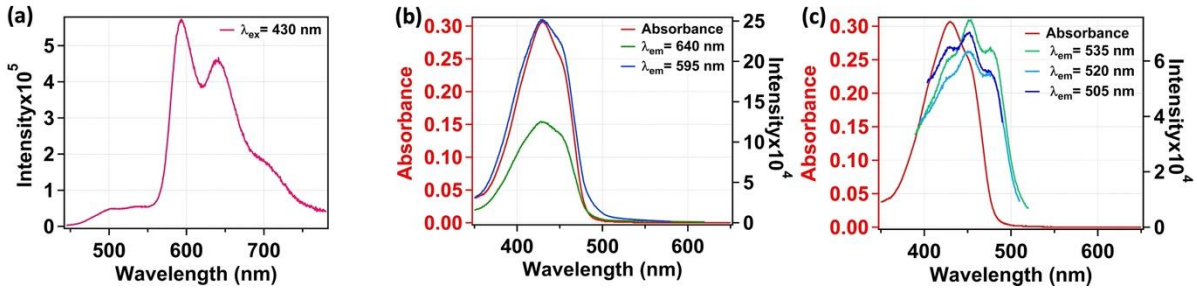

Figure 4.2.13. (a) Steady-state emission spectra of TC1 inside the octa acid (OA) cavity in borate buffer solution (excitation wavelength 430 nm) at room temperature; (b) Excitation spectra for the 595 and 640 nm emission bands and comparison with the absorption spectrum; (c) Excitation spectra for three different fluorescence emission regions (505, 520, and 535 nm) and comparison with the absorption spectrum. All the measurements were done in aerated condition.

The steady-state emission spectra of TC1@OA_2 exibits a strong band in 560-750 nm region and a weak band around 490-550 nm (see Figure 4.2.13a). The band above 550 nm resembles the phosphorescence measured under nitrogen purged condition in hexane (Figure 4.2.3a). Thus, we assigned the low energy band as phosphorescence, and the high energy band as fluorescence. The excitation spectra for both the emission bands are shown in Figures 4.2.13b,c. The excitation spectra for the phosphorescence band match very well with the absorption spectrum of TC1. On the other hand, the excitation spectra for the fluorescence band are found to be red-shifted to the absorption spectrum. These results undoubtedly suggest that fluorescence mainly originating from a low lying singlet excited state, while the phosphorescence is mainly coupled to the high energy singlet exited state through ISC. This suggests that the internal conversion from upper to lower singlet is slower than ISC. Further, the probability of transition from the ground state to the high energy singlet state is higher compared to the same to the low energy singlet excited state. Thus, the study of TC1 within OA cavity helps us to prove the existence of two closely spaced excited singlet states. The state with high transition probability from the ground state have the higher energy and is dark. This high energy state is mainly responsible for the generation of triplets, leading to the observation of phosphorescence. The low energy state is somewhat bright state but have very low transition probability from the ground state. This state is mainly responsible for the fluorescence.

The fluorescence lifetime of TC1 in OA cavity monitored at selected wavelengths were fitted into three components (0.3 ps, 30 ps and 420 ps; see Figure 14, fitted parameters are tabulated in Table 5). Within the OA cavity, the singlet state lifetime of TC1 is found to be ultrafast, similar to that in hexane. The two fast time components (0.3 ps, 30 ps) were assigned to the two nearly degenerate singlet states. The long component (420 ps) most likely is due to the contribution of phosphorescence.

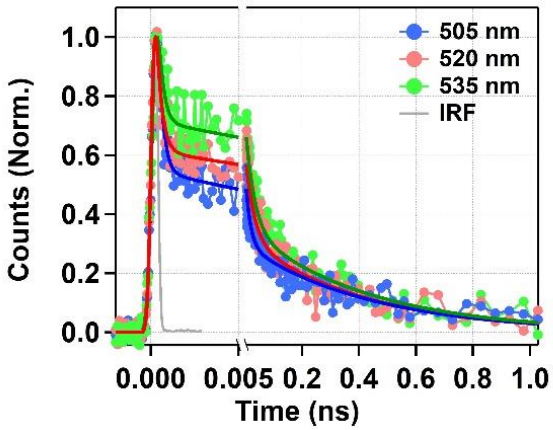

Figure 4.2.14. Normalized fluorescence decays of TC1 inside the octa acid (OA) cavity at three emission wavelengths: 505 (blue), 520 (red), and 535 nm (green) (λ_{ex}=400 nm) at 25 °C. All the measurements are done in nitrogen-purged conditions.

Table 4.2.5: Fitted kinetic parameters of the fluorescence lifetime decay of TC1 inside the octa acid

Wavelength (nm)	**a_1**	**τ_1 (ps)**	**a_2**	**τ_2 (ps)**	**a_3**	**τ_3 (ps)**
500	0.72	0.26	0.13	17	0.15	440
520	0.62	0.29	0.18	30	0.20	420
535	0.59	0.27	0.21	31	0.20	430

Error in fitted time constants: ±30 fs for the ultrafast component, ±2 ps for the intermediate picosecond component, and ±20 ps for the long component

Table 4.2.6: Fitted data of single point kinetic analysis of TC1 inside the octa acid

Wavelength (nm)	**a_1**	**τ_1 (ps)**	**a_2**	**τ_2 (ps)**	**a_3**	**τ_3 (ps)**	**a_4**	**τ_4 (ns)**
520±2	-0.0048	0.17	-0.0004	12	0.0004	950	0.002	>10
600±2	-0.0039	0.36	-0.0007	14	0.0012	1750	0.003	>10
700±2	-0.0250	0.42	-0.0003	22	0.0006	1600	0.003	>10

Error in fitted time constants: ±30 fs for the ultrafast growth component, ±2 ps for the intermediate picosecond component, and ±50 ps for the long component

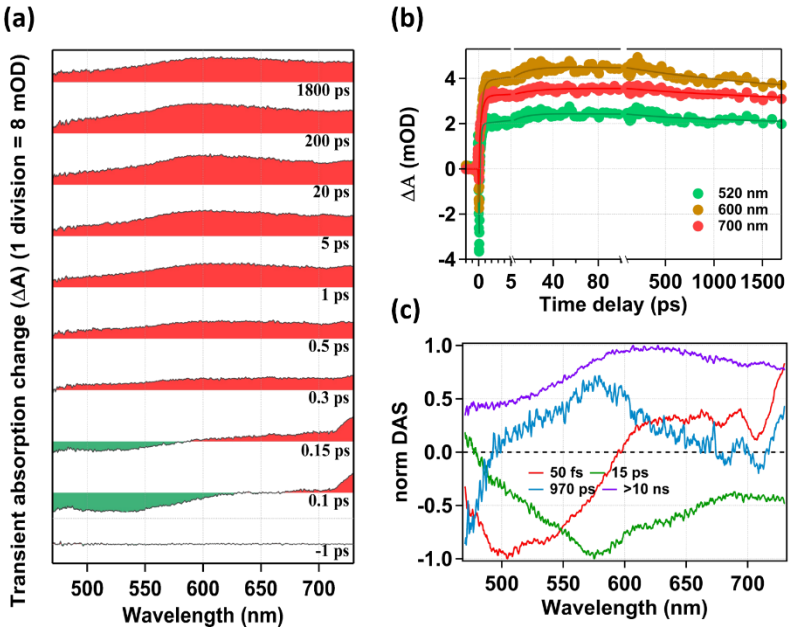

Figure 4.2.15. Transient absorption response (pump, 400 nm, probe, 460-730 nm) of TC1 inside the octa acid (OA) cavity. (a) TA spectra at some representative delay times. In the OA cavity, the TA spectra consist of SE around 480-550 nm (Green) and ESA above 600 nm (red). (b) Fitted kinetics of TC1 in OA at three selective wavelengths of the whole probe window spectra. (520, 600, and 700 nm) (c) Decay-associated spectra from the global analysis of TA data in octa acid (OA). For TC1 in OA, four global time constants are 50 fs, 15 ps, 970 ps, and > 10 ns. The transient measurement was performed in N_2-purged condition.

The TA spectra of TC1@OA_2 have a SE band in 480-550 nm region in the early time, which converted to a broad ESA band at later time (see Figure 4.2.15). The transient spectral analysis shows that the SE band is short lived, and the triplet-related ESA arises quickly. To understand the timescale of excited state processes, we performed the kinetic analysis of the transient data in three selective wavelengths i.e. 520, 600, and 700 nm (see Figure 4.2.15b). From the fitted parameters of the transient data (See Table 4.2.6) we see two rise time components (~0.3 ps and 15 ps) in the triplet state formation, indicating a ultrafast population growth of the triplets. From the global analysis of the TA data we found four DAS components of TC1 in OA capsule (see Figure 4.2.15c). The time component of DAS suggests that the first two components (50 fs and 15 ps) are SE type, and the other two components (970 ps and >10 ns) are ESA type. The results show that inside the OA cavity the rate of ISC is extremely fast (~10^{11} s^{-1}), which is probably due to the non-polar environment of

the cavity.[60] The results within OA capsule resembles those in hexane. It is known that the capsular interior is non-polar. A comparison of the results in the three solvents (hexane, acetonitrile and dichloromethane) and within OA cavity suggest that the excited state dynamics of TC1 is highly dependent on the polarity of the solvent. Given that the excited state electronic nature may be subjected to charge transfer from the 7-amino group to the thiocarbonyl side, such a solvent dependence is not unanticipated. To gain a better understanding of the excited state manifold of TC1 and the origin of ultrafast ISC, we performed TDDFT calculations whose results are presented below.

4.2.3 TDDFT calculation. Spectra of of TC1 in acetonitrile computed using TDDFT and the cLR-PCM method, revealed two closely spaced singlet states, S_1 (2.86 eV) and S_2 (2.92 eV), with nπ* and ππ* characters, respectively, at the Franck-Condon (FC) point (see Figure 4.2.16 and Tables 4.2.7,4.2.8). The latter state is brighter and also involves intramolecular charge transfer from the amino to the thiolactone end, similar to that reported in substituted coumarins.[61] This is consistent with the larger dipole moment for the excited state inferred in the experiments above. The first two singlet excited states are 0.6 eV apart in the gas phase. However, they are brought closer together in a polar solvent by opposite solvatochromic effects (~0.3 eV) on the two states (also see Table 4.2.11). The presence of diethylamino group at the 7-position promotes charge transfer across TC1 upon excitation, subsequently leading to the large solvatochromic effect and the subsequent reduction of the S_1 - S_2 gap. The latter effect is robust to the details of the DFT method applied (see Tables 4.2.9 and 4.2.10). It is tempting to assign these two states as the two closely spaced singlets responsible for the difference between absorption and excitation spectra of fluorescence. However, given that a similar behaviour is also observed in OA, where the environment is presumably non-polar, it is unclear whether the same two states would continue to be responsible. One possibility is that these two states are also proximal within OA due to interaction of excited charge densities with the OA cage.

However, given the expense entailed in computation of TDDF spectra for the OA bound TC1 molecule, we are yet to confirm this possibility.

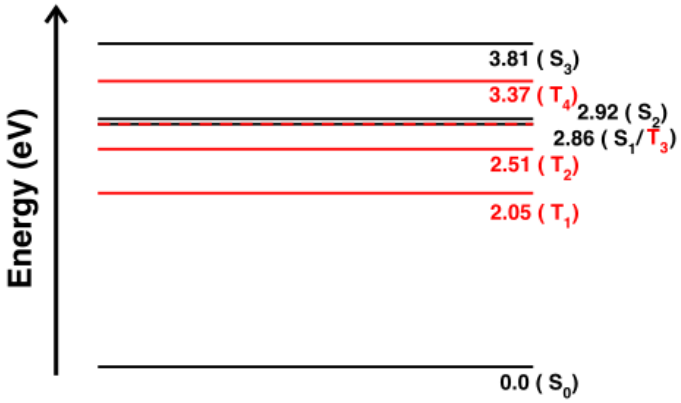

Figure 4.2.16. Vertical electronic excitation energies of low-lying electronic states TC1 in acetonitrile (ACN) in (cLR-) PCM method.

Table 4.2.7: Vertical excitation energies of TC1 to singlet states computed using TD-DFT/B3LYP/6-31+G(d,p) in gas phase and in acetonitrile solution using linear response (LR-) and corrected linear response (cLR-) PCM methods

State	Gas Phase (eV)	LR-PCM (eV)	cLR-PCM (eV)	Oscillator strength	Orbital character
S_1	2.60	2.92	2.86	0.0054	nπ*
S_2	3.22	2.97	2.92	0.5401	ππ*/charge transfer
S_3	3.88	3.79	3.81	0.1335	ππ*

Table 4.2.8: Vertical excitation energies of TC1 to triplet states computed using TD-DFT/B3LYP/6-31+G(d,p) in gas phase and in acetonitrile solution using linear response (LR-) and corrected linear response (cLR-) PCM methods

State	Gas Phase (eV)	LR-PCM (eV)	cLR-PCM (eV)	Orbital character
T_1	2.00	2.06	2.05	ππ*/charge transfer
T_2	2.30	2.74	2.51	nπ*
T_3	2.97	2.89	2.86	ππ*/charge transfer
T_4	3.44	3.38	3.37	-

From the calculations we observed that the triplet state T_2 is only 0.35 eV away from S_2, while the T_3 state is degenerate with S_1 and T_1 is about 0.87 eV below it. The proximity of the T_2 and T_3 states to the first two excited singlet states suggests the possibility of a population transition between the two spin channels. To assess the orbital feasibility of ISC using the El-Sayed rule, frontier molecular orbitals of TC1 in acetonitrile at the FC geometry were computed for different electronic states (see Figure 4.2.17).[62] The S_2/T_2 transition is found to be of ππ*→nπ* character, while, the S_2/T_3 transition have the ππ*→ππ* character. Therefore, the $S_2 \rightarrow T_2$ transition is both energetically and orbitally feasible. Similarly, both S_1/T_3 and S_1/T_1 are characterized by nπ*→ππ*, making them also feasible. The conclusion drawn here parallels the one proposed recently for thionucleobases. In the latter systems also the fast ISC from excited singlet to triplet manifold is attributed to the heavy mixing of nπ* and ππ* triplet states. However, the role of the charge transfer contribution of the diamino group at the 7 position in effecting a fast ISC is not obvious.

Table 4.2.9: Vertical excitation energies of TC1 (in eV) to lowest singlet and triplet levels using various exchange-correlation functionals. In each case, the spectrum was computed on the geometry optimized at the corresponding level of theory and using the LR-PCM method for implicit solvation in acetonitrile. The basis set used throughout was 6-31+G(d,p).

Excited States	PBE	B3LYP	CAM-B3LYP
S_1	3.02	2.92	3.27
S_2	3.06	2.96	3.36
S_3	3.92	3.79	4.37
T_1	2.03	2.06	2.17
T_2	2.80	2.74	3.11
T_3	2.90	2.89	3.12
T_4	3.33	3.38	3.64

Table 4.2.10: Solvatochromic shifts (in eV) of the lowest three singlet levels, defined as the difference in excitation energies between the gas phase and solvated molecules. Here, the $(\pi\pi^*)_1$ and $(\pi\pi^*)_2$ levels correspond to the first and second ππ* levels which also have charge transfer characteristics.

XC Functional	Solvatochromic shifts ($E_{gas} - E_{ACN}$) for the first three singlets (eV)		
	nπ*	$(\pi\pi^*)_1$	$(\pi\pi^*)_2$
PBE	-0.80	-0.24	-0.59
B3LYP	-0.37	0.30	0.09
CAM-B3LYP	-0.32	0.23	0.17

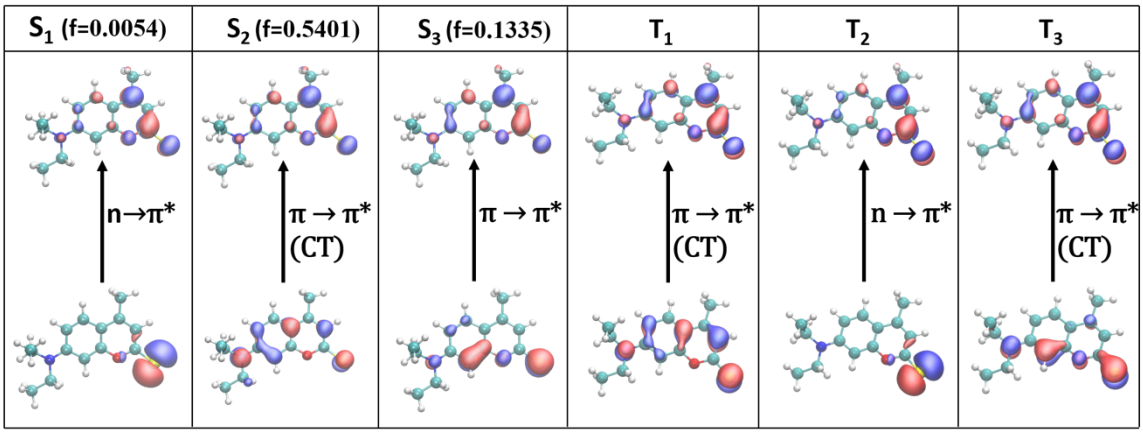

Figure 4.2.17. Electronic structure of the S_1, S_2, S_3, T_1, T_2, and T_3 state of TC1 in ACN through TDDFT calculation. A significant change in orbital character in the transition between S_2 to T_2 (ππ* → nπ*) However, there is no change in the orbital character in the transition between S_2 to T_3 (ππ* → ππ*), and S_2 to T_1 (ππ* → ππ*) transition. So, the S_2/T_2 transition follows the El Sayed rule of intersystem crossing (ISC). Similarly, S_1/T_1 transition has orbital character nπ* → ππ* and thus follows El Sayed rule. In the figure, charge transfer transitions are written as CT in short and the values of the oscillator strength of different transitions is written with the symbol f.

Table 4.2.11: Evolution of the excited state energies (given in eV) of TC1 with increasing solvent polarity. The nature of the transition for each excited state is mentioned in paranthesis in the corresponding table entry.

Solvent	**S_1**	**S_2**	**S_3**	**T_1**	**T_2**	**T_3**
Hex	2.63 (nπ*)	3.12 (ππ*)	3.82 (ππ*)	2.02 (ππ*)	2.34 (nπ*)	2.90 (ππ*)
DCM	2.76 (nπ*)	2.99 (ππ*)	3.81 (ππ*)	2.05 (ππ*)	2.49 (nπ*)	2.86 (ππ*)
ACN	2.86 (nπ*)	2.92 (ππ*)	3.81 (ππ*)	2.05 (ππ*)	2.57 (nπ*)	2.86 (ππ*)

The theoretical results presented here are consistent with our experimental observations of fast ISC. Although we have confirmed the existence of fast ISC in TC1 we are unable to unequivocally identify the origin. In general, molecules possessing thiocarbonyl chromophore are reported to have almost unit quantum yield of ISC from excited singlet state. Early studies on thioketones revealed the occurrence of quantitative and fast ISC from both S_2 and S_1.[4, 12-13, 32] In these cases the energy gap between the two states ranges between 35 to 50 kcal/mole. Apart from heavy atom effect due to sulfur, the rapid and quantitative intersystem crossing in alicyclic thioketones from S_2 is suggested to be facilitated by intramolecular C—H vibration.[52] Thioesters and thiocoumarins possessing O-(C=S) chromophore were also reported to undergo quantitative and rapid ISC from excited singlet state.[40, 47] Unlike in thioketones, in these molcules the gap between S_2 and S_1 is small (5-10 kcal/mole). This makes identification of the electronic nature of the states involved in crossing difficult. In TC the fast and effiecient ISC is attributed to mixing of nπ* and ππ* states and heavy atom effect.[47] One of the most extensively studied thiocarbonyl system is sulfur substituted thio-nucleobases N-(C=S). These molecules also, similar to other thiocarbonyl derivatives, possess ultra short singlet lifetime and quantitative ISC. Because of the close energies of S_2 and S_1, in these molecules also it is not easy to pindown the electronic identity of the S_2, S_1, T_2, and T_1. Because of the closeness, all these states are likely to have both nπ* and ππ*

characters. This mixing of states is thought to be the reason for the fast and quantitative ISC in thio-nucleobases.[49-50] Similiarity between thiocoumarins, thioesters and thio-nucleobases is obvious. Clearly replacing the 'O' with 'S' in all these systems, independent of the energy gap between S_2 and S_1, leads to fast and quantitative ISC. In our opinion, there is something more than Kasha's heavy atom effect and El-Sayed's orbital mixing[63] that is responsible for the unusual and interesting excited state properties of thiocarbonyl compounds.

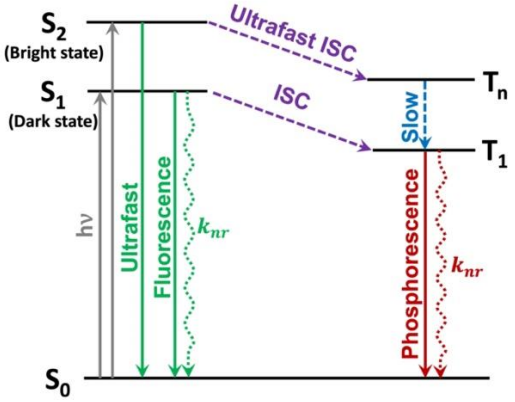

Scheme 4.2.1. Schematic representation of possible relaxation pathway of TC1.

4.3 Conclusions

The steady-state experiment reveals weak fluorescence quantum yield and room-temperature phosphorescence (RTP) behavior of TC1 in bulk solvents like hexane, acetonitrile and dichloromethane, which are distinctly different compared to the oxygen analogue, C1. This structural modification also changes the electronic energy levels, and an appearance of two decoupled singlet states with a very short lifetime (sub-ps to ps) has been noticed. Out of these two states, the state with a high absorption coefficient displays low fluorescence characteristics and vice-versa. Fluorescence upconversion measurement in bulk solvent reveals that the photoexcited singlet states of TC1 only sustains up to several picoseconds, indicating extensive population loss in a very short time. Detailed femtosecond transient

absorption (TA) study reveals an ultrafast (sub-ps) ISC process is probably the major non-radiative channels operating in the excited singlet state of the molecule. Furthermore, TA analysis reveals that both singlet states play a role in the formation of triplet populations. Higher-order triplets integrate into the lowest triplet state through the IC mechanism in 10s of picoseconds. Inside the isolated octa acid (OA) media, TC1 shows very strong phosphorescence along with a weak fluorescence, which further enunciate our proposition.

The excitation spectral measurement for fluorescence and phosphorescence bands deciphers their different origins on photoexcited singlet states and supports the speculation of decoupled singlet states involved in the ISC process. Fluorescence lifetime measurement inside the OA cavity has revealed a similar bulk solvent-like ultrashort lifetime of the singlet manifolds. TA analysis reveals the ultrafast triplet generation characteristics inside the OA cavity. Theoretical calculations of vertical transition energies in bulk ACN solvent depict the presence of two closely spaced singlets. The low energy gap and the required orbital characteristics of singlet-triplet transition allow us to support the experimental observation of fast ISC behavior. A more detailed theoretical analysis will be reported in a subsequent study.

References

1. Ramamurthy, V., Thiocarbonyl Photochemistry. In *Organic Photochemistry*, Padwa, A., Ed. 1985; Vol. 7, pp 231-328.
2. Steer, R.; Ramamurthy, V., Photophysics and Intramolecular Photochemistry of Thiones in Solution. *Acc. Chem. Res.* **1988**, *21*, 380-386.
3. de Mayo, P., Thione Photochemistry, and the Chemistry of the S_2 State. *Acc. Chem. Res.* **1976**, *9*, 52-59.
4. Maciejewski, A.; Steer, R. P., The Photophysics, Physical Photochemistry, and Related Spectroscopy of Thiocarbonyls. *Chem. Rev.* **1993**, *93*, 67-98.
5. Hui, M. H.; de Mayo, P.; Suau, R.; Ware, W. R., Thione Photochemistry:Fluorescence from Higher Excited States. *Chem. Phys. Lett.* **1975**, *31*, 257-263.
6. Turro, N. J.; Ramamurthy, V.; Cherry, W.; Farneth, W., The Effect of Wavelength on Organic Photoreactions in Solution. Reactions from Upper Excited States. *Chem. Rev.* **1978**, *78*, 125-145.
7. Jézéquel, Y. A.; Svěrák, F.; Ramundo, A.; Orel, V. c.; Martínek, M.; Klán, P., Structure–Photoreactivity Relationship Study of Substituted 3-Hydroxyflavones and 3-Hydroxyflavothiones for Improving Carbon Monoxide Photorelease. *J. Org. Chem.* **2024**, *89*, 4888-4903.
8. Tang, J.; Wang, L.; Loredo, A.; Cole, C.; Xiao, H., Single-Atom Replacement as a General Approach Towards Visible-Light/near-Infrared Heavy-Atom-Free Photosensitizers for Photodynamic Therapy. *Chem. Sci.* **2020**, *11*, 6701-6708.
9. Tang, J.; Robichaux, M. A.; Wu, K.-L.; Pei, J.; Nguyen, N. T.; Zhou, Y.; Wensel, T. G.; Xiao, H., Single-Atom Fluorescence Switch: A General Approach toward Visible-Light-Activated Dyes for Biological Imaging. *J. Am. Chem. Soc.* **2019**, *141*, 14699-14706.

10. Wang, J. Y. J.; Blyth, M. T.; Sherburn, M. S.; Coote, M. L., Tuning Photoenolization-Driven Cycloadditions Using Theory and Spectroscopy. *J. Am. Chem. Soc.* **2022**, *144*, 1023-1033.

11. Liu, R. S. H.; Ramamurthy, V., Self-Quenching in Photocycloaddition of Thiobenzophenone to Crotononitrile: A Case of Energy Transfer from S2. *Mol. Photochem.* **1971**, *3*, 261-265.

12. Lawrence, A. H.; Liao, C. C.; de Mayo, P.; Ramamurthy, V., Thione Photochemistry. Cycloaddition in a Saturated Alicyclic System. *J. Am. Chem. Soc.* **1976**, *98*, 2219-2226.

13. Lawrence, A. H.; Liao, C. C.; de Mayo, P.; Ramamurthy, V., Thione Photochemistry. Mechanism of the Short-Wavelength Cycloaddition of Adamantanethione: Evidence for an Excimer Derived from S2. *J. Am. Chem. Soc.* **1976**, *98*, 3572-3579.

14. Devanathan, S.; Ramamurthy, V., Photochemistry Of. Alpha.,. Beta.-Unsaturated Thiones: Cycloaddition of Thiocoumarin to Electron-Rich and Electron-Deficient Olefins from T1. *J. Org. Chem.*, **1988**, *53*, 741-744.

15. Rao, V. P.; Ramamurthy, V., Photochemistry Of. Alpha.,. Beta.-Unsaturated Thiones. Cycloaddition to Electron-Deficient Olefins from Higher Excited States. *J. Org. Chem.* **1988**, *53*, 332-339.

16. Bhattacharyya, K.; Das, P. K.; Ramamurthy, V.; Rao, V. P., Triplet-State Photophysics and Transient Photochemistry of Cyclic Enethiones. A Laser Flash Photolysis Study. *J. Chem. Soc., Faraday Trans. 2* **1986**, *82*, 135-147.

17. Becker, R. S.; Chakravorti, S.; Gartner, C. A.; Miguel, M. G., Photosensitizers: Comprehensive Photophysics/Phootochemistry and Theory of Coumarins, Chromones, Their Homologues and Thione Analogues. *J. Chem. Soc., Faraday Trans.* **1993**, *89*, 1007-1019.

18. Das, A.; Sharma, G.; Kamatham, N.; Prabhakar, R.; Sen, P.; Ramamurthy, V., Ultrafast Solvation Dynamics Reveal That Octa Acid Capsule's Interior Dryness Depends on the Guest. *J. Phys. Chem. A* **2019**, *123*, 5928-5936.

19. Nandi, N.; Bhattacharyya, K.; Bagchi, B., Dielectric Relaxation and Solvation Dynamics of Water in Complex Chemical and Biological Systems. *Chem. Rev.* **2000**, *100*, 2013-2045.

20. Vajda, S.; Jimenez, R.; Rosenthal, S. J.; Fidler, V.; Felming, G. R.; Castner Jr., E. W., Femtosecond to Nanosecond Solvation Dynamics in Pure Water and inside the γ-Cyclodextrin Cavity. *J. Chem. Soc. Faraday Trans.* **1995**, *91*, 867-873.

21. Jarzeba, W.; Walker, G. C.; Johnson, A. E.; Kahlow, M. A.; Barbara, P. F., Femtosecond Microscopic Solvation Dynamics of Aqueous Solutions *J. Chem. Phys.* **1988**, *92*, 7039-7041.

22. Kahlow, M. A.; Jarzeba, W.; Kang, T. J.; Barbara, P. F., Femtosecond Resolved Solvation Dynamics in Polar Solvents. *J. Chem. Phys.* **1989**, *90*, 151-158.

23. Horng, M. L.; Gardecki, J. A.; Papazyan, A.; Maroncelli, M., Subpicosecond Measurements of Polar Solvation Dynamics: Coumarin 153 Revisited. *J. Phys. Chem.* **1995**, *99*, 17311-17337.

24. Maroncelli, M.; Fleming, G. R., Picosecond Solvation Dynamics of Coumarin 153: The Importance of Molecular Aspects of Solvation. *J. Chem. Phys.* **1987**, *86*, 6221-6239.

25. Givens, R. S.; Matuszewski, B., Photochemistry of Phosphate Esters: An Efficient Method for Generation of Electrophiles. *J. Am. Chem. Soc.* **1984**, *106*, 6860-6861.

26. Kamatham, N.; Mendes, D. C.; Da Silva, J. P.; Givens, R. S.; Ramamurthy, V., Photorelease of Incarcerated Caged Acids from Hydrophobic Coumaryl Esters into Aqueous Solution. *Org. Lett.* **2016**, *18*, 5480-5483.

27. Nguyen, H. D.; Abe, M., Crucial Roles of Leaving Group and Open-Shell Cation in Photoreaction of (Coumarin-4-yl) Methyl Derivatives. *J. Am. Chem. Soc*. **2024,** *146*, 10993-11001.
28. Halder, D.; Paul, A., Understanding the Role of Aromaticity and Conformational Changes in Bond Dissociation Processes of Photo-Protecting Groups. *J. Phys. Chem. A* **2020**, *124*, 3976-3983.
29. Maciejewski, A.; Demmer, D. R.; James, D. R.; Safarzadeh-Amiri, A.; Verrall, R. E.; Steer, R. P., Relaxation of the Second Excited Singlet States of Aromatic Thiones: The Role of Specific Solute-Solvent Interactions. *J. Am. Chem. Soc.* **1985**, *107*, 2831-2837.
30. Rajee, R.; Ramamurthy, V., Oxidation of Thiones by Singlet and Triplet Oxygen. *Tetrahedron Lett.* **1978**, *19*, 5127-5130.
31. Rajee, R.; Ramamurthy, V., Energy Wastage in Organic Photochemistry: Self-Quenching in Thiones. *J. Photochem.* **1979**, *11*, 135-138.
32. de Mayo, P.; Shizuka, H., On the Mechanism of Photocycloaddition of Thiobenzophenone at 366 nm. *J. Am. Chem. Soc.* **1973**, *95*, 3942-3947.
33. Kemp, D. R.; de Mayo, P., The Detection of Transients in Thiocarbonyl Flash Photolysis. *J. Chem. Soc., Chem. Commun.* **1972**, 233-234.
34. Rao, V. J.; Muthuramu, K.; Ramamurthy, V., Oxidations of Thio Ketones by Singlet and Triplet Oxygen. *J. Org. Chem.* **1982**, *47*, 127-131.
35. Rao, V. J.; Ramamurthy, V., Oxidation of Thioketens by Singlet Oxygen and Ozone. *J. Chem. Soc., Chem. Commun.* **1981**, 638-639.
36. Rao, V. J.; Ramamurthy, V.; Schaumann, E.; Nimmesgern, H., Oxidation of Thioketenes by Singlet Oxygen. *J. Org. Chem.* **1984**, *49*, 615-621.
37. Szymański, M.; Balicki, M.; Binkowski, M.; Kubicki, J.; Maciejewski, A.; Pawłowska, E.; Wróżowa, T., Effects of Solute-Solvent Interactions on

Radiationless Decay of Thioketones Excited to Their S_2-and T_1-States. *Acta Phys. Pol. A* **1996**, *89*, 527-546.

38. Maciejewski, A., The Application of Perfluoroalkanes as Solvents in Spectral, Photophysical and Photochemical Studies. *J. Photochem. Photobiol. A: Chem.* **1990**, *51*, 87-131.

39. Barton, D. H. R.; Bolton, M.; Magnus, P. D.; West, P. J.; Porter, G.; Wirz, J., Mechanism of Thiobenzoic Acid O-Ester Photolysis. *J. Chem. Soc., Chem. Commun.* **1972**, 632-633.

40. Wirz, J., Photolysis of Aromatic Thioacid O-Esters: The Nature of the Reactive Excited State. *J. Chem. Soc., Perkin Trans. 2.* **1973**, 1307-1312.

41. Gibb, C. L.; Gibb, B. C., Well-Defined, Organic Nanoenvironments in Water: The Hydrophobic Effect Drives a Capsular Assembly. *J. Am. Chem. Soc.* **2004**, *126*, 11408-11409.

42. Ramamurthy, V., Photochemistry within a Water-Soluble Capsule. *Acc. Chem. Res.* **2015**, *48*, 2904-2917.

43. Ramamurthy, V.; Jockusch, S.; Porel, M., Supramolecular Photochemistry in Solution and on Surfaces: Encapsulation and Dynamics of Guest Molecules and Communication between Encapsulated and Free Molecules. *Langmuir* **2015**, *31*, 5554-5570.

44. Ramamurthy, V.; Sen, P.; Elles, C. G., Ultrafast Excited State Dynamics of Spatially Confined Organic Molecules. *J. Phys. Chem. A* **2022**, *126*, 4681-4699.

45. Ramamurthy, V., Photochemistry in a Capsule: Controlling Excited State Dynamics Via Confinement. *Chem. Commun.* **2022**, *58*, 6571-6585.

46. Ghosh, S. K.; Valloli, L. K.; Unny, D.; Sivaguru, J.; Jockusch, S.; Ramamurthy, V., Room Temperature Phosphorescence of 2-Thioxo-Coumarins in Aqueous

Solution Promoted by Octa Acid Inclusion. *J. Photochem. Photobiol. A: Chem.* **2024**, 115510.

47. Burdzinski, G.; Ziolek, M.; Karolczak, J.; Maciejewski, A., S2 and S1 States Deactivation of Thiocoumarin in n-Hexane and Acetonitrile Studied by Femtosecond Fluorescence Upconversion and Transient Absorption Spectroscopies. *J. Phys. Chem. A* **2004**, *108*, 11160-11164.

48. Szymański, M.; Maciejewski, A.; Kozłowski, J.; Koput, J., Photophysics of the S2 State of Thiocoumarin: A Vibrationally Unequilibrated Luminophore. *J. Phys. Chem. A* **1998**, *102*, 677-683.

49. Mai, S.; Pollum, M.; Martínez-Fernández, L.; Dunn, N.; Marquetand, P.; Corral, I.; Crespo-Hernández, C. E.; González, L., The Origin of Efficient Triplet State Population in Sulfur-Substituted Nucleobases. *Nat. Commun* **2016**, *7*, 13077.

50. Ashwood, B.; Pollum, M.; Crespo-Hernández, C. E., Photochemical and Photodynamical Properties of Sulfur-Substituted Nucleic Acid Bases. *Photochem. Photobiol.* **2019**, *95*, 33-58.

51. Brister, M. M.; Gustavsson, T.; Crespo-Hernández, C. E., Excited State Lifetimes of Sulfur-Substituted DNA and RNA Monomers Probed Using the Femtosecond Fluorescence up-Conversion Technique. *Molecules* **2020**, *25*, 584.

52. Falk, K. J.; Steer, R. P., Photophysics and Intramolecular Photochemistry of Adamantanethione, Thiocamphor, and Thiofenchone Excited to Their Second Excited Singlet States: Evidence for Subpicosecond Photoprocesses. *J. Am. Chem. Soc.* **1989**, *111*, 6518-6524.

53. Lawrence, A. H.; de Mayo, P., Thione Photochemistry. Chemical Evidence for Intersystem Crossing from a Second Excited Singlet State. *J. Am. Chem. Soc.* **1973**, *95*, 4084-4085.

54. Law, K. Y.; de Mayo, P., Thione Photochemistry. Adamantanethione as a Model for Singlet π,π* Hydrogen Abstraction. *J. Am. Chem. Soc.* **1979**, *101*, 3251-3260.

55. Ho, K. W.; de Mayo, P., Thione Photochemistry. On the Mechanism of Photocyclization of Aralkyl Thiones. *J. Am. Chem. Soc.* **1979**, *101*, 5725-5732.

56. Pollum, M.; Crespo-Hernández, C. E., The Dark Singlet State as a Doorway State in the Ultrafast and Efficient Intersystem Crossing Dynamics in 2-Thiothymine and 2-Thiouracil. *J. Chem. Phys.* **2014**, *140*, 071101.

57. Jones, G.; Jackson, W. R.; Choi, C. Y.; Bergmark, W. R., Solvent Effects on Emission Yield and Lifetime for Coumarin Laser Dyes. Requirements for a Rotatory Decay Mechanism. *J. Phys. Chem.* **1985**, *89*, 294-300.

58. Brackmann, U., *Lambdachrome® Laser Dyes*, 3rd ed.; Lambda Physik AG D-37079 Göttingen · Germany, 2000.

59. Sen, P.; Roy, D.; Mondal, S. K.; Sahu, K.; Ghosh, S.; Bhattacharyya, K., Fluorescence Anisotropy Decay and Solvation Dynamics in a Nanocavity: Coumarin 153 in Methyl β-Cyclodextrins. *J. Phys. Chem. A.* **2005**, *109*, 9716-9722.

60. Porel, M.; Jayaraj, N.; Kaanumalle, L. S.; Maddipatla, M. V. S. N.; Parthasarathy.A.; Ramamurthy, V., Cavitand Octa Acid Forms a Nonpolar Capsuleplex Dependent on the Molecular Size and Hydrophobicity of the Guest. *Langmuir* **2009**, *25*, 3473-3481.

61. Barik, A.; Kumbhakar, M.; Nath, S.; Pal, H., Evidence for the TICT Mediated Nonradiative Deexcitation Process for the Excited Coumarin-1 Dye in High Polarity Protic Solvents. *Chem. Phys.* **2005**, *315*, 277-285.

62. El-Sayed, M. A., Triplet state. Its radiative and nonradiative properties. *Acc. Chem. Res.* **1968,** *1*, 8-16.

63. Turro, N. J.; Ramamurthy, V.; Scaiano, J. C., *Modern Molecular Photochemistry of Organic Molecules*; University Science Books: Sausalito, CA, 2010, pp.277-287; 306-308.

This page left blank intentionally

Chapter 5

Effect of Hydrogen Bonding on the Ultrafast Intersystem Crossing in 7-diethylaminothiocoumarin

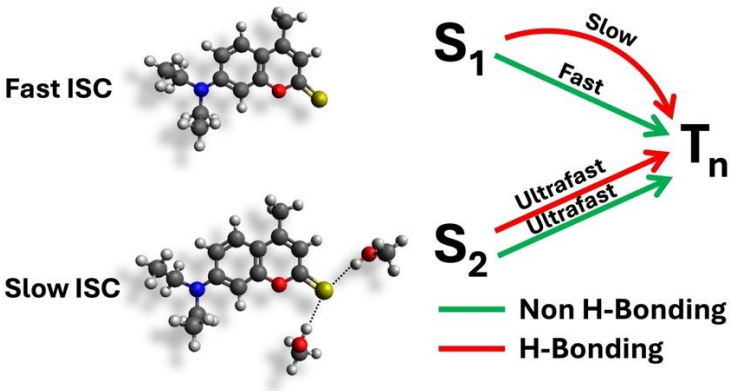

Abhijit Dutta, Suman Bhowmik, Sujit Kumar Ghosh, Vaidhyanathan Ramamurthy and Pratik Sen. *J. Phys. Chem. A* **2025** (Accepted)

Thiocarbonyls exhibit unique photophysical properties, characterized by rapid intersystem crossing (ISC) due to favourable singlet-triplet energetics and enhanced spin-orbit coupling. However, the role of hydrogen bonding in modulating ISC remains underexplored. This study investigates the effect of solvent-solute hydrogen bonding on the ISC dynamics of 7-(diethylamino)-4-methyl-2-sulfanylidene-2H-chromen-2-one (thiocoumarin 1, TC1) using steady-state and time-resolved spectroscopy, complemented by theoretical calculations. Experimental data reveal that in methanol, hydrogen bonding leads to increased fluorescence quantum yield, prolonged singlet-state lifetime, and reduced triplet yield compared to aprotic acetonitrile. Time-resolved spectroscopy identifies an additional long-lived emissive singlet state in methanol, attributed to a hydrogen-bonded state, which slows ISC. Theoretical calculations demonstrate that hydrogen bonding alters the electronic structure and constrains ISC along key nuclear coordinates, including the C=S bond vibration and dihedral angles, leading to decreased triplet formation. These findings provide mechanistic insights into hydrogen bonding-mediated control of ISC in thiocoumarins, with implications for designing functional materials with tunable photophysical properties.

5.1 Introduction

Hydrogen bonding interactions between the solute and the solvent are crucial for defining the properties and functions of molecules.[1–13] These interactions, stemming from weak bonding between a hydrogen atom and electronegative atoms like oxygen, nitrogen, or fluorine, have a profound impact on molecular geometry, stability, and reactivity.[14–17] Without hydrogen bonds, essential biomolecules such as proteins and nucleic acids would lose their structural integrity, preventing them from fulfilling their biological roles. In the past several decades, extensive research has illuminated the critical importance of hydrogen bonds across various fields, including organocatalysis, synthetic materials, crystal engineering, macrocyclic assembly, supramolecular strategy, and biomolecules.[1,3,5–7,14,17–20] Moreover, it is important to note that hydrogen bond formation is not confined solely to traditional electronegative atoms; even weakly electronegative sulfur atoms can act as potential acceptors in hydrogen bonding.[21–30] While the research on hydrogen bonding involving thiocarbonyl groups has made strides, a significant portion of the focus has remained on the intramolecular hydrogen bonds,[4,21,24,30–35] leaving the effect of inter-molecular hydrogen bonding on molecular property less explored. Exploring this lesser-known area could pave the way for innovative breakthroughs.

On the other hand, sulfur containing molecules play a critical role in various photophysical and photochemical applications, such as organic electronics, fluorescence quenching, and photodynamic therapy.[21,23,27,36–49] Their unique ability to facilitate ISC also makes them valuable in studying triplet state dynamics and designing functional materials for light-emitting and energy transfer systems. Understanding ISC in such a system provides insights into their photochemical behavior and enables the development of advanced materials and technologies.[26,29,45,50] Among varieties of sulfur-containing molecules, aromatic thioketones are particularly valuable for investigating photophysical and photochemical processes.[26,30,51–54] These molecules, derived from their parent ketones, are notable for their pronounced ability to generate triplet states on ultrafast timescales.[22,48,55] The photophysical behavior of aromatic thioketones is highly

dependent on the solvent environment; for instance, alkanes efficiently quench fluorescence from their higher excited singlet states[28,56–59] In addition to exhibiting room-temperature phosphorescence (RTP), these compounds also display thermally activated delayed fluorescence (TADF) from the first excited singlet state in various solvents, including acetonitrile and hydrocarbons.[44–46,48,55] Notably, these unique photophysical properties are intrinsic to the molecular structure of aromatic thioketones, making them valuable for exploring solvent-dependent photodynamic interactions.[60] Recent studies have primarily focused on the intersystem crossing behavior of thio-analogs of nucleobases and coumarins.[22,23,52,59]

Earlier reports on thiocoumarins describe ultrafast intersystem crossing (ISC) dynamics in aprotic solvents.[51,61] In this study, we investigate how the solvent-solute hydrogen bonding influence the photophysical behaviour of thiocoumarin 1 (TC1) (Scheme 5.1.1). Steady-state and femtosecond transient absorption/emission measurements were conducted for the TC1 in polar aprotic acetonitrile, polar protic methanol, and their mixtures. The measured data indicate a ~10-fold enhancement in fluorescence quantum yield and average lifetime in methanol solvent, alongside a ~10-fold reduction in the triplet yield. In methanol, global analysis of transient results reveals the presence of an additional emissive singlet state, likely attributable to a hydrogen-bonded structure. Kinetic analysis of the triplet signal indicates slower triplet formation dynamics in methanol, contrasting with the ultrafast dynamics observed in acetonitrile. Theoretical calculations of vertical transition energies highlight the influence of hydrogen bonding interactions on the energetics of the singlet and triplet manifolds, leading to less efficient triplet generation. A potential energy coordinate (PEC) scan along the C=S bond vibration coordinate further illustrates the negative impact of hydrogen bonding on triplet generation from the lowest excited singlet state. Additionally, two other reaction coordinates related to singlet-to-triplet formation have been investigated, emphasizing the potential inhibitory role of hydrogen bonding on ISC efficiency.

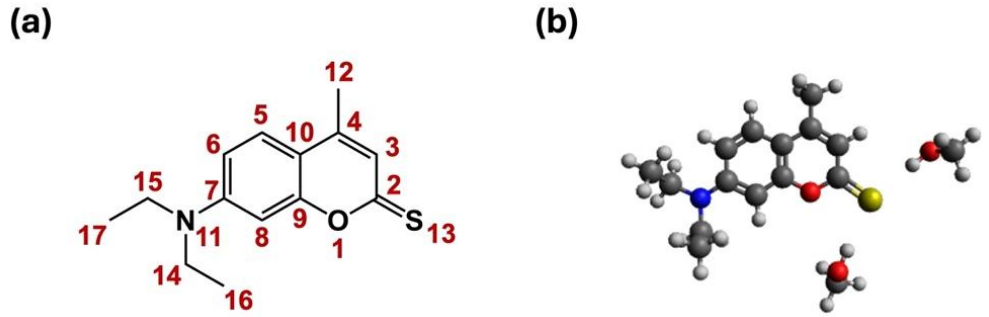

Scheme 5.1.1. Structure of (a) 7-diethylamino-4-methyl thiocoumarin (Thiocoumarin-1 or TC1) (b) TC1:$(CH_3OH)_2$ complex.

5.2. Results and Discussion

Our preliminary report on thiocoumarin (TC1) provided insights into the factors contributing to its extremely low fluorescence quantum yield and ultrashort singlet lifetimes observed in both non-polar and polar aprotic solvents.[61] However, that report did not explore the dynamics of the excited state in polar protic solvents. The present study aims to investigate how hydrogen bonding between the solute and the solvent influences the excited state photophysical properties, particularly the intersystem crossing (ISC) process of the TC1 molecule. To achieve this, we conducted a series of steady-state and time-resolved experiments in polar aprotic acetonitrile (ε ~ 35.9) and polar protic methanol (ε ~ 32.6), as well as in mixtures of acetonitrile and methanol.

5.2.1. Steady-State and Time-Resolved Absorption and Emission Studies

Figures 5.2.1a and 5.2.1b display the steady-state absorption and emission spectra of TC1 in acetonitrile/methanol solvent mixtures with varying compositions. A gradual shift in emission spectra was observed upon increasing the volume percentages of methanol in acetonitrile, but no shift is observed in the absorption spectra. To explore this further, the Stokes' shift $(\Delta\bar{\upsilon} = \bar{\upsilon}_{abs}^{max} - \bar{\upsilon}_{em}^{max})$ of the dye was correlated with the solvent polarity parameter, $\Delta f \left(= \frac{\varepsilon-1}{2\varepsilon+1} - \frac{n^2-1}{2n^2+1}\right)$ according to the Lippert-Mataga equation (equation 5.2.1).

$$\Delta\bar{\nu} = \Delta\bar{\nu}_0 + \frac{2\Delta\mu^2}{hcr^3}\Delta f \qquad (5.2.1)$$

Where, $\Delta\mu$ is the difference between the excited state (μ_e) and ground state (μ_g) dipole moments of the dye, h is the Planck's constant, c is the light velocity, and r is the Onsager radius of interaction. From Figure 5.2.1c, it is evident that Stokes' shift of TC1 does not obey the linear expression of solvent polarity function, i.e., Δf, which infers that apart from the solvent polarity, there must be some other factor that influences the deexcitation behavior of the singlet excited state. Methanol is a polar protic solvent, indicating that solute-solvent hydrogen bonding interactions likely a factor influencing the energetics of the singlet excited state.

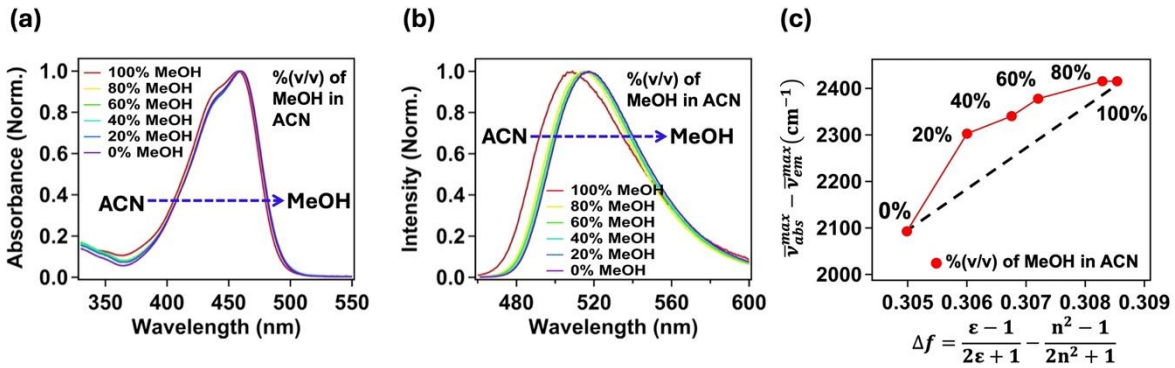

Figure 5.2.1. Steady-state (a) absorption spectra and (b) emission spectra of TC1 in pure acetonitrile (ACN) and methanol (MeOH) and in their mixtures at 298K upon exciting at 440 nm. (c) Lippert-Mataga plot for TC1 in methanol/acetonitrile mixtures.

Table 5.2.1. Experimentally observed photophysical parameters of TC1 in aprotic acetonitrile, protic methanol and their mixtures.

% (v/v) of methanol in acetonitrile	λ_{abs}^{max} (nm)	λ_{em}^{max} (nm)	ε	ϕ_f	a_1	τ_1 (fs)	a_2	τ_2 (fs)	a_3	τ_3 (fs)	τ_{avg} (ps)*	$\phi_{singlet\ O_2}$	$\phi_{Triplet}$
0%	458	508.5	35.9	2.98×10^{-4}	0.43	1200	0.57	4700			3.2	0.579	0.602
20%	458	514.5	36.2	9.43×10^{-4}	0.34	340	0.47	4264	0.19	37639	9.3	0.328	0.341
40%	458	515.5	35.6	14.70×10^{-4}	0.42	345	0.32	4702	0.26	47562	14.0	0.161	0.167
60%	458	516.5	34.9	20.41×10^{-4}	0.36	400	0.32	5453	0.32	60530	21.3	0.129	0.134
80%	458	517.5	33.9	24.62×10^{-4}	0.38	320	0.31	5706	0.31	77150	25.8	0.075	0.078
100%	458	517.5	32.6	35.91×10^{-4}	0.36	500	0.29	5500	0.35	101000	35.3	0.061	0.063

Furthermore, the fluorescence quantum yield and lifetime of TC1 were recorded in acetonitrile, methanol, and their mixtures, as depicted in Figure 5.2.2. With an increase in the volume percentage of methanol in acetonitrile, an increase in fluorescence quantum yield and lifetime is observed. The fluorescence quantum yield and the average fluorescence lifetime of TC1 increase by ~10-fold from acetonitrile to methanol (see Table 5.2.1). Additionally, in methanol rich mixtures and in pure methanol, an extra lifetime component for TC1 is observed in the fluorescence transient, which is believed to originate from the hydrogen-bonded excited state. To investigate hydrogen bonding interactions in other protic alcohols, we performed steady-state and time-resolved measurements in a series of short-chain alcohols ethanol, isopropyl alcohol, butanol and pentanol (see Figure 5.2.3). In all cases a methanol-like hydrogen bonding induced stabilization of the emissive singlet state, leading to a red-shifted emission spectra despite the lower polarity of these solvents (see Table 5.2.2) are observed. Moreover, the fluorescence quantum yield of TC1 in these alcohols was significantly enhanced compared to that in the more polar acetonitrile (see Table 5.2.2). Fluorescence transients of TC1 in these alcoholic solvents also exhibited a long-lived component, similar to that in methanol.

Table 5.2.2. Fluorescence quantum yield and the average lifetime of Thiocoumarin 1 in other alcohols

Alcoholic Solvents	$\boldsymbol{\lambda_{abs}^{max}}$ **(nm)**	$\boldsymbol{\lambda_{em}^{max}}$ **(nm)**	$\boldsymbol{\varepsilon}$	$\boldsymbol{\phi_f}$	$\boldsymbol{a_1}$	$\boldsymbol{\tau_1}$ **(fs)**	$\boldsymbol{a_2}$	$\boldsymbol{\tau_2}$ **(fs)**	$\boldsymbol{a_3}$	$\boldsymbol{\tau_3}$ **(ps)**
Ethanol (EtOH)	458	514	24.3	19.8×10^{-4}	0.54	330	0.30	4364	0.16	100000 (fixed)
Isopropyl Alcohol (IPA)	457	509	18.0	14.8×10^{-4}	0.61	340	0.26	4817	0.13	100000 (fixed)
Butanol (BuOH)	457	509	17.8	18.70×10^{-4}	0.59	380	0.27	4556	0.14	100000 (fixed)
Pentanol (PnOH)	457	508	14.8	21.50×10^{-4}	0.59	420	0.27	5797	0.14	100000 (fixed)

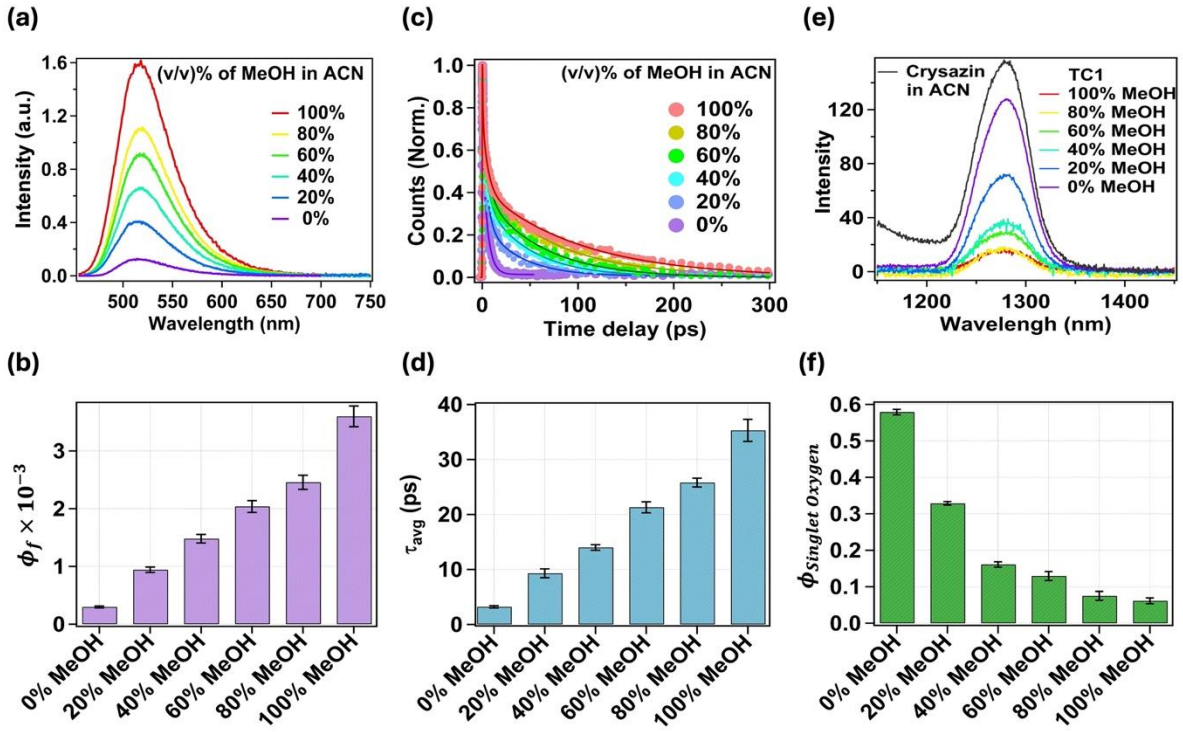

Figure 5.2.2. (a) Steady-state emission spectra and (b) fluorescence quantum yield (ϕ_f) of TC1 in methanol, acetonitrile and their mixtures upon exciting at 440 nm at 298K. (c) Fluorescence decay traces and (d) average fluorescence lifetime (τ_{avg}) of TC1 in methanol, acetonitrile and their mixtures upon exciting at 400 nm at 298K. (e) Singlet oxygen emission measured by exciting TC1 at 440 nm in oxygen-saturated methanol, acetonitrile, and their mixtures at 283K. The spectrum for the standard molecule (i.e. chrysazin) in acetonitrile is also shown. (f) Singlet oxygen yield of TC1 in methanol, acetonitrile and their mixtures at 283K.

These findings suggest that hydrogen-bonding solvents play a critical role in reducing non-radiative decay processes in the excited state of TC1. In contrast, the oxygen analogue of TC1, i.e. coumarin-1 (C1), displays an opposite effect: hydrogen bonding interactions reduce both the fluorescence quantum yield and lifetime (see Figure 5.2.4 and Table 5.2.3), likely due to TICT-mediated non-radiative decay processes.[69] However, for TC1, there is no experimental evidence of TICT states; rather, the triplet state is populated in an ultrafast time scale.[61] It is hypothesized that hydrogen bonding interactions slow down triplet formation in TC1, leading to enhanced fluorescence quantum yield and prolonged lifetime.

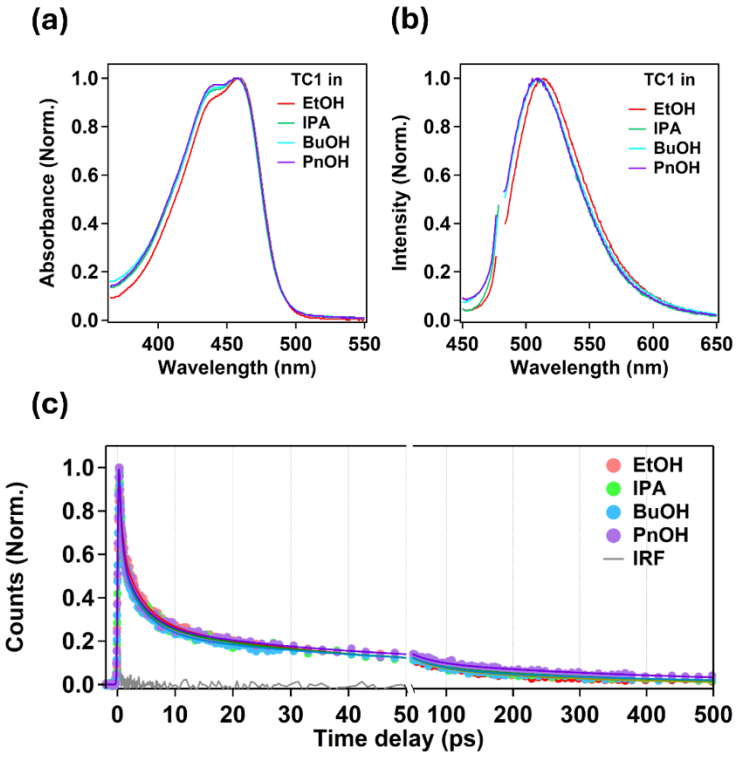

Figure 5.2.3. Steady-state (a) absorption (b) emission spectra of TC1 in ethanol (EtOH), isopropyl alcohol (IPA), butanol (BuOH), and pentanol (PnOH) with the excitation wavelength of $\lambda_{ex} = 420\,nm$, (c) fluorescence lifetime decay of TC1at the corresponding emission maxima. The concentration of the TC1 dye was 10 µM. All the steady-state measurements were performed at 25°C.

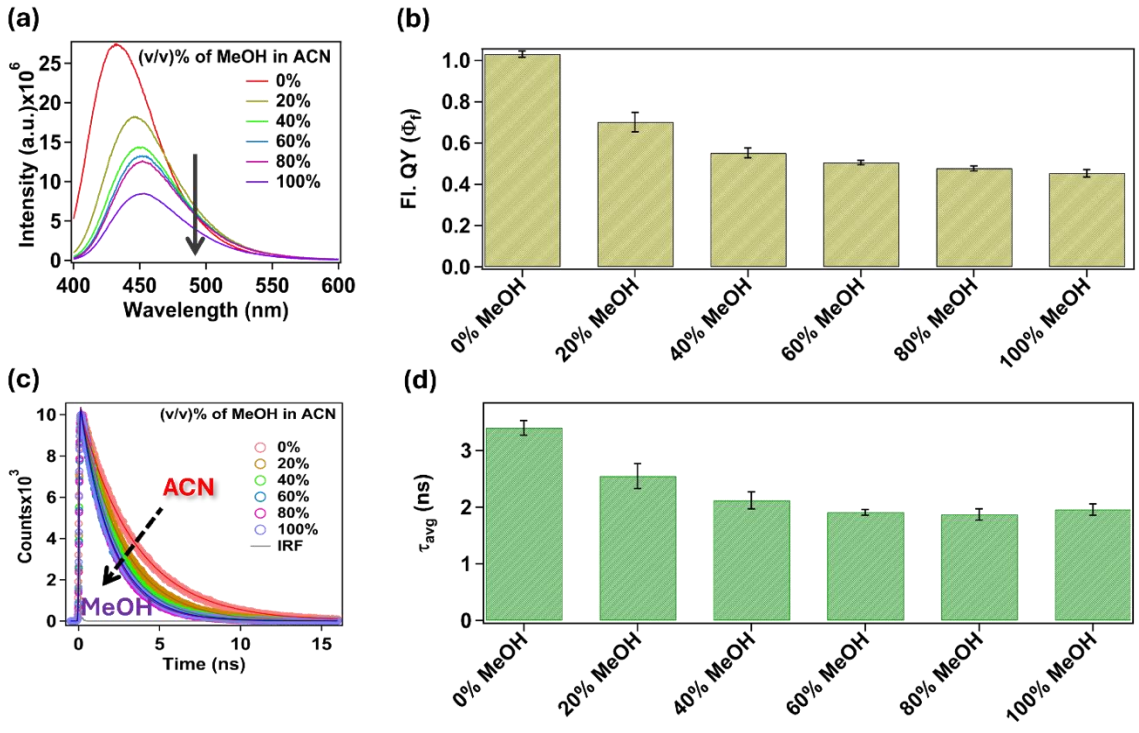

Figure 5.2.4. (a) Steady-state emission spectra ($\lambda_{ex} = 380\,nm$) (b) Fluorescence quantum yield (Φ_f) (c) Fluorescence lifetime decay (d) Average fluorescence lifetime (τ_{avg}) of Coumarin 1 (C1) upon increasing the volume percentage of (v/v %) of methanol (MeOH) in acetonitrile (ACN). Coumarin 1 in pure acetonitrile was taken as the fluorescence standard to measure the relative fluorescence quantum yield of C1. The concentration of the TC1 dye was 10 µM. All the steady-state measurements were performed at 25°C.

Table 5.2.3. Fluorescence quantum yield and the average lifetime of coumarin 1 in (v/v) % of Acetonitrile-Methanol mixture

% (v/v) of Methanol in Acetonitrile	$\emptyset_f$	τ_{avg} **(ps)**
0%	1.03	3.40
20%	0.70	2.55
40%	0.55	2.12
60%	0.50	1.91
80%	0.48	1.87
100%	0.45	1.96

To better understand how hydrogen bonding interactions influence the formation of the triplet state, we recorded the singlet oxygen emission intensity for TC1 in various acetonitrile/methanol mixtures. Figure 5.2.2e displays the singlet oxygen emission band centered at 1270 nm for TC1 in different acetonitrile/methanol mixtures. In reference to chrysazin in acetonitrile, the singlet oxygen quantum yield is converted to the triplet quantum yield of TC1, which is depicted in Figures 5.2.2e, 5.2.2f and tabulated in Table 5.2.1. We observed a 10-fold decrease in the triplet yield of TC1 from acetonitrile to methanol, which indicates that intermolecular hydrogen bonding between TC1 and solvent significantly inhibits triplet generation.

Femtosecond transient absorption (fs-TA) measurements were performed to capture the formation kinetics of the triplet state in TC1 in various methanol/acetonitrile mixtures. Earlier, we performed fs-TA experiment in acetonitrile (Figure 5.2.5a) and reported two triplet state formation time constants of ~0.5 ps and ~2 ps.[61] The origin of these two time constants were attributed to the formation of triplet state from two different energetically close (S_1 and S_2) singlet states. In this case, the global analysis

of the TA spectra yielded four decay-associated spectra (DAS) with two negative and two positive bands (Figure 5.2.5b).[61] The negative bands are attributed to the stimulated emission (SE) of the low-lying singlet states (S_2 and S_1), whereas the positive bands are assigned to the higher-order triplet state (T_n) and the lowest triplet state (T_1). In the case of pure methanol, the global analysis of TA spectra yielded five DAS (see Figures 5.2.5c and 5.2.5d). Of these, three are negative bands (0.5 ps, 4.2 ps, and 66 ps), and two are positive ESA bands (20 ps and >2 ns). Comparing the DAS features of TC1 in methanol and acetonitrile, it can be inferred that the 0.5 ps and 4.2 ps components are due to the SE of the S_2 and S_1 states, while the 20 ps and >2 ns components correspond to the T_n and T_1 states, respectively. Notably, in methanol, an additional long-lived SE emission feature has been observed, which was not present in acetonitrile. This highlights the distinct excited-state deactivation behavior of TC1 in protic methanol compared to aprotic acetonitrile. Based on our observation of a specific interaction of TC1 with methanol in Lippert-Mataga analysis, the 66 ps SE component is inferred to have originated from a hydrogen-bonded singlet excited state. Thus, the formation of the triplet state is retarded in methanol compared to acetonitrile and could explain the observed long fluorescence lifetime of TC1 in methanol ($\tau_{avg} = 35.3$ ps) compared to 3.2 ps in acetonitrile (see Figure 5.2.2b and Table 5.2.1).

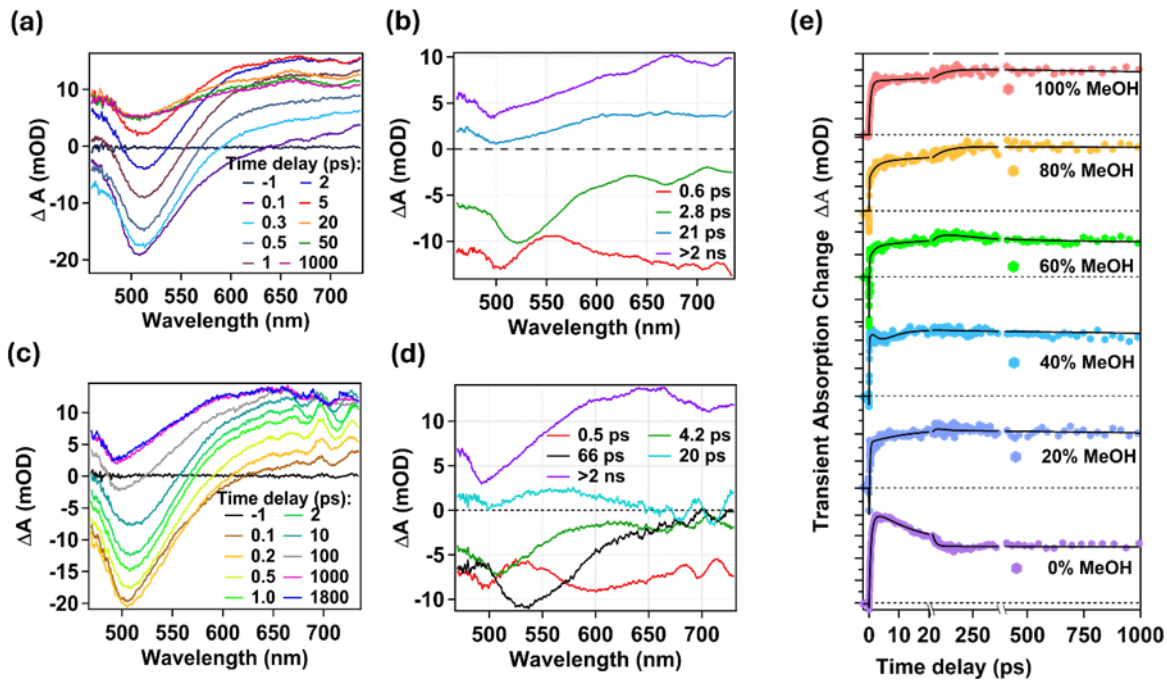

Figure 5.2.5. Transient absorption (TA) spectra (pump: 400 nm, probe: 460-730 nm) of TC1 at some representative delay times (a) in acetonitrile (ACN) and (c) in methanol (MeOH), in aerated condition at 298K. Decay-associated spectra from the global analysis of TA data in ACN and MeOH are presented in (b) and (d), respectively. For TC1 in ACN solvent, four global components are 0.6 ps, 2.8 ps, 21 ps, and >2 ns, and in MeOH, the observed five global components are 0.5 ps, 4.2 ps, 20 ps, 66 ps, and >2 ns. (e) Fitted transient absorption (TA) triplet state kinetics (at 700 nm) of TC1 in ACN and MeOH and in their mixtures (% v/v).

To obtain further insight into the time scale of triplet formation in methanol, we have the triplet formation kinetics. Our previous report established that the broad absorption feature of excited TC1 beyond 600 nm is mainly attributed to the ESA of the triplet species.[61] Therefore, we have performed a kinetic analysis of the transient data at 700±2 nm. Figures 5.2.5e depicts the triplet formation kinetics of TC1 in methanol/acetonitrile mixtures along with the pure counterparts, and the fitting data are tabulated in Table 5.2.4 (for TA spectra, see Figure 5.2.6). By looking at the kinetic features of the data, it is evident that triplet formation kinetics are drastically different for pure methanol and acetonitrile. Our previous work established that in pure acetonitrile, both low-lying excited singlet states generate triplet species on an ultrafast timescale (0.5 ps and 2.0 ps). Subsequently, the high-energy triplets (T_n) relax to the lowest triplet state (T_1), where they persist for several nanoseconds.

However, in pure methanol or methanol/acetonitrile mixtures, the triplet generation dynamics differ significantly, exhibiting a slower rise

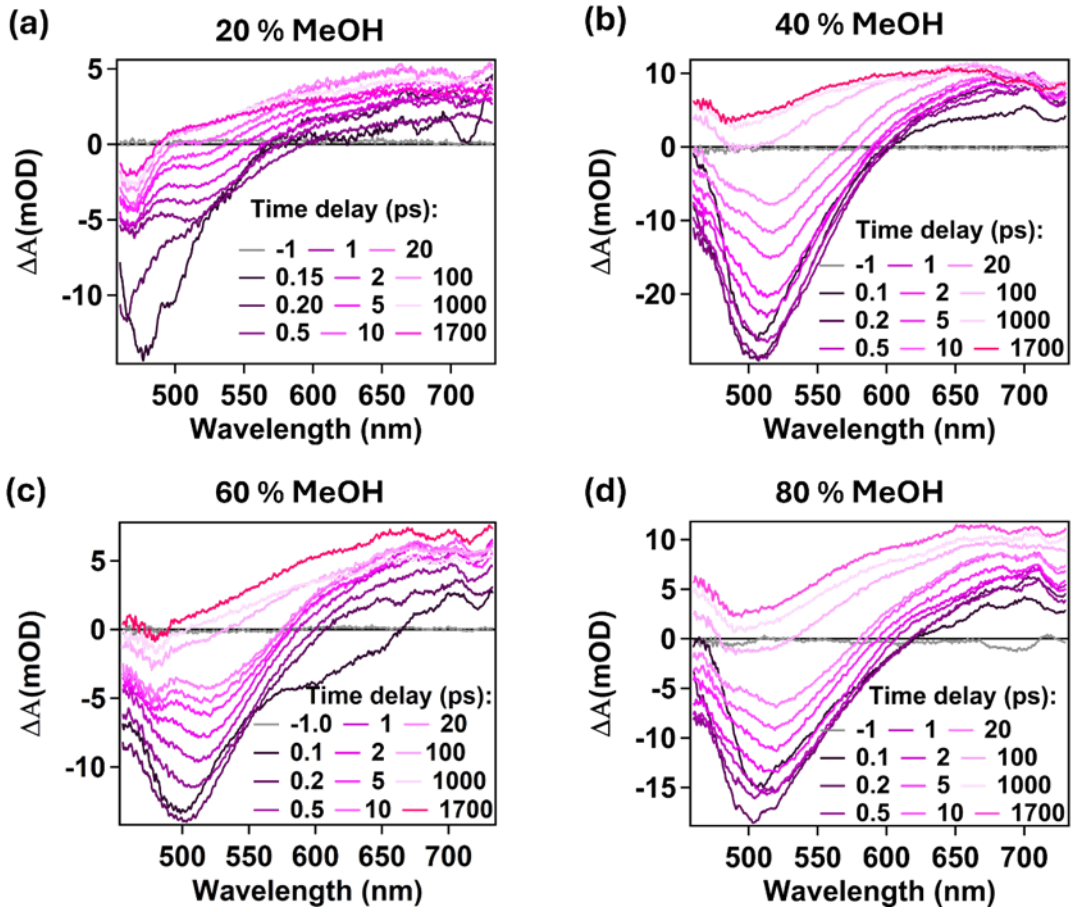

Figure 5.2.6. Transient absorption response (pump, 400 nm, probe 460-730 nm) of TC1 in four different acetonitrile (ACN)/methanol (MeOH) volume mixtures: (a) 20 % methanol (b) 40 % Methanol (c) 60 % methanol and (d) 80 % methanol

Table 5.2.4. Triplet state formation time constants of TC1 extracted from the fitted TA kinetics data at 700±2 nm, in acetonitrile, methanol and their mixtures at 298K.

(v/v) % of Methanol in Acetonitrile	Spectral range (nm)	τ_1 (ps)	τ_2 (ps)	τ_3 (ps)
0% Methanol	698-702	0.55	1.54	-
20% Methanol	698-702	0.52	1.99	32
40% Methanol	698-702	0.55	1.88	39
60% Methanol	698-702	0.53	1.77	45
80% Methanol	698-702	0.55	2.63	85
100% Methanol	698-702	0.53	7.16	94

A comparison of the kinetics in pure acetonitrile, methanol, and their binary mixtures reveals that an increase in the methanol volume fraction (v/v %) results in progressively slower triplet formation kinetics. Notably, TC1 exhibits three distinct growth components in the triplet formation process when in methanol and its mixtures, which differs from its behaviour in pure acetonitrile. Two of these components are attributed to triplet generation from two low-lying singlet states, similar to what is observed in acetonitrile. The third growth component likely originates from a hydrogen-bonded singlet excited state. As the methanol volume fraction in acetonitrile increases from 20% to 100%, the time associated with this third growth component extends from 32 ps to 94 ps. This indicates that as the strength of solvent-solute hydrogen bonding increases, triplet formation occurs more slowly.

This conclusion is further supported by ultrafast fluorescence decay measurements, which reveal a longer singlet state lifetime for TC1 in solvents capable of forming hydrogen bonds. The time-resolved experimental findings highlight the significant effect of intermolecular hydrogen bonding interactions on the excited-state dynamics of TC1. We propose that these hydrogen bonding interactions modify the energetics of the singlet and triplet states, as well as the spin-orbit coupling factor in TC1, ultimately affecting the intersystem crossing (ISC) process. To test this hypothesis, we conducted several theoretical calculations, which are presented in the following sections.

5.2.2. Quantum chemical calculations

5.2.2.1. Energy level ordering

Using the ground state optimized structures, the vertical transition energies of singlet and triplet manifolds of TC1 in acetonitrile and methanol were computed through time-dependent density functional theory (TDDFT) method using conductor-like polarizable continuum model (CPCM). At the Franck-Condon (FC) point, the calculated excitation energies to various singlet and triplet states are shown in Figure 5.2.7 and tabulated in Table 5.2.5 for both the solvents. In acetonitrile, the

excitation energies to S_1 and S_2 sates are found to be 2.993 eV and 3.048 eV, respectively, with oscillator strengths/characters of dark/nπ* and bright/ππ*, respectively (see Table 5.2.5). In methanol, the energies of S_1 and S_2 states are found to be 3.019 eV and 3.079 eV, respectively, with similar oscillator strengths and characters, as those observed in acetonitrile. In acetonitrile, the energies of the triplet states are 2.114 eV (T_1), 2.773 eV (T_2), and 2.964 eV (T_3), with their corresponding characters being ππ*, nπ*, and ππ* (see Figure 5.2.7). In methanol, a similar orbital characteristic (i.e. T_1: ππ*, T_2: nπ*, and T_3: ππ*) have been observed (see Table 5.2.5 and Figure 5.2.7).

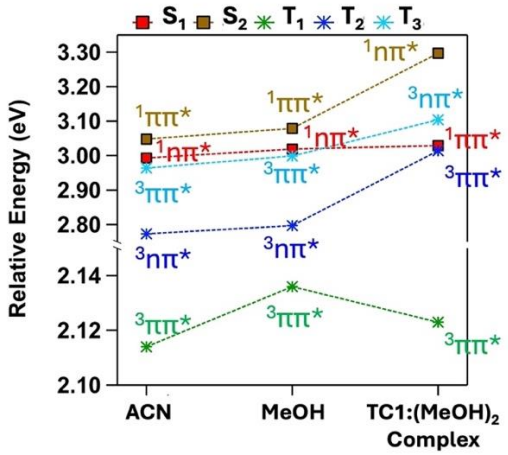

Figure 5.2.7. Vertical electronic excitation energies of electronic exited states of TC1 in acetonitrile (ACN), methanol (MeOH) without explicit hydrogen bonds, and that for TC1:$(MeOH)_2$ complex in methanol, obtained through TDDFT calculation.

Table 5.2.5. Vertical transition energies of TC1 in Acetonitrile, Methanol-no Hydrogen Bond (MeOH-noHB), TC1:MeOH (1:2 complex) in Methanol solvent

Acetonitrile				**Methanol**				**TC1(MeOH)$_2$ complex**			
States	**Electronic Character**	**Energy (eV)**	**Osc. strength**	**States**	**Electronic Character**	**Energy (eV)**	**Osc. strength**	**States**	**Electronic Character**	**Energy (eV)**	**Osc. strength**
S_1	nπ*	2.993	0.00006	S_1	nπ*	3.019	0.00023	S_1	ππ*	3.029	0.67270
S_2	ππ*	3.048	0.66691	S_2	ππ*	3.079	0.67080	S_2	nπ*	3.297	0.00027
S_3	ππ*	3.921	0.23001	S_3	ππ*	3.959	0.23360	S_3	ππ*	3.943	0.24920
T_1	ππ*	2.114	-	T_1	ππ*	2.136	-	T_1	ππ*	2.123	-
T_2	nπ*	2.773	-	T_2	nπ*	2.797	-	T_2	ππ*	3.014	-
T_3	ππ*	2.964	-	T_3	ππ*	2.999	-	T_3	nπ*	3.104	-
$\Delta E (S_1/T_1)$	-	0.879	-	$\Delta E (S_1/T_1)$	-	0.883	-	$\Delta E (S_1/T_1)$	-	0.906	-
$\Delta E (S_1/T_2)$	-	0.220	-	$\Delta E (S_1/T_2)$	-	0.222	-	$\Delta E (S_1/T_2)$	-	0.015	-
$\Delta E (S_1/T_3)$	-	0.029	-	$\Delta E (S_1/T_3)$	-	0.020	-	$\Delta E (S_1/T_3)$	-	-0.075	-
$\Delta E (S_2/T_1)$	-	0.934	-	$\Delta E (S_2/T_1)$	-	0.943	-	$\Delta E (S_2/T_1)$	-	1.174	-
$\Delta E (S_2/T_2)$	-	0.275	-	$\Delta E (S_2/T_2)$	-	0.282	-	$\Delta E (S_2/T_2)$	-	0.283	-
$\Delta E (S_2/T_3)$	-	0.084	-	$\Delta E (S_2/T_3)$	-	0.080	-	$\Delta E (S_2/T_3)$	-	0.193	-

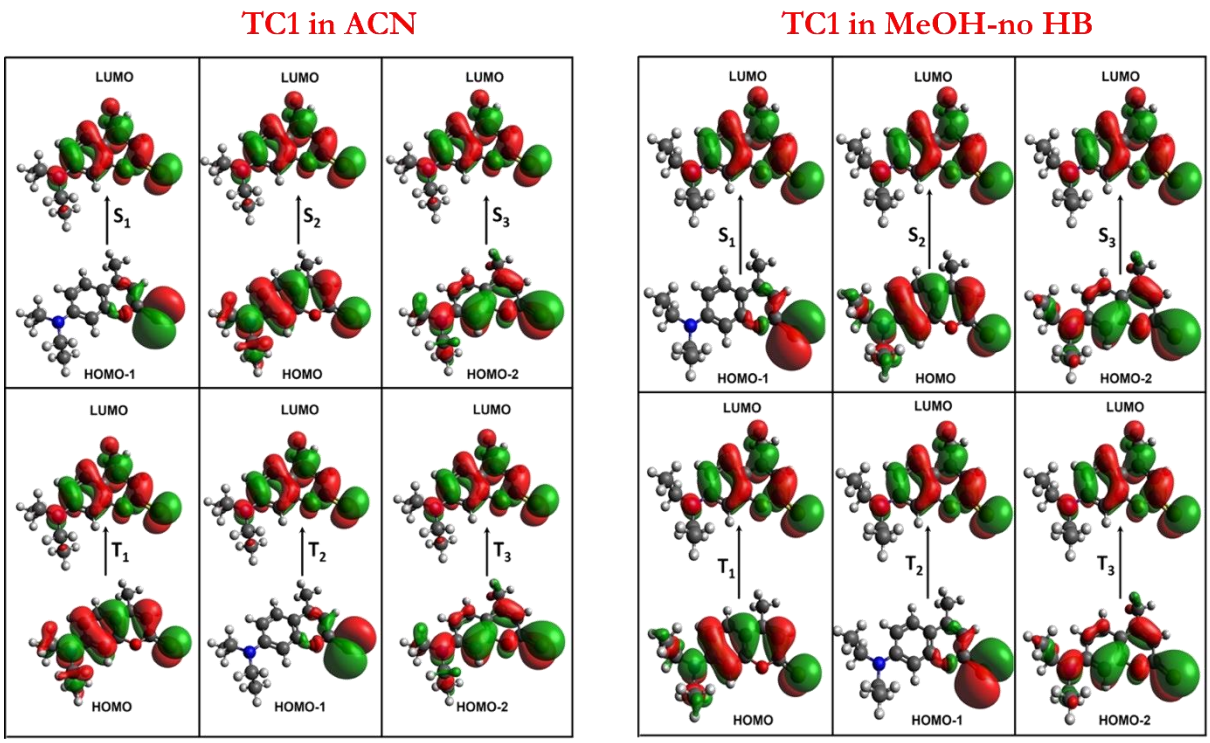

Figure 5.2.8. Electronic structures of the S_1, S_2, S_3, T_1, T_2, and T_3 states of TC1 in Acetonitrile (ACN) and Methanol (MeOH) without explicit solvents through TDDFT calculation

Table 5.2.6. Spin orbit coupling constants (SOC) of TC1 in Acetonitrile, Methanol-no Hydrogen Bond (MeOH-noHB), TC1: MeOH (1:2 complex) in Methanol solvent

Electronic states	Acetonitrile		Methanol-no HB		TC1(MeOH)$_2$ complex	
	Transition Type	SOC (cm^{-1})	Transition Type	SOC (cm^{-1})	Transition Type	SOC (cm^{-1})
$S_1 - T_1$	nπ*-ππ*	96.80	nπ*-ππ*	66.84	ππ*-ππ*	0.11
$S_1 - T_2$	nπ*-nπ*	0.82	nπ*-nπ*	1.63	ππ*-ππ*	3.16
$S_1 - T_3$	nπ*-ππ*	103.8	nπ*-ππ*	103.60	ππ*-nπ*	61.82
$S_2 - T_1$	ππ*-ππ*	0.88	ππ*-ππ*	1.86	nπ*-ππ*	86.27
$S_2 - T_2$	ππ*-nπ*	66.30	ππ*-nπ*	63.39	nπ*-ππ*	107.84
$S_2 - T_3$	ππ*-ππ*	0.93	ππ*-ππ*	2.08	nπ*-nπ*	6.56

To analyze the transition probabilities from the low-lying singlet to nearby triplet states, we calculated singlet-triplet energy gaps and spin-orbit coupling constants

(SOCs) (see Table 5.2.5 and Table 5.2.6). The energy gap between S_1(nπ*) and T_1(ππ*) states in acetonitrile is found to be 0.879 eV, which remains similar in methanol (0.883 eV). The SOC value between S_1(nπ*) and T_1(ππ*) sates is calculated to be 96.8 cm^{-1} and 66.8 cm^{-1} for acetonitrile and methanol, respectively. More importantly, the energy gap between S_1(nπ*) and T_3(ππ*) states in acetonitrile is found to be quite low (0.029 eV), which remains similar in methanol (0.020 eV). Perhaps, the S_1(nπ*) state can rapidly transition to the isoenergetic T_3(ππ*) state, with high SOC value (~104 cm^{-1}) in both the solvents. Although the S_1 and T_2 states are energetically closer compared to S_1 and T_1 states, the nπ* character of the T_2 state does not satisfy the El-Sayed rule for ISC, which is substantiated by the extremely small SOC value between S_1 and T_2 states (0.82 cm^{-1} for acetonitrile and 1.63 cm^{-1} for methanol).

Similarly, the population of the S_2(ππ*) state can also yield triplet population via multiple pathways. For the S_2(ππ*)→T_1(ππ*) transition, the energy gap is moderately high ($\Delta E_{S_2-T_1} = 0.934$ eV and 0.943 eV, respectively, for acetonitrile and methanol), and the transition does not obey the orbital change criteria (El Sayed's rule) for ISC, which is supported by the very small SOC values (0.88 cm^{-1} for acetonitrile and 1.86 cm^{-1} for methanol). The situation is similar for the S_2(ππ*)→T_3(ππ*) transition with SOC values of 0.93 cm^{-1} in acetonitrile and 2.08 cm^{-1} in methanol, though it is energetically favourable ($\Delta E_{S_2-T_3}$=0.084 eV for acetonitrile and 0.080 eV for methanol). In contrast, the S_2(ππ*)→T_2(nπ*) transition displays a high SOC value (66.3 cm^{-1} for acetonitrile and 63.4 cm^{-1} for methanol) and adheres to the El Sayed's rule, with a moderate energy gap ($\Delta E_{S_2-T_2} \sim 0.28\ eV$) for both the solvents. Overall, results suggest that at the FC point TC1 might have three dominant ISC channels, namely, (a) S_1(nπ*)→T_1(ππ*), (b) S_1(nπ*)→T_3(ππ*), and (c) S_2(ππ*)→T_2(nπ*).

The above calculations suggest a similar photophysics of TC1 in both acetonitrile and methanol. However, experimentally, we observed a marked difference in the photophysics of TC1 in acetonitrile and methanol, where the excited state lifetime

of TC1 in methanol is about 10-times more and has 10-times less triplet yield than that in acetonitrile. Recently, Fang *et al*. reported that an alteration in the bond parameters in the excited state through hydrogen-bonding plays a crucial role in modulating the photophysical properties of aromatic thioketone systems.[30] Inspired by these findings, we hypothesize that similar interactions may be present in TC1-methanol system, which acts as a potential barrier for the triplet generation in TC1. To verify such a possibility, the vertical transition energies of the low-lying singlet and triplet states of TC1 in methanol were calculated by incorporating explicit solvent interactions.

For this, we first performed the ground state optimization of TC1 along with two methanol molecules. The initial location of the two methanol molecules is decided based on chemical intuition. In spite of low electronegativity, sulfur has been considered as a potential hydrogen bond acceptor.[21,30,31,58] A detailed analysis of the C−H···S interactions in biomolecular systems has shown that the C−H···S interaction meets the requirements of a H-bond.[70–72] In view of these results, we considered the sulfur atom of TC1 as the potential hydrogen-bond acceptor and placed the two methanol molecules close the sulfur atom so that the methanolic -OHs form hydrogen bonds with the sulfur atom of TC1 forming a TC1:$(CH_3OH)_2$ complex. TDDFT calculation was performed for the ground state optimized structure of the TC1:$(CH_3OH)_2$ complex to determine the energies of singlet and triplet states along with the SOC values between them.

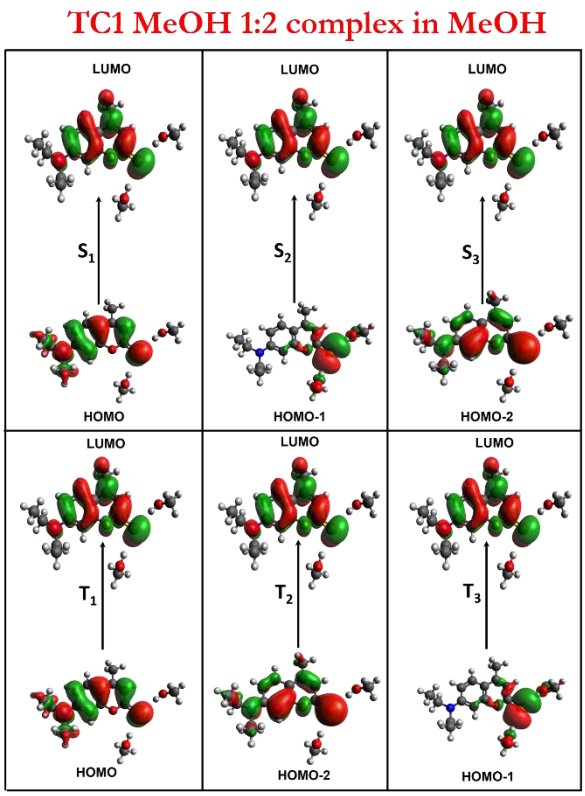

Figure 5.2.9. Electronic structure of the S_1, S_2, S_3, T_1, T_2, and T_3 states of TC1 in Methanol and two methanol (1:2 complex) explicit structures in methanol through TDDFT calculation

In TC1:$(CH_3OH)_2$ complex, the vertical transition energies to S_1 and S_2 states are found to be 3.029 eV and 3.297 eV (see Table 5.2.5), respectively, with their characters being ππ* and nπ* (see Figure 5.2.9). The oscillator strengths of these singlet states are reversed (f_{S_1} = 0.67270 and f_{S_2} = 0.00027) compared to TC1 in acetonitrile and methanol continuum solvent, and is believed due to the specific hydrogen bonding interactions. The S_3 state is much higher in energy at 3.943 eV and exhibits a ππ* character. The low-lying triplet states (T_1, T_2, and T_3) have energies of 2.123 eV (ππ*), 3.014 eV (ππ*), and 3.104 eV (nπ*), respectively (see Figure 5.2.9). The results indicate that S_1 to T_1 and T_2 population transfer is much less probable due to poor SOC values of 0.11 cm^{-1} and 3.16 cm^{-1}, respectively. In contrast, the T_3 state, characterized by nπ* orbital contributions, meets the orbital criteria for intersystem crossing (ISC) with S_1 state with a high SOC value of ~62 cm^{-1}. However, the T_3 state lies energetically above the S_1 state (see Table 5.2.5). Thus, the ISC from the S_1 state is not feasible for TC1:$(CH_3OH)_2$ complex.

The energy gaps between S_2 and T_1, T_2, T_3, respectively, are 1.174 eV, 0.283 eV, 0.193 eV, with SOC values of 86.27 cm^{-1}, 107.84 cm^{-1}, 6.56 cm^{-1} (see Table S3 of the SI). The $S_2(n\pi^*) \rightarrow T_1(\pi\pi^*)$ and $S_2(n\pi^*) \rightarrow T_2(\pi\pi^*)$ transitions are allowed according to El-Sayed rule, however, the $S_2(n\pi^*) \rightarrow T_3(n\pi^*)$ transition is not feasible due to their orbital character. This suggests that the S_2 state population in the TC1:$(CH_3OH)_2$ complex has a high likelihood of transitioning to the triplet states. However, the calculations also suggest that the oscillator strength for the S_2 state is much lower compared to the S_1 state for photoexcitation, and thus the ISC yield in TC1:$(CH_3OH)_2$ complex must be very low compared to TC1 in acetonitrile/methanol continuum solvent. This is exactly what we have observed in the experiment. As a whole, the results illustrate how hydrogen bonding interactions influence the energies and characters of the electronic states, the feasibility of transitions, and the ISC efficiency of TC1 in different media, these are summarized in Scheme 5.2.2.

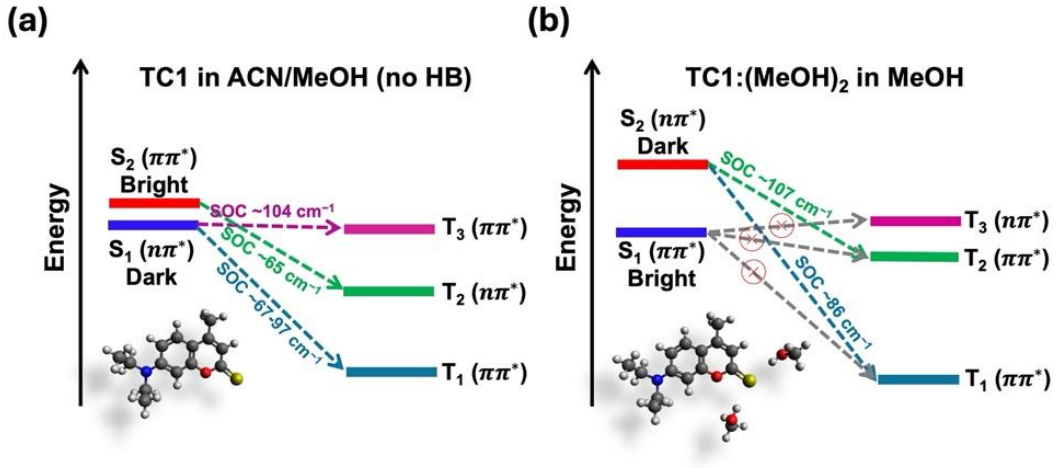

Scheme 5.2.2. Schematic representation of the singlet and triplet energy levels of TC1 in non-hydrogen-bonding solvent, and of TC1:$(MeOH)_2$ complex along with possible triplet formation channels with SOC values.

5.2.2.2 Possible ISC coordinate

Beyond the FC geometry, photoexcited singlet states may undergo intersystem crossing (ISC) during the excited state relaxation process. Earlier reports indicate that upon photoexcitation, the oxygen version of TC1 (i.e., coumarin 1) forms a

twisted intramolecular charge transfer (TICT) state in polar solvents along the rotation coordinate of -NEt_2 with respect to the coumarin ring, specifically through a change in the C_{14}-N_{11}-C_7-C_8 dihedral angle.[69,73] We first checked the role of C_{14}-N_{11}-C_7-C_8 dihedral angle rotation in the TC1 molecule in the ISC process. Figure 5.2.10 depicts the potential energy coordinate (PEC) scan along this C_{14}-N_{11}-C_7-C_8 coordinate in both acetonitrile and methanol continuum solvents. It is evident that, as the C_{14}-N_{11}-C_7-C_8 angle increases, the energy of the S_1 state increases until 50°, then begins to decrease, reaching a minimum near 90° angle, which suggests the presence of the same TICT state (see Figure 5.2.10). Along this coordinate, two triplet states (T_2 and T_3) cross the S_1 state at two specific dihedral angles (~65° for S_1/T_3 and 80° for S_1/T_2). Among these two, the S_1/T_3 the transition follows the El Sayed rule criteria for ISC. To reach the S_1/T_3 crossing point, the system must cross a potential energy barrier of 0.30 eV and 0.35 eV in acetonitrile and methanol, respectively, which is significantly high and unattainable at the room temperature. Based on this observation we conclude that the rotation of -NEt_2 group through the C_{14}-N_{11}-C_7-C_8 dihedral coordinate might not be the ISC coordinate in TC1.

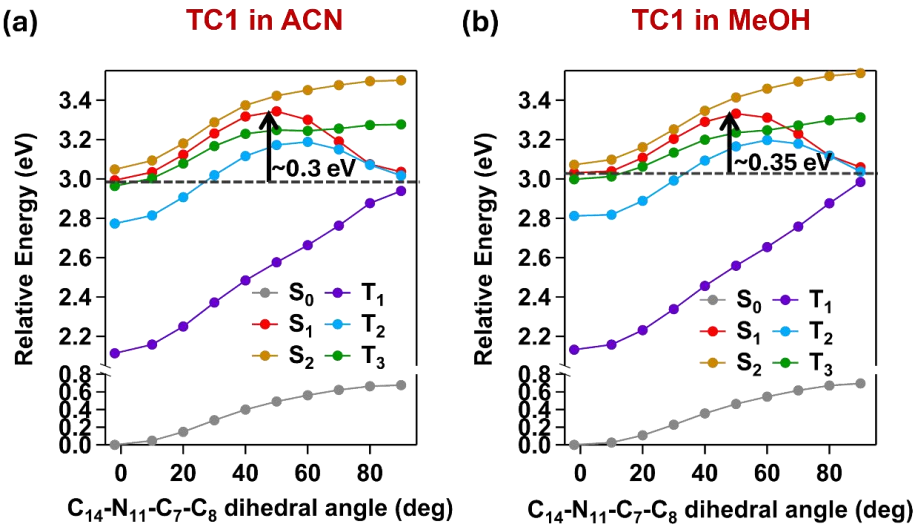

Figure 5.2.10. Potential energy coordinate (PEC) scan along the C_{14}-N_{11}-C_7-C_8 dihedral of the TC1 (a) in Acetonitrile (ACN), (b) in Methanol (MeOH)

Recent studies on thioketone systems have shown significant changes in bond parameters upon photoexcitation, notably the stretching of the C=S bond.[30,74,75] To investigate this phenomenon further, a PEC scan along the C_2=S_{13} bond length was conducted, providing insights into how the vibrations of the C_2=S_{13} bond might contribute to the ISC process. The potential energies along the C_2=S_{13} bond vibration coordinate for the different singlet and triplet manifolds of TC1 in acetonitrile and methanol continuum solvent and of TC1:$(CH_3OH)_2$ complex are depicted in Figure 5. In acetonitrile, starting from the FC state, the lowest singlet excited state (S_1) and the T_3 state stabilize through bond stretching. During the stabilization, they become isoenergetic around 6% stretch of the C_2=S_{13} bond, with a spin-orbit coupling (SOC) value of ~110 cm^{-1}, which can lead to efficient ISC in acetonitrile (see Figures 5.2.11a and 5.2.11d).

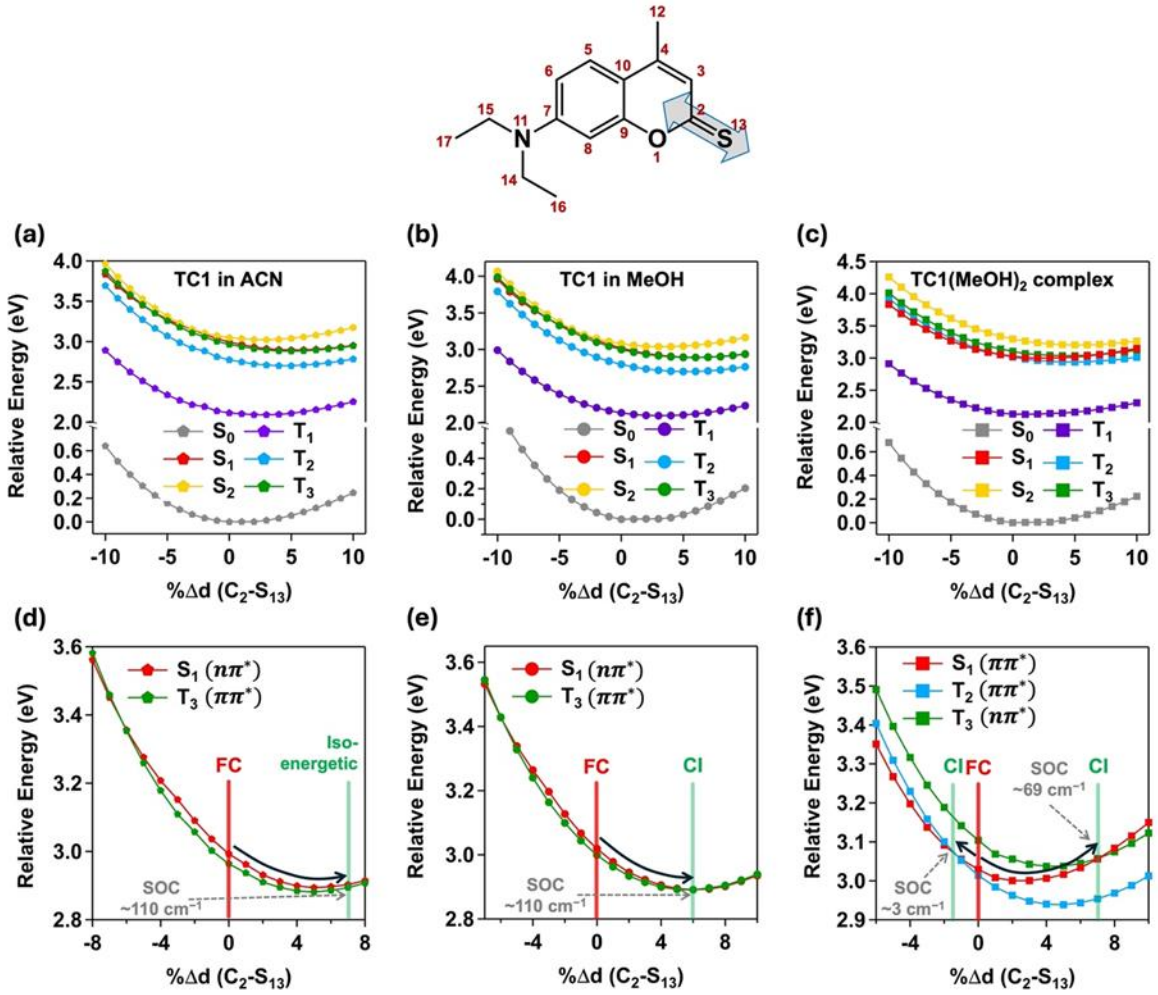

Figure 5.2.11. Potential energy coordinate (PEC) scan along the C_2=S_{13} bond vibrations coordinate in (a) TC1 in acetonitrile (ACN), (b) TC1 in methanol (MeOH), and (c) TC1$(MeOH)_2$ complex. A zoomed version around S_1 energy level of (a), (b) and (c) is represented in (d), (e) and (f), respectively, along with the SOC values (cm^{-1}) at the singlet-triplet crossing/isoenergetic points and orbital characters.

A similar high ISC probability from the S_1 state to the T_3 state, with high SOC values (~110 cm^{-1}), is observed in methanol without explicit hydrogen bonding, occurring at a similar bond stretched condition (see Figures 5.2.11b and 5.2.11e). Thus, the nature of the S_1-T_3 crossover in both acetonitrile and methanol is quite similar. Notably, no singlet-triplet crossing point is observed for the S_2 state with the triplet manifolds along the C_2=S_{13} bond vibration coordinate.

However, in TC1:$(CH_3OH)_2$ complex, the S_1-T_3 crossing point occurs at ~7% C_2=S_{13} bond stretched region and lies energetically above the FC state of S_1 manifold. Moreover, the SOC value drops to ~68.7 cm^{-1} at this crossing point (see Figures 5.2.11c and 5.2.11f). We observed another crossing point between S_1 and T_2 states at ~1% C_2=S_{13} bond compressed condition with a SOC value of 3.2 cm^{-1}. This crossing point is also energetically higher compared to the S_1 FC state. As a result, the rate of triplet generation in TC1:$(CH_3OH)_2$ complex is likely to be significantly reduced compared to in acetonitrile, which we have observed experimentally (see Table 5.2.1). Thus, we conclude that the C=S bond vibration is an important ISC coordinate in TC1 molecule. To evaluate the viability of other ISC coordinates, we have examined the PEC along two dihedral coordinates (C_4-C_3-C_2-S_{13} and C_9-O_1-C_2-S_{13}) containing the S-atom.

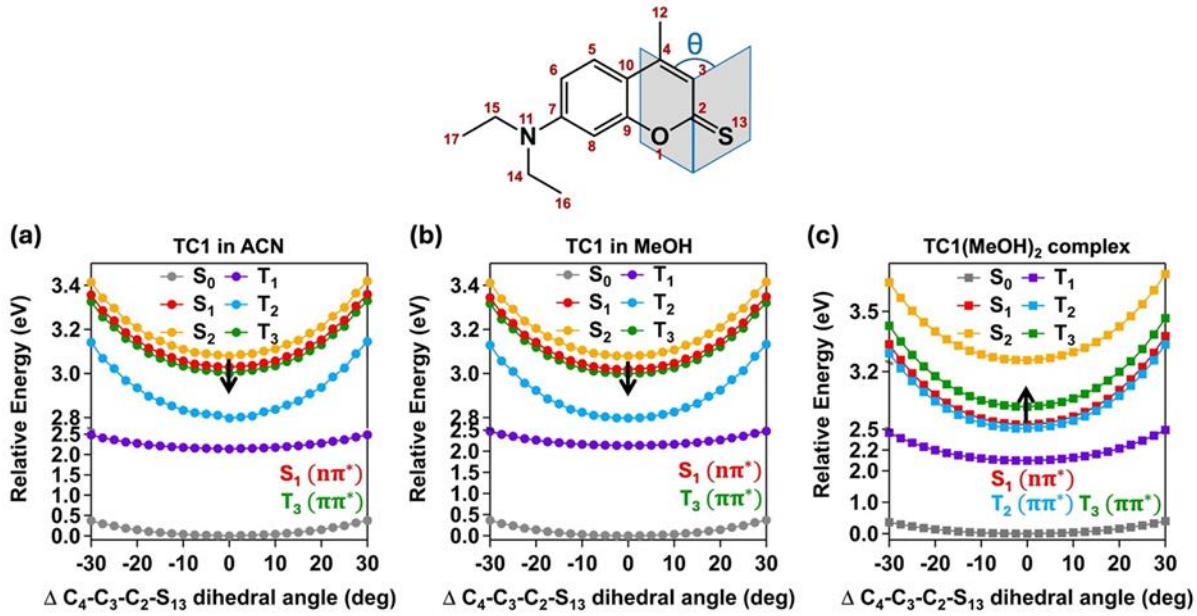

Figure 5.2.12: Potential energy coordinate (PEC) scan along the C_4-C_3-C_2-S_{13} dihedral angle of (a) TC1 in acetonitrile (ACN), (b) TC1 in methanol (MeOH), and (c) TC1$(MeOH)_2$ complex.

Figures 5.2.12a,b illustrates the PEC scan of TC1 in both acetonitrile and methanol without explicit methanol solvent along the C_4-C_3-C_2-S_{13} dihedral coordinate. Throughout this dihedral coordinate, the S_1 and T_3 states are nearly isoenergetic and follow El-Sayed's rule for intersystem crossing (ISC). However, in TC1:$(CH_3OH)_2$ complex, S_1 and T_2 states are nearly isoenergetic (Figure 5.2.12c), but they do not satisfy the orbital exchange criteria (El Sayed's rule) necessary for ISC. Consequently, ISC from the S_1 state is anticipated to be slower compared to non-hydrogen bonded solvent, as observed in the experiment. Thus, the results suggest that the C_4-C_3-C_2-S_{13} coordinate might also have a role in the ISC process in TC1.

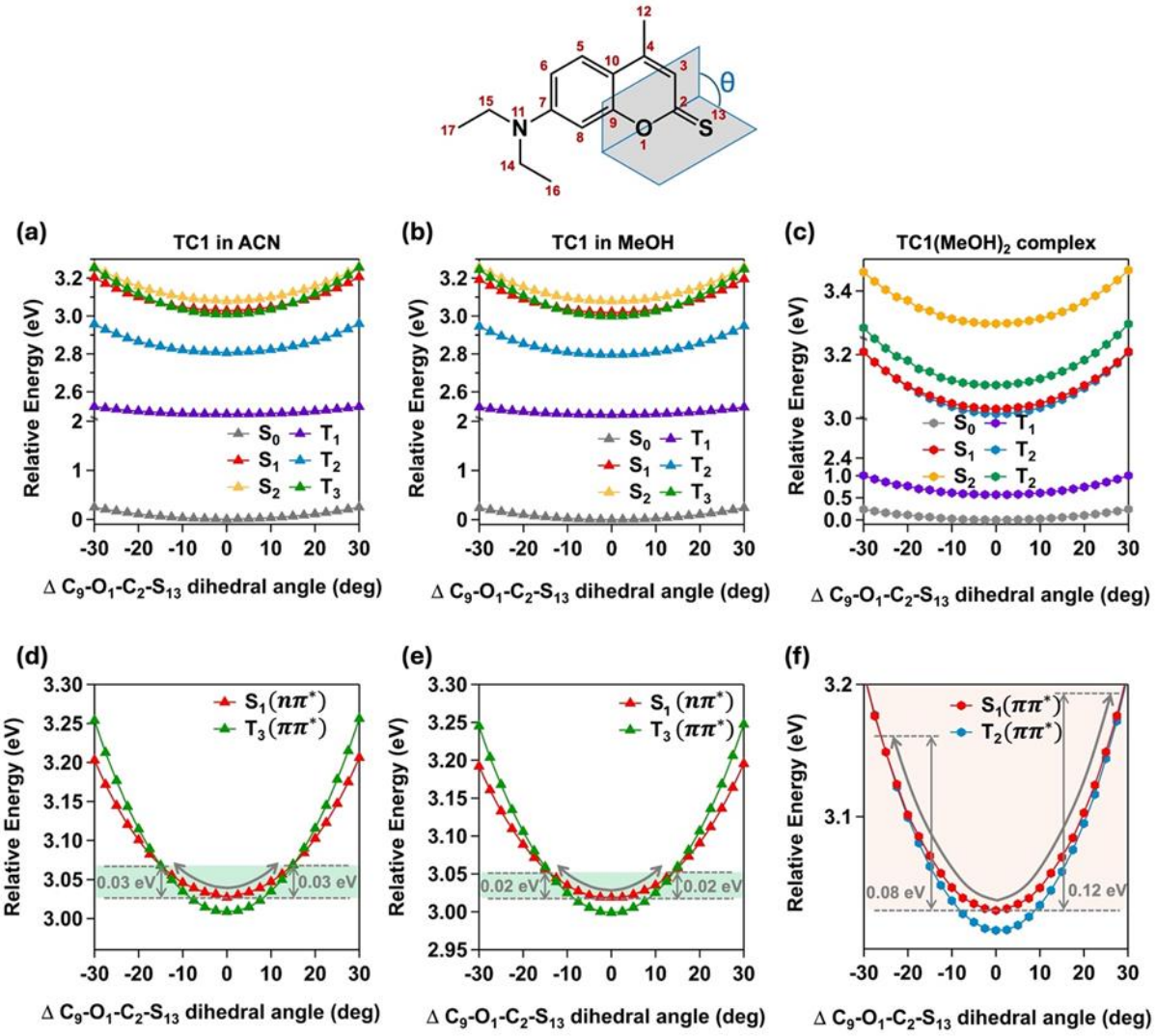

Figure 5.2.13. Potential energy coordinate (PEC) scan along the C_9-O_1-C_2-S_{13} dihedral angle of (a) TC1 in acetonitrile (ACN), (b) TC1 in methanol (MeOH), and (c) TC1$(MeOH)_2$ complex. A zoomed version around S_1 energy level of (a), (b) and (c) is represented in (d), (e) and (f), respectively, along with the orbital characters. In acetonitrile and methanol, the S_1/T_3 crossing are energetically feasible, whereas in TC1$(MeOH)_2$ complex the S_1/T_2 crossing is energy activated.

The potential energy coordinate scan (PEC) scan of TC1 in acetonitrile and methanol (without hydrogen bonding) along the C_9-O_1-C_2-S_{13} dihedral coordinate is depicted in Figures 5.2.13a, 5.2.13b, 5.2.13d, and 5.2.13e. Along this symmetric nuclear coordinate, a crossing between the S_1 and T_3 states has been observed with an energy barrier of ~0.025 eV from the S_1 FC state, which is achievable at the room temperature. In addition, the $S_1 \longrightarrow T_3$ transition is orbitally feasible (El-Sayed allowed), and, therefore, may contribute to efficient triplet generation from the S_1

state. However, in TC1:$(CH_3OH)_2$ complex, the energy gap between the S_1 and T_3 states increased appreciably, and S_1 and T_2 states crosses each other around ±20° change in C_9-O_1-C_2-S_{13} dihedral angle (see Figures 5.2.13c and 5.2.13f), with an activation energy close to 0.1 eV from the S_1 FC state. Moreover, the orbital character of the S_1 and T_2 states does not satisfy El-Sayed rule for ISC. Based on these observations we conclud that the C_9-O_1-C_2-S_{13} dihedral coordinate also plays a role in triplet formation in TC1, and the presence of hydrogen bonding interactions modifies this coordinate in such a way that the ISC is less efficient.

Overall, the quantum chemical calculations predict a possible role of three vibrational modes (i.e., C_2=S_{13} bond stretch, C_4-C_3-C_2-S_{13} dihedral angle, and C_9-O_1-C_2-S_{13} dihedral angle) in the ISC of TC1 molecule. The results also predict that the energy landscape is modulated through hydrogen bonding in polar protic solvent and attenuate the triplet yield in the molecule.

5.3 Conclusions

In conclusion, we have investigated how intermolecular hydrogen bonding influences the photophysical properties of thiocoumarin 1 (TC1) using steady-state and time-resolved spectroscopic techniques. Our steady-state fluorescence measurements showed that in protic methanol, the fluorescence quantum yield and lifetime of TC1 are approximately ten times greater than in the aprotic acetonitrile solvent, whose polarity is similar to that of methanol. This increase in fluorescence quantum yield and lifetime in methanol was accompanied by a tenfold reduction in triplet yield, underscoring the inhibitory role of hydrogen bonding in triplet-state generation. Further, time-resolved absorption experiments revealed the emergence of an additional emissive state in protic methanol, which was not present in acetonitrile. This state likely represents the hydrogen-bonded singlet state. Kinetic analysis of the transient data revealed that triplet generation in methanol arises from three singlet states (with time constants ~0.5 ps, ~2.0 ps, and ~90 ps), while in acetonitrile, it involves only two states (with time constants ~0.5 ps and ~2.0 ps).

Additionally, as the proportion of protic solvent (methanol) increases in the aprotic acetonitrile, the triplet generation slows down monotonically.

TDDFT calculations indicated that hydrogen bonding influences the energetics and electronic characteristics of low-lying singlet states in a manner that disfavors triplet formation from the Franck-Condon excitation point. Further analysis identified at least three possible reaction coordinates for triplet generation: the C_2=S_{13} bond vibration along with a change in C_4-C_3-C_2-S_{13} and C_9-O_1-C_2-S_{13} dihedral angles. Perhaps the solvent-solute hydrogen bonding at the sulfur atom significantly affects the feasibility of triplet generation along these coordinates by altering both energetics and orbital properties. This observation is consistent with the noted reduction in fluorescence quantum yield and lifetime of TC1 in protic methanol.

Our experimental and theoretical findings bring out the intricate role of hydrogen bonding interactions in modulating triplet state generation and the overall dynamics of photoexcited thiocoumarin 1, which is summarized in Scheme 5.3.1. This research offers new insights into how hydrogen bonding interactions reshape the landscape of photo-excited molecules.

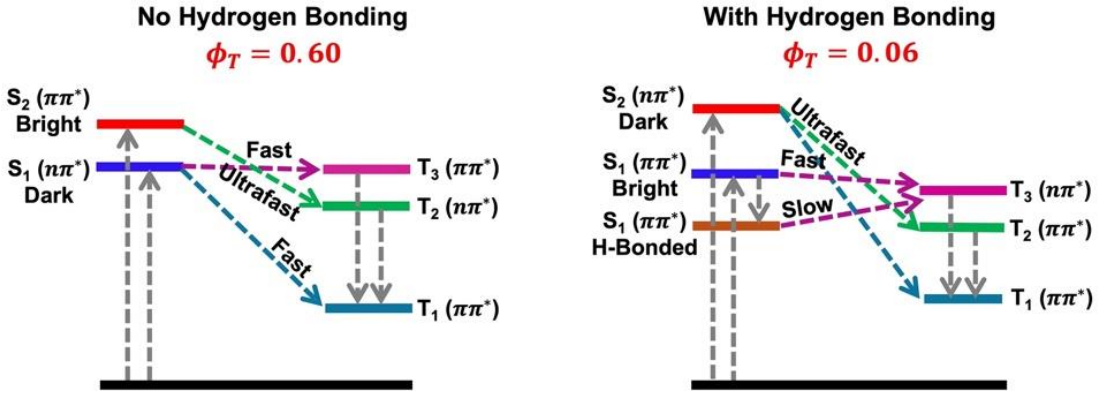

Scheme 5.3.1. A schematic representation of possible relaxation coordinate of TC1 in non-hydrogen bonded and hydrogen bonded solvent.

References:

(1) Grayson, M. N.; Yang, Z.; Houk, K. N. Chronology of CH···O Hydrogen Bonding from Molecular Dynamics Studies of the Phosphoric Acid-Catalyzed Allylboration of Benzaldehyde. *J. Am. Chem. Soc.* **2017**, 139, 7717–7720.

(2) Yi, X.; Chen, W.; Xiao, Y.; Liu, F.; Yu, X.; Zheng, A. Spectroscopically Visualizing the Evolution of Hydrogen-Bonding Interactions. *J. Am. Chem. Soc.* **2023**, 145, 27471–27479.

(3) Heyden, M.; Tobias, D. J. Spatial Dependence of Protein-Water Collective Hydrogen-Bond Dynamics. *Phys. Rev. Lett.* **2013**, *111*, 218101.

(4) Burdzinski, G.; Maciejewski, A.; Buntinx, G.; Poizat, O.; Toele, P.; Zhang, H.; Glasbeek, M. Femtosecond Fluorescence Up-Conversion and Transient Absorption Studies of the S_2 State in the Hydrogen-Bonded Benzopyranthione–Water Complex. *Chem. Phys. Lett.* **2004**, 393, 102–106.

(5) Su, Y.; Li, K.; Yu, X. Theoretical Studies on the Fluorescence Enhancement of Benzaldehydes by Intermolecular Hydrogen Bonding. *J. Phys. Chem. B* **2019**, *123*, 884–890.

(6) Nishio, M. The CH/π Hydrogen Bond in Chemistry. Conformation, Supramolecules, Optical Resolution and Interactions Involving Carbohydrates. *Phys. Chem. Chem. Phys.* **2011**, *13*, 13873–13900.

(7) Galle Kankanamge, S. R.; Ma, J.; Mackin, R. T.; Leonik, F. M.; Taylor, C. M.; Rubtsov, I. V.; Kuroda, D. G. Proving and Probing the Presence of the Elusive C−H···O Hydrogen Bond in Liquid Solutions at Room Temperature. *Angew. Chem. Int. Ed.* **2020**, *59*, 17012–17017.

(8) Das, K.; Sappati, S.; Bisht, G. S.; Hazra, P. Proton-Coupled Electron Transfer in the Aqueous Nanochannels of Lyotropic Liquid Crystals:

Interplay of H-Bonding and Polarity Effects. *J. Phys. Chem. Lett.* **2021**, *12*, 2651–2659.

(9) Aizawa, T.; Takahashi, S.; Isobe, A.; Datta, S.; Sotome, H.; Miyasaka, H.; Kajitani, T.; Yagai, S. Fluorescent Supramolecular Polymorphism Driven by Distinct Hydrogen Bonding Lattice. *Chem. Lett.* **2020**, *49*, 1009–1012.

(10) Sotome, H.; Kamada, K.; Kuzuhara, D.; Yamada, H.; Abulikemu, A.; Sakagami, Y.; Heck, C.; Miyasaka, H. Near-Infrared-to-Visible Photon Upconversion via Triplet-Triplet Annihilation of a Solid-State System Fabricated by Rapid Drying Casting. *JSAP-OSA Joint Symposia*, **2019**.

(11) Pullanchery, S.; Kulik, S.; Rehl, B.; Hassanali, A.; Roke, S. Charge Transfer across C-H···O Hydrogen Bonds Stabilizes Oil Droplets in Water. *Science* **2021**, *374*, 1366–1370.

(12) Rabe, E. J.; Goldwyn, H. J.; Hwang, D.; Masiello, D. J.; Schlenker, C. W. Intermolecular Hydrogen Bonding Tunes Vibronic Coupling in Heptazine Complexes. *J. Phys. Chem. B* **2020**, *124*, 11680–11689.

(13) Fan, M.; Tang, Y.; Li, C.; Chen, B.; Wang, T.; Zhou, P.; Cui, X. Enhanced Fluorescence by Inter/Intramolecular Hydrogen Bonding in Si-Substituted Coumarins. *J. Phys. Chem. B* **2023**, *127*, 3187–3196.

(14) JUNE SUTOR, D. The C–H…O Hydrogen Bond in Crystals. *Nature* **1962**, *195*, 68–69.

(15) Taylor, R.; Kennard, O. Crystallographic Evidence for the Existence of C-H···O, C-H···N, and C-H···Cl Hydrogen Bonds. *J. Am. Chem. Soc.* **1982**, *104*, 5063–5070.

(16) Desiraju, G. R. The C-H···O Hydrogen Bond in Crystals: What Is It? *Acc. Chem. Res.* **1991**, *24*, 290–296.

(157) Boyken, S. E.; Chen, Z.; Groves, B.; Langan, R. A.; Oberdorfer, G.; Ford, A.; Gilmore, J. M.; Xu, C.; DiMaio, F.; Pereira, J. H.; Sankaran, B.; Seelig, G.; Zwart, P. H.; Baker, D. De Novo Design of Protein Homo-Oligomers with Modular Hydrogen-Bond Network–Mediated Specificity. *Science* **2016**, *352*, 680–687.

(18) Liu, Y.; Zhao, W.; Chen, C.-H.; Flood, A. H. Chloride Capture Using a C–H Hydrogen-Bonding Cage. *Science* **2019**, *365*, 159–161.

(19) Krystkowiak, E.; Bachorz, R. A.; Maciejewski, A. Hydrogen-Bonded 4H-1-Benzopyrane-4-Thione–Water Complexes Properties in the S_2 Excited State: The Mechanism and Dynamics of Deactivation. *Phys. Chem. Chem. Phys.* **2016**, *18*, 492–502.

(20) Decato, D. A.; Sun, J.; Boller, M. R.; Berryman, O. B. Pushing the Limits of the Hydrogen Bond Enhanced Halogen Bond—the Case of the C–H Hydrogen Bond. *Chem. Sci.* **2022**, *13*, 11156–11162.

(21) Liu, Z.-Y.; Hu, J.-W.; Huang, C.-H.; Huang, T.-H.; Chen, D.-G.; Ho, S.-Y.; Chen, K.-Y.; Li, E. Y.; Chou, P.-T. Sulfur-Based Intramolecular Hydrogen-Bond: Excited-State Hydrogen-Bond On/Off Switch with Dual Room-Temperature Phosphorescence. *J. Am. Chem. Soc.* **2019**, *141*, 9885–9894.

(22) Mai, S.; Pollum, M.; Martínez-Fernández, L.; Dunn, N.; Marquetand, P.; Corral, I.; Crespo-Hernández, C. E.; González, L. The Origin of Efficient Triplet State Population in Sulfur-Substituted Nucleobases. *Nat. Commun.* **2016**, *7*, 13077.

(23) Ashwood, B.; Pollum, M.; Crespo-Hernández, C. E. Photochemical and Photodynamical Properties of Sulfur-Substituted Nucleic Acid Bases, *Photochem. Photobiol.* **2019**, *95*, 33–58.

(24) Biswal, H. S.; Bhattacharyya, S.; Bhattacherjee, A.; Wategaonkar, S. Nature and Strength of Sulfur-Centred Hydrogen Bonds: Laser Spectroscopic

Investigations in the Gas Phase and Quantum-Chemical Calculations. *Int. Rev. Phys. Chem.* **2015**, *34*, 99–160.

(25) Chand, A.; Sahoo, D. K.; Rana, A.; Jena, S.; Biswal, H. S. The Prodigious Hydrogen Bonds with Sulfur and Selenium in Molecular Assemblies, Structural Biology, and Functional Materials. *Acc. Chem. Res.* **2020**, 53, 1580–1592.

(26) Mondal, J. A.; Ghosh, H. N.; Mukherjee, T.; Palit, D. K. Ultrafast Relaxation Dynamics of the Excited States of Michler's Thione. *J. Phys. Chem. A* **2006**, *110*, 12103–12112.

(27) Gemenetzidis, E.; Shavorskaya, O.; Xu, Y. Z.; Trigiante, G. Topical 4-Thiothymidine Is a Viable Photosensitiser for the Photodynamic Therapy of Skin Malignancies. *J. Dermatolog Treat.* **2011**, *24*, 209–214.

(28) Maciejewski, A.; Demmer, D. R.; James, D. R.; Safarzadeh-Amiri, A.; Verrall, R. E.; Steer, R. P. Relaxation of the Second Excited Singlet States of Aromatic Thiones: The Role of Specific Solute-Solvent Interactions. *J. Am. Chem. Soc.* **1985**, 107, 2831–2837.

(29) Maciejewski, A.; Sikorski, M.; Augustyniak, W.; Fidecka, M. The Quenching of Short-Lived S2 States of Aromatic Thioketones by Hydrocarbons. I. Important Contributions of the Transient Effect from Steady-State Measurements. *J. Photochem. Photobiol. A: Chem* **1996**, *94*, 119–127.

(30) Fang, Y.-G.; Fang, W.-H. Nature of Excited-State Dependent Hydrogen Bonds and Their Critical Role in Determining the Photophysical Properties of Aromatic Thioketones. *Phys. Chem. Chem. Phys.* **2022**, *24*, 17059–17067.

(31) Fargher, H. A.; Sherbow, T. J.; Haley, M. M.; Johnson, D. W.; Pluth, M. D. C–H···S Hydrogen Bonding Interactions. *Chem. Soc. Rev.* **2022**, *51*, 1454–1469.

(32) Mundlapati, V. R.; Gautam, S.; Sahoo, D. K.; Ghosh, A.; Biswal, H. S. Thioamide, a Hydrogen Bond Acceptor in Proteins and Nucleic Acids. *J. Phys. Chem. Lett.* **2017**, *8*, 4573–4579.

(33) Culik, R. M.; Jo, H.; DeGrado, W. F.; Gai, F. Using Thioamides To Site-Specifically Interrogate the Dynamics of Hydrogen Bond Formation in β-Sheet Folding. *J. Am. Chem. Soc.* **2012**, *134*, 8026–8029.

(34) Reddi, R.; Singarapu, K. K.; Pal, D.; Addlagatta, A. The Unique Functional Role of the C–H···S Hydrogen Bond in the Substrate Specificity and Enzyme Catalysis of Type 1 Methionine Aminopeptidase. *Mol. BioSyst.* **2016**, *12*, 2408–2416.

(35) Krystkowiak, E.; Koput, J.; Maciejewski, A. Hydrogen Bond Effects in the Ground and Excited Singlet States of 4H-1-Benzopyrane-4-Thione in Water—Theory and Experiment. *Phys. Chem. Chem. Phys.* **2012**, *14*, 8842–8851.

(36) Cui, X.; Fan, J.; Lyu, Y.; Zhou, X.; Meng, Q.; Zhang, C. Quasi-Intrinsic Thiobase Derivatives as Potential Targeted Photosensitizers in Two-Photon Photodynamic Therapy. *Spectrochim. Acta. A. Mol Biomol. Spectrosc.* **2024**, *316*, 124311.

(37) He, P.; Ren, X.; Zhang, Y.; Tang, B.; Xiao, C. Recent Advances in Sulfur Dioxide Releasing Nanoplatforms for Cancer Therapy. *Acta. Biomaterialia. Acta. Materialia. Inc.* **2024**, 91–103.

(38) Tong, S.; Cheng, Y.; Liu, H.; Pang, Y.; Lin, X.; Hu, Z.; Wu, F. Thionation of Conjugated Porphyrin with Enhanced Photodynamic and Photothermal

Effects for Cancer Therapy. *J Photochem. Photobiol. A Chem* **2025**, *459*, 116085.

(39) Yu, J.; Xu, J.; Jiang, R.; Yuan, Q.; Ding, Y.; Ren, J.; Jiang, D.; Wang, Y.; Wang, L.; Chen, P.; Zhang, L. Versatile Chondroitin Sulfate-Based Nanoplatform for Chemo-Photodynamic Therapy against Triple-Negative Breast Cancer. *Int. J. Biol. Macromol.* **2024**, *265*.

(40) Khatun, M. N.; Nandy, S.; Roy, H.; Ghosh, S. S.; Kumar, S.; Iyer, P. K. Sulphur-Atom Positional Engineering in Perylenimide: Structure-Property Relationships and H-Aggregation Directed Type-I Photodynamic Therapy. *Chem. Sci.* **2024**, *15*, 9298–9317.

(41) Pu, Y.; Cai, X.; Qu, Y.; Cui, W.; Li, L.; Li, C.; Zhang, Y.; Wang, Y. Spiro-Carbon-Locking and Sulfur-Embedding Strategy for Constructing Deep-Red Organic Electroluminescent Emitter with High Efficiency. *Angew. Chem. Int. Ed.* **2024**, *e202420253*,1-8.

(42) Pu, Y.; Jin, Q.; Zhang, Y.; Li, C.; Duan, L.; Wang, Y. Sulfur-Locked Multiple Resonance Emitters for High Performance Orange-Red/Deep-Red OLEDs. *Nat. Commun.* **2025**, *332*.

(43) Fan, T.; Liu, Q.; Zhang, H.; Wang, X.; Zhang, D.; Duan, L. Enhancing Spin–Orbit Coupling in an Indolocarbazole Multiresonance Emitter by a Sulfur-Containing Peripheral Substituent for a Fast Reverse Intersystem Crossing. *Adv. Mater.* **2024**, *36*, 2408816.

(44) Güven, Z.; Dolati, H.; Wessel, L.; Frank, R. Facile Synthetic Access Towards Sulfur- and Selenium-Functionalized Boron-Based Multiresonance TADF Emitters. *Molecules* **2024**, *29*, 5819.

(45) Mahaan, R.; John Bosco, A. Sulfur Oxidation State and Substituents Influenced Multifunctional Organic Luminophores in BTP Core for OLEDs:

A Computational Study on RTP, TADF Emitter and Sensitizer. *J. Phys. Chem. A* **2023**, *127*, 10570–10582.

(46) Karakurt, O.; Demirgezer, E. F.; Dastemir, M.; Cakmaktepe, S. C.; Miranda-Salinas, H.; Aksoy, E.; Danos, A.; Monkman, A.; Yildirim, E.; Cirpan, A. Design and Performance of Sulfur and Selenium-Substituted Triarylboron D3-A TADF Emitters for OLED Applications. *Org. Electron.* **2024**, 134, 107130.

(47) Wang, Y.; Tian, X.; Wang, X.; Wang, S.; Shao, S.; Wang, L. Boron-, Sulfur- and Nitrogen-Doped Decacyclic Multiple Resonance Emitters for Narrowband Deep Blue Electroluminescence. *Org. Electron.* **2024**, *128*, 107045.

(48) Wang, Z.; Li, Y.; Cai, X.; Chen, D.; Xie, G.; Liu, K. K.; Wu, Y. C.; Lo, C. C.; Lien, A.; Cao, Y.; Su, S. J. Structure-Performance Investigation of Thioxanthone Derivatives for Developing Color Tunable Highly Efficient Thermally Activated Delayed Fluorescence Emitters. ACS Appl. Mater. Interfaces. **2016**, *8*, 8627–8636.

(49) Piontkowski, Z.; McCamant, D. W. Excited-State Planarization in Donor-Bridge Dye Sensitizers: Phenylene versus Thiophene Bridges. *J. Am. Chem. Soc.* **2018**, *140*, 11046–11057.

(50) Lazarides, T.; McCormick, T. M.; Wilson, K. C.; Lee, S.; McCamant, D. W.; Eisenberg, R. Sensitizing the Sensitizer: The Synthesis and Photophysical Study of Bodipy-Pt(II)(Diimine)(Dithiolate) Conjugates. *J. Am. Chem. Soc.* **2011**, *133*, 350–364.

(51) Maciejewski, A.; Sikorski, M.; Augustyniak, W.; Fidecka, M. The Quenching of Short-Lived S2 States of Aromatic Thioketones by Hydrocarbons. I. Important Contributions of the Transient Effect from

Steady-State Measurements. *J. Photochem. Photobiol. A: Chem.* **1996**, *94*, 119–127.

(52) Mohamadzade, A.; Nenov, A.; Garavelli, M.; Conti, I.; Ullrich, S. Double Thionated Pyrimidine Nucleobases: Molecular Tools with Tunable Photoproperties. *J. Am. Chem. Soc.* **2023**, *145*, 11945–11958.

(53) Iyer, A.; Clay, A.; Jockusch, S.; Sivaguru, J. Evaluating Brominated Thioxanthones as Organo-Photocatalysts. *J. Phys. Org. Chem.* **2017**, *30*, e3738.

(54) Raghunathan, R.; Jockusch, S.; Sibi, M. P.; Sivaguru, J. Evaluating Thiourea/Urea Catalyst for Enantioselective 6π-Photocyclization of Acrylanilides. *J. Photochem. Photobiol. A: Chem.* **2016**, *331*, 84–88.

(55) Ruduss, A.; Jece, A.; Stucere, K. A.; Chen, K. W.; Turovska, B.; Belyakov, S.; Vembris, A.; Chang, C. H.; Traskovskis, K. Sulfonyl-Functionalized Benzo[d]Imidazo[5,1-b]Thiazole-Based Carbenes as Building Blocks for Two-Coordinate Cu(i) Complexes Exhibiting Fast and Efficient Thermally Activated Delayed Fluorescence. *J. Mater. Chem. C* **2024**, *12*, 2968–2980.

(56) Szymański, M.; Balicki, M.; Binkowski, M.; Kubicki, J.; Maciejewskia, A.; Pawłowska, E.; Wróżowa, T. Effects of Solute-Solvent Interactions on Radiationless Decay of Thioketones Excited to their S_2-and T_1-States. *ACTA. PHYSICA. POLONICA. A* **1996**, *89*, 527–546.

(57) Maciejewski, A. The Application of Perfluoroalkanes as Solvents in Spectral, Photophysical and Photochemical Studies. *J. Photochem. Photobiol. A: Chem.* **1990**, *51*, 87–131.

(58) Law, K. Y.; De Mayo, P. Thione Photochemistry. Adamantanethione as a Model for Singlet $\pi\pi^*$ Hydrogen Abstraction. *J. Am. Chem. Soc.* **1979**, *101*, 3251–3260.

(59) Pollum, M.; Crespo-Hernández, C. E. Communication: The Dark Singlet State as a Doorway State in the Ultrafast and Efficient Intersystem Crossing Dynamics in 2-Thiothymine and 2-Thiouracil. *J. Chem. Phys.* **2014**, *140*, 071101.

(60) Acquah, C.; Hoehn, S.; Krul, S.; Jockusch, S.; Yang, S.; Seth, S. K.; Lee, E.; Xiao, H.; Crespo-Hernández, C. E. Electronic Relaxation Pathways in Thio-Acridone and Thio-Coumarin: Two Heavy-Atom-Free Photosensitizers Absorbing Visible Light. *Phys. Chem. Chem. Phys.* **2024**, *26*, 28980-28991.

(61) Dutta, A.; Ghosh, S. K.; Mandal, S.; Srinivasan, V.; Ramamurthy, V.; Sen, P. Ultrafast Processes in Upper Excited Singlet States of Free and Caged 7-Diethylaminothiocoumarin. *J. Phys. Chem. A* **2024**, *128*, 6853–6863.

(62) Ghosh, S. K.; Chatterjee, S.; Boruah, P. P.; Mandal, S.; Da Silva, J. P.; Srinivasan, V.; Ramamurthy, V. A Supramolecular Approach towards the Photorelease of Encapsulated Caged Acids in Water: 7-Diethylaminothio-4-Coumarinyl Molecules as Triggers. *Photochem. Photobiol. Sci.* **2024**, *23*, 2057–2073.

(63) Ghosh, S. K.; Valloli, L. K.; Unny, D.; Sivaguru, J.; Jockusch, S.; Ramamurthy, V. Room Temperature Phosphorescence of 2-Thioxo-Coumarins in Aqueous Solution Promoted by Octa Acid Inclusion. *J. Photochem. Photobiol. A: Chem.* **2024**, *451*, 115510.

(64) Gollnick+, K.; Held, S.; Martire, D. 0; Braslavsky, S. E. Hydroxyanthraquinones as Sensitizers of Singlet Oxygen Reactions: Quantum Yields of Triplet Formation and Singlet Oxygen Generation in Acetonitrile. *J. Photochem. Photobiol. A: Chem.* **1992**, *69*, 155-165.

(65) Dutta, A.; Bhowmik, S.; Sen, P. Triplet State Photophysics of Bis(Dimethylphenanthroline)Copper(I) Might Involve Volume-Changing

Molecular Motion: Ultrafast Absorption and Emission Studies. *Chem. Phys. Lett.* **2024**, *839*, 141108.

(66) Sen, A.; Dutta, A.; Bose, A. L.; Sen, P. Oleylammonium Fluoride Passivated Blue-Emitting 2D $CsPbBr_3$ Nanoplates with near-Unity Photoluminescence Quantum Yield: Safeguarding against Threats from External Perturbations. *Chem. Sci.* **2025**, *16*, 735–752.

(67) Das, N.; Tarif, E.; Dutta, A.; Sen, P. Associated Water Dynamics Might Be a Key Factor Affecting Protein Stability in the Crowded Milieu. *J. Phys. Chem. B* **2023**, *127*, 3151–3163.

(68) Neese, F.; Wennmohs, F.; Becker, U.; Riplinger, C. The ORCA Quantum Chemistry Program Package. *J. Chem. Phys.* **2020**, *152*, 224108.

(69) Barik, A.; Kumbhakar, M.; Nath, S.; Pal, H. Evidence for the TICT Mediated Nonradiative Deexcitation Process for the Excited Coumarin-1 Dye in High Polarity Protic Solvents. *Chem. Phys.* **2005**, *315*, 277–285.

(70) Tagliavini, V.; Duan, P. C.; Chatterjee, S.; Ferretti, E.; Dechert, S.; Demeshko, S.; Kang, L.; Peredkov, S.; DeBeer, S.; Meyer, F. Cooperative Sulfur Transformations at a Dinickel Site: A Metal Bridging Sulfur Radical and Its H-Atom Abstraction Thermochemistry. *J. Am. Chem. Soc.* **2024**, *146*, 23158–23170.

(71) Scheiner, S. Participation of S and Se in Hydrogen and Chalcogen Bonds. *CrystEngComm* **2021**, *23*, 6821–6837.

(72) Tsagkalidis, W.; Rehder, D. Characterization of Bio-Related Vanadium and Zinc Complexes Containing Tetradentate Dithiolate-Disulfide, -Diamine and -Amine-Amide Ligands. *J. Biol. Inorg. Chem.* **1996**, *1*, 507–514.

(73) Barik, A.; Nath, S.; Pal, H. Effect of Solvent Polarity on the Photophysical Properties of Coumarin-1 Dye. *J. Chem. Phys.* **2003**, *119*, 10202–10208.

(74) Acquah, C.; Hoehn, S.; Krul, S.; Jockusch, S.; Yang, S.; Seth, S. K.; Lee, E.; Xiao, H.; Crespo-Hernández, C. E. Electronic Relaxation Pathways in Thio-Acridone and Thio-Coumarin: Two Heavy-Atom-Free Photosensitizers Absorbing Visible Light. Phys. *Chem. Chem. Phys.* **2024**, *26*, 28980–28991.

(75) Jena, S.; Mohanty, P.; Rout Rout, S.; Kumar Pati, S.; Biswal, H. S. Thio and Seleno-Psoralens as Efficient Triplet Harvesting Photosensitizers for Photodynamic Therapy. *Chem. Eur. J.* **2024**, *30*, e202400733.

Chapter 6

Inhibitory Effect of Charge Transfer on Ultrafast Triplet Formation in Thiocoumarins

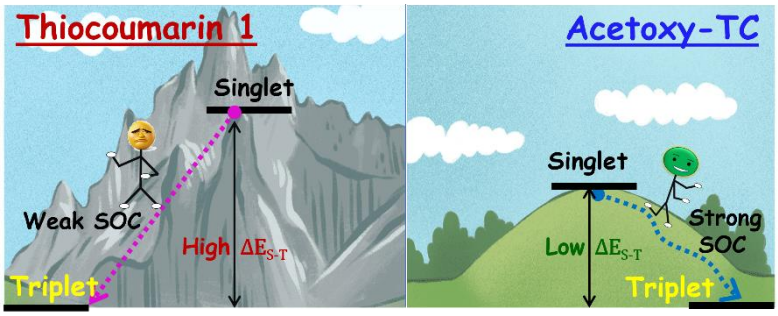

• Less-efficient triplets • Efficient triplets

Abhijit Dutta, Sujit Kumar Ghosh, Vaidhyanathan Ramamurthy and Pratik Sen (*Manuscript Under Preparation*)

Thiocarbonyl-containing compounds are known for their distinctive photophysical properties, particularly their rapid intersystem crossing (ISC), facilitated by favorable singlet–triplet energetics and enhanced spin–orbit coupling (SOC). However, the ISC efficiency and resulting triplet yields can vary significantly depending on molecular factors. This study explores the role of intramolecular charge transfer (CT) in modulating triplet state generation in thiocoumarins. Specifically, the introduction of a diethylamino group at the 7-position of the thiocoumarin ring (Thiocoumarin 1, or TC1) induces CT character, yielding a moderate singlet oxygen generation efficiency (50–60%) and solvent polarity-dependent fluorescence with a low quantum yield (~10^{-4}). In contrast, the 7-acetoxy-substituted derivative (Acetoxy-TC) shows extremely weak fluorescence (quantum yield ~10^{-6}) but achieves remarkably high singlet oxygen yields (80–90%) that are largely independent of the solvent environment. Time-resolved spectroscopic measurements reveal an ultrashort fluorescence lifetime and concomitant ultrafast triplet state population in Acetoxy-TC across solvents, indicating highly efficient ISC. On the other hand, TC1 displays a more stable singlet excited state and slower ISC dynamics, consistent with its steady state photophysical behavior. Complementary theoretical calculations further support these observations: Acetoxy-TC exhibits solvent-independent high SOC values and a small singlet–triplet energy gap, both conducive to efficient ISC. In contrast, TC1 shows less favorable ISC parameters. These findings underscore the importance of molecular design specifically avoiding CT states in achieving efficient triplet state generation in thiocarbonyl systems.

6.1 Introduction

In the field of photophysical studies of molecular systems, numerous reports have highlighted the role of photoinduced charge transfer (CT) processes in various solvent environments and their applications across areas such as biology and imaging. [1–16] Owing to its dipolar nature, this CT state exhibits solvent-dependent behavior in both absorption and emission spectra.[17–19] Among the diverse range of CT-state forming systems, amino-coumarin derivatives are among the most extensively studied. These molecules absorb light in the near-UV to visible region[20–24] and have been widely used as solvatochromic probes in fluorescence sensing and imaging applications. [25,26] Upon photoexcitation, these aminocoumarin molecules get promoted to the Franck–Condon (FC) excited state, from which intramolecular charge transfer occurs typically from the amino group to the fused benzopyrone ring forming the CT state. [20–22] In coumarin systems, this singlet-CT state has high quantum yields and nanosecond-scale lifetimes, primarily due to restricted non-radiative decay channels.[20–22] Moreover, their triplet states exhibit significantly different energy levels and often violate the El-Sayed rule for intersystem crossing (ISC). [27,28] In polar protic solvents, the CT state can further evolve into a twisted intramolecular CT (TICT) state, which is readily decays to the ground state and leads to reduced fluorescence quantum yield. [20,29] Thus, the formation and stabilization of the CT state play a crucial role in maintaining the high fluorescence efficiency of aminocoumarin systems.

In contemporary research, there is a growing interest in triplet states due to their applications in optoelectronics and photodynamic therapy.[30–34] Consequently, strategies are needed to suppress fluorescence and redirect singlet-state decay pathways toward triplet-state generation. Numerous studies have shown that external heavy atoms can effectively promote ISC in various aromatic compounds.[35–38] Several reports explored that apart from heavy-atom effect, particularly the sulfur atom incorporation at the carbonyl oxygen of carbonyl compounds potentially promotes the ISC dynamics. [32,39–55] A similar thionation also potentially impacts the

ISC dynamics in DNA/RNA nucleobases.[32,56–60] In this regards, visible light absorbing thiocoumarin derivative are also attractive for the study of triplet formation dynamics. Interestingly, these thio-derivatives often exhibit very low fluorescence quantum yields and ultrashort fluorescence lifetimes, indicating efficient ISC to nearby triplet states.[61,62] Recently, Ramamurthy's group investigated the photophysical properties of various thio-aminocoumarin derivatives, both in bulk solvents and within the confined environment of an octa acid (OA) cavity.[63] Their findings revealed that molecules bearing an amino group at the 7-position of the thiocoumarin core exhibited solvent polarity-dependent behavior in both absorption and emission spectra. This contrasted with unsubstituted or acetoxy/alkoxy-substituted thiocoumarins, indicating the formation of a CT state specifically in the amino-substituted thio-derivatives. Our investigations into the photophysical properties of Thiocoumarin 1 have revealed unique excited-state dynamics, including ultrafast triplet generation in both bulk solvents and confined environments like octa acid cavities. Notably, many of the observed ISC transitions in these systems conform to the El-Sayed rule and exhibit high spin-orbit coupling constants (SOC), further confirming efficient triplet generation.[64] Generally, the presence of a CT singlet state is associated with a smaller energy gap between the singlet and nearby triplet states, which typically leads to reduced fluorescence and enhanced ISC efficiency.[22,65–69] However, experimental observations showed that the 7-amino-thiocoumarin derivatives exhibit relatively strong fluorescence, both in ethanol glass at 77 K and within the OA cavity, compared to their non-amino counterparts.[63] Moreover, the phosphorescence-to-fluorescence intensity ratio $\left(\frac{I_{Phos}}{I_{Fl}}\right)$ was found to be higher for non-CT-based thiocoumarins than for the 7-amino derivatives, indicating more efficient triplet generation in the absence of CT character. These results suggest that the presence of a CT state in thiocoumarins may counteract efficient triplet formation, highlighting a complex interplay between CT character and ISC efficiency in these systems.

With this comprehensive introduction, we started to present our work on how the CT state in amino-functionalized thiocoumarins decreases the triplet formation efficiency, we have selectively chosen the 7-acetoxy (Acetoxy-TC) and 7-diethyl amino-thiocoumarin (TC1, with CT character) (see Scheme 6.1.1) derivatives and studied the steady-state and time-resolved measurements and quantum chemical calculations in bulk solvents as well as inside the caged octa acid (OA) cavity (see Scheme 6.1.1).

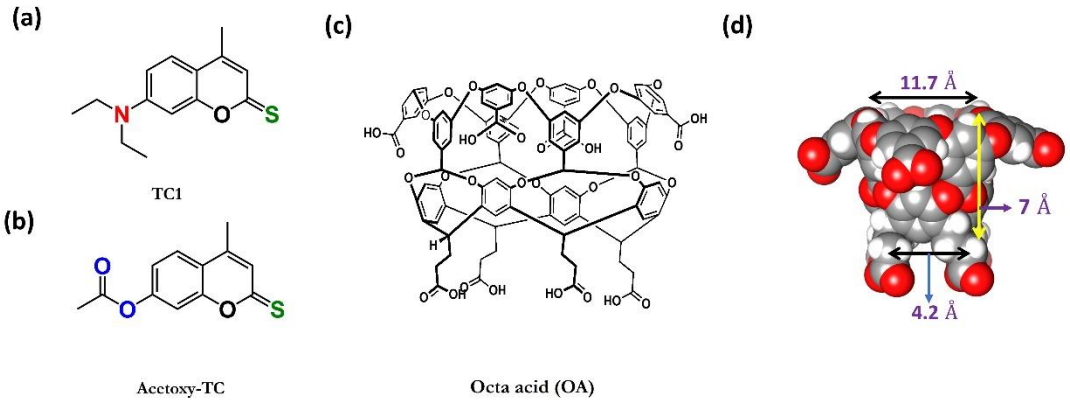

Scheme 6.1.1. Structure of (a) 7-Diethylaminothiocoumarin (Thiocoumarin 1 or TC1), (b) 4-methyl-2-thioxo-2H-chromen-7-yl acetate (7-Acetoxy Thiocoumarin or Acetoxy-TC), (c) Chemical structure of water-soluble octa-acid (OA) cavitand, (d) Three-dimensional structure of OA cavitand

6.2. Results and Discussion

Our preliminary results reveal that the 7-acetoxy-substituted thiocoumarin (Acetoxy-TC) exhibits an extremely low fluorescence quantum yield (~10^{-6}) and an ultrashort fluorescence lifetime (~150 fs), in stark contrast to thiocoumarin 1, which shows a higher fluorescence quantum yield (~10^{-4}) and a singlet state lifetime in the picosecond range when studied in bulk solvents. Notably, TC1 displays solvent polarity-dependent shifts in both its absorption and emission spectra, indicative of the presence of a charge transfer (CT) state.[64] These contrasting excited state behaviors in thiocoumarins prompted us to undertake advanced time-resolved

spectroscopic studies, complemented by computational analyses, to further elucidate the role of CT states in the photoexcited-state dynamics of thiocoumarins as efficient triplet forming system. The results of these investigations are detailed in the sections that follow.

6.2.1. Steady-State and Time-Resolved Absorption/Emission Studies in Solution.

Figures 6.2.1(a–b) and 6.2.1(d–e) depict the steady-state absorption and emission spectra of TC1 and Acetoxy-TC molecules in solvents of increasing polarity hexane, acetone, and acetonitrile. A spectral shift in both the absorption and emission bands is observed for the TC1 molecule, suggesting the presence of a charge transfer (CT) excited state, unlike in the case of the Acetoxy-TC molecule. From the emission spectra, it is also evident that the Acetoxy-TC molecule exhibits relatively strong room-temperature phosphorescence (RTP) emission bands in both polar and non-polar solvents, unlike the TC1 molecule, which shows weak RTP bands relative to its fluorescence emission. More interestingly, the fluorescence quantum yield of the Acetoxy-TC molecule is ~100 times lower than the TC1 molecule (See Figures 6.2.1c and 6.2.1f). This indicates that the molecule bearing a diethylamino moiety at the 7-position forms a CT state and exhibits higher fluorescence compared to the Acetoxy-TC molecule, which contains an acetoxy group at the 7-position of the thiocoumarin. To assess the efficiency of triplet generation, the singlet oxygen quantum yields of both molecules were measured (see Figure 6.2.2a). Upon comparison, the singlet oxygen yield is approximately 1.7 times higher for the 7-acetoxy TC molecule than for the TC1 molecule. Therefore, steady-state measurements indicate that the CT state formation TC1 is less conducive to triplet generation.

Further to understand the origin of the fluorescence emission band, the excitation spectra of Acetoxy-TC were recorded, and compared those with the absorption spectra are presented in Figures 6.2.3. It is already established that the excitation

spectra of the fluorescence band in TC1 are red-shifted relative to the absorption band, which we interpreted as evidence for a hidden low-energy singlet state (possibly S_1) with very poor oscillator strength, but relatively strong fluorescence compared to the higher oscillator strength singlet state (S_2). This interpretation is further supported by the excitation wavelength-dependent variations in fluorescence quantum yield values. However, in Acetoxy-TC, the excitation spectra of fluorescence band almost approximately match with the absorption spectra (see Figure 6.2.3). This indicates that in Acetoxy-TC fluorescence comes only due to excitation the main absorptive state.

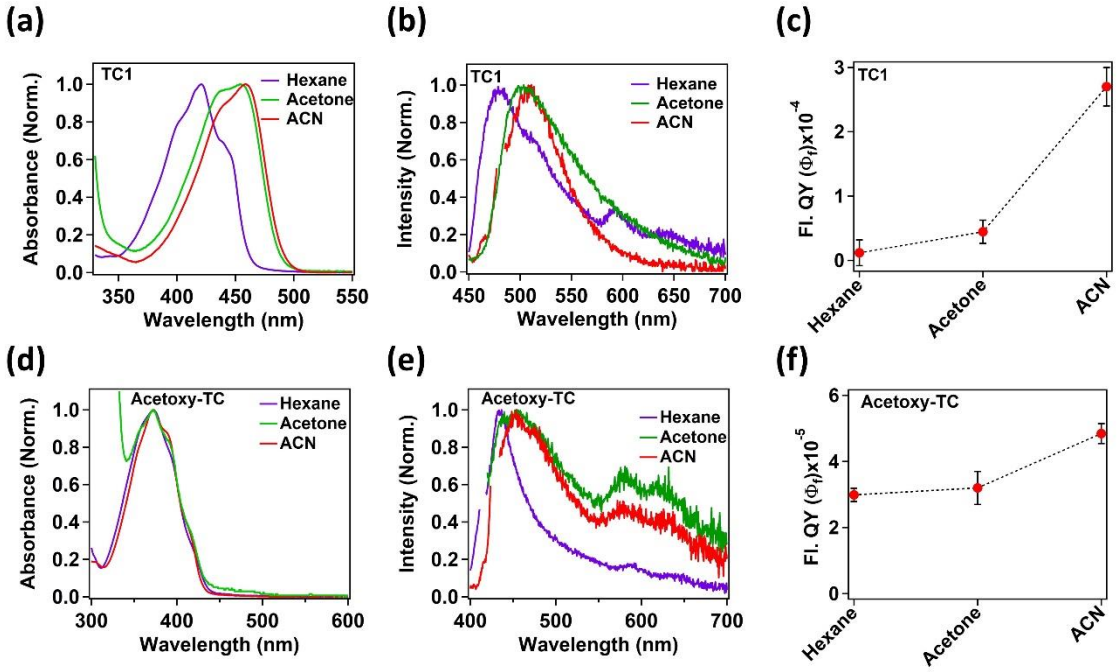

Figure 6.2.1: Steady-State (a) absorption and (b) emission spectra of TC1 in hexane (purple; λ_{ex} = 400 nm), acetone (green; λ_{ex} = 420 nm), and acetonitrile, ACN (red; λ_{ex} = 420 nm). Steady-State (d) absorption and (e) emission spectra of acetoxy-TC in hexane (purple; λ_{ex} = 370 nm), acetone (green; λ_{ex} = 370 nm), and acetonitrile, ACN (red; λ_{ex} = 380 nm). (c, f) Fluorescence quantum yield of TC1 and acetoxy-TC in previously mentioned solvents. All these measurements were done in an aerated condition at 25 °C without any special treatment.

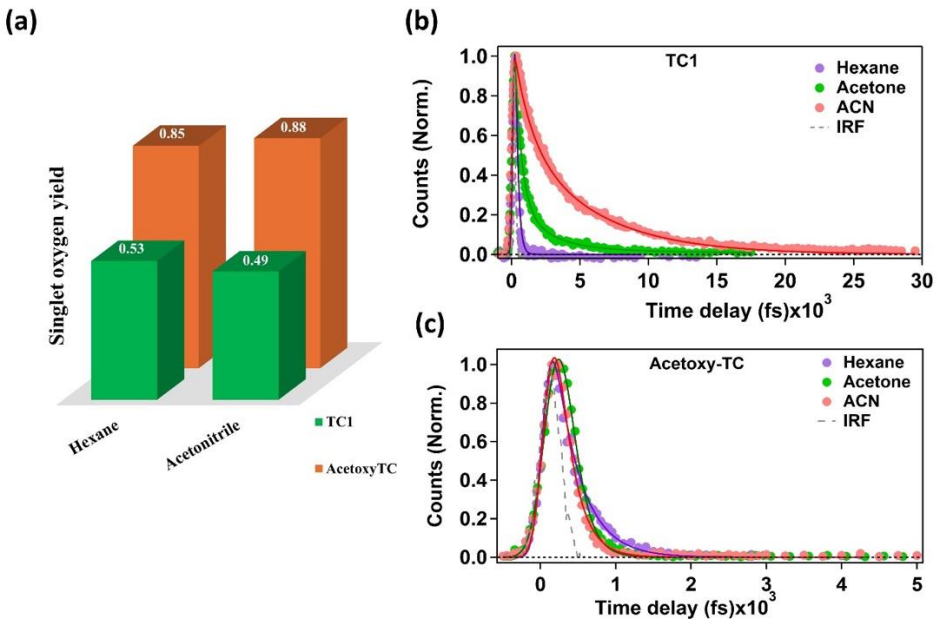

Figure 6.2.2: Steady state (a) Singlet oxygen yield and (b, c) fluorescence lifetime of thiocoumarin 1 (TC1) and Acetoxy-TC in solvents with different polarities i.e. hexane, acetone, and acetonitrile (ACN). Singlet oxygen quantum yield measurements were performed at 10 °C by taking chrysazin molecule in acetonitrile as a singlet oxygen standard (Φ_{SO}=0.69).[70] Fluorescence lifetimes were recorded at 25 °C at their corresponding emission maxima.

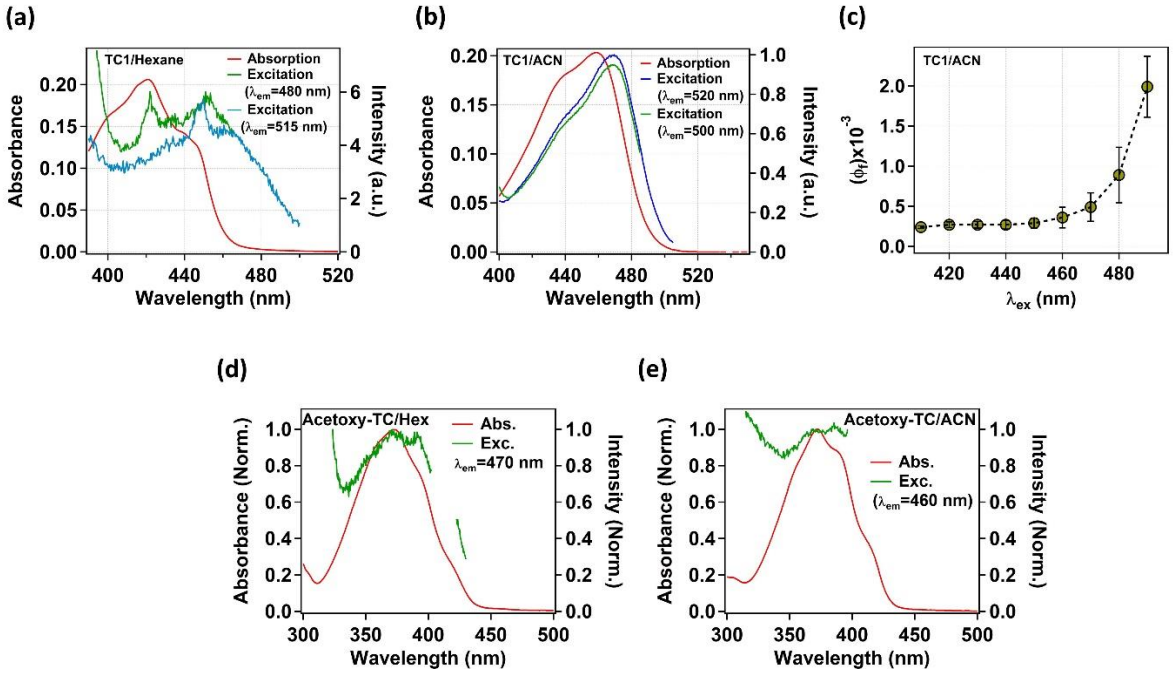

Figure 6.2.3: Steady-state excitation spectral measurement and fluorescence quantum yield measurement: excitation spectra (right axis) and absorption spectra (left axis) of TC1 in (a) hexane (Hex) and (b) acetonitrile (ACN) in an aerated condition at 25 °C (λ_{em} for excitation

spectral measurements are indicated in the figures). Excitation spectra of Acetoxy-TC in (d) hexane (Hex) and (e) acetonitrile (ACN) in an aerated condition at 25 °C (c) Excitation wavelength-dependent fluorescence quantum yield of TC1 in ACN solvent in an aerated condition at 25 °C (using the reference quantum yield 0.032 of coumarin 481 in 50% ethanol).

Further to get the time information of triplet generation, fluorescence lifetime of both the molecules (Acetoxy-TC and TC1) are recorded at their corresponding emission maxima is measured using the femtosecond fluorescence up-conversion technique; decay traces are displayed in Figure 6.2.2b, 6.2.2c. In hexane, fluorescence lifetime of both the molecules are found to be ultrafast with a time constants of ~ 200 ps. As the solvent polarity increases (from hexane to acetone to acetonitrile), the fluorescence lifetime of the TC1 molecule increases in a regular fashion. In contrast, no significant change is observed in the lifetime decay of the Acetoxy-TC molecule with changing the solvents. This suggests that, in the case of the TC1 molecule, in polar solvents, leading to a longer fluorescence lifetime due to the presence of CT state. In all the solvents, the fluorescence decay profiles were fitted, and time constants are tabulated in Table 6.2.1. In acetonitrile, time components of fluorescence decays of TC1 are 1.2 ps and 4.7 ps, which likely arise from the emission of the two lowest-lying singlet states (S_1 and S_2), as previously reported.[64] In the moderately polar acetone solvent, fast two-time components are 0.5 ps (79 %) and 2.2 ps (19 %). One additional component (13 ps, 2%) possibly arises from the specific interaction of the TC1 with the acetone. A similar result of slow fluorescence decay also observed in weakly polar dichloromethane solvent with time components of 0.6 ps (83 %) and 4.2 ps (17 %). This indicates that increased solvent polarity enhances the lifetime of the emissive states. The combined fluorescence quantum yield and lifetime data suggest that the polar solvents stabilize the CT state which leads to reduce the efficiency of triplet formation.

Table 6.2.1: Fitted kinetic parameters of TC1 in specified solvents in their fluorescence emission maximum.

Solvent	a_1	τ_1 (ps)	a_2	τ_2 (ps)	a_3	τ_3 (ps)
Hexane	1	0.15	-	-		
ACN	0.43	1.2	0.57	4.7		
DCM	0.83	0.6	0.17	4.2		
Acetone	0.79	0.5	0.19	2.2	0.02	13

Error in fitted time constants: ±30 fs for ultrafast growth component, ±0.2 ps for picosecond component

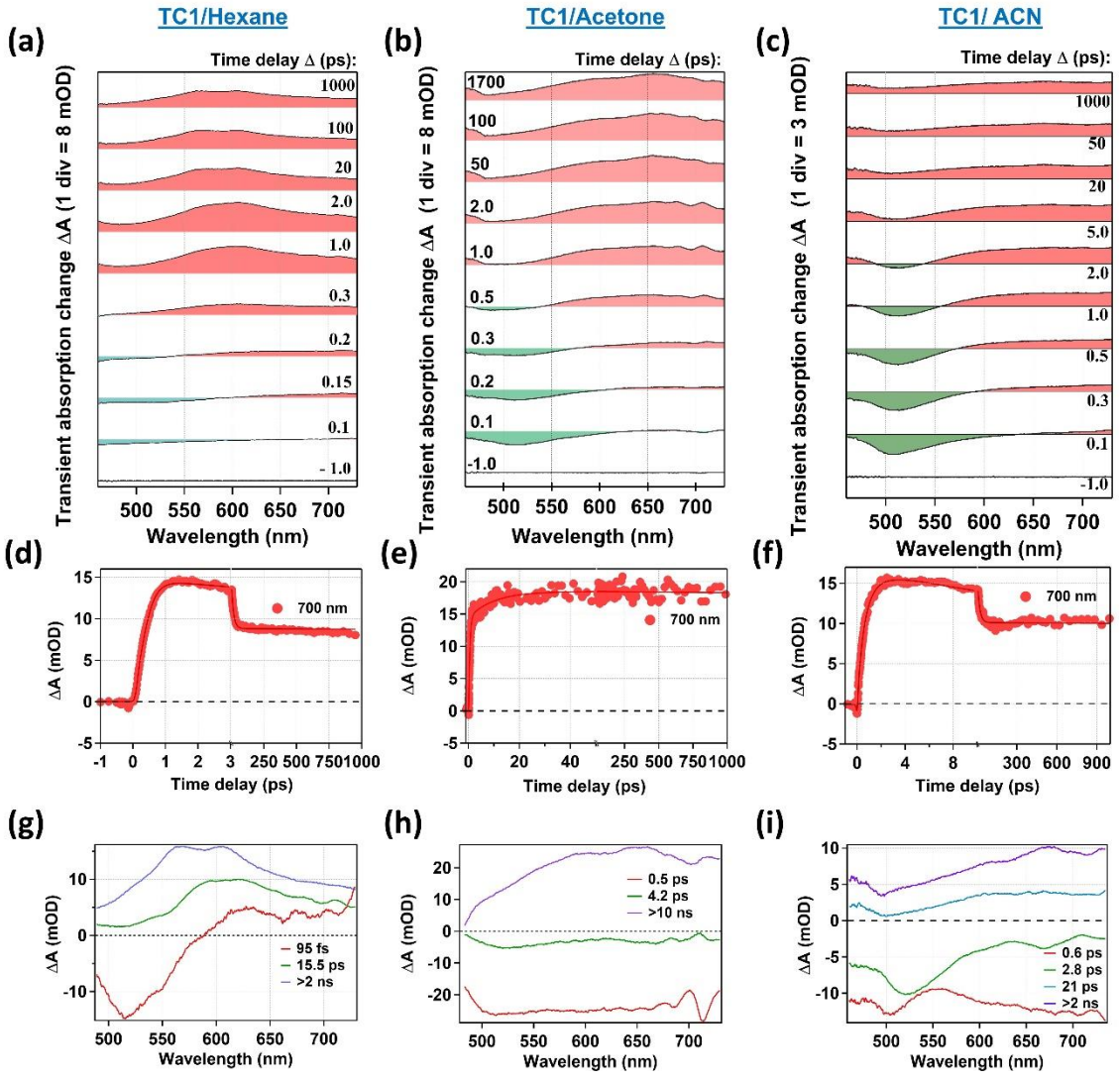

Figure 6.2.4: Transient absorption (TA) response (pump, 400 nm, probe, 460−730 nm) of TC1 in hexane (left panel), acetone (middle), and acetonitrile (ACN) (right panel). (a, b, c) TA

spectra at some representative delay times for hexane, acetone and acetonitrile (ACN), respectively. In hexane, the TA spectra consist of extremely feeble SE around 470-650 nm (green) and strong ESA over the whole probe spectral window (red). In acetone and ACN, spectra consist of SE around 470-600 nm (green) and ESA above 600 nm (red). (d, e, f) Fitted kinetics of TC1 in hexane, acetone, and ACN solvent at 700±5 wavelength of the spectra. (g, h, i) Decay-associated spectra from the global analysis of TA data in hexane, acetone, and ACN solvent. In hexane, two global time constants are 95 fs, 15.5 ps, and >10 ns, in acetone three global time constants are 0.5 ps, 4.2 ps and >10 ns and in ACN solvent, four global time constants are 0.6 ps, 2.8 ps, 21 ps and >10 ns. All the transient measurements were done in an aerated condition.

To further validate this hypothesis and get the time information about the triplet formation dynamics, femtosecond transient absorption (TA) studies were conducted for both molecules. Figure 6.2.4(a–c) displays the transient absorption spectra of TC1 in three different solvents. From these transients, it is evident that at early times (sub-picosecond to a few picoseconds), a negative band appears within the steady-state emission spectral range. This feature is attributed to stimulated emission (SE), and it is observed consistently across all solvents. In hexane, this negative SE band rapidly converts into a broad positive band within a few sub-picoseconds and remains unchanged up to 2 ns (the time window of our measurement). In contrast, in polar solvents such as acetone and acetonitrile, the SE feature persists for picoseconds. The broad positive band observed in the 460–730 nm region is assigned to the excited-state absorption (ESA) of triplet states according to our earlier report.[64] This observation strongly supports our initial speculation regarding the stabilization of the CT state in polar solvents, leads to create one additional slow ISC channel. However, the transient spectral features of the Acetoxy-TC molecule are markedly different, exhibiting a stimulated emission (SE) band in the 460–600 nm range with an ultrashort lifetime; approximately 0.3 ps (see Figure 6.2.5a–c). Regardless of the solvent, this emissive feature rapidly transforms into a broad excited-state absorption (ESA) band on a sub-picosecond timescale and remains unchanged throughout the entire experimental time window (>2 ns). This behavior strongly indicates the involvement of the triplet state.

Table 6.2.2: Triplet state rise time components of TC1 and Acetoxy-TC are extracted from the fitted TA kinetics data at 700±2 nm (average 700 nm) for TC1 and 475±5 nm (average 475 nm) for Acetoxy-TC, in hexane, Acetone, and acetonitrile at 298K.

Solvent	TC1			Acetoxy-TC	
	Spectral range (nm)	τ_1 (ps)	τ_2 (ps)	Spectral range (nm)	τ_1 (ps)
Hexane	698-702	0.25	-	470-480	0.40
Acetone		0.45	10.4		0.28
Acetonitrile		0.45	2.45		0.23

Error in fitted time constants: ±30 fs for ultrafast growth component, ±0.2 ps for picosecond growth components

Transient kinetics at the triplet absorption regions (700 nm for TC1 and 475 nm for Acetoxy-TC) were fitted using multiexponential functions (see Figure 6.2.4d–f). In our earlier report, we found that in acetonitrile, the triplet kinetics of TC1 fit a biexponential model, with triplet generation time constants of 0.55 ps and 1.54 ps.[64] In acetone, similar biexponential behavior is observed, with time constants of 0.45 ps and 10.4 ps (see Table 6.2.2). In contrast, in hexane, a single ultrafast component (~0.25 ps) is sufficient to fit the triplet formation kinetics. These results suggest that in polar solvents, the presence of a CT state introduces an additional singlet state channel, from which triplet generation occurs more slowly. However, for the Acetoxy-TC molecule, the kinetics of triplet generation are totally ultrafast with time constants of approximately 0.3 ps, regardless of solvent polarity. Therefore, TA kinetic analysis suggests that in polar solvents, TC1 accesses two distinct singlet state channels (ultrafast and slow) for triplet state population, exhibiting strong

polarity dependence. In contrast, ultrafast triplet generation in Acetoxy-TC occurs exclusively through the initially excited singlet state, having no CT character.

To better understand the involvement of multiple excited states in the photophysical processes of TC1, we compared the decay-associated spectra (DAS) obtained through the global analysis of the TA data. In hexane, global parameters are 95 fs, 15.5 ps, and 2 ns. Out them, 95 fs components display characteristic of stimulated emission (SE) and 15.5 ps, and 2 ns components exhibit excited-state absorption (ESA) feature, corresponding to the initial (T_n) and final triplet state (T_1). (see Figure 6.2.4g) With changing solvent to ACN, one more relatively slow SE type global time component (2.8 ps) appears in the excited state dynamics. (see Figure 6.2.4i) In acetone, three global time parameters are identified with time constants 0.5 ps and 4.2 ps (SE-type) and >10 ns (ESA type) (see Figure 6.2.4h). Therefore, in polar solvents, TC1 has at least two emissive singlet states which strongly correlates with our fluorescence upconversion results.

For the Acetoxy-TC molecule, however, the DAS analysis reveals a complete lack of solvent polarity dependence, with consistent global time constants of ~0.2 ps (SE) and >10 ps (ESA) across all solvents (see Figures 6.2.5g–i). This result indicates apart from the initially excited singlet state, no other long-lived low-energy emissive singlet states are generated in Acetoxy-TC. The overall transient absorption data analysis strongly supports our initial hypothesis that no CT state forms in Acetoxy-TC, in contrast to TC1. In TC1, the formation of CT state activates one additional triplet generation pathway. However, this pathway is significantly slower than the ultrafast triplet formation from the initially excited Franck–Condon (FC) state. As a result, TC1 exhibits high fluorescence quantum yield and a pronounced fluorescence lifetime in polar solvents, accompanied by a reduced triplet yield. Therefore, the collective experimental findings clearly indicate that CT state formation in aminothiocoumarins plays a counteractive role in triplet state population generation.

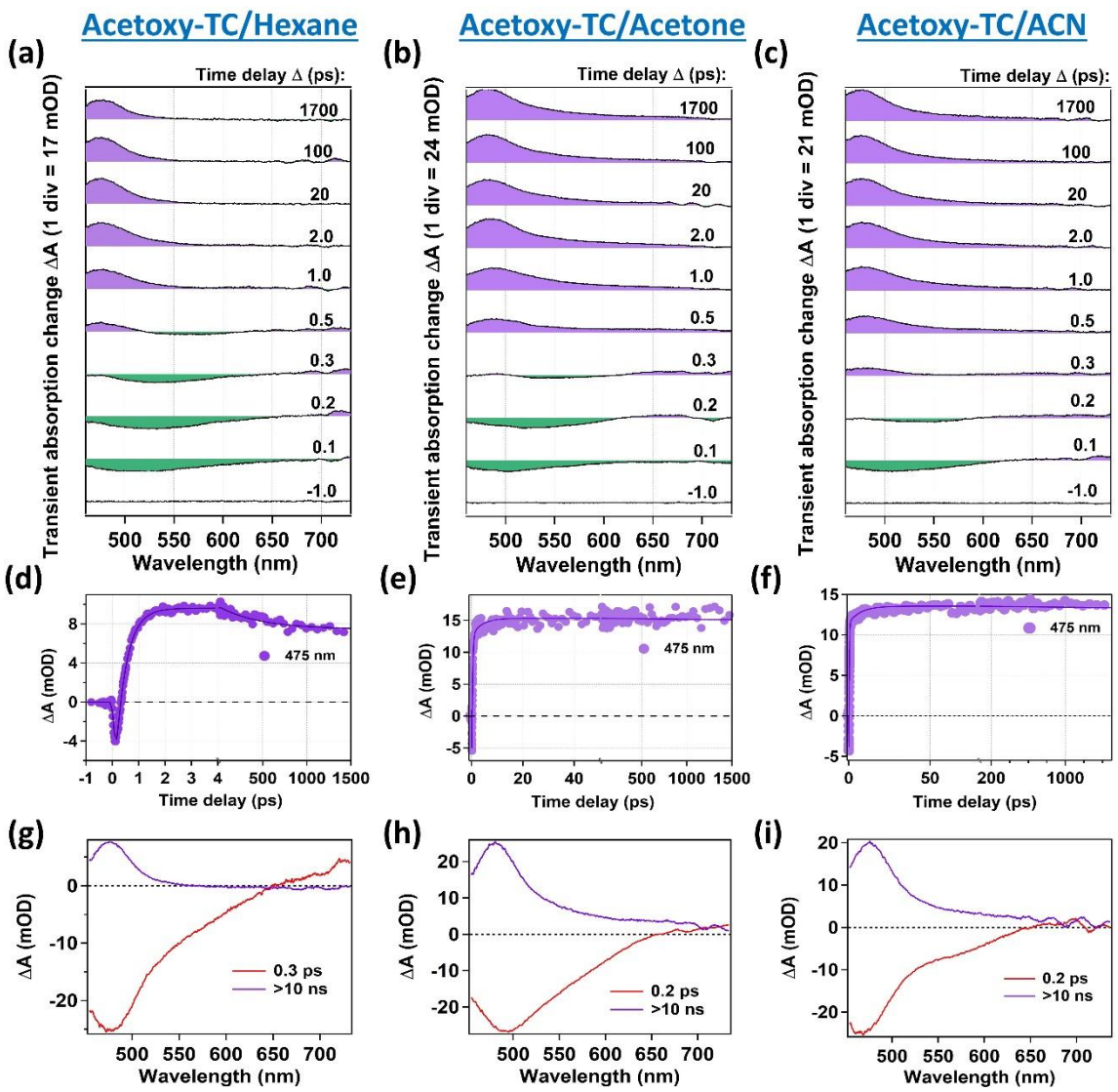

Figure 6.2.5: Transient absorption response (pump, 400 nm, probe, 460−730 nm) of Acetoxy-TC in hexane (left panel), acetone(middle), and acetonitrile (right panel). (a, b, c) TA spectra at some representative delay times for hexane, acetone and acetonitrile (ACN), respectively. In all three solvents i.e. hexane, acetone and acetonitrile (ACN) the TA spectra consist of extremely feeble SE around 470-650 nm (green) and strong ESA over the whole probe spectral window (purple). (d, e, f) Fitted kinetics of Acetoxy-TC data in hexane, acetone, and ACN solvents are at 475±5 nm wavelength of the transient spectra. (g, h, i) Decay-associated spectra from the global analysis of TA data in hexane, acetone, and ACN solvent. In all three solvents, global time constants are 0.2-0.3 ps and >10 ns. All the transient measurements were done in an aerated condition.

6.2.2. Steady-State and Time-Resolved Absorption/Emission Studies within a Confined Capsule.

Octa-acid (OA) is known to form closed capsular host–guest complexes with a variety of guest molecules.[71–73] Octa-acid (OA) is known to form closed capsular host–guest complexes with a variety of guest molecules. Since excited thioketones are known to be highly reactive in organic solvents and often relax via interactions with C–H bonds,[44,54,74,75] a well-defined and restricted medium such as the OA capsule is ideal for gaining deeper insights into the role of CT states formation in intersystem crossing dynamics in thiocoumarins. Recently, we demonstrated via ^{1}H NMR spectroscopy that OA forms a 2:1 host–guest complex with both TC1 and Acetoxy-TC dyes in borate buffer solution (pH 7.4).[63] The steady-state absorption and emission spectra of TC1@OA_2 and Acetoxy-TC@OA_2 show a strong band in the 570–750 nm range and a weaker band around 460–560 nm (see Figure 6.2.6a, 6.2.6b). The band above 570 nm resembles the phosphorescence observed in gated emission spectra measured in ethanol glass at 77 K, and is thus assigned to phosphorescence, while the higher-energy band is attributed to fluorescence.

To identify the origin of the emission bands, excitation spectra for both the fluorescence and phosphorescence emissions were recorded and compared them with the absorption spectra (see Figure 6.2.6c-6.2.6f). For both TC1@OA_2 and Acetoxy-TC@OA_2 complexes, the excitation spectrum of the phosphorescence band exactly matches the main absorption band. In contrast, the excitation spectrum of the fluorescence band appears red-shifted relative to the absorption spectrum in TC1@OA_2 which we interpreted and proved as the presence of a low-energy, weakly absorbing but strongly emissive hidden singlet state within the main absorption band. However, the fluorescence excitation spectrum of Acetoxy-TC@OA_2 is blue-shifted relative to the absorption band. This implies that in this case the fluorescence arises from excitation into a higher-order singlet state, and no other low-energy hidden singlet state (relative to main singlet absorption band) is involved in fluorescence emission.

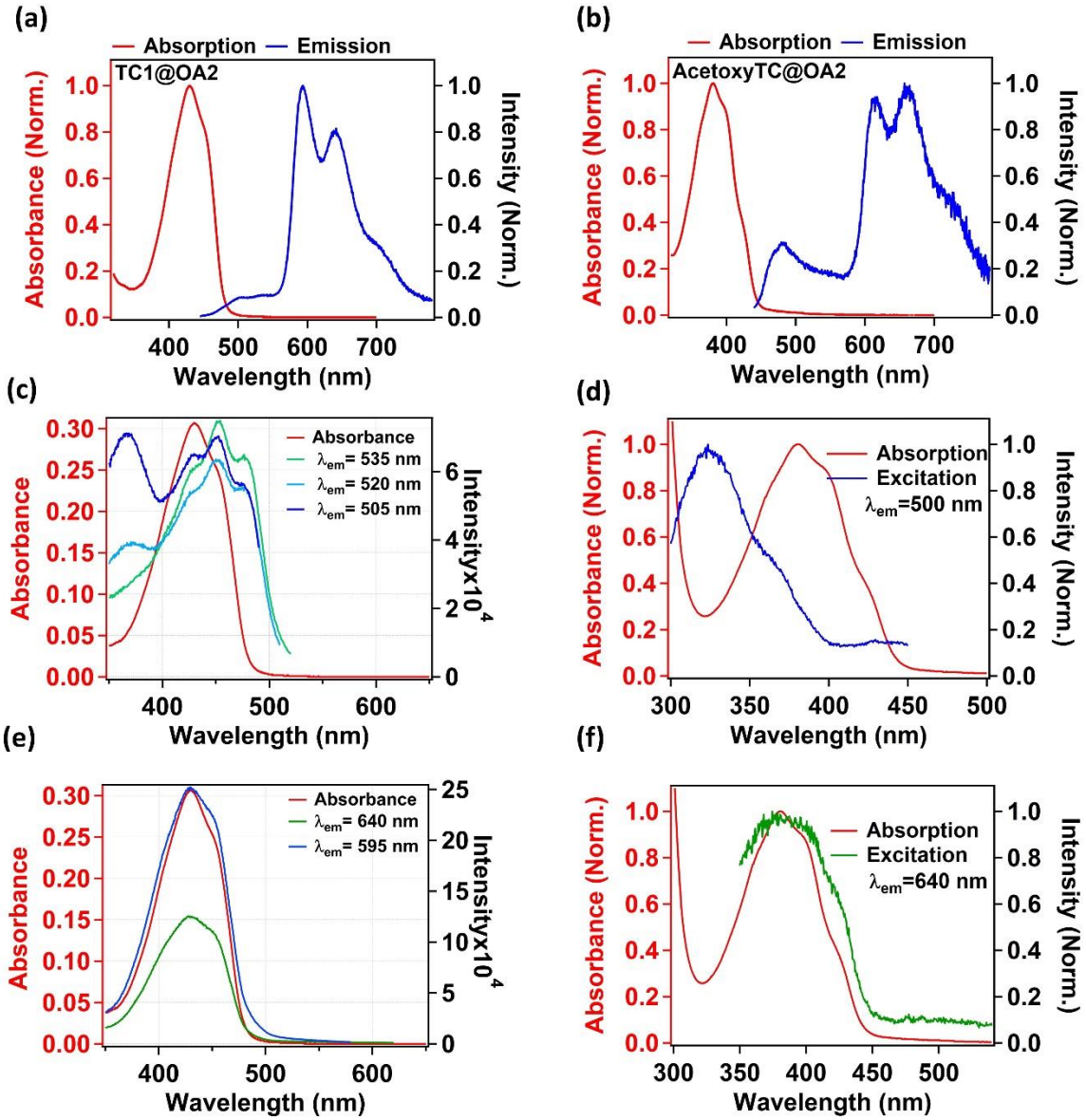

Figure 6.2.6: Steady-state absorption, emission, and excitation spectra of (a) TC1 and (b) Acetoxy-TC inside the octa acid (OA) cavity in borate buffer solution i.e. TC1@OA_2 and Acetoxy-TC@OA_2 respectively: (a) Absorption and Emission spectra of TC1@OA_2 (excitation wavelength 430 nm) and (b) Acetoxy-TC@OA_2 (excitation wavelength 400 nm); (c) Excitation spectra for three different fluorescence emission regions (505, 520, and 535 nm) of TC1@OA_2 and (d) Excitation spectra of Acetoxy-TC@OA_2 (500 nm) comparison with the absorption spectrum; (e) Excitation spectra for the 595 and 640 nm emission bands and comparison of TC1@OA_2 with the absorption spectrum; (f) Excitation spectra for the 640 nm emission bands Acetoxy-TC@OA_2 and comparison with the absorption spectrum All the measurements were done in aerated condition and at room temperature.

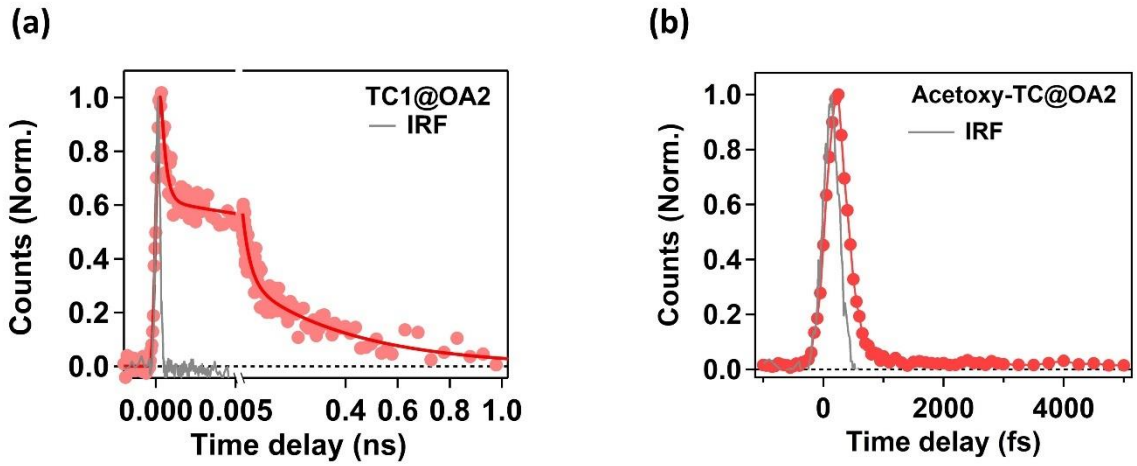

Figure 6.2.7: Normalized fluorescence decays of TC1 and Acetoxy-TC inside the octa acid (OA) cavity at emission wavelengths: 520 nm (for TC1@OA_2) and 500 nm (for Acetoxy-TC@OA_2) (λ_{ex}=400 nm) at 25 °C. All the measurements are done in nitrogen-purged conditions.

The fluorescence lifetime of TC1 within the OA cavity, and the fitted time components (0.59 ns, 12.8 ns, and >1 ns) are obtained from our earlier report. (See Figure 6.2.7a).[64] Out them, the first two components we interpreted as the lifetimes of two closely lying emissive singlet states, one of which is attributed to a charge transfer (CT) character as evident by our earlier report as well. Interestingly, for Acetoxy-TC@OA_2, the fluorescence decay is characterized by a single ultrafast component (~0.2 ps). (See Figure 6.2.7b) This singlet state lifetime is very similar to that observed in solvents, suggesting that Acetoxy-TC lacking a CT state has highly unstable singlet excited state that undergoes rapid non-radiative decay on an ultrafast timescale.

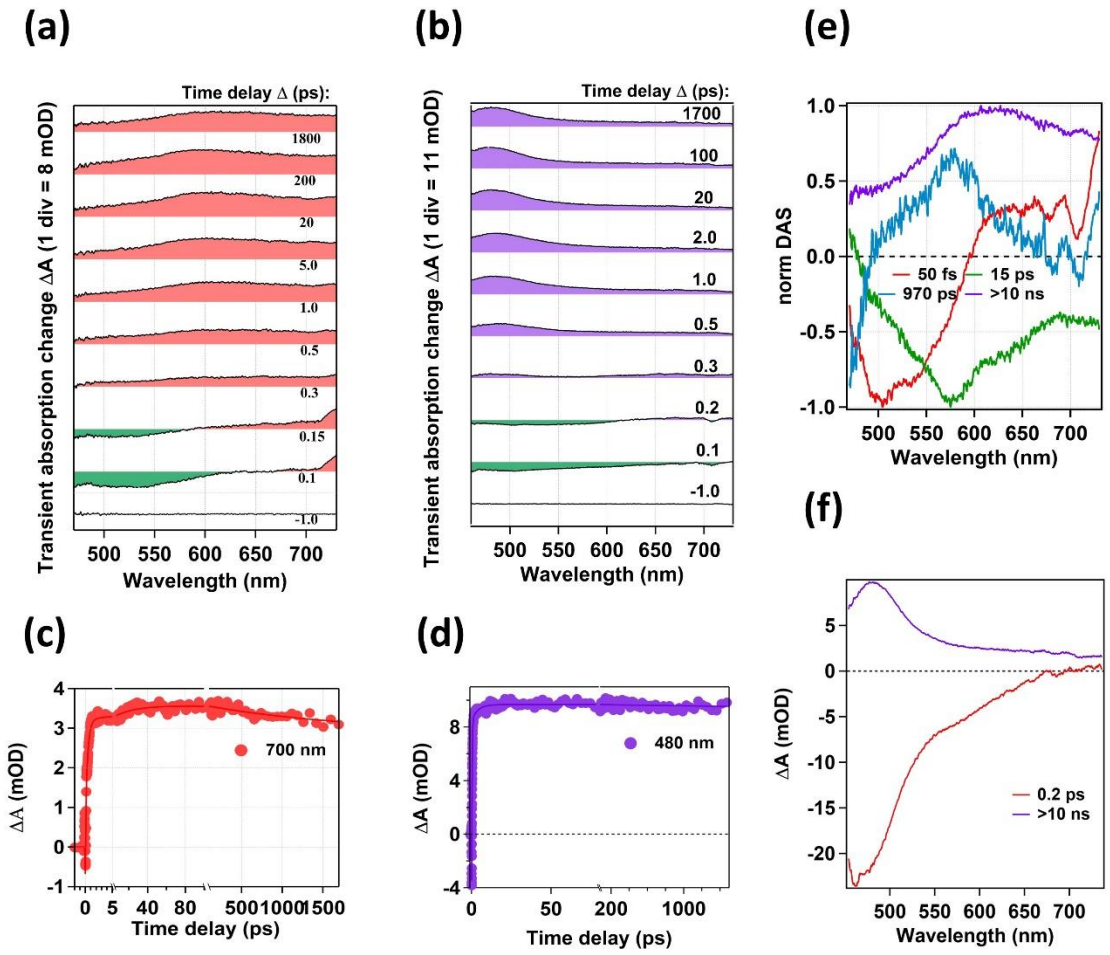

Figure 6.2.8. Transient absorption response (pump, 400 nm, probe, 460–730 nm) of TC1 and Acetoxy-TC inside the octa acid (OA) cavity. TA spectra of (a) TC1 and (b) Acetoxy-TC at some representative delay times. In the OA cavity, the TA spectra of TC1 consist of SE around 480–550 nm (green) and ESA above 600 nm (red), TA spectra of Acetoxy-TC consist of a short-lived SE band around 470–600 nm (green), a strong ESA band centered around 480 nm (purple) appears rapidly. Fitted kinetics at the triplet ESA region (700 nm for TC1 and 480 nm for Acetoxy-TC) of (c) TC1 (d) Acetoxy-TC inside the OA. Decay-associated spectra from the global analysis of TA data (OA) of (e) TC1 and (f) Acetoxy-TC in octa acid. For TC1 in OA, four global time constants are 50 fs, 15 ps, 970 ps, and >10 ns. For Acetoxy-TC in OA global time constants are 0.2 ps and 10 ns. The transient measurement was performed in a N_2-purged condition. All the transient measurements were done in an aerated condition.

To gain deeper insights into triplet state formation dynamics, we performed transient absorption (TA) measurements of OA-encapsulated Acetoxy-TC and compared with the encapsulated TC1. Representative TA spectra at some time delays are presented in Figure 6.2.8. In our earlier report, we found that for TC1@OA_2, a short-lived stimulated emission (SE) band appears in the 470–600 nm range at early times, which subsequently evolves into a broad excited-state absorption (ESA) band at later

times (see Figure 6.2.8a).[64] In contrast, Acetoxy-TC@OA_2 exhibits distinctly different triplet spectral characteristics. Following a short-lived SE band (470–600 nm), a strong ESA band centered around 475 nm appears rapidly (see Figure 6.2.8b). To understand the kinetics of these excited-state processes, we compared the transient decay at the respective triplet spectral regions (700 ± 2 nm for TC1@OA_2 and 475 ± 5 nm for Acetoxy-TC@OA_2) (see Figures 6.2.8c and 6.2.8d). In our previous finding, we reported that two rise components for TC1@OA_2, indicating the involvement of both ultrafast and slower intersystem crossing (ISC) pathways in triplet state formation. However, for Acetoxy-TC@OA_2, only a single ultrafast rise component was observed, suggesting a much faster and more direct ISC process. These findings clearly show that, as in solvents, triplet state formation for CT-state forming TC1 is slower than for the Acetoxy-TC, even within the confined environment of the OA capsule. Global analysis of the TA data for TC1@OA_2 revealed four decay-associated spectral (DAS) components (see Figure 6.2.8e). The first two components (50 fs and 15 ps) correspond to SE features, while the third and fourth components (970 ps and >10 ns) is associated with the ESA of the triplet state. For Acetoxy-TC@OA_2, only two global time components were identified: a 200 fs SE-type component and a >10 ns ESA-type component which indicates the presence of only one emissive singlet state and one triplet state in the overall excited state dynamics. (see Figure 6.2.8f). A comparative analysis of the results in three solvents (hexane, acetone, and acetonitrile) and within the OA cavity demonstrates that the excited-state dynamics of TC1 are highly sensitive to solvent polarity. This behavior is consistent with the notion that excited-state dynamics in TC1 involve charge transfer from the 7-amino group to the thiocarbonyl moiety. To further understand the solvent polarity-dependent triplet state formation in the CT-state-forming TC1, and to uncover the reason behind the solvent independent ultrafast ISC observed in Acetoxy-TC, we performed time-dependent density functional theory (TDDFT) calculations, the results of which are discussed in the following section.

6.2.3. TDDFT Calculation.

Theoretical calculations were carried out using TDDFT for both molecules in three solvents: hexane, acetone, and acetonitrile and vertical excitation energies and the electronic characters of the states are depicted in Figure 6.2.10. In hexane, the low-lying singlet excited states of TC1 appear at 2.759 eV (S_1) and 3.216 eV (S_2), corresponding to $n\pi^*$ and $\pi\pi^*$ character, respectively, at the Franck–Condon (FC) point (see Figure 6.2.9 and Table 6.2.4). Among them, the S_2 state is optically brighter and involves an intramolecular charge transfer (CT) from the amino group to the thiolactone moiety. The energy gap between the first two singlet states is approximately 0.457 eV in hexane. In acetonitrile solvent, the S_1 and S_2 states bring them closer in energy, and the computed energies for S_1 and S_2 in acetonitrile are 2.993 eV and 3.048 eV, respectively. A similar trend of energy and characteristics is also observed in acetone, an intermediately polar solvent with energies 3.006 eV(S_1) and 3.078 eV (S_2). The presence of the amino group at the 7-position facilitates intramolecular charge transfer excitation, which in turn leads to a strong solvatochromic response and a reduction in the S_1–S_2 energy gap. These theoretical results are consistent with our experimental observations of difference between the excitation and absorption spectra in solvents. A similar excitation spectral shift is observed in OA (octa acid), where the microenvironment is assumed to be non-polar. However, due to the computational expense of simulating TDDFT spectra for the OA-bound TC1 complex, it remains unclear whether the same two excited states are responsible in that system.

Table 6.2.3. Vertical transition energies of TC1 in Hexane, Acetone and Acetonitrile solvents

Hexane				Acetone				Acetonitrile			
States	**Character**	**Energy (eV)**	**Osc. strength**	**States**	**Character**	**Energy (eV)**	**Osc. strength**	**States**	**Character**	**Energy (eV)**	**Osc. strength**
S_1	nπ*	2.759	0.00001	S_1	nπ*	3.066	0.00014	S_1	nπ*	2.993	0.00006
S_2	ππ*	3.216	0.72070	S_2	ππ*	3.078	0.68310	S_2	ππ*	3.048	0.66691
S_3	ππ*	3.975	0.15800	S_3	ππ*	3.956	0.23000	S_3	ππ*	3.921	0.23001
T_1	ππ*	2.165	-	T_1	ππ*	2.138	-	T_1	ππ*	2.114	-
T_2	nπ*	2.497	-	T_2	nπ*	2.782	-	T_2	nπ*	2.773	-
T_3	ππ*	3.044	-	T_3	ππ*	3.000	-	T_3	ππ*	2.964	-
$\Delta E (S_2/S_1)$	-	0.457	-	$\Delta E (S_2/S_1)$	-	0.012	-	$\Delta E (S_2/S_1)$	-	0.055	-
$\Delta E (S_1/T_1)$	-	0.594	-	$\Delta E (S_1/T_1)$	-	0.928	-	$\Delta E (S_1/T_1)$	-	0.879	-
$\Delta E (S_1/T_2)$	-	0.262	-	$\Delta E (S_1/T_2)$	-	0.284	-	$\Delta E (S_1/T_2)$	-	0.220	-
$\Delta E (S_1/T_3)$	-	-0.285	-	$\Delta E (S_1/T_3)$	-	0.066	-	$\Delta E (S_1/T_3)$	-	0.029	-
$\Delta E (S_2/T_1)$	-	1.051	-	$\Delta E (S_2/T_1)$	-	0.940	-	$\Delta E (S_2/T_1)$	-	0.934	-
$\Delta E (S_2/T_2)$	-	0.719	-	$\Delta E (S_2/T_2)$	-	0.296	-	$\Delta E (S_2/T_2)$	-	0.275	-
$\Delta E (S_2/T_3)$	-	0.172	-	$\Delta E (S_2/T_3)$	-	0.078	-	$\Delta E (S_2/T_3)$	-	0.084	-

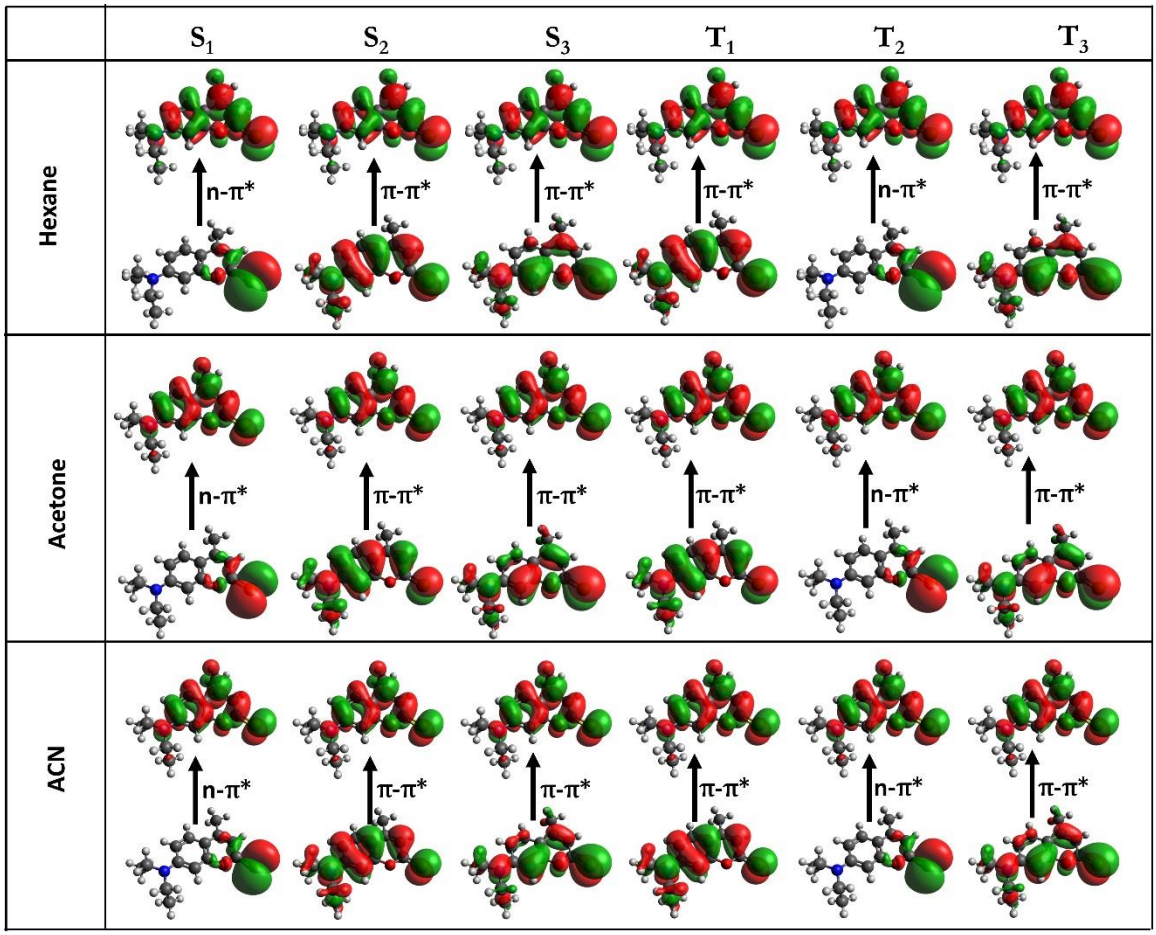

Figure 6.2.9. Electronic structures of the S_1, S_2, S_3, T_1, T_2, and T_3 states of TC1 in Hexane, Acetone and Acetonitrile (ACN) solvents through TDDFT calculation

Table 6.2.4. Spin orbit coupling constants (SOC) of TC1 in Hexane, Acetone, and acetonitrile solvent

Electronic states	Hexane		Acetone		Acetonitrile	
	Transition Type	SOC (cm^{-1})	Transition Type	SOC (cm^{-1})	Transition Type	SOC (cm^{-1})
$S_1 - T_1$	nπ*-ππ*	115.2	nπ*-ππ*	97.72	nπ*-ππ*	96.8
$S_1 - T_2$	nπ*-nπ*	0.71	nπ*-nπ*	1.33	nπ*-nπ*	0.82
$S_1 - T_3$	nπ*-ππ*	83.56	nπ*-ππ*	102.75	nπ*-ππ*	103.8
$S_2 - T_1$	ππ*-ππ*	0.19	ππ*-ππ*	1.45	ππ*-ππ*	0.88
$S_2 - T_2$	ππ*-nπ*	71.78	ππ*-nπ*	64.25	ππ*-nπ*	66.3
$S_2 - T_3$	ππ*-ππ*	0.18	ππ*-ππ*	1.59	ππ*-ππ*	0.95

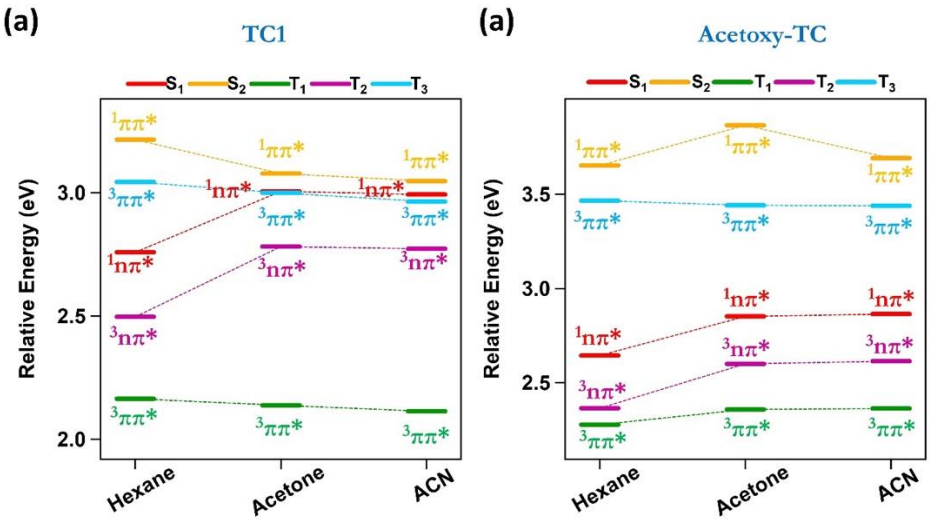

Figure 6.2.10: Vertical electronic excitation energies and their characters of electronic exited states of TC1 and Acetoxy-TC in Hexane, Acetone and acetonitrile (ACN) obtained through TDDFT calculation.

Triplet state calculations revealed that lower lying triplet states (T_1, T_2, and T_3) are close in energy to the S_1 and S_2 states, suggesting the possibility of population transfer between the singlet and triplet manifolds across solvents (see Table 6.2.3). With changing solvents from hexane to polar solvents (acetone or acetonitrile,) $S_1 \rightarrow T_1$ energy gaps increases but $S_2 \rightarrow T_2$ gap decreases. Therefore, in polar solvents, the $S_1 \rightarrow T_1$ transition may become energetically unfavorable, whereas the $S_2 \rightarrow T_2$ transition may become more energetically favorable. To assess the orbital feasibility of such intersystem crossing (ISC) events, El-Sayed's rule was applied by examining the frontier molecular orbitals of TC1 in all three solvents at the FC geometry (see Figure 6.2.9). Additionally, spin–orbit coupling (SOC) values were computed for all low-lying singlet–triplet pairs (see Table 6.2.4). In hexane, the $S_2 \rightarrow T_2$ transition involves $\pi\pi^* \rightarrow n\pi^*$ character with a SOC value of ~72 cm^{-1}, while the $S_2 \rightarrow T_3$ transition involves a $\pi\pi^* \rightarrow \pi\pi^*$ configuration. Therefore, ISC from S_2 to T_2 is both energetically and orbitally feasible. Similarly, the $S_1 \rightarrow T_1$ transition, involving $n\pi^*$ and $\pi\pi^*$ character, has a high SOC value of ~115 cm^{-1}, indicating a highly favorable ISC pathway. In acetonitrile, $S_1 \rightarrow T_1$, $S_1 \rightarrow T_3$, and $S_2 \rightarrow T_2$ transitions follows the energy and orbital criteria (El Sayed rule) with SOC value of ~ 97 cm^{-1}, ~104 cm^{-1},

and ~66 cm^{-1}. All other ISC transitions are orbitally forbidden. In acetone, probability of ISC transitions is very similar to the acetonitrile, with SOC values ~ 97 cm^{-1} ($S_1 \rightarrow T_1$), ~103.8 cm^{-1} ($S_1 \rightarrow T_3$), and ~66 cm^{-1} ($S_2 \rightarrow T_2$). Therefore, it indicates that in TC1, solvent switch from hexane to polar solvents (acetone or acetonitrile), not only the $S_1 \rightarrow T_1$ energy gaps increase but the SOC values also decrease which may be responsible for diverted and slow ISC of TC1 in polar solvents. However, through the SOC values for ($S_2 \rightarrow T_2$) transition decrease in polar solvents but which may be compensated by the decreased $S_2 \rightarrow T_2$ energy gap which leads to show solvent independency in the ultrafast triplet generation from the S_2 state in TC1.

On the other hand, the S_1 state of Acetoxy-TC possesses $n\pi^*$ character (weakly allowed), while the S_2 state exhibits bright $\pi\pi^*$ character, and this state ordering remains unchanged across all three solvents (see Table 6.2.5 and Figure 6.2.11). In hexane, the energies of the S_1 and S_2 states are 2.645 eV and 3.653 eV, respectively. Upon switching the solvent to acetonitrile, both states shift to higher energies 2.865 eV (S_1) and 3.692 eV (S_2). A similar energy trend is also noted in acetone, where the S_1 and S_2 energies are 2.852 eV and 3.866 eV, respectively.

Table 6.2.5. Vertical transition energies of Acetoxy-TC in Hexane, Acetone and Acetonitrile solvents

Hexane				Acetone				Acetonitrile			
States	**Character**	**Energy (eV)**	**Osc. strength**	**States**	**Character**	**Energy (eV)**	**Osc. strength**	**States**	**Character**	**Energy (eV)**	**Osc. strength**
S_1	nπ*	2.645	0.00014	S_1	nπ*	2.852	0.000014	S_1	nπ*	2.865	0.000014
S_2	ππ*	3.653	0.64540	S_2	ππ*	3.866	0.70567	S_2	ππ*	3.692	0.70300
S_3	nπ*	4.201	0.00008	S_3	ππ*	4.248	0.02358	S_3	ππ*	4.242	0.02345
T_1	ππ*	2.278	-	T_1	ππ*	2.359	-	T_1	ππ*	2.364	-
T_2	nπ*	2.365	-	T_2	nπ*	2.601	-	T_2	nπ*	2.615	-
T_3	ππ*	3.466	-	T_3	ππ*	3.442	-	T_3	ππ*	3.439	-
$\Delta E (S_1/T_1)$	-	0.367	-	$\Delta E (S_1/T_1)$	-	0.493	-	$\Delta E (S_1/T_1)$	-	0.501	-
$\Delta E (S_1/T_2)$	-	0.280	-	$\Delta E (S_1/T_2)$	-	0.251	-	$\Delta E (S_1/T_2)$	-	0.250	-
$\Delta E (S_1/T_3)$	-	-0.821	-	$\Delta E (S_1/T_3)$	-	-0.590	-	$\Delta E (S_1/T_3)$	-	-0.574	-
$\Delta E (S_2/T_1)$	-	1.375	-	$\Delta E (S_2/T_1)$	-	1.507	-	$\Delta E (S_2/T_1)$	-	1.328	-
$\Delta E (S_2/T_2)$	-	1.288	-	$\Delta E (S_2/T_2)$	-	1.265	-	$\Delta E (S_2/T_2)$	-	1.077	-
$\Delta E (S_2/T_3)$	-	0.187	-	$\Delta E (S_2/T_3)$	-	0.424	-	$\Delta E (S_2/T_3)$	-	0.05	-

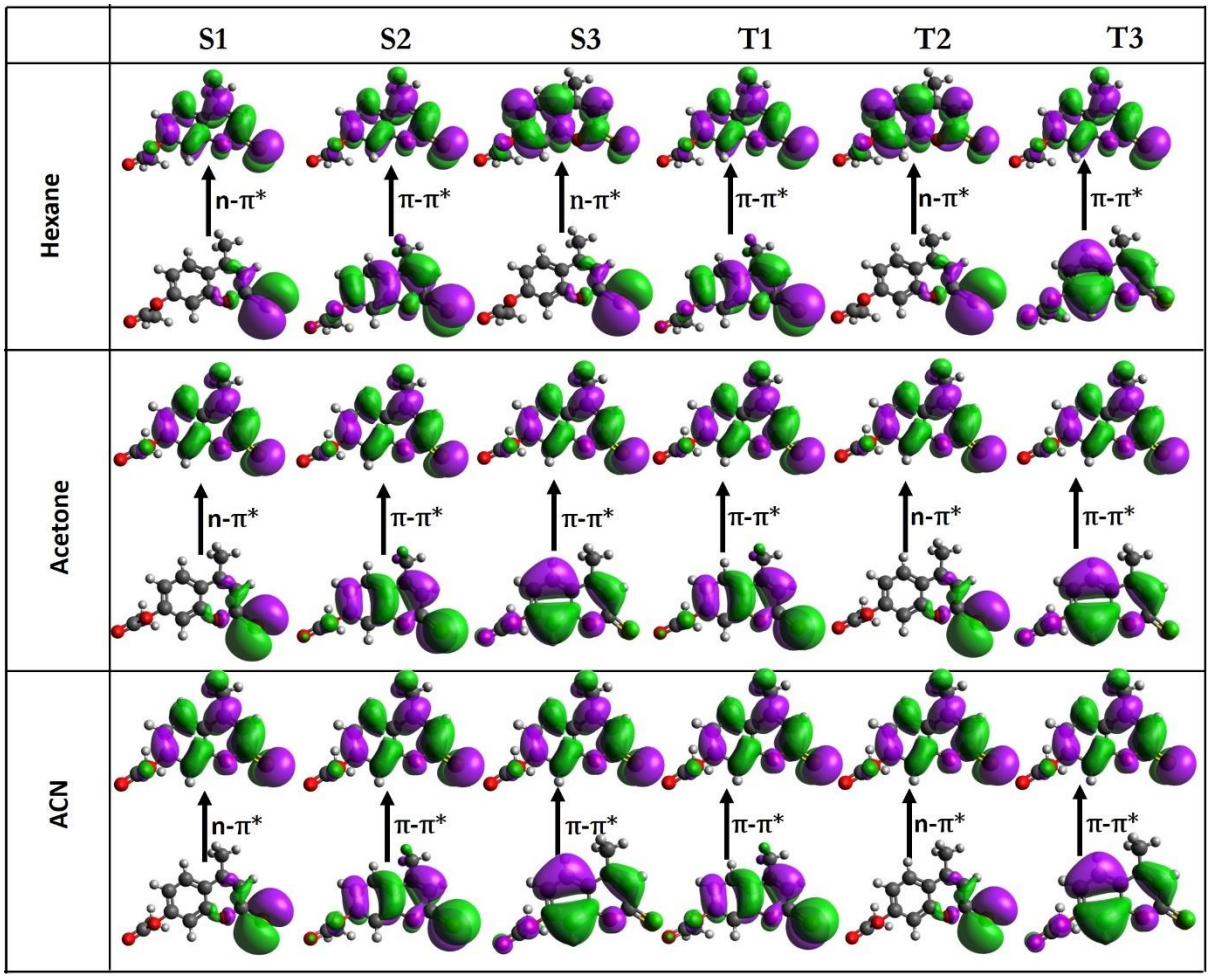

Figure 6.2.11. Electronic structures of the S_1, S_2, S_3, T_1, T_2, and T_3 states of TC1 in Hexane, Acetone and Acetonitrile (ACN) solvents through TDDFT calculation

Table 6.2.6. Spin orbit coupling constants (SOC) of Acetoxy-TC in Hexane, Acetone, and acetonitrile solvent

Electronic states	Hexane		Acetone		Acetonitrile	
	Transition Type	SOC (cm^{-1})	Transition Type	SOC (cm^{-1})	Transition Type	SOC (cm^{-1})
$S_1 - T_1$	nπ*-ππ*	133.8	nπ*-ππ*	132.7	nπ*-ππ*	132.6
$S_1 - T_2$	nπ*-nπ*	1.45	nπ*-nπ*	0.69	nπ*-nπ*	0.69
$S_1 - T_3$	nπ*-ππ*	36.79	nπ*-ππ*	36.01	nπ*-ππ*	35.88
$S_2 - T_1$	ππ*-ππ*	1.10	ππ*-ππ*	0.17	ππ*-ππ*	0.17
$S_2 - T_2$	ππ*-nπ*	116.62	ππ*-nπ*	118.27	ππ*-nπ*	118.18
$S_2 - T_3$	ππ*-ππ*	0.05	ππ*-ππ*	0.05	ππ*-ππ*	0.05

Interestingly, in Acetoxy-TC, the S_1 and S_2 states are not energetically close, with an energy gap greater than 0.9 eV, unlike in the case of TC1. However, neither S_1 nor S_2 exhibits any charge transfer (CT) character (See Figure 6.2.11). Calculations reveal that in hexane, the energies of the low-lying triplet states are 2.278 eV (T_1), 2.365 eV (T_2), and 3.466 eV (T_3), indicating that singlet-to-triplet transitions are energetically favorable. Furthermore, the transitions $S_1(n\pi^*) \rightarrow T_1(\pi\pi^*)$ and $S_2(\pi\pi^*) \rightarrow T_2$ ($n\pi^*$) adhere to El-Sayed's rule and are associated with high spin–orbit coupling (SOC) values of 133.84 cm^{-1} and 116.62 cm^{-1}, respectively (see Table 6.2.6 and Figure 6.2.11), suggesting a strong likelihood of ultrafast triplet formation. Upon switching the solvent to acetone and acetonitrile, the energies and electronic characters of the triplet states (T_1, T_2, T_3) remain largely unchanged (see Figure 6.2.10 and Table 6.2.5). In addition, the SOC values of these energetically and orbitally allowed singlet–triplet transitions remain nearly constant across solvents, reinforcing the prediction of efficient triplet generation in all three media. Therefore, overall theoretical result strongly supports our experimental observation of ultrafast and quantitative triplet formation in Acetoxy-TC (having no CT character) regardless of solvent polarity. In contrast, in TC1, we believe that due to the CT state, solvent-dependent modulation of electronic state energies and electronic couplings in polar solvents diminishes singlet–triplet orbital mixing efficiency. Overall, this analysis underscores that the CT character of singlet states in aminothiocoumarins can counteract fast and efficient triplet generation.

6.3 Conclusions

The steady state experiment revealed that in TC1 has CT behavior and shows relatively high fluorescent characteristics and yields less triplets in solvents. However, in Acetoxy-TC, fluorescence quantum yield is exceptionally low and yield almost a quantitative triplet and relatively strong room temperature phosphorescence (RTP) emission irrespective of the solvent polarities having no CT character in the singlets. In addition, fluorescence excitation spectra of TC1 are red shifted to the

absorption spectra which indicates the presence of a hidden low energy singlet excited state band inside the main absorption band having emissive characteristics. However, in Acetoxy-TC, the fluorescence excitation spectra completely match with the absorption band irrespective of the solvents indicates that the fluorescence is coming from excitation of the main absorption band only. Inside the OA cavity, both the TC1 and Acetoxy-TC has strong RTP characteristics, and those bands completely originate from the excitation of the main absorptive state only. Fluorescence upconversion measurement in bulk solvent reveals that the photoexcited singlet states of TC1 sustain up to several femtoseconds in hexane indicating extensive population loss suddenly. Lifetime increases abruptly up to several picoseconds upon changing solvents of different polarities. However, fluorescence lifetime decays of Acetoxy-TC having no CT states sustain only up to hundreds of femtoseconds and it is independent of solvent polarities. A detailed femtoseconds transient absorption (TA) measurements reveal that ultrafast ISC is the major non-radiative decay channel in Acetoxy-TC. Furthermore, TA analysis also reveals that in hexane, TC1, a similar ultrafast ISC behavior like Acetoxy-TC across solvents. However, in polar solvents, triplet state generation of TC1 is relatively slow and both the lowest singlet states involve in ISC process which is possibly due to the presence of CT singlet state. Inside the OA cavity fluorescence lifetime decays of TC1 is relatively slow over the Acetoxy-TC. We believe, the same CT states formation in TC1 might the responsible length picosecond fluorescence lifetime and retarded ISC behavior of TC1 inside the OA cavity. Such behavior is not observed for the Acetoxy-TC molecule, likely due to misalignment of the donor moiety with the thiocoumarin ring or due to forbidden charge transfer resulting from the higher electronegativity of the oxygen atom at the 7-position of the ring. Theoretical TDDFT calculation of vertical excitation energies, singlet-triplet coupling values strongly supports the experimental observations of environment independent ultrafast ISC behavior of Acetoxy-TC having unlike strongly retarded ISC in TC1 having a CT singlet state. The overall study highlights the possible role charge transfer singlet state in the triplet state formation dynamics in thiocoumarins.

References:

(1) Liu, D.; El-Zohry, A. M.; Taddei, M.; Matt, C.; Bussotti, L.; Wang, Z.; Zhao, J.; Mohammed, O. F.; Di Donato, M.; Weber, S. Long-lived Charge-transfer State Induced by Spin-Orbit Charge Transfer Intersystem Crossing (SOCT-ISC) in a Compact Spiro Electron Donor/Acceptor Dyad. *Angew. Chem. Int. Ed.* **2020**, *59*, 11591–11599.

(2) Dong, Y.; Sukhanov, A. A.; Zhao, J.; Elmali, A.; Li, X.; Dick, B.; Karatay, A.; Voronkova, V. K. Spin-Orbit Charge-Transfer Intersystem Crossing (SOCT-ISC) in Bodipy-Phenoxazine Dyads: Effect of Chromophore Orientation and Conformation Restriction on the Photophysical Properties. *J. Phys. Chem. C* **2019**, *123*, 22793–22811.

(3) Hou, Y.; Zhang, X.; Chen, K.; Liu, D.; Wang, Z.; Liu, Q.; Zhao, J.; Barbon, A. Charge Separation, Charge Recombination, Long-Lived Charge Transfer State Formation and Intersystem Crossing in Organic Electron Donor/Acceptor Dyads. *J. Mater. Chem. C* **2019**, *7*, 12048–12074.

(4) Pullanchery, S.; Kulik, S.; Rehl, B.; Hassanali, A.; Roke, S. Charge Transfer across C-H···O Hydrogen Bonds Stabilizes Oil Droplets in Water. *Science* **2021**, *374*, 1366–1370.

(5) Shen, D.; Chen, W. C.; Lo, M. F.; Lee, C. S. Charge-Transfer Complexes and Their Applications in Optoelectronic Devices. *Mater Today Energy* **2021**, *20*, 100644.

(6) Das, A.; Jha, A.; Gera, R.; Dasgupta, J. Photoinduced Charge Transfer State Probes the Dynamic Water Interaction with Metal−Organic Nanocages. *J. Phys. Chem. C* **2015,** *119***,** 21234–21242.

(7) Sulas-Kern, D. B.; Miller, E. M.; Blackburn, J. L. Photoinduced Charge Transfer in Transition Metal Dichalcogenide Heterojunctions-towards next Generation Energy Technologies. *Energy Environ. Sci* **2020**, *13*, 2684.

(8) Ramírez-Wierzbicki, I.; Cotic, A.; Cadranel, A. Photoinduced Intervalence Charge Transfers: Spectroscopic Tools to Study Fundamental Phenomena and Applications. *ChemPhysChem* **2022**, *23*, e202200384.

(9) Park, H.; Kim, H.-I.; Moon, G.-H.; Choi, W. Photoinduced Charge Transfer Processes in Solar Photocatalysis Based on Modified TiO_2. *Energy Environ. Sci* **2016**, *9*, 411–433.

(10) Coropceanu, V.; Chen, X.-K.; Wang, T.; Zheng, Z.; Brédas, J.-L. Charge-Transfer Electronic States in Organic Solar Cells. *Nat Rev Mater* **2019**, *4*, 689–707.

(11) Lv, M.; Wang, X.; Wang, D.; Li, X.; Liu, Y.; Pan, H.; Zhang, S.; Xu, J.; Chen, J. Unravelling the Role of Charge Transfer State during Ultrafast Intersystem Crossing in Compact Organic Chromophores. *Phys. Chem. Chem. Phys.* **2021**, *23*, 25455-25466.

(12) Hustings, J.; Bonné, R.; Cornelissen, R.; Morini, F.; Valcke, R.; Vandewal, K.; Manca, J. V. Charge-Transfer States in Photosynthesis and Organic Solar Cells. *Frontiers in Photonics* **2022**, *3*.

(13) Liu, X.; Rand, B. P.; Forrest, S. R. Engineering Charge-Transfer States for Efficient, Low-Energy-Loss Organic Photovoltaics. *Trends Chem* **2019**, *1*, 815–829.

(14) Das, A.; Bhattacharyya, A.; Guchhait, N. Achieving Solvent Specific Charge Transfer Damped Excited State Proton Transfer by Controlling Chain Length and Charge Donor Torsion: Implications in Nanomolar Fe^{3+} Sensing. *J. Photochem. Photobiol. A Chem* **2024**, *453*.

(15) Ito, F.; Nagamura, T. Photochemical and Photophysical Properties of Ion-Pair Charge Transfer Complexes for All-Optical Information Processing. *J. Photochem. Photobiol. C: Photochem. Rev.* **2007**, *8*, 174–190.

(16) Vlc' Ek, A. *Mechanistic Roles of Metal-to-Ligand Charge-Transfer Excited States in Organometallic Photochemistry*; 1998; Vol. 177.

(17) Liu, X.; Cole, J. M.; Xu, Z. Substantial Intramolecular Charge Transfer Induces Long Emission Wavelengths and Mega Stokes Shifts in 6-Aminocoumarins. *J. Phys. Chem. C* **2017**, *121*, 13274–13279.

(18) Ravi, M.; Samanta, A.; Radhakrishnan, T. P. Excited State Dipole Moments from an Efficient Analysis of Solvatochromic Stokes Shift Data. *J. Phys. Chem.* **1994**, *98*, 9133–9136.

(19) Kovalenko, S.; Ernsting, N. Ultrafast Stokes Shift and Excited-State Transient Absorption of Coumarin 153 in Solution. *Chem. Phys. Lett.* **1997**, *271*, 40–50.

(20) Dahiya, P.; Kumbhakar, M.; Mukherjee, T.; Pal, H. Effect of Protic Solvents on Twisted Intramolecular Charge Transfer State Formation in Coumarin-152 and Coumarin-481 Dyes. *Chem. Phys. Lett.* **2005**, *414*, 148–154.

(21) Nad, S.; Kumbhakar, M.; Pal, H. Photophysical Properties of Coumarin-152 and Coumarin-481 Dyes: Unusual Behavior in Nonpolar and in Higher Polarity Solvents. *J. Phys. Chem. A* **2003**, *107*, 4808–4816.

(22) Barik, A.; Nath, S.; Pal, H. Effect of Solvent Polarity on the Photophysical Properties of Coumarin-1 Dye. *J. Chem. Phys.* **2003**, *119*, 10202–10208.

(23) Molotsky, T.; Huppert, D. Solvation Statics and Dynamics of Coumarin 153 in Hexane−Propionitrile Solvent Mixtures. *J. Phys. Chem. A* **2002**, *106*, 8525–8530.

(24) Molotsky, T.; Huppert, D. Site Specific Solvation Statics and Dynamics of Coumarin Dyes in Hexane−Methanol Mixture. *J. Phys. Chem. A* **2003**, *107*, 2769–2780.

(25) Karami, B.; Kiani, M. Application of 7-Amino Coumarins for the Synthesis of Novel and Thermally Stable Water-Insoluble Azo-Coumarin Dyes. *J. IRAN. CHEM. SOC.* **2016**, *13*, 111–116.

(26) Woronoff, G.; El Harrak, A.; Mayot, E.; Schicke, O.; Miller, O. J.; Soumillion, P.; Griffiths, A. D.; Ryckelynck, M. New Generation of Amino Coumarin Methyl Sulfonate-Based Fluorogenic Substrates for Amidase Assays in Droplet-Based Microfluidic Applications. *Anal. Chem.* **2011**, *83*, 2852–2857.

(27) Sayed, M.; Maity, D. K.; Pal, H. A Comparative Photophysical Study on the Structurally Related Coumarin 102 and Coumarin 153 Dyes. *J. Photochem. and Photobiol. A: Chem.* **2023**, *434*, 114265.

(28) Das, A.; Ghosh, S. K.; Ramamurthy, V.; Sen, P. Vibration-Assisted Intersystem Crossing in the Ultrafast Excited-State Relaxation Dynamics of Halocoumarins. *J. Phys. Chem. A* **2022**, *126*, 1475–1485.

(29) Barik, A.; Kumbhakar, M.; Nath, S.; Pal, H. Evidence for the TICT Mediated Nonradiative Deexcitation Process for the Excited Coumarin-1 Dye in High Polarity Protic Solvents. *Chem. Phys.* **2005**, *315*, 277–285.

(30) Xiao Yao; Huang Xiaoyu; Feng Jiao; Ni Zhigang; Gai Lizhi; Xiao Xuqiong; Sui Xinbing; Lu Hua. A Simple Route toward Triplet-Forming Thionated BODIPY-Based Photosensitizers. *Dyes and Pigments* **2022**, *200*, 110167.

(31) Hasegawa, R.; Iwakiri, S.; Kubo, Y. Synthesis and Triplet Sensitization of Bis(Arylselanyl)BOPHYs; Potential Application in Triplet-Triplet Annihilation Upconversion. *New J. Chem.* **2021**, *45*, 6091–6099.

(32) Tong, S.; Cheng, Y.; Liu, H.; Pang, Y.; Lin, X.; Hu, Z.; Wu, F. Thionation of Conjugated Porphyrin with Enhanced Photodynamic and Photothermal Effects for Cancer Therapy. *J. Photochem. Photobiol. A: Chem.* **2025**, *459* 116085.

(33) Khatun, M. N.; Nandy, S.; Roy, H.; Ghosh, S. S.; Kumar, S.; Iyer, P. K. Sulphur-Atom Positional Engineering in Perylenimide: Structure-Property Relationships and H-Aggregation Directed Type-I Photodynamic Therapy. *Chem. Sci.* **2024**, *15*, 9298–9317.

(34) Gemenetzidis, E.; Shavorskaya, O.; Xu, Y. Z.; Trigiante, G. Topical 4-Thiothymidine Is a Viable Photosensitiser for the Photodynamic Therapy of Skin Malignancies. *Journal of Dermatological Treatment* **2011**, *24*, 209–214.

(35) Hung, M.-K.; uen-Wei Tsai, K.; Sharma, S.; Chen, S.-A. Polymer Light-Emitting Diodes Acridan-Grafted Poly(Biphenyl Germanium) with High Triplet Energy, Low Polarizability,a Nd an External Heavy-Atom Effect for Highly Efficient Sky-Blue TADF Electroluminescence. *Angew. Chem. Int. Ed.* **2019**, *58*, 11317.

(36) Yan, Z.-A.; Lin, X.; Sun, S.; Ma, X.; Tian, H.; Yan, Z.; Lin, X.; Sun, S.; Ma, X.; Tian, H. Activating Room-Temperature Phosphorescence of Organic Luminophores via External Heavy-Atom Effect and Rigidity of Ionic Polymer Matrix. *Angew. Chem. Int. Ed.* **2021**, *60*, 19735.

(37) Wang, F.; Ye, J.; Liu, J.; Chen, X. K.; Yang, Y.; Bin, Z.; You, J. Synthesis of Selenium-Doped Heteroacenes: Unveiling the External Heavy-Atom Effect in Host Materials. *Angew. Chem. Int. Ed.* **2025**, *64*, e202502380.

(38) Li, H.; Ma, H.; Zhang, P.; An, Z.; He, X. Room-Temperature Phosphorescence Modulating Room-Temperature Phosphorescence of Phenothiazine Dioxide via External Heavy Atoms. *Angew. Chem. Int. E* **2024**, *64*, e2024193.

(39) Coyle, J. D. The Photochemistry of Thiocarbonyl Compounds. *Tetrahedron* **1985**, *41*, 5393–5425.

(40) Rao, V. P. The Photoreactivity of Thiocarbonyl Compounds. *Sulfur Reports* **1992**, *12*, 359–399.

(41) Raghunathan, R.; Jockusch, S.; Sibi, M. P.; Sivaguru, J. Evaluating Thiourea/Urea Catalyst for Enantioselective 6π-Photocyclization of Acrylanilides. *J. Photochem. Photobiol. A: Chem.* **2016**, *331*, 84–88.

(42) Piontkowski, Z.; McCamant, D. W. Excited-State Planarization in Donor-Bridge Dye Sensitizers: Phenylene versus Thiophene Bridges. *J. Am. Chem. Soc.* **2018**, *140*, 11046–11057.

(43) Maciejewski, A.; Safarzadeh-Amiri, A.; Verrall, R. E.; Steer, R. P. Radiationless Decay of the Second Excited Singlet States of Aromatic Thiones: Experimental Verification of the Energy Gap Law. *Chem Phys* **1984**, *87*, 295–303.

(44) Lawrence, A. H.; Liao, C. C.; de Mayo, P.; Mayo, de; Ramamurthy, V. Thione Photochemistry. Cycloaddition in a Saturated System. *J. Am. Chem. Soc.* **1976**, *98*, 2219–2226.

(45) Bailey, W. F.; Bartelson, A. L.; Wiberg, K. B. Contrasting Reactions of Ketones and Thioketones with Alkyllithiums: A Coordinated Experimental and Computational Investigation. *J. Am. Chem. Soc.* **2012**, *134*, 3199–3207.

(46) Mondal, J. A.; Ghosh, H. N.; Mukherjee, T.; Palit, D. K. Ultrafast Relaxation Dynamics of the Excited States of Michler's Thione. *J. Phys. Chem. A* **2006**, *110*, 12103–12112.

(47) Xu, J.; Zeng, H.; Wang, K.; Peng, S.; Chen, X.; Zhang, Y.; Wu, D.; Xia, J. High-Yield Triplet States from Charge-Transfer-Mediated Intersystem Crossing in a Thionated Perylene Dimer. *J. Phys. Chem. C* **2024**, *128*, 20967–20973.

(48) Law, K. Y.; De Mayo, P. Thione Photochemistry. Adamantanethione as a Model for Singlet π, π* Hydrogen Abstraction. *J. Am. Chem. Soc.* **1979**, *101*, 3251–3260.

(49) Szymański, M.; Maciejewski, A.; Steer, R. P. Photophysics of Thione Triplets in Solution: Factors Controlling the Rates of Radiationless Decay. *Chem Phys* **1988**, *124*, 143–154.

(50) Fang, Y.-G.; Fang, W.-H. Nature of Excited-State Dependent Hydrogen Bonds and Their Critical Role in Determining the Photophysical Properties of Aromatic Thioketones. *Phys. Chem. Chem. Phys.* **2022**, *24*, 17059–17067.

(51) Szymański, M.; Balicki, M.; Binkowski, M.; Kubicki, J.; Maciejewskia, A.; Pawłowska, E.; Wróżowa, T. EFFECTS OF SOLUTE-SOLVENT INTERACTIONS ON RADIATIONLESS DECAY OF THIOKETONES EXCITED TO THEIR S_2-AND T_1-STATES. *Acta Phys Pol A* **1996**, *89*, 527–546.

(52) Lawrence, A. H.; Liao, C. C.; de Mayo, P.; Ramamurthy, V. Thione Photochemistry. Mechanism of the Short-Wavelength Cycloaddition of Adamantanethione: Evidence for an Excimer Derived from S_2. *J. Am. Chem. Soc.* **1976**, *98*, 3572–3579.

(53) LAW, K. Y.; DE MAYO, P. PHOTOCHEMICAL SYNTHESIS. 72. THIONE PHOTOCHEMISTRY. ADAMANTANETHIONE AS A MODEL FOR SINGLET π, π* HYDROGEN ABSTRACTION. *J. Am. Chem. Soc.* **1979**, *10*, 3251–3260.

(54) Mayo, de; of Adamantanethione, C. Thione Photochemistry. Mechanism of the Short- Wavelength Cycloaddition of Adamantanethione: Evidence for an Excimer Derived from S_2. *J. Am. Chem. Soc.* **1976**, *98*, 3572–3579.

(55) Fang, Y.-G.; Zhu, C.; Shen, L.; Wang, H.; Fang, W.-H. Synergistic Effects of Unconventional Hydrogen Bonds and π-Stacking Interaction and Their Excited-State Dependence: The Origin of Unusual Photophysical Properties of Aromatic Thioketones in Acetonitrile and Hydrocarbons. *J. Am. Chem. Soc* **2024**, *146*, 28845–28855.

(56) Borrego-Varillas, R.; Teles-Ferreira, D. C.; Nenov, A.; Conti, I.; Ganzer, L.; Manzoni, C.; Garavelli, M.; Maria De Paula, A.; Cerullo, G. Observation of the Sub-100 Femtosecond Population of a Dark State in a Thiobase Mediating Intersystem Crossing. *J. Am. Chem. Soc.* **2018**, *140*, 16087–16093.

(57) Mai, S.; Pollum, M.; Martínez-Fernández, L.; Dunn, N.; Marquetand, P.; Corral, I.; Crespo-Hernández, C. E.; González, L. The Origin of Efficient Triplet State Population in Sulfur-Substituted Nucleobases. *Nat. Commun.* **2016**, *7*, 13077.

(58) Ashwood, B.; Pollum, M.; Crespo-Hernández, C. E. Photochemical and Photodynamical Properties of Sulfur-Substituted Nucleic Acid Bases. *Photochem. Photobiol.* **2019**, *95*, 33–58.

(59) Mai, S.; Marquetand, P.; González, L. A Static Picture of the Relaxation and Intersystem Crossing Mechanisms of Photoexcited 2-Thiouracil. *J. Phys. Chem. A* **2015**, *119*, 9524–9533.

(60) Sánchez-Rodríguez, J. A.; Mohamadzade, A.; Mai, S.; Ashwood, B.; Pollum, M.; Marquetand, P.; González, L.; Crespo-Hernández, C. E.; Ullrich, S. 2-Thiouracil Intersystem Crossing Photodynamics Studied by Wavelength-Dependent Photoelectron and Transient Absorption Spectroscopies. *Phys. Chem. Chem. Phys.* **2017**, *19*, 19756–19766.

(61) Burdzinski, G.; Ziolek, M.; Karolczak, J.; Maciejewski, A. S_2 and S_1 States Deactivation of Thiocoumarin in *n*-Hexane and Acetonitrile Studied by

Femtosecond Fluorescence Upconversion and Transient Absorption Spectroscopies. *J. Phys. Chem. A* **2004**, *108*, 11160–11164.

(62) Szyman´ski, M.; Szyman´ski, S.; Maciejewski, A.; Kozłowski, J.; Koput, J. Photophysics of the S_2 State of Thiocoumarin: A Vibrationally Unequilibrated Luminophore. *J. Phys. Chem. A* **1997**, *102*, 677–683.

(63) Ghosh, S. K.; Valloli, L. K.; Unny, D.; Sivaguru, J.; Jockusch, S.; Ramamurthy, V. Room Temperature Phosphorescence of 2-Thioxo-Coumarins in Aqueous Solution Promoted by Octa Acid Inclusion. *J. Photochem. Photobiol. A: Chem.* **2024**, *451*, 115510.

(64) Dutta, A.; Ghosh, S. K.; Mandal, S.; Srinivasan, V.; Ramamurthy, V.; Sen, P. Ultrafast Processes in Upper Excited Singlet States of Free and Caged 7-Diethylaminothiocoumarin. *J. Phys. Chem. A* **2024**, *128*, 6853–6863.

(65) Marian, C. M. Spin-Orbit Coupling and Intersystem Crossing in Molecules. *Wiley Interdiscip Rev Comput Mol Sci* **2012**, *2*, 187–203.

(66) Gould, I. R.; Boiani, J. A.; Gaillard, E. B.; Goodman, J. L.; Farid, S. Intersystem Crossing in Charge-Transfer Excited States. *J. Phys. Chem. A* **2003**, *107*, 3515–3524.

(67) Verhoeven, J. W. On the Role of Spin Correlation in the Formation, Decay, and Detection of Long-Lived, Intramolecular Charge-Transfer States. *J. Photochem. and Photobiol. C: Photochem. Rev.* **2006**, *7*, 40–60.

(68) Yeldman, D.; Chopin, S. M. A.; Meskers, S. C. J.; Janssen, R. A. J. Enhanced Intersystem Crossing via a High Energy Charge Transfer State in a Perylenediimide-Perylenemonoimide Dyad. *J. Phys. Chem. A* **2008**, *112*, 8617–8632.

(69) Dance, Z. E. X.; Mickley, S. M.; Wilson, T. M.; Ricks, A. B.; Scott, A. M.; Ratner, M. A.; Wasielewski, M. R. Intersystem Crossing Mediated by

Photoinduced Intramolecular Charge Transfer: Julolidine - Anthracene Molecules with Perpendicular π Systems. *J. Phys. Chem. A* **2008**, *112*, 4194–4201.

(70) Gollnick+, K.; Held, S.; Martire, D. 0; Braslavsky, S. E. Hydroxyanthraquinones as Sensitizers of Singlet Oxygen Reactions: Quantum Yields of Triplet Formation and Singlet Oxygen Generation in Acetonitrile. *J. Photochem. Photobiol. A: Chem.* **1992**, *69*, 155–165.

(71) Ramamurthy, V.; Jockusch, S.; Porel, M. Supramolecular Photochemistry in Solution and on Surfaces: Encapsulation and Dynamics of Guest Molecules and Communication between Encapsulated and Free Molecules. *Langmuir* **2015**, *31*, 5554–5570.

(72) Ramamurthy, V. Photochemistry in a Capsule: Controlling Excited State Dynamics via Confinement. *Chem. Commun.* **2022**, *58*, 6571–6585.

(73) Ramamurthy, V. Photochemistry within a Water-Soluble Organic Capsule. *Acc Chem Res* **2015**, *48*, 2904–2917.

(74) Law, K. Y.; de Mayo, P. Thione Photochemistry. Adamantanethione as a Model for Singlet π, π* Hydrogen Abstraction. *J. Am. Chem. Soc.* **1979**, *101*, 3251–3260.

(75) de Mayo, P. Thione Photochemistry, and the Chemistry of the S_2 State. *Acc. Chem. Res.* **1976**, *9*, 52–59.

Chapter 7

Conclusion and Future Outlook

In molecular systems, intersystem crossing (ISC) from singlet to triplet states is influenced by various factors including substituents in the molecular structure, its geometry, inherent vibrations, intermolecular hydrogen bonding, and the surrounding medium's viscosity.[1–6] Detailed photophysical investigations can elucidate the mechanisms behind triplet state formation via ISC. This knowledge paves the way for designing innovative triplet-generating molecular systems with broad applications.

In this thesis, I investigated the intersystem crossing (ISC) dynamics of several triplet-generating molecules in both bulk solvents and confined environments, such as AOT reverse micelles and octa acid (OA) cavities. In particular, the excited-state study of the $Cu(dmphen)_2Cl$ complex in viscous and confined reverse micelle media revealed that triplet-state generation and its decay involve volume-changing vibrational motions and proceeds over an activation barrier of approximately 5.9 kJ/mol.[7] These findings advance our understanding of the vibrational contributions to triplet formation and support ongoing efforts to identify and explore triplet forming metal-ligand complex systems.

Current research on triplet systems is increasingly focused on identifying heavy-atom-free molecules. In this context, I have investigated the unique photophysical properties of the thionated coumarin 1 molecule (called TC1), which exhibits a notably low fluorescence quantum yield and an ultrashort fluorescence lifetime, both in bulk solvents and within the octa acid (OA) cavity.[8] It has been observed that on an ultrashort timescale, the singlet state population rapidly transitions to the triplet state. Theoretical analysis of the energy and orbital characteristics aligns well with the experimental findings, confirming the rapid ISC behavior. This study demonstrates how thionation significantly alters the photophysical properties of coumarin-type molecules and opens avenues for developing new, quantitatively efficient triplet-generating systems.

Hydrogen bonding interactions significantly impact various ground and excited state processes, profoundly influencing the photoexcited properties of molecular systems.

[2,9–14] My research has shown that in the hydrogen bond-forming protic solvent methanol, the fluorescence quantum yield and lifetime of TC1 are approximately ten times higher than in the similarly polar, but aprotic, solvent acetonitrile, with a concomitant tenfold decrease in triplet yield. Time-resolved studies revealed an additional hydrogen-bonded singlet state in methanol,[15] which is responsible for slower ISC dynamics and reduced triplet yield. Theoretical calculations were conducted to understand how hydrogen bonding alters the energy and orbital characteristics of thiocoumarin 1 in methanol. These calculations also elucidated how solvent-solute hydrogen bonding interactions energetically and orbitally constrain ISC across different molecular vibrational coordinates. This research delineates the inhibitory role of hydrogen bonding in the efficiency of triplet generation in the thiocoumarin 1 molecule, providing insights into the complex interplay between molecular interactions and photophysical behavior.

I have delved into how intramolecular charge transfer (CT) influences triplet state generation in thiocoumarin systems. Photophysical analyses of two thiocoumarin derivatives indicated that amino-thiocoumarins, which possess CT properties, generate fewer triplets than the non-CT acetoxy-thiocoumarin molecules in solvents, pointing to varying triplet formation mechanisms. Time-resolved studies revealed the presence of ultrafast components in triplet generation for non-CT thiocoumarins, while amino-thiocoumarin (TC1) displays two growth components, one fast and one slow with a dependency on solvent polarity. Theoretical calculations have elucidated how the energetics and spin-orbit coupling factors (SOC) promote rapid and efficient intersystem crossing (ISC) in acetoxy-thiocoumarin molecules. Conversely, the solvent polarity in CT-forming TC1 appears to decelerate ISC. This effect of intramolecular charge transfer on triplet formation was similarly observed in studies within OA-caged environments. Overall, these studies highlight how intramolecular charge transfer significantly affects the photophysical behavior of thiocoumarin systems, critical for efficient triplet generation.

References

(1) Thomas J. Penfold; Gindensperger, E.; Daniel, C.; Marian, C. M. Spin-Vibronic Mechanism for Intersystem Crossing. *Chem. Rev.* **2018**, *118*, 6975–7025.

(2) Bhowmik, S.; Dutta, A.; Sen, P. Ultrafast Intersystem Crossing in Benzanthrone: Effect of Hydrogen Bonding and Viscosity. *J. Phys. Chem. A* **2024**, *128*, 6864–6878.

(3) Liu, Z.-Y.; Hu, J.-W.; Huang, C.-H.; Huang, T.-H.; Chen, D.-G.; Ho, S.-Y.; Chen, K.-Y.; Li, E. Y.; Chou, P.-T. Sulfur-Based Intramolecular Hydrogen-Bond: Excited-State Hydrogen-Bond On/Off Switch with Dual Room-Temperature Phosphorescence. *J. Am. Chem. Soc.* **2019**, *141*, 9885–9894.

(4) Burdzinski, G.; Maciejewski, A.; Buntinx, G.; Poizat, O.; Toele, P.; Zhang, H.; Glasbeek, M. Femtosecond Fluorescence Up-Conversion and Transient Absorption Studies of the S_2 State in the Hydrogen-Bonded Benzopyranthione–Water Complex. *Chem. Phys. Lett.* **2004**, *393*, 102–106.

(5) Das, A.; Ghosh, S. K.; Ramamurthy, V.; Sen, P. Vibration-Assisted Intersystem Crossing in the Ultrafast Excited-State Relaxation Dynamics of Halocoumarins. *J. Phys. Chem. A* **2022**, *126*, 1475–1485.

(6) Kim, P.; Valentine, A. J. S.; Roy, S.; Mills, A. W.; Chakraborty, A.; Castellano, F. N.; Li, X.; Chen, L. X. Ultrafast Excited-State Dynamics of Photoluminescent Pt(II) Dimers Probed by a Coherent Vibrational Wavepacket. *J. Phys. Chem. Lett.* **2021**, *12*, 6794–6803.

(7) Dutta, A.; Bhowmik, S.; Sen, P. Triplet State Photophysics of Bis(Dimethylphenanthroline)Copper(I) Might Involve Volume-Changing Molecular Motion: Ultrafast Absorption and Emission Studies. *Chem. Phys. Lett.* **2024**, *839* (141108), 1–7.

(8) Dutta, A.; Ghosh, S. K.; Mandal, S.; Srinivasan, V.; Ramamurthy, V.; Sen, P. Ultrafast Processes in Upper Excited Singlet States of Free and Caged 7-Diethylaminothiocoumarin. *J. Phys. Chem. A* **2024**, *128*, 6853–6863.

(9) Shimada, H.; Nakamura, A.; Yoshihara, T.; Tobita, S. Intramolecular and Intermolecular Hydrogen-Bonding Effects on Photophysical Properties of 2′-Aminoacetophenone and Its Derivatives in Solution. *Photochem. Photobiol. Sci.* **2005**, *4*, 367–375.

(10) Kumar Venkatraman, R.; Kayal, S.; Barak, Ar.; Orr-Ewing, A. J.; Umapathy, S. Intermolecular Hydrogen Bonding Controlled Intersystem Crossing Rates of Benzophenone. *J. Phys. Chem. Lett.* **2018**, *9*, 1642–1648.

(11) Fan, M.; Tang, Y.; Li, C.; Chen, B.; Wang, T.; Zhou, P.; Cui, X. Enhanced Fluorescence by Inter/Intramolecular Hydrogen Bonding in Si-Substituted Coumarins. *J. Phys. Chem. B* **2023**, *127*, 3187–3196.

(12) Su, Y.; Li, K.; Yu, X. Theoretical Studies on the Fluorescence Enhancement of Benzaldehydes by Intermolecular Hydrogen Bonding. *J. Phys. Chem. B* **2019**, *123*, 884–890.

(13) Zhao, G. J.; Han, K. L. Role of Intramolecular and Intermolecular Hydrogen Bonding in Both Singlet and Triplet Excited States of Aminofluorenones on Internal Conversion, Intersystem Crossing, and Twisted Intramolecular Charge Transfer. *J. Phys. Chem. A* **2009**, *113*, 14329–14335.

(14) Nath, S.; Kumbhakar, M.; Pal, H. *Effect of H-Bonding on the Photophysical Behaviour of Coumarin Dyes*; K.-L. Han and G.-J. Zhao, Ed.; John Wiley & Sons, Ltd, 2010; Vol. 1.

(15) Dutta, A.; Bhowmik, S.; Ghosh, S. K.; Ramamurthy, V.; Sen, P. Effect of Hydrogen Bonding on Ultrafast Intersystem Crossing in 7-Diethylaminothiocoumarin. *J. Phys. Chem. A* **2025**, *129*, 4414–4425.

This page left blank intentionally

List of Publications

#1. Effect of Hydrogen Bonding on the Ultrafast Intersystem Crossing in 7-diethylaminothiocoumarin.

Abhijit Dutta, Suman Bhowmik, Sujit Kumar Ghosh, Vaidhyanathan Ramamurthy and Pratik Sen. *J. Phys. Chem. A* **2025**, *129*, 4414–4425.

2. Synergistic Mitigation of Phase Segregation and Blinking Suppression Along with Enhanced Electrocatalytic Activity in $CsPbBrI_2$ Perovskite Nanocrystals via Ascorbic Acid Surface Treatment.

Subarna Biswas, Mrinal Kanti Panda, Shovon Chatterjee, Jit Satra, Shilendra Kumar Sharma, Jyotisman Rath, **Abhijit Dutta**, Debopam Acharjee, Sudip Chakraborty, Subhadip Ghosh, Nimai Mishra. *Adv. Funct. Mater*. **2025**, 2505506.

3. Pivotal Role of Binding on Ultrafast Hole Transfer from $CsPbBr_3$ Nanocrystals to Isomeric Diaminobenzenes.

Patralekha Sarkar, Arghya Sen, **Abhijit Dutta**, Rakesh Kumar, Pratik Sen, *J. Phys. Chem. C* **2025**, *129*, 2, 1252–1259.

4. Oleylammonium Fluoride Passivated Blue-Emitting 2D $CsPbBr_3$ Nanoplates with Near Unity Photoluminescence Quantum Yield: Safeguarding against Threats by External Perturbations.

Arghya Sen, **Abhijit Dutta**, Abir Lal Bose and Pratik Sen, *Chem. Sci*. **2025**,*16,* 735-752.

#5. Ultrafast Processes in Upper Excited Singlet States of Free and Caged 7-Diethylaminothiocoumarin.

Abhijit Dutta, Sujit Kumar Ghosh, Satyajit. Mandal, Varadharajan Srinivasan, Vaidhyanathan Ramamurthy and Pratik Sen *J. Phys. Chem. A* **2024**, *128*, 6853-6863.

6. Ultrafast Intersystem Crossing in Benzanthrone: Effect of Hydrogen Bonding and Viscosity.

Suman Bhowmik, **Abhijit Dutta,** Pratik. Sen *J. Phys. Chem. A* **2024**, *128*, 6864-6878.

#7. Triplet state photophysics of bis (dimethylphenanthroline) copper (I) might involve volume-changing molecular motion: Ultrafast absorption and emission studies.

Abhijit Dutta, Suman Bhowmik, Pratik Sen, *Chem. Phys. Lett.* **2024**, *839*, 141108.

8. Associated water dynamics might be a key factor affecting protein stability in the crowded milieu.

Nilimesh Das, Ejaj Tarif, **Abhijit Dutta**, Pratik Sen, *J. Phys. Chem. B* **2023**, *127*, 3151–3163.

9. CdS/$CuCo_2S_4$ dots-on-rods boosting charge separation and hydrogen evolution

Amit Gautam, Saddam Sk, B. Moses Abraham, **Abhijit Dutta**, Pratik Sen, Ujjwal Pal *International Journal of Hydrogen Energy*, **2022**, *47*, 23632-23643.

10. Marcus Inversion is Observed for Excited State Proton Transfer in the Adiabatic Limit using Naphthol based Photoacids.

Aritra Das, Pratyush Ghosh, **Abhijit Dutta**, Pratik Sen, *Chem. Phys. Impact* **2021**, *3*, 100044,1-6.

Works in this thesis are based on the publications marked with #

Front pages of these four published articles are given in the following pages.